

FOR REFERENCE ONLY

**The Nottingham Trent University
Library & Information Services
SHORT LOAN COLLECTION**

Date	Time	Date	Time
12 JUL 2002 <i>XXXXX</i>	<i>LGF</i>		

Please return this item to the issuing library.
Fines are payable for late return.

THIS ITEM MAY NOT BE RENEWED

Short Loan 01

40 0720793 3



ProQuest Number: 10183508

All rights reserved

INFORMATION TO ALL USERS

The quality of this reproduction is dependent upon the quality of the copy submitted.

In the unlikely event that the author did not send a complete manuscript and there are missing pages, these will be noted. Also, if material had to be removed, a note will indicate the deletion.



ProQuest 10183508

Published by ProQuest LLC (2017). Copyright of the Dissertation is held by the Author.

All rights reserved.

This work is protected against unauthorized copying under Title 17, United States Code
Microform Edition © ProQuest LLC.

ProQuest LLC.
789 East Eisenhower Parkway
P.O. Box 1346
Ann Arbor, MI 48106 – 1346

Dynamics of Four-Wheeled Mobile Robots on Uneven Surface Applications

Assefa Ayalew, BSc., Dott.-Ing

A thesis submitted in partial fulfilment of the requirements of the
Nottingham Trent University for the degree of
Doctor of Philosophy

This research programme was carried out in the
Department of Mechanical & Manufacturing Engineering,
Faculty of Engineering and Computing,
The Nottingham Trent University,
Burton Street, Nottingham NG1 4BU, UK

October 2001

Acknowledgement:

I would like to thank my supervisory team including Dr. Eugene Lai for his tireless support, Dr. S. O. Oyadiji of the University of Manchester for his priceless advice, Mr. Brian Dobbins, the administrative and technical staff at the Nottingham Trent University, Mechanical and Manufacturing Engineering Department for their direct and indirect help. Most importantly I am very grateful to my parents who gave me the opportunity to study mechanical engineering.

Assefa Ayalew (BSc., Dott-Ing)

List of Figures

2.1	Some common types of WMRs for flat surface application	9
2.2	Comparison of manoeuvrability between: a car-like robot and a synchro-drive WMR during parallel parking	10
2.3	Comparison of manoeuvrability between a car-like robot and an independently 4-wheeeel steered WMR during tight cornering	
2.4	Axle-length varying mechanism of a WMR to prevent wheel side slipping.	12
2.5	A variable mode WMR	13
2.6	SHRIMP: A rover for rugged terrain applications.	13
2.7	A stationary manipulator interacting with the environment	24
3.1	The tyre coordinate system, and definition of kinematic and force variables.	29
3.2	The variations of the lateral (μ_l) and traction (μ_a) friction coefficients with wheel slip λ and slip-angle α .	31
3.3	Diagram for the derivation of the relationship between wheel-slip ratio and driving torque.	32
4.1	Definition of WMR coordinate axes.	36
4.2	The free-body diagram of a steered wheel in contact with uneven ground surface.	40
4.3	A WMR traversing a ramp front obstacle (laterally symmetrical).	47
4.4	The effect of the profile angle γ on the front wheel contact.	52
4.5	The effect of the magnitude and mode of traction on wheel contact loss.	53
4.6	The Laboratory robot used in the case study	54
4.7	Contour plot of normal jerk of vehicle driven/braked by rear wheels.	57
4.8	The relationship between the ideal traction force and the longitudinal velocity of the vehicle.	58
4.7	Dependence of the ideal traction force needed for a zero normal jerk motion, with respect to vehicle dimensions and speed.	60
4.8	Implementation of the control scheme.	62

5.1	A mobile platform with front obstacle (laterally symmetrical).	64
5.2	Displacement, velocity, acceleration and jerk versus time plots of a polynomial trajectory function.	69
5.3	The time parametrised ramp profile angle considered in the simulation.	71
5.4	Traction force requirement when manoeuvre time span $T \leq 1.38s$.	73
5.5	Traction force requirement when manoeuvre time span $T \geq 1.38s$.	74
6.1	An application of a mobile robot climbing a step obstacle .	76
6.2	A WMR colliding with a ramp obstacle.	77
6.3	Deformation of a cylindrical wheel due to central load and contact reaction.	81
6.4	Definition of wheel deformation coordinate.	82
6.5	The effect of variation of h_1 on the settling time after impact at the front wheels.	86
6.6	The effect of variation of h_0 on the settling time after impact at the front wheels.	87
6.7	Variation of the wheel deformations.	90
6.8	Variation of the actuation forces.	91
6.9	The dependency of the actuation effort on the stiffness of the wheel	92
6.10	The planned trajectory for the front wheel deformations for differing duration of the control.	95
6.11	Comparison of the tracking errors for a step input and planned trajectory input.	97
6.12	A finite element model of the WMR used in the case study.	98
6.13	A finite element model of one wheel of the WMR.	99
6.14	Variation of the front wheel reaction force from finite element simulations of uncontrolled impact and controlled impact.	102
6.15	Variation of the rear wheel reaction force from finite element simulations of uncontrolled impact and controlled impact.	102
7.1	Common forms of shock pulses	107
7.2	Quarter car model.	108
7.3	Comparison between the amplitudes of a Fourier series of a rectangular	

	pulse of period 3s and the Fourier integral of a rectangular pulse.	114
7.4	Points of excitation on a 4-wheeled WMR.	119
8.1	The chassis of the WMR considered in the case studies.	118
8.2	The first 25 natural frequencies of the chassis of the WMR considered for the shock response analysis.	122
8.3	Modes of vibration 1 to 4. Vehicle coordinate is measured from rear to front along the length and from left to right along the width.	127
8.4	Modes of vibration 5 to 8. Vehicle coordinate is measured from rear to front along the length and from left to right along the width.	128
8.5	Modes of vibration 9 to 12. Vehicle coordinate is measured from rear to front along the length and from left to right along the width.	129
8.6	Plot of two rectangular pulses employed in the simulations.	130
8.7	The sinusoidal Fourier coefficients of two rectangular pulses of different duration	131
8.8	The cosinusoidal Fourier coefficients of two rectangular pulses of different duration	132
8.9	Acceleration response map of a rectangular platform to one front wheel excitation with 0.05s rectangular pulse	134
8.10	Acceleration response map of a rectangular platform to one front wheel excitation	135
8.11	Comparison of acceleration responses between 0.05 s pulse and 0.08 s pulse excitations at station 1.	136
8.12	Acceleration response map of a rectangular platform to diagonal wheel excitations	139
8.13	Comparison of modal participation factor between single-wheel and diagonal-wheel excitations.	139
8.14	Comparison of acceleration response between 4-wheel excitations and diagonal-wheels excitations.	140
8.15	Comparison of modal participation factors between diagonal and 4-wheel wheel excitations.	142
10.1	Fifth-wheel technique for measuring obstacle geometry.	154
10.2	A wheel that makes multiple contacts with the ground surface.	156

List of tables

4.1	Dimension of the WMR used in the simulation	53
5.1	Dimensions of the mobile platform for used in the case study	72
6.1	Dimensions of the WMR used in the simulation.	89
6.2	Summary of the characteristics of the finite element model of the WMR.	101
8.1	Dimensions and structural properties of a WMR used in the case study.	124

List of symbols

\vec{a}_c	acceleration
F_a	traction/actuation force
F_{tr}	rear-wheels traction force
F_n	normal reaction force
\vec{F}_w	resultant wheel force
g	acceleration due to gravity
I	moment of inertia matrix
I_y	pitch moment of inertia
k	index
L_f, L_r	axle distances
M	mass matrix
\vec{T}	moment
m	mass
\vec{n}	normal vector
p	pitch angular displacement
\vec{r}	position vector

R	wheel radius
x, y, z	coordinates
$\ddot{\alpha}$	angular acceleration
α_p	pitch angular acceleration
δ	steering angle
μ_l	coefficient of lateral friction
γ	road profile gradient angle
ζ	damping coefficient
$\vec{\omega}$	angular velocity
ω	angular natural frequency
ω_p	pitch angular velocity

Contents

Acknowledgement	i	
List of figures	ii	
List of tables	v	
List of symbols	v	
Abstract	xii	
Chapter 1	<i>Introduction</i>	1
1.1	Background	1
1.2	Project Overview	5
1.3	Aim	6
1.4	Objectives	6
1.5	Thesis Overview	6
Chapter 2	<i>Literature Review</i>	8
2.1	Classification of WMRs	8
2.2	Modelling of WMRs	14
2.2.1	Kinematics Based Work	14
2.2.2	Work Based on Two-dimensional Dynamics	17
2.2.3	Work Based on Uneven Terrain Dynamics	20
2.3	Impact modelling and Control in Manipulators	23
Chapter 3	<i>Wheel Modelling</i>	28
3.1	Introduction	28
3.2	Wheel Modelling	28

3.3	Wheel -Slip Control	32
3.4	Summary Comments	34
Chapter 4	<i>Rigid body Dynamics Modelling</i>	36
4.1	Introduction	36
4.2	Mathematical Modelling	38
4.2.1	Translational Acceleration	42
4.2.2	Centrifugal Acceleration	42
4.2.3	Angular Acceleration	42
4.2.4	The Normal Components of Acceleration	44
4.2.5	Wheel Unilateral Constraints	44
4.3	Dynamics of a WMR Climbing a Ramp	44
4.4	Sensitivity of the Unilateral Constraint	51
4.5	Smoothness of Manoeuvre	54
4.6	A Case Study	57
4.7	Summary Comments	62
Chapter 5	<i>Trajectory Planning and Control of WMR Pitch Dynamics</i>	63
5.1	Introduction	63
5.2	Modelling and Control of Impact for WMRs	65
5.3	Localised Trajectory Planning	68
5.4	Summary Comments	75
Chapter 6	<i>Wheel Impact Control</i>	76
6.1	Introduction	76
6.2	Modelling and Control of Impact for WMRs	80
6.3	Case Study	87
6.4	State-Space Formulation	93
6.5	Control with Trajectory Planning	94
6.6	Implementation Issues	98

6.7	Finite Element Simulation	99
6.8	Summary Comments	103
Chapter 7	<i>Shock Response Analysis of WMRs - Modelling</i>	104
7.1	Introduction	104
7.2	Modelling	108
7.3	Eigenvalue Problem Formulation	110
7.4	Response Computation	111
7.5	Projection of the Excitation Force	113
7.6	Summary Comments	121
Chapter 8	<i>Shock Response Analysis of WMRs - Application</i>	122
8.1	Introduction	122
8.2	Modes of Vibration	124
8.3	Analysis of the Shock Load	130
8.4	Single Wheel Excitation	132
8.5	Diagonal Wheel Excitation	137
8.6	Four wheel Excitation	141
8.7	Summary Comments	143
Chapter 9	<i>Discussion</i>	145
9.1	Discussion	145
Chapter 10	<i>Conclusions and Further Work</i>	152
10.1	Conclusions	152
10.2	Further Work	153
	10.2.1 Ground Profile Measurement	154
	10.2.2 Measuring Jerk	154
	10.2.3 Trajectory Planning	155
	10.2.4 Multiple Wheel-Ground Contact	155

- Appendix A *Computation of Normal Jerk*
- Appendix B *Expression for the Pitch Angular Acceleration*
- Appendix C *Shock Response Computation*
- Appendix D *Publications*

Abstract

Although wheeled locomotion has existed for many decades the application of intelligent techniques to guide mobile platforms, referred to as Wheeled Mobile Robots (WMR) has awaited the advance in information and computation technology. Still the development of wheeled mobile robots lags behind that of stationary manipulators where considerable research effort has been spent. However, the unique advantage of mobile robots, which is their mobility, has attracted significant attention recently in various areas, including industrial material transfer, underground mining, various operations in hazardous environments and unmanned explorations.

So far most of the research work on WMRs application has been limited to indoor environment with smooth and flat ground surface. There is a distinctive lack of understanding of the behaviour of WMRs when the smooth and flat working surface conditions are not met. The interaction between wheels and ground surface obstacles has so far been ignored. This has made impossible the operational autonomy of wheeled mobile robots in arbitrary ground surface conditions where wheel level obstacles are present.

This work has been undertaken to close the gap between the lack of understanding of WMRs dynamic behaviour and the need to have a complete autonomy of WMRs in any geometrical condition of the ground surface. An analytical modelling approach of the dynamics problem has been followed. For this purpose a rigid-body-dynamics model of a WMR that navigates an uneven ground surface of an arbitrary geometry has been formulated. Undesired dynamic effects such as wheel-ground contact loss, payload instability and harshness of motion of the WMR have been identified as problems of uneven terrain manoeuvre. Analytical expressions that relate the above-mentioned problems to: (a) the geometry of the ground surface (b) the wheel drive forces of the WMR and (c) the velocity of the WMR have been derived. These relationships permit the development of a jerk-minimisation technique.

The rigid body dynamics model of the WMR has been extended to take into account wheel deformations that occur during wheel-obstacle collision. A traction control scheme that enables permanent wheel-ground grip during impact has been proposed. Simulation results of the proposed scheme have shown the effectiveness of the technique to controlling impact between WMRs and wheel obstacles. A mathematical tool has also been devised to enable the estimation of the shock acceleration response at various points on a WMR when its wheels are excited by impact load. Simulation study suggests that this tool may be used in conjunction with the proposed jerk-minimisation technique and the impact-control scheme to improve the safe motion planning and control of WMRs in an environment with wheel level obstacles.

Chapter 1

Introduction

1.1 Background

In the classical definition of the term a robot is stated as: *a programmable, multifunction manipulator designed to move material, parts, tools, or specialised devices through variable programmed motions for the performance of a variety of tasks* [1]. This definition is restricted to manipulators. A better operational definition specifically for Wheeled Mobile Robots (WMR) has been given in [2] where a WMR has been defined as: *a robot capable of locomotion on a surface through the actuation of wheel assemblies mounted on the robot and in contact with the surface. A wheel assembly is a device which provides or allows relative motion between its mount and a surface on which it is intended to have a single point of rolling contact.*

The predecessors of Wheeled Mobile Robots (WMRs), Autonomous Guided Vehicles (AGVs) have been around for several decades. According to an article in the Modern Materials Handling Magazine [3], the first AGV was installed by the Cravens Company at Mercury Motor Express in Columbia, USA in 1954 for materials handling purposes. However, the use of AGVs did not enjoy much popularity and by the early 80s the investment by US firms in AGVs was less than 70 Million dollars. The technology nevertheless got the attention of several European companies that rapidly evolved it. The present trend is towards the development of the more intelligent forms of AGVs, i.e. WMRs, for various industrial applications.

The traditional AGVs follow predefined paths marked by either reflective tapes or buried wires in their working environment. In contrast, WMRs can intelligently plan their path in a working environment clustered with avoidable obstacles which are detected with the help of sonar or laser range finders or other image processing tools. The avoidable obstacles could be static, as in the case of walls and fixed machinery, or mobile, as in the case of people, vehicles or other mobile robots. In addition to planning the path of the WMR, intelligent control methods are applied to track the planned path enabling complete autonomy of the WMR's operations. The complete autonomy of WMRs and the functional flexibility they offer makes them a more

attractive option to the further development of the now almost obsolete technology of AGVs.

While there has been a lot of interest in developing mobile robots of different kinds, including aerial, aquatic and walking, the most successful advancement has been observed in the wheeled mobile robotics for indoor applications. At present it is possible to purchase commercial wheeled mobile robots for unmanned security patrols. Potential applications of WMRs are in the areas of industrial material transfer, underground mining operations, fire fighting, various operations in nuclear plants, unmanned space explorations and land-mine removal [4-5].

Despite their promising future a great deal of research effort is required before WMRs become a common tool in day to day industrial, military and civil activities. Ideally, WMRs will need to have the capability to tackle rugged, non-ideal, variable characteristics rough outdoor and indoor terrain where small ground surface unevenness is unavoidable. A number of open questions remain unanswered in the development of intelligent and dynamic path planers. Obstacle detection techniques need to become more accurate and faster [6]. Vehicle guidance techniques need to be more reliable.

Common applications of a WMR involve the planning of the motion of the WMR and an automatic control to enable it to follow the planned motion. The main tasks in WMR motion planning and control can be split into three major phases: *path planning, trajectory planning and trajectory tracking*. The path planning phase involves the selection of a geometric path based on the satisfaction of a combination of criteria such as: obstacle avoidance, minimum distance and vehicle kinematic constraints (steering angle limits, for example). The planned path needs to be parametrised with time in order to generate vehicle velocity and acceleration commands. The velocities and accelerations are generated so that some criteria governing the availability of drive torque and ground surface friction are satisfied. This phase corresponds to the trajectory planning. The trajectory-tracking phase involves the control of the WMR by using either a kinematic or dynamics based control algorithm so that the WMR follows the planned trajectory.

While these problems have been tackled in several previous works for WMRs navigating a smooth and flat environment [7-10], the lack of understanding of WMR dynamic behaviour in uneven terrain has limited similar advances to be achieved in uneven ground surface applications. Although there is an intuitive human understanding of the undesired effects of driving a WMR over an obstacle, the robot needs some framework to estimate the potential hazard, and a mathematical model that can relate the vehicle characteristics, working conditions, ground surface geometry, vehicle response and driving inputs.

Jerk, the rate of change of acceleration, is a good measure of harshness of the dynamic response of mechanical structures [11]. In the context of WMRs navigating an uneven ground surface, a high level of jerk corresponds to a higher potential of payload instability, and possible damage to sensitive measurement instrument and computational hardware aboard the robot.

The effect of collisions between the wheels and a stationary ground obstacle on the structural dynamic response of a WMR also needs to be considered with aim of enabling the WMR motion planner to assess the potential damages caused by such events so that counteractive actions could be taken.

For a WMR to be manoeuvrable it is necessary that the wheels be in contact with the ground at all times so that traction as well as steering forces can be generated. However, collisions with stationary obstacles can cause these contacts to fail making the WMR uncontrollable.

The present study seeks to improve the understanding of path and trajectory planning problems and the development of motion control tools, by providing a basis on which the adverse effects of uneven surface manoeuvre can be quantified. A new criterion, that is the satisfaction of minimum jerk requirement, will be introduced as a means of designing a feasible trajectory for manoeuvres of WMRs on uneven ground surface. An impact control scheme based on an extended model of the rigid body dynamics of WMRs, that incorporates wheel deformations, will be proposed to improve wheel-grip characteristics of WMRs during impact. The technique thus

developed will be tested in a finite element simulation environment by using the LS-Dyna® programme.

There are two types of modelling problems of mechanical structures in general and robots in particular. The first one is the kinematics modelling problem and the second one is the dynamics modelling problem. Kinematics relates the geometry of the structure and the external constraints to the motion variables, namely, displacement, velocity and acceleration, of various members of a mechanical object. Dynamics adds the forces into the motion equations. In this thesis mainly the dynamics modelling problem will be considered.

There are two basic problems in dynamics modelling of robots. The first is the inverse dynamics modelling while the second is the forward dynamics modelling. An inverse modelling problem can be stated as follows. Given the motion in terms of displacement, velocity or acceleration of some points on the robot, determine the forces/torques needed to be applied at the actuation points in order to achieve the specified motion. A forward dynamics problem seeks to determine the resulting motion of the robot's components to a given set of external actuation forces/torques. While inverse dynamics is used for devising control strategy forward dynamics is mainly used to simulate the response of a robot to prescribed inputs.

In mathematical terms the difference between the inverse and forward dynamics problems can be stated as follows. Let \vec{q} be a vector of generalised coordinates describing the configuration (i.e. position and orientation) of a WMR, thus the equation of motion of the robot can be written in two forms:

$$\vec{F} = g(\vec{q}, \vec{\dot{q}}, \vec{\ddot{q}}) \quad (1.1)$$

or

$$\vec{\ddot{q}} = f(\vec{q}, \vec{\dot{q}}, \vec{F}) \quad (1.2)$$

where $\vec{\dot{q}}$ is the velocity vector, $\vec{\ddot{q}}$ is the acceleration vector, \vec{F} is the vector of external forces/torques, and g and f are functions. Thus Equation (1.1) represents the inverse dynamics problem while Equation (1.2) specifies the forward dynamics problem of the robot.

This research work is motivated by the inadequate understanding of both the inverse and forward dynamics of WMRs in uneven surface applications. The non-existence of realistic mathematical models that can adequately describe the behaviour of WMRs when they interact with ground surface irregularities means that:

- It may not be possible to devise control strategies that are capable of dealing with undesired dynamic effects of uneven terrain manoeuvre. Thus the objective of tracking the motion of a WMR along a prescribed path from a specified departure point to a desired destination can not be achieved.
- The safety of payload and instrumentation aboard the WMR may be compromised.

Before any attempt could be made to rectify the above problems a model that exposes the physics of the interaction between the ground surface and the WMR has to be devised. Any undesired effects have to be identified qualitatively and described quantitatively. Finally control strategies could be devised in order to minimise the undesired effects and the effectiveness of the devised techniques needs to be evaluated.

1.2 Project Overview

This work has been undertaken at The Nottingham Trent University, Mechanical and Manufacturing Engineering Department as part of a plan to develop an expertise in the area of Wheeled Mobile Robot technology. A preceding PhD project has focused on the kinematics and construction of a prototype WMR. The present work is mainly concerned with the dynamics of WMRs that navigate in the presence of ground surface obstacles. Technical advice and collaborations were obtained from the University of Manchester, School of Engineering.

1.3 Aim

- To develop an understanding of the dynamic effects of WMR manoeuvre on uneven ground surface.

1.4 Objectives

- To devise a mathematical model of the rigid body dynamics of a 4-wheel steered WMR whose wheels interact with ground surface obstacles of arbitrary geometry.
- To determine the relationships between the vehicle characteristics, obstacle geometry, driving input and the rigid-body jerk response of the WMR and to propose a technique for the minimisation of the rigid-body dynamics jerk.
- To develop a mathematical model for the wheel-ground impact problem, propose a control scheme and validate the performance of the technique by using finite element simulation.
- To develop an analytical tool for the estimation of the potential damage due to shock response of WMRs due to wheel-ground obstacle collisions.

1.5 Thesis Overview

The thesis is divided into two main parts. The first part deals with the rigid body dynamics and modelling of WMRs. The second part concentrates on the non-rigid body dynamics.

In Chapter 2 a review of existing work on kinematic and dynamic modelling of WMRs is given starting with the structural classification of common WMR designs. This section is subdivided into three major topics covering the two-dimensional kinematics, two-dimensional dynamics and three-dimensional dynamics of WMRs. In Chapter 3 a background theory on wheel force modelling techniques is presented.

Chapter 4 details the derivation of a generalised dynamics model of a WMR that navigates on a ground surface of an arbitrary geometry, with the WMR having

arbitrary steering angles. A case study of a straight-line motion of a WMR while traversing a ground obstacle of ramp geometry is presented.

Chapter 5 deals with the pitch dynamics of a WMR moving along a straight-line while encountering a front wheel obstacle of an arbitrary geometry. A new methodology for planning the trajectory and controlling the pitching motion of the WMR is presented.

Throughout the rigid body dynamics analysis smooth transition between planar motion and three-dimensional motion will be assumed. If the smooth transition assumption can not be justified the analysis calls for non-rigid body dynamic models.

By extending the rigid-body dynamics model presented in Chapter 4 in order to include wheel deformations, Chapter 6 deals with the dynamics and control of wheel-ground impact with an aim to achieving permanent wheel-ground grip. A control technique will be proposed and evaluated by means of simulations.

Chapter 7 continues the non-rigid body dynamic analysis by dealing with the vibration caused by the shock loading during wheel obstacle impact. A mathematical tool that is used to estimate the acceleration response at various points on the chassis of the WMR is presented. The model developed will be applied in case studies that are presented in Chapter 8. A discussion on the results of the project is provided in Chapter 9 followed by concluding remarks, which are given in Chapter 10.

Chapter 2

Literature Review

2 Literature Review

In this chapter the state-of-the-art of Wheeled Mobile Robot (WMR) technology will be reviewed with an emphasis on the modelling and control. The limitations of previous modelling approaches will be discussed. The historical development of WMRs is preceded with a brief review of the types of WMRs found in the open literature.

2.1 Classification of WMRs

Various designs of WMRs are found in the literature. In Figure 2.1 some of the most common types of WMRs for indoor applications have been shown. Figure 2.1.a shows the car-like WMR with front actuated steering wheels. The synchro-drive WMR (Figure 2.1.b) has equal actuated steering angles on all its wheels and is often driven by a synchronous drive, with all the wheels interconnected by a chained mechanism. It is evident that the motion of the synchro-drive WMR is always translational, except when the steering angle is changed while the robot is in motion in which case a transient yawing motion may ensue. The 4-wheel independently steered WMR is a highly manoeuvrable WMR (Figure 2.1.c). The most widely investigated WMR, mainly because of its simplicity, is the wheelchair-like robot with its differentially-driven fixed rear wheels and one or more self steering castor front wheels (Figure 2.1.d).

Although most of the analysis to be discussed in later chapters can be extended to other types of WMRs, particular attention will be given to 4-wheeled WMRs with independent steering. The car, one of the most common devices in modern day activities, has been considered for a WMR in some research works [7,12]. However this structure has poor manoeuvrability in many situations some of which have been demonstrated in Figures 2.2 and 2.3. In Figure 2.2 a comparison has been made

between a car-like WMR and a synchro-drive WMR for parallel parking manoeuvre in a space between two parked WMRs (A and B). The car-like robot has

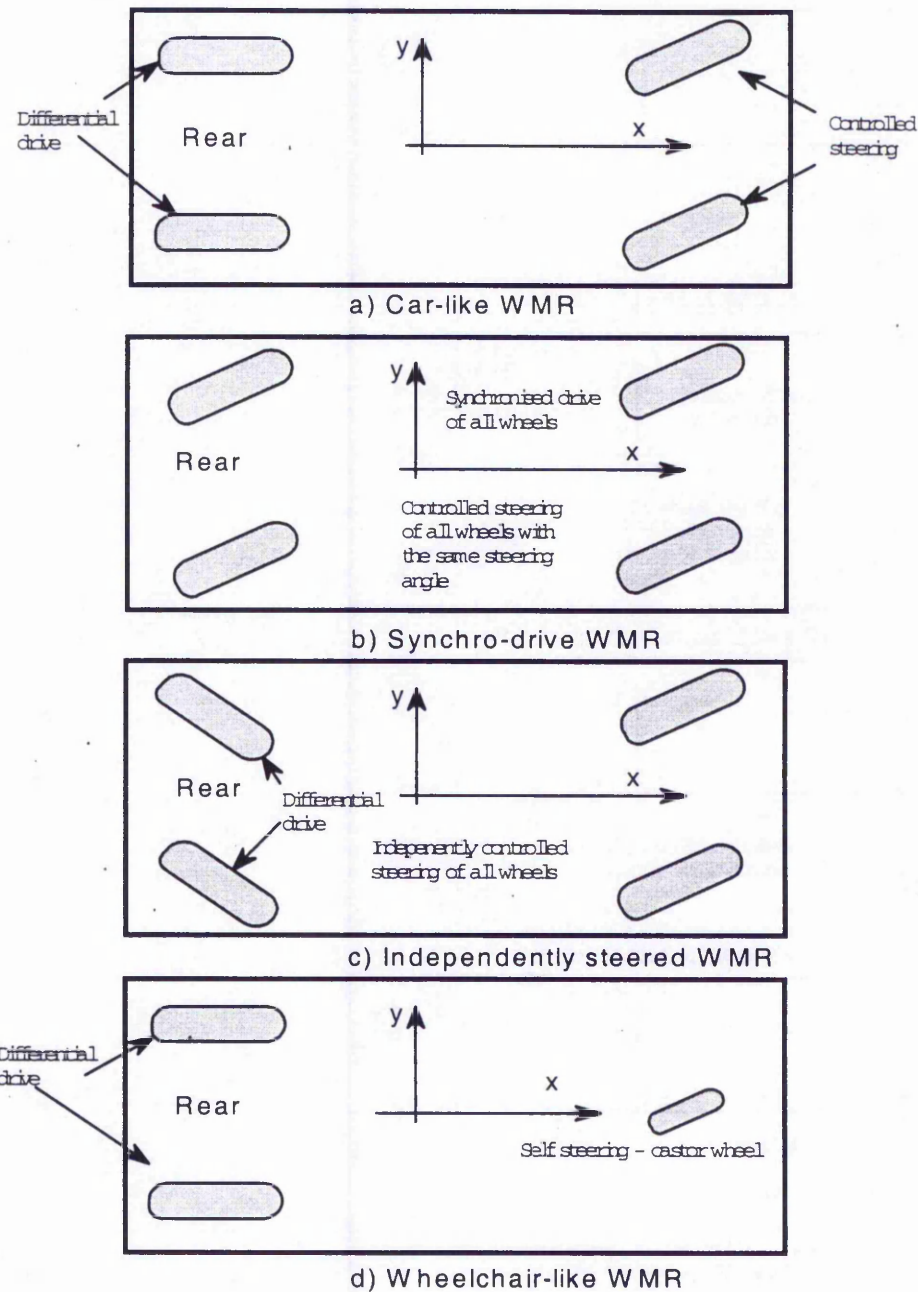


Figure 2.1 Some common types of WMRs for flat surface application.

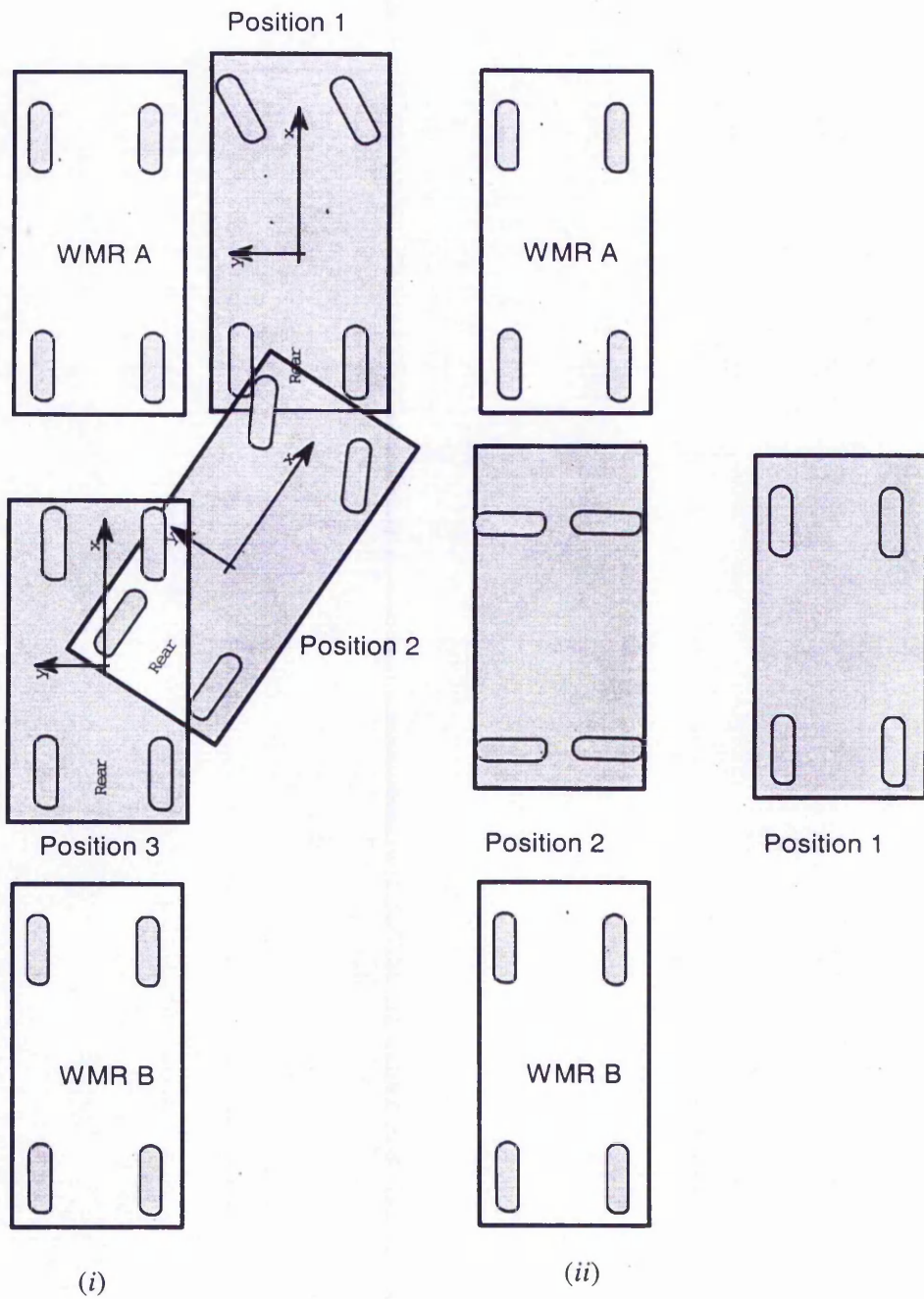


Figure 2.2 Comparison of manoeuvrability between: (i) a car-like robot and (ii) a synchro-drive WMR during parallel parking.

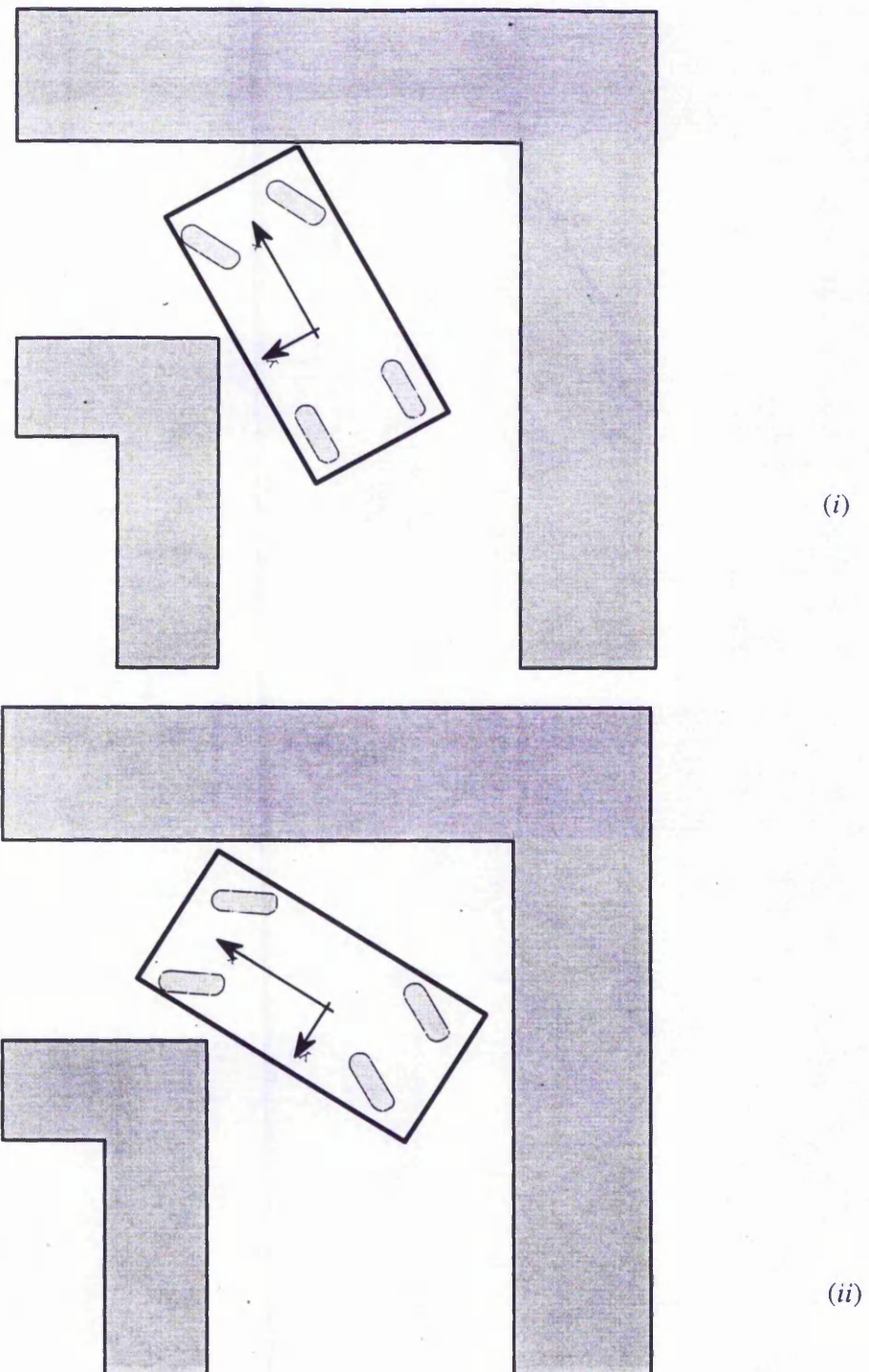


Figure 2.3 Comparison of manoeuvrability between (i) a car-like robot and (ii) an independently 4-wheeled steered WMR during tight cornering.

to go through a longer and a more complex manoeuvre to reach the desired destination (position 3), whereas the synchro-drive WMR reaches the desired target with a manoeuvre of two simple steps. It can be shown that the 4-wheeled WMR with independent steering has a capability to do a manoeuvre similar to that of the synchro-drive WMR.

In Figure 2.3 another manoeuvrability test involving a tight cornering of a car-like robot has been demonstrated. It is evident that the car-like robot may have to undergo a reversing manoeuvre before it may complete the cornering motion. The independently steered WMR, having a superior angular turn could go around the tight corner with relative ease. A difficult manoeuvre is required to get the synchro-drive WMR around the tight corner while maintaining its front along the heading direction.

Uneven surface navigation necessitates the use of articulated WMR chassis designs to facilitate static wheel-ground contact. Ground clearance of the chassis is another essential feature of WMRs that navigate a highly rugged terrain. The chassis designs that enable the WMR to satisfy the above requirements are, however, done on an ad-hoc basis. The kinematics and the mechanisms employed are often treated as

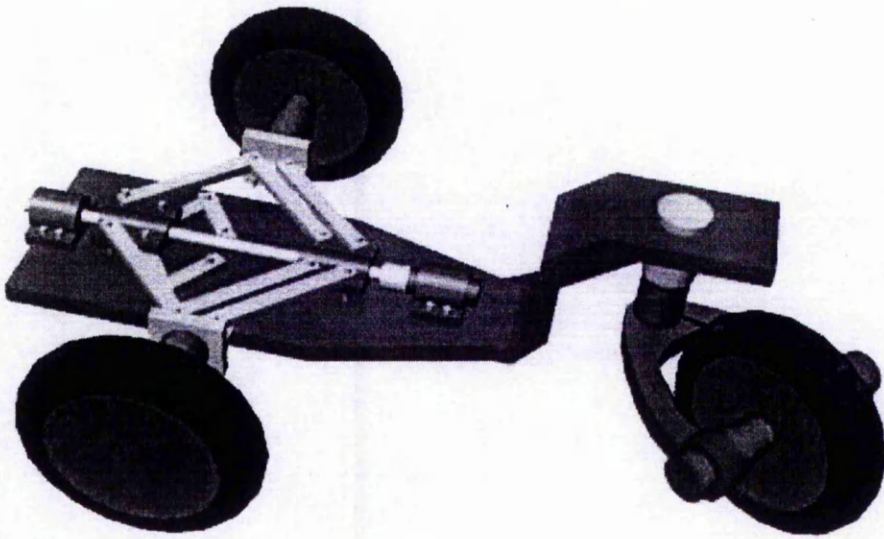


Figure 2.4 Axe-length varying mechanism of a WMR to prevent wheel side slipping [14].

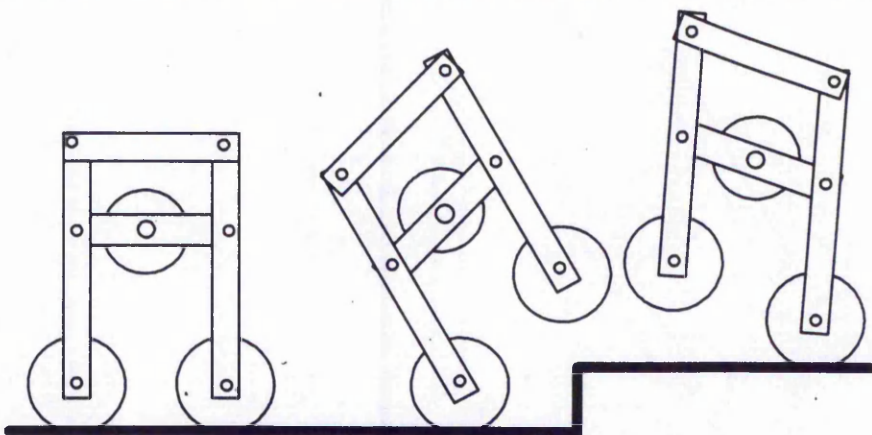


Figure 2.5 A variable mode WMR [15].

commercially confidential information. However, a few of these mechanisms are available in the open literature and will be discussed below.

The vehicle design employed by Choi and Sreenivasan [14] features a variable length axle that is introduced in order to reduce wheel sliding brought about by kinematic incompatibility (Figure 2.4). A variable structure, four-wheeled mobile robot (Figure 2.5) that can pass over a step obstacle has been proposed in [15]. This WMR can switch between two running modes. When the robot is working on a smooth surface it has a car-like, four-wheeled structure. When it passes over an obstacle the

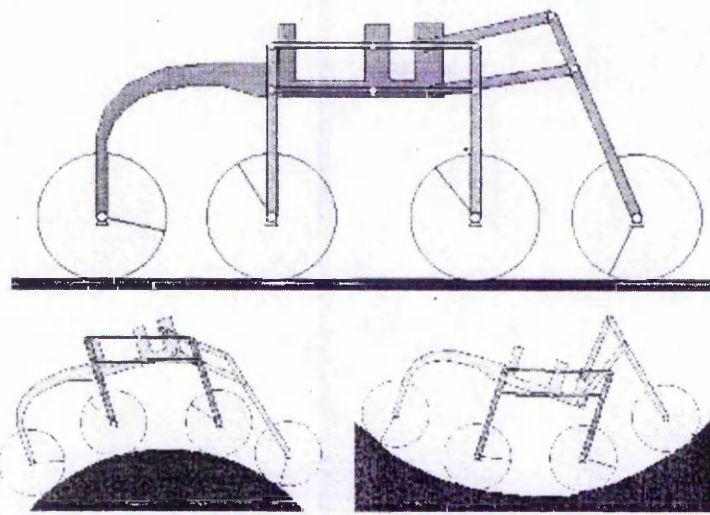


Figure 2.6 SHRIMP: A rover for rugged terrain applications [16].

vehicle changes its structure and becomes a two-wheeled robot running like a wheeled inverted pendulum. SHRIMP [16] is another fascinating articulated WMR design devised for highly irregular, outdoor terrain (Figure 2.6). As ingenious they may seem, the above chassis designs are not suitable for handling heavy payloads, and the likely missions of the robots are limited to simple tasks such as inspection. This is because the highly articulated linkages prohibit an inclusion of a payload platform in most cases.

2.2 Modelling of WMRs

An extensive amount of work has been done on kinematic and dynamic modelling of WMRs. However, the majority of the past research work is based on an assumption that the working surface of the WMR is smooth and flat. More recently, attempts have been made to address issues related to the behaviour of WMRs during uneven terrain manoeuvre. After an extensive literature survey the research work on WMRs may be classified as follows:

- i. Work based on pure kinematics.
- ii. Work based on smooth and flat ground surface dynamics: 2-dimensional dynamics.
- iii. Work that takes account of surface unevenness.

2.2.1 Kinematics Based Work

Kinematic modelling of WMRs seeks to relate the translational and rotational motions of the platform of a WMR to the rotational motions of the wheels as well as the steering angles. In contrast to stationary manipulators the WMRs have nonholonomic kinematics because their constraint equations are not integrable. This makes the devising of control strategies generally more complex as coordinates can not be eliminated by using the constraint equations like in holonomic systems such as manipulators.

Zhang et al [8] considered the tracking control of a differentially-steered wheeled mobile robot. Three posture variables are employed to uniquely define the configuration of the WMR travelling on a level flat surface. These posture variables are expressed in Cartesian coordinates x and y to specify the position of the tracking point (i.e. a fixed point on the platform used as a reference), and an angular variable, θ , describing the orientation of a fixed line on the platform with respect to a globally fixed axis. An algorithm has been developed to control the position and orientation of the vehicle by differentially controlling the rotational speeds of the two driving wheels. This work highlighted that the three posture variables can not be controlled concurrently unless the tracking point lies on the line connecting the two driving wheels. This is a practical constraint associated with differentially-steered WMRs. WMRs with conventionally steered wheels have been shown to be free from this constraint so that the tracking point can be placed anywhere on the platform [9].

Alexander and Maddocks [9] developed a forward and inverse kinematics model of a WMR that has an arbitrary number of axles with conventionally steered wheels. It was assumed that for sufficiently small manoeuvring speeds where the available friction force was not saturated, kinematic control with pure rolling motion of the wheels was possible. This assumption is in fact contradictory to a well established principle in the tyre modelling literature where it is stated that the lateral friction force that can be developed by a pure rolling wheel is zero [17]. This lateral force is however essential for balancing centrifugal forces developed when the vehicle travels along a curved trajectory. Hence the kinematic steering condition can be satisfied only when the vehicle's heading speed is zero (or when the vehicle is weightless), which do not have any relevance in practice. For the WMR travelling at a speed greater than zero there will be unbalanced lateral forces, which in turn can cause the robot to drift from the intended trajectory. This work did not provide a good basis for investigating the control of WMRs of a significant weight and speed while travelling on curved trajectories.

The major advantage of the kinematic modelling approach is that it allows simple control algorithms to be devised that are computationally fast. Based on these

simplified kinematic models several feedback control algorithms have been proposed and implemented both for the mechanically simple, wheelchair-like WMRs [8,47-48] and WMRs with conventional, omni-directional, and spherical wheels [8,10-11]. Yun and Sarkar [93] considered a dynamic feedback control of a conventionally steered WMR having a steerable wheel on both the front and rear axles based on a kinematics model. The authors demonstrated that static feedback control based on inverse kinematics is not possible for conventionally steered WMRs due to the singularity of the decoupling matrix of the system. To overcome this problem a dynamic non-linear feedback control has been introduced. The work further enabled the control of the orientation of the WMR independently from the position of the WMR. This way the WMR's heading direction need not be tangent to the path of the WMR. The fact that the model is a kinematic one means, however, that the work is limited to low speed manoeuvres.

Muir and Neuman [2] extended the kinematic modelling formalism used in manipulators for WMR modelling applications. This work, which was the first attempt to formalise kinematic modelling of WMRs, introduced a recursive computation algorithm of the kinematic variables. The modelling approach accommodates special characteristics of WMRs such as multiple closed-link kinematic chains, higher-pair contact points between a wheel and a surface, and unactuated and unsensed wheel degrees of freedom. As in most kinematic modelling approaches the work is based on the assumption of pure rolling of wheels.

Although kinematic models facilitate the devising of feedback control schemes, they are based on a critical assumption that the inertia forces are negligible. This assumption may fail when a WMR travels on a curved trajectory and has a significant weight. The unbalanced lateral forces may cause lateral-sliding motion of the WMR. To regain the robot's localisation information lost due to vehicle lateral slipping some authors have proposed techniques of kinematic modelling with wheel sliding which have been successfully implemented [19-21]. However the proposed techniques are limited to smooth and flat terrain navigation applications.

In summary, kinematic based models do not provide a sufficiently good basis to represent the actual behaviour of WMRs with significant inertia and high working speed, even for flat and smooth surface applications.

2.2.2 Work Based on Two-dimensional Dynamics

The necessity to account for the effect of side inertia forces has motivated several researchers to base control strategies on dynamic models rather than on kinematic ones. Deng and Brady [22] formulated the dynamic equations of motion of a three-wheeled mobile robot by using the Lagrangian approach. The robot had a single steered front wheel and two rear driving wheels. Constraint forces were assigned in lateral and longitudinal directions and pure rolling kinematic constraints were imposed on the wheels. However, for the same reason mentioned in the kinematic modelling pure rolling assumption is invalid for WMRs with large inertia and/or significant speed travelling on a curved trajectory.

Some research works have extended the two-dimensional dynamics of WMRs to incorporate tyre modelling in the formulation of the equations of the WMR's motion. Boyden and Velinsky [23] showed, with analytical and experimental work, that robot control based on pure rolling assumptions, as used in kinematic models are subjected to large unrecoverable drifts from the intended curved trajectory in heavy load applications. In this work a WMR with two rear differentially steered wheels and a conventionally steered front wheel was considered. The dynamics model of the WMR incorporated a tyre model based on an empirical formula. While the findings regarding the importance of tyre modelling in the description of vehicle dynamics has been an important contribution of this work, the approach which was based on a relatively complicated empirical formula for the wheel forces did not make the model suitable for devising control techniques. This is because empirical equations contain non-linear terms that complicate the differential equations governing the motion of the WMR.

Hemami and Mehrabi [24] presented a dynamic model of a WMR using analytical description for the wheel forces. The WMR under investigation consisted of two driven rear wheels and two passive front-caster wheels. Although the work provided a more realistic dynamic model for WMRs with convenient analytical relationships for the wheel forces the investigation was limited to differentially driven WMRs navigating on flat surfaces.

A theoretical and experimental comparison between kinematics and dynamics based path-tracking controllers for a WMR with a front wheel conventional steering executing tight cornering manoeuvres was presented in [49]. One more aspect of the weakness of kinematic based controlled in tight manoeuvring condition has been pointed out in this work. Because of their intrinsic structures kinematic models do not admit dynamic constraints such as saturation of the drive torque. One way of ensuring that the saturation torque is not reached during a kinematic based controlled manoeuvre is by tuning the controller with respect to the path to be tracked. In contrast it was shown that dynamic based controllers do not need to be tuned for various paths in order to satisfy maximum torque requirements because this constraint can be embedded in the dynamics model. An evaluation of the performance of the two controllers was performed in a case study by driving a WMR around a 90° corner. The kinematics based controller failed to track the path, stalling the WMR after attempting a rather high steering angle. In contrast the dynamics based controller managed to negotiate the path despite being computationally more intensive.

Rajagopalan et al [25] adopted Kane's dynamic modelling approach [26], for use in WMR dynamic modelling. The Kane's dynamic modelling approach also known as the Lagrange's form of d'Alembert's principle (or the principle of virtual power) is a relatively new and powerful formalism used to derive equations of motion of complex systems. The work by Rajagopalan et al [25] resulted in a substantial shift from the traditional Newton-Euler and Lagrangian approaches often used for modelling WMR dynamics. The authors showed that the use of Kane's modelling approach provides advantages over the traditional Newton-Euler and Lagrangian techniques by focusing on the degrees of freedom of the motion rather than on the

configuration of the WMR. The equations of motion were also found to be simpler and more suitable for devising feedback control. The work however was limited to flat surface manoeuvre where it is easy to formulate the motion constraints.

Mazur [50] devised an adaptive control strategy for WMRs. The proposed control algorithm requires the knowledge of the robot's dynamics to devise a control law that stabilises the WMR along a desired trajectory. The control action has however been shown to result in an overshoot immediately after application, making it unsuitable for sudden manoeuvres near obstacles.

Cheng et al [51] proposed a control strategy for a front and rear wheel steered WMR based on a Newton-Euler dynamics model. A control law that relates the command steering angles to the offset error of the centre of mass of the WMR and its orientation error relative to the desired position and orientation was devised. The superior path-tracking performance of multiple-steered WMRs was shown by comparing them with car-like robots. However the work has been evaluated only for straight line motion.

An often overlooked issue in the two-dimensional kinematics and dynamics modelling of WMRs is the wheel-slip associated with the generation of the traction forces. Shekhar [52] presented a work demonstrating that dead-reckoning based on pure wheel rolling with no slip condition is not a reliable method of ascertaining the position and orientation of WMRs for a long distance. By employing the theory of elastic bodies in contact, an analytical model of the traction forces generated by the rolling of wheels was introduced. Nonlinear control theory on the accessibility and controllability were used to prove that lateral and longitudinal constraints imposed by the wheels can not in general be preserved by a WMRs. It was pointed out that the tracking point of the WMR has zero accessibility and controllability as long as the angular orientation and of the plane of the wheel has zero velocity. The work concluded that wheel slip was inevitable for the traditional WMR wheel types of fixed, off-centred and omni-directional wheels.

Two-dimensional vehicle handling dynamics, with particular emphasis on road vehicles, has been an issue for several works [27-29]. But the working conditions as

well as the construction aspect of road vehicles differ significantly to those of wheeled mobile robots. Road vehicle handling dynamics is often based on the assumption that the vehicle is insensitive to small road irregularities (which are normally taken up by the suspension system including pneumatic wheels), and the vehicle is manoeuvring at high speed with low payload. WMRs do not usually have a well-defined suspension system and are sensitive to small unevenness. Also the working speed of WMRs is likely to be relatively low and common indoor applications may involve heavy payload handling.

In summary, research work based on two-dimensional dynamics has extended kinematic modelling techniques so that inertia forces of a robot travelling along a curved trajectory could be taken into account. Furthermore, in several works consideration was given to tyre-ground surface interaction by means of various tyre-modelling techniques. However, as in the case of the kinematic based research work, the working surface of the robots has been assumed to be flat and smooth, a scenario that can be satisfied in limited applications only.

2.2.3 Work Based on Uneven Terrain Dynamics

The work discussed so far is based on smooth and flat surface manoeuvres. The effect of road surface unevenness on the handling and payload stability of a WMR has not been considered. Recently however there is a growing interest in dealing with the surface unevenness of the navigation environment. Most of the work in this regard has been carried out by authors researching on path-planning where the aim is to find a feasible path joining a departure and a destination point on an uneven working surface.

Ben Amar [30] introduced a method to find the feasible path of a 4-wheeled planetary vehicle moving on an uneven terrain. The geometric compatibility of the vehicle platform and the terrain had been enhanced by a special design of the front axle, which was connected by a revolute joint to the platform. By ignoring the inertia forces, the overall dynamics of the WMR had been simplified to the case of a system in

statics. The shortest path between the goal points that guarantees vehicle static stability was then selected as the feasible path. The model used is rather simplistic as the dynamics of the WMR is completely ignored.

Shiller and Gwo [13] considered the dynamics of a standard, four-wheeled, fixed rear axle and front wheel steered mobile platform moving on a rough surface. A concept of 'an average steering angle' of the front axle was introduced, which reduces the four-wheel kinematics problem to a three-wheeled vehicle kinematics. When considering the vehicle dynamics, the WMR was further reduced to a point mass and the rotational motion and inertia are ignored. Based on a set of criteria, covering the satisfaction of motor-torque constraint, wheel-sliding constraint, geometric constraint of wheel to ground-surface contact and tip-over constraint, a feasible path for the robot between two positions is selected. However, the model neglects the rotational dynamics of the WMR. The stability constraint was based on the assumption of static equilibrium of the platform, which may not be valid for vehicles with large inertia either due to their large mass or because of the large accelerations or both.

Siméon and Wright [31] addressed the problem of geometric placement of wheeled vehicles on a rough terrain, whose geometrical description is known *a priori*. The WMR was fitted with a suspension system to ensure compliance of the platform to guarantee continuous wheel-terrain contact. One of the criteria used for selecting the feasible path was the length by which the suspension springs would extend if the vehicle follows a certain path to reach a specified target point. Another criteria was static stability (tip-over avoidance) which was determined by whether a particular path guarantees a configuration such that the line of action of the gravitational force passed inside the polygon described by the contact points of the wheels. No consideration was given to other constraints such as the availability of friction force that drives the vehicle along a specified path. Furthermore, the analysis that was based on satisfying static stability was not valid when the vehicle is accelerating, either due to a change of speed or a change of heading direction or both.

Dynamic constraints were considered along with kinematic and geometric constraints in the path planning technique for off-road vehicles proposed by Cherif and

Laugier [32]. This new approach considers the vehicle as a body made up of discrete bodies interconnected by spring-damper connectors. Safe and executable paths are then generated for the WMR that satisfy the geometric, kinematic and dynamic constraints. The work however neglected the dynamic interaction between the wheels and the terrain.

Necsulescu et al [33] proposed a tip-over, wheel-torque-saturation and wheel slippage avoidance control schemes for a WMR. The vehicle was assumed to travel on a flat horizontal or inclined plane and the analysis was limited to these particular cases. Despite the fact that this work addressed some of the issues related to the vehicle's dynamic stability, the work considered only two-dimensional, inclined flat surface, motion.

Borenstein et al [34] proposed the integration of wheel encoders and gyroscopes to minimise the vehicle orientation errors, encountered while traversing road obstacles. Orientation information obtained from gyroscopes was suggested to supplement odometric data, which was affected adversely when the wheels drive over humps, dents and other surface irregularities. The work, which was purely experimental, did not establish a mathematical model that depicts the physics of interaction between the WMR and the obstacles and it has been concerned with only a straight-line manoeuvre.

In this category of work most of the contribution came from researchers on path planning which are motivated by the determination of safe and time-optimal paths a mobile platform may traverse to travel between two given positions. The mathematical analysis is based on very simplified assumptions, where in most of the cases the dynamics problem has been simplified to a statics problem. Vehicle inertia has been ignored and little consideration has been given to wheel-road interaction. Moreover, the analyses are based on various types of chassis designs of the vehicles, which make it difficult to draw a generalised conclusion about the behaviour of mobile platforms on uneven terrain.

The approach in the present work proposes the use of a complete dynamic model of the WMR and the utilisation of the jerk to measure the smoothness of

manoeuvre in uneven ground surface. The undesirable effects of jerk, which increases position errors and which induces manipulator vibration, are well understood in the stationary robotics literature. Piazzì and Visoli [11] proposed an algorithm that enables minimum jerk manipulation of robotic arms where an optimisation method is introduced for obtaining cubic spline joint trajectories with continuity of velocities and accelerations. It will be shown that a similar jerk minimisation strategy can be utilised for WMRs that need to traverse an obstacle having a known geometry.

2.3 Impact Modelling and Control in Manipulators

The wheels of a WMR often collide with stationary ground surface irregularities where there is a discontinuity in the ground surface profile. Such collisions may be followed by a repetitive rebound of the wheels. This is an undesired situation as it makes the WMR less controllable. This is because WMR control forces (traction and steering) require the existence of the contact between the wheels and the ground surface. Therefore there is a need to control impact so that WMR wheels grip characteristics can be enhanced. No previous work, to the best of the knowledge of the author, has dealt with this problem in the context of mobile robots. However there have been several works that discussed the subject of impact control in stationary manipulators.

Fixed robots or manipulators interact with the environment in several applications such as assembling, pushing, scrapping, grinding, polishing, drilling and pounding (Figure 2.7). The robotic manipulator literature classifies the modes of operation of robot arms into three general categories namely; free space motion, impact and constrained motion. Free-space motion control, also known as position control, has been extensively investigated and various control strategies such as PID, computed torque control and adaptive control, have been implemented successfully [35]. Similarly for constrained motion control techniques based on force feedback have been implemented. Schutter et al [36] summarise these techniques as pure force

control (also known as compliance control), pure impedance control, parallel force/position control and hybrid impedance control.

While a transition from a constrained motion to unconstrained motion presents little difficulties, the reverse process is rather complex because it involves the little understood physical phenomena *impact*. Early research work on robotic manipulator control considers this phenomenon as negligible transient, leaving impact dynamics out of the model and control during the transient dynamics. Recently, however, as manipulator designs got lighter and more flexible a motivation has arisen to include the effects of impact in the model and control because of its potential to induce excessive vibrations which in turn affect the performance of the robot. Uncontrolled impacts are

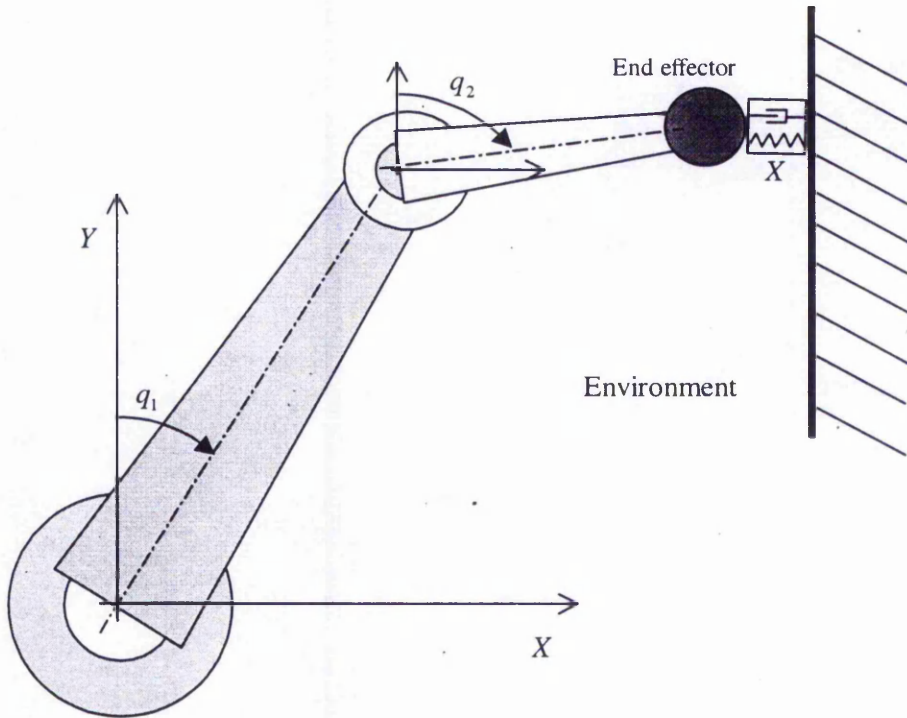


Figure 2.7 A stationary manipulator interacting with the environment

often followed by rebound, and hence multiple collisions. This is detrimental to the performance of the controller that will be subjected to repetitive discontinuities. The robot's structure may also be subjected to a series of impulsive loads that worsen the vibration initiated at the initial impact.

From the control point of view it is customary to use position control in free space motion and force control for constrained motion. A theoretical method that treats constrained and unconstrained motion in a single control strategy has been proposed in [37]. The proposed strategy replaces the force discontinuity in the manipulator by a velocity discontinuity of the constraint surface necessitating a need for an accurate geometrical description of the constraint surface well in advance of encountering it.

The two most common ways of controlling impact/contact in stationary manipulators are impedance control and force control. The equations of motion of a dynamic system such as a manipulator is usually given in the joint coordinates \vec{q} as:

$$D(\vec{q})\ddot{\vec{q}} + E(\vec{q}, \dot{\vec{q}}) = \vec{\tau} + J_x^T \vec{F} \quad (2.1)$$

where $D(\vec{q})$ is the inertia tensor in the joint coordinates \vec{q} , $E(\vec{q}, \dot{\vec{q}})$ is the sum of velocity and configuration dependent forces, $\vec{\tau}$ is the actuator torque, J is the Jacobian of the system and \vec{F} is the contact force, i.e. the reaction force from the environment on the manipulator. The end-effector position (also referred to as task space displacement), \vec{X} , is a function of the generalised coordinates, \vec{q} , related by a kinematic constraint relationship and its velocity $\dot{\vec{X}}$ is related to the joint coordinate velocity $\dot{\vec{q}}$. The aim of impedance control is to establish desired mechanical impedance that specifies a dynamical relationship between end-effector position \vec{X} , a specified reference end-effector position \vec{X}_r and the contact force \vec{F} [38]. This system enables to regulate the contact force indirectly through the regulation of the mechanical impedance that relates the contact force and the end-effector position.

Another technique for controlling contact force between a robot and its environment is what is known as explicit force control. This technique is similar to impedance control; the only difference being while in impedance control the tracked variable is displacement of the end effector in explicit force control the contact force is employed as the tracking variable. The advantage of this system over impedance control is that it is easier to measure force than position during contact dynamics. This

is because accurate measurement of small structural deformations is quite difficult to carry out, while at the same time the penalty due to a small error in deformation measurement causes large error in contact force values because of the usually high contact stiffness between the environment and the end-effector.

A contact force tracking system that combines the advantages of both impedance and explicit force control techniques for manipulators was proposed by Seraji and Colbaugh [38]. It was shown that impedance control could be used both for constrained and unconstrained motion by setting a zero tracking force in the case of an unconstrained motion. However impedance control may result in contact force overshoot as force is not a directly controlled variable. After introducing a relationship that replaced the end-effector position by the contact force as the tracking variable, the authors proposed an adaptive control scheme that tracks the contact force in an environment whose contact stiffness is not known *a priori*. The proposed control scheme did not consider the transition phase between constrained and unconstrained motion that generally involves impact.

Marth et al [53] proposed an event based control approach to handle impact between a manipulator and a contact environment. The proposed technique intends to achieve a transition between constrained and unconstrained motion by dividing the task into three events; i.e. free space motion control, contact detection and constrained motion control. The authors devised a simple algorithm for achieving the above objective that can be stated as:

- i. approach the constraining surface with a planned velocity using free space control
- ii. on detection of contact switch over to constrained motion control
- iii. if bouncing occurs switch over to free space motion control to bring the manipulator back to contact.

The technique however needs very fast sensors to detect contact especially if the approach velocity is high.

Allotta and Buttazzo [54] proposed a proximity based control approach to handle the transition between constrained and unconstrained motion of a robot. The

proposed system sought to achieve a smooth transition by employing a control signal which is a weighted mixture of free space motion control signal and constrained motion control signal. The weighting parameter in turn was chosen as a smooth function of the distance between the manipulator and the constraining surface which is measured by ultrasound or infrared sensors.

In summary the impact/contact problem has been addressed in the robotic manipulator literature. While impedance and force control have been used to control a 'collision-free' transition between constrained and unconstrained motion the consideration of impact calls for additional strategies such as an event based strategy or the proximity based control scheme discussed above. However, there are no similar literature works for the mobile robot discipline.

Chapter 3

Wheel Modelling

3.1 Introduction

The wheel is probably the most essential element in the study of the dynamics of a WMR. The wheel forces play a major role by being a link between the vehicle and the ground surface. An accurate representation of these forces is thus essential in order to have a realistic model of the WMR dynamics.

The wheels of WMRs are most commonly made of solid rubber in contrast to road vehicles where pneumatic wheels are usually used. For most wheel kinematic and dynamic analysis, however, the modelling techniques used for pneumatic wheels are valid for solid rubber wheels.

The wheels, apart from supporting the normal force mainly due to the weight of the WMR, generate traction/braking forces as well as cornering forces during a manoeuvre around a curved path. The actual mechanism for the generation of wheel forces is still a little-understood phenomenon [39]. The widely accepted theory is the tyre mechanics based on the shear force analysis of the wheel-ground surface patch [40] which is discussed below.

3.2 Wheel Modelling

A detailed wheel kinematic and dynamic representation often used for passenger car dynamic analysis is given in Figure 3.1. The wheel camber angle defined in the figure is often ignored either for simplifying the analysis or because it is equal to zero as in the case of most WMR designs. For the sake of simplicity the wheel rolling resistance and the aligning torque are also ignored in the following discussion of wheel forces.

Techniques of varying degree of complexity for determining the wheel forces have been proposed in the literature. The Magic formula [41-42] is an empirical relationship that is employed to compute the longitudinal and cornering forces by means of curve fitting of experimental data. A more simplified tyre force model is the

one devised by Dugoff [40]. In this model the friction forces are characterised by two regimes:

- Stick regime: in this case it is assumed that the patch of the wheel in contact with the ground surface does not slide relative to the surface. The wheel traction and cornering forces are proportional to the elastic stiffness of the wheel in the respective directions. This is the situation of the wheel in most manoeuvring conditions.
- Slide: in this situation the wheel slides relative to the ground surface and the wheel interface forces are functions of the friction property of the ground surface.

The wheel forces also depend on two other kinematic parameters, the wheel-slip ratio λ and the slip angle α . These two parameters are described below.

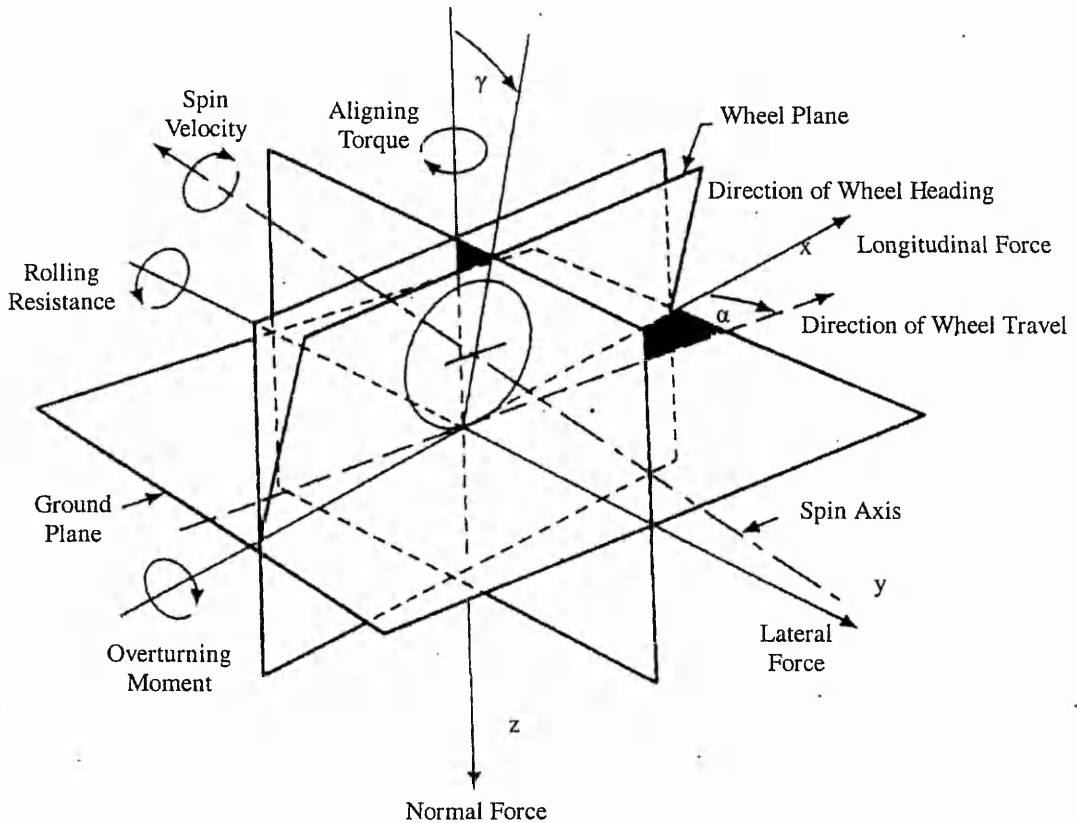


Figure 3.1 The tyre coordinate system, and definition of kinematic and force variables [94].

For an accelerating vehicle the wheel-slip ratio, λ , is defined as:

$$\lambda = \frac{(R\omega - V)}{R\omega} \quad (3.1)$$

During braking the wheel-slip ratio is defined as:

$$\lambda = \frac{(R\omega - V)}{V} \quad (3.2)$$

R is the effective wheel radius, V is the velocity of the vehicle and ω is the rotational velocity (spin) of the wheel. The wheel-slip ratio is an important parameter that determines the magnitude of the traction force generated at the wheel-ground interface. In tyre mechanics it is generally accepted that there exists a finite wheel-slip, although small in magnitude, in the wheel-ground sticking regime as well.

The slip angle α is the angle between the direction in which the wheel is heading to (the direction of the velocity of the centre of the wheel) and the plane of the wheel. Even though this parameter is named a slip-angle in actuality the wheel may not be sliding on the road at the contact zone. A non-zero slip angle indicates that the wheel is not doing a pure rolling motion, instead it is moving sideways as well as it is rolling. This parameter greatly influences the magnitude of the lateral force and is an essential mechanism through which cornering forces are generated.

The dependence of wheel traction and lateral forces on wheel-slip ratio and slip-angle has been summarised in Figure 3.2. In this figure the variables, the traction and lateral force coefficients are defined as:

$$\mu_l = \frac{F_l}{F_n}$$

$$\mu_a = \frac{F_a}{F_n}$$

where μ_l is the lateral friction coefficient, μ_a is the longitudinal friction coefficient, F_l is the lateral wheel force, F_a is the longitudinal wheel force, and F_n is the normal wheel reaction force. As can be noted in Figure 3.2, as the steering angle increases the cornering force coefficient increases and the coefficient of the traction force decreases. Although the above discussion has concentrated on traction (acceleration) an

analogous dependency exists when the wheel is subject to a braking action, the only difference being the definition of the wheel-slip ratio (Equations 3.1-3.2).

3.3 Wheel-Slip Control

At several stages of this work reference will be given to the traction/braking control technique. Rigorous treatment of the subject has been given elsewhere in the literature [43-46] and in this section highlight of the state-of-the-art of traction control technique will be given.

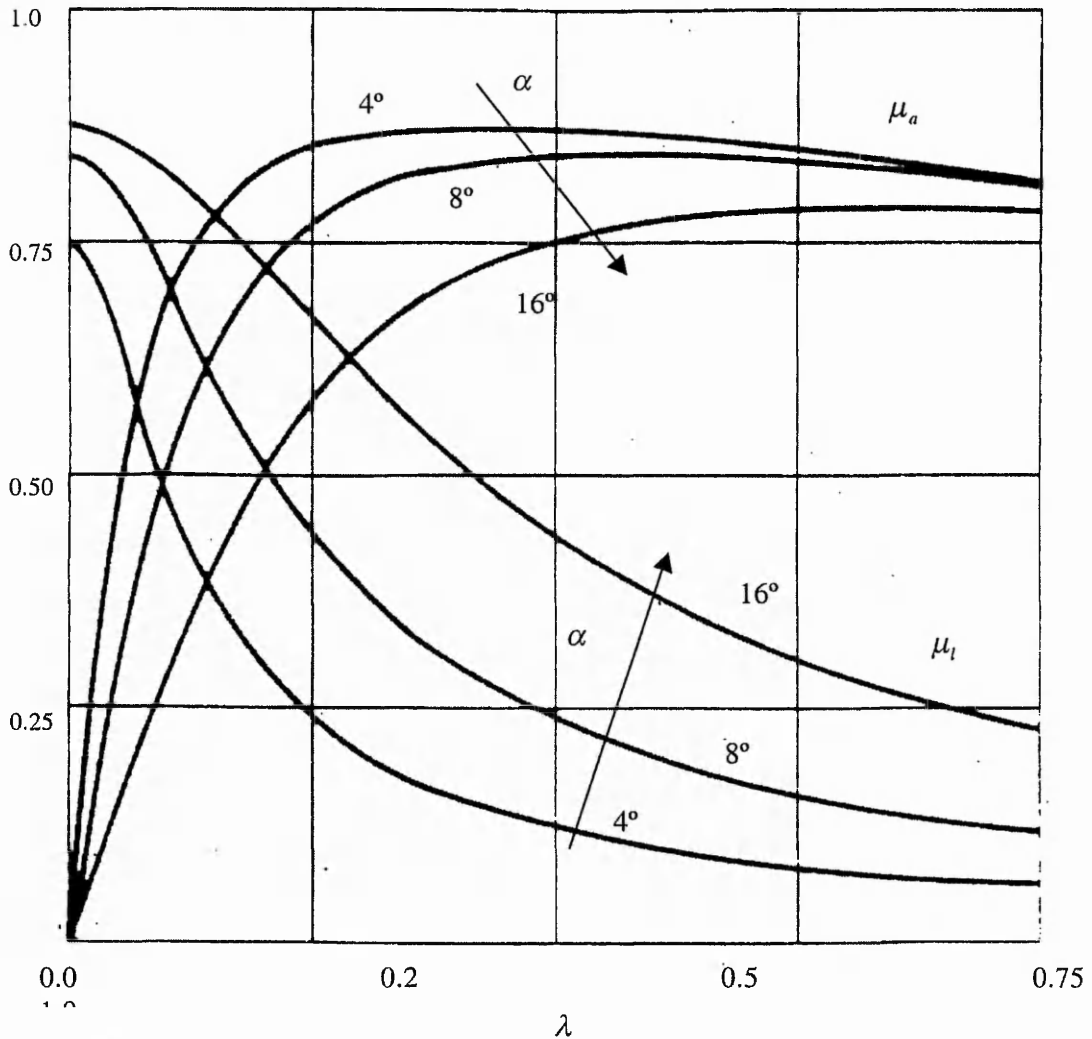


Figure 3.2 The variations of the lateral (μ_l) and traction (μ_a) friction coefficients with wheel slip λ and slip-angle α [94].

Traction control system (TCS) is becoming a standard technology in the automotive industry to provide anti-spin acceleration for road vehicles [44]. This technique has contributed to road safety in conjunction with the slightly older technology of anti-lock braking system (ABS). WMRs are more suited to the applications of these techniques in that they are driven by electric motors that can generate wheel-torque more precisely and more quickly in comparison to internal combustion engines.

From control and modelling point of view the regulation of the traction force requires the regulation of the wheel-slip-ratio, λ , which characterises the coefficient of friction of the traction surface. For the purpose of simplicity in the discussion that follows it is assumed that the wheel has a zero slip angle. Further it is also assumed that the vehicle has only one wheel (Figure 3.3). This is a purely theoretical assumption, which can not be achieved in practice without some sort of a balancing

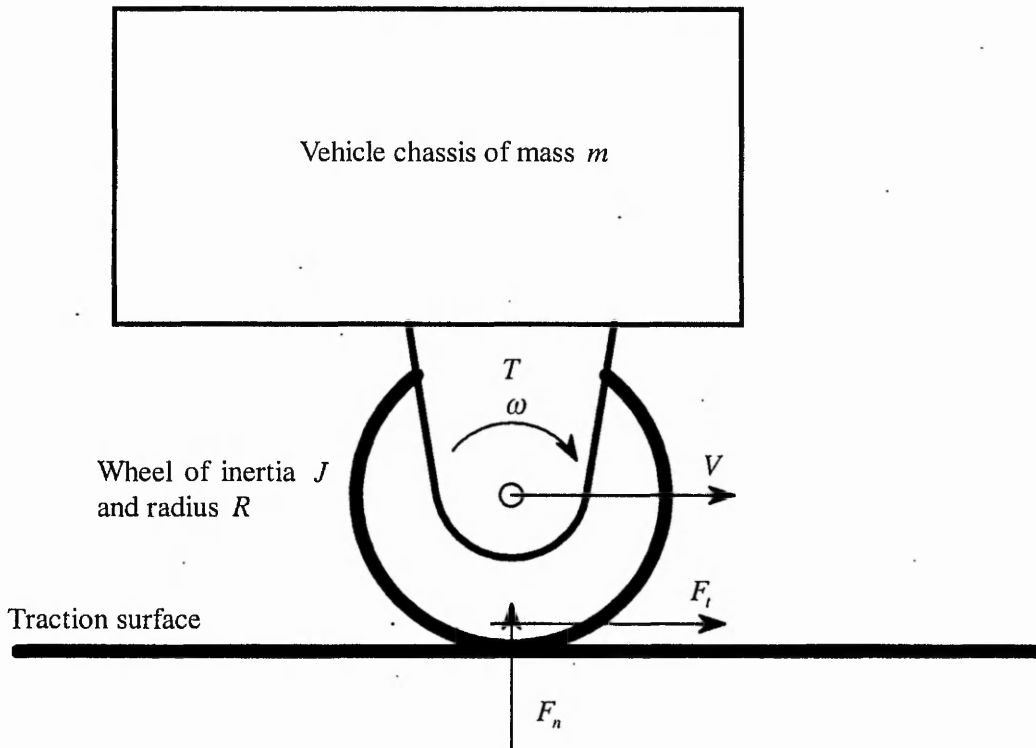


Figure 3.3 Diagram for the derivation of the relationship between wheel-slip ratio and driving torque.

mechanism, which keeps the vehicle in the upright position. However the above assumption simplifies the analysis by eliminating the consideration of the redistribution of normal force among multiple wheels due to inertia loading and helps us to focus on the dynamic relationship between wheel-slip ratio and wheel drive torque which is the main objective here.

The traction force is related to the wheel's longitudinal coefficient of friction (which is a function of the wheel-slip ratio for a given surface type and condition) as:

$$F_t = \mu_a(\lambda) F_n \quad (3.3)$$

where F_t is the traction force and F_n is the normal (reaction) force that acts between the wheel and the traction surface. The transfer function between the wheel slip ratio and the drive-motor torque for the ideal single-wheel vehicle is derived as follows.

The longitudinal acceleration, \dot{V} , and the traction force, F_t , are related by:

$$F_t = m\dot{V} \quad (3.4)$$

where m is the mass of the vehicle. The rate of change of the wheel's rotational velocity, $\dot{\omega}$, is related to the motor torque, T , and the traction force by:

$$T - F_t R = J_w \dot{\omega} \quad (3.5)$$

where J_w is the wheel's mass moment of inertia about a rotational axis through its centre and R is the wheel's radius.

From Equation (3.1) the following perturbation system can be derived [46]:

$$\Delta\lambda = \frac{\partial\lambda}{\partial V} \Delta V + \frac{\partial\lambda}{\partial\omega} \Delta\omega \quad (3.6)$$

Substituting Equation (3.1) for λ in the right hand side of Equation (3.6):

$$\Delta\lambda = -\frac{1}{R\omega} \Delta V + \frac{V}{R\omega^2} \Delta\omega \quad (3.7)$$

At the operation point where $V = V_o$ and $\omega = \omega_o$ Equation (3.7) becomes:

$$\Delta\lambda = -\frac{1}{R\omega_o} \Delta V + \frac{V_o}{R\omega_o^2} \Delta\omega \quad (3.8)$$

After performing Laplace transformations on Equations (3.4) and (3.5) we have:

$$V = \frac{F_t}{sm} \quad (3.9)$$

and

$$\omega = \frac{T - F_t R}{s J_w} \quad (3.10)$$

The perturbations of Equations (3.9) and (3.10) are respectively given by:

$$\Delta V = \frac{\Delta F_t}{sm} \quad (3.11)$$

$$\Delta \omega = \frac{\Delta T - \Delta F_t R}{s J_w} \quad (3.12)$$

Defining k as the gradient of the $\mu - \lambda$ curve we have:

$$\Delta \mu_a = k \Delta \lambda$$

Therefore from Equation (3.3) we have:

$$\Delta F_t = F_n \Delta \mu = F_n k \Delta \lambda \quad (3.13)$$

Substituting Equation (3.11) for ΔV , Equation (3.12) for $\Delta \omega$ into Equation (3.88) we have:

$$\Delta \lambda = -\frac{1}{R \omega_o} \frac{\Delta F_t}{sm} + \frac{V_o}{R \omega_o^2} \frac{\Delta T - \Delta F_t R}{s J_w} \quad (3.14)$$

Substituting for ΔF_t from Equation (3.13) into Equation (3.14):

$$\Delta \lambda = -\frac{1}{R \omega_o} \frac{F_n k \Delta \lambda}{sm} + \frac{V_o}{R \omega_o^2} \frac{\Delta T - F_n k \Delta \lambda R}{s J_w}$$

solving for $\Delta \lambda$ and rearranging we have:

$$\Delta \lambda = \frac{V_o}{(R \omega_o^2 J_w) s + (V_o R - \omega_o \frac{J_w}{m}) F_n k} \Delta T \quad (3.15)$$

That is,

$$\Delta \lambda = H \Delta T$$

where

$$H = \frac{V_o}{(R\omega_o^2 J_w)s + (V_0 R - \omega_o \frac{J_w}{m})F_n k} \quad (3.16)$$

H is the transfer function between the wheel-slip ratio and the drive torque.

3.4 Summary Comments

Wheel modelling is a fairly well treated subject mainly in the context of road vehicles where it is usually referred to as tyre modelling. Most of the concepts used in wheel modelling in the automotive literature are also valid for WMR analysis purposes. Wheel slip control is an important contribution of the work on wheel modelling and will be employed in the present work to generate traction forces needed to counteract undesired effects of uneven terrain WMR dynamics.

Rigid Body Dynamics Modelling of WMRs

4.1 Introduction

Existing research work on wheeled mobile robots (WMRs) are based on the assumption that the working surface is smooth and flat. This consideration is inadequate to describe the dynamics of a mobile robot when its wheels encounter inevitable ground obstacles such as humps, ground cables and cracks. These obstacles may either be irregularities in a generally smooth and flat ground surface, as in the case of most indoor applications, or the characteristic features of a generally uneven terrain to be navigated, as in the case of most outdoor applications.

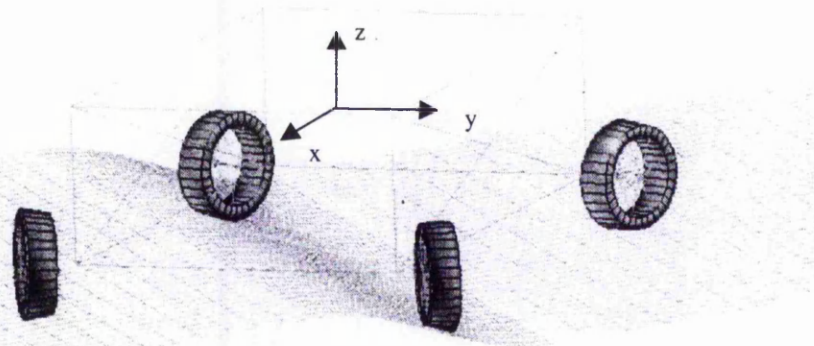


Figure 4.1 Definition of WMR coordinate axes.

The interaction between wheels and obstacles may give rise to a WMR motion in the 3-dimensional Cartesian space, namely: translational motions along the x , y , z , axes and rotational motions referred to as pitching, rolling and yawing. This is as opposed to the planar motion observed when the surface is flat, which consists of translational motions along the x and y axes and a yawing rotational motion. The addition of new degrees of freedom to the robot's motions due to the

obstacles brings with it more challenges. The problem of localising the robot, i.e. determining its absolute location with respect to the environment, becomes more complex. The controllability of the platform may be compromised as a result of any potential wheel-ground contact loss during uneven terrain navigation. The maintenance of contact between the wheels and the ground is essential in order to generate control forces in the form of traction and steering. If wheel ground contact is lost, subsequent reestablishment of contact will generally be accompanied by undesirable impact between the wheel and the ground. This in turn may give rise to impulsive forces causing excessive vibrations on the robot's chassis and recurrent contact losses. The effects of vibration caused by wheel-contact loss could compromise accuracy and safety of guidance and control hardware aboard the WMR. These may include visual sensors, wheel rotation encoders, accelerometers, rate gyros and computing hardware.

To minimise the undesired effects noted above it is essential to maintain continuous wheel-ground contact at best, or at least to reduce the frequency of the occurrence of contact loss. When the WMR is stationary the problem of achieving all-wheels-to-ground contact is purely geometrical and has been addressed by authors researching in the field of path planning who dealt with static vehicle placement problem [23,31,55-57]. Geometric path planning presumes that the WMR has the ability to track a path planned by ignoring the vehicle dynamics. The shortcomings of geometric based strategies of WMRs are well documented for smooth floor applications [57]. The major limitation of such techniques is that unmodelled inertia forces can cause significant drift of the WMR from its intended trajectory.

In this chapter derivation of the mathematical model of the dynamics of a WMR navigating an uneven terrain is carried out. The jerk response of the rigid body motion will be considered analytically and used as a measure of the undesirable effects of uneven ground surface motion dynamics, such as payload stability and WMR controllability. An investigation will be carried out to obtain ways of minimising the jerk response of a WMR traversing ramp obstacles. In this regard a control scheme that relates the traction force, the dimensions and working speed of the WMR as well as the geometry of the road profile will be proposed to minimise the normal jerk of the WMR while traversing a laterally symmetric obstacle.

4.2 Mathematical Modelling

In this first part of the mathematical analysis, the WMR is assumed to constitute a single rigid body. The WMR is actually composed of several wheels and a platform (including payload). However, the mass and inertia of the wheels are considered to be very small relative to those of the platform and payload. Thus the robotic vehicle can be modelled as a single body with mass and inertia of that of the platform and payload. Analysis that accommodates the flexibility of the WMR's chassis and its wheels will be considered in Chapters 6 to 8.

In robotics, rigid-body dynamic equations are derived by using either the Lagrangian or the Newton-Euler formalisms. Each technique has a merit of its own based on the type of problem being considered. Lagrange's approach is well suited to problems where explicit kinematic constraints are readily available. Such kinematic constraints which relate the various coordinates used to describe the position and orientation of a WMR travelling over an arbitrary rough ground surface are very difficult to formulate. The Newton-Euler method of deriving equations of motion, which does not rely on the kinematic constraints, is preferred to formulate the equations of motion of a WMR navigating an uneven ground surface.

For convenience, a reference coordinate system attached to the WMR's centre of mass has been defined as shown in Figure 4.1. The equations of motion, Equations 4.1-4.2, are expressed with respect to this coordinate system which translates as well as rotates with the robotic vehicle.

The sum of forces in the longitudinal (x), lateral (y), and normal (z) directions is given by:

$$\sum \bar{F} = M \bar{a}_c \quad (4.1)$$

The sum of moments about the x , y , and z axes is given by:

$$\sum \bar{T} = I \bar{\alpha} \quad (4.2)$$

where \bar{a}_c is the acceleration of the centre of mass of the WMR, $\bar{\alpha}$ is the angular acceleration of the WMR, M is the mass of the vehicle and I is its moment of inertia tensor about the centeroidal coordinate system. The free body diagram of a wheel travelling over an uneven surface is shown in Figure 4.2. Provided that the

wheel is in contact with the road surface, it will be subjected to the applied traction force and the reaction forces from the ground and the WMR's chassis. However for the sake of clarity only wheel-ground interaction forces are shown in Figure 4.2.

$$\vec{F}_{Rk} = \vec{A}_k F_{ak} + \vec{N}_k F_{nk} \quad (4.3)$$

where F_{ak} is the traction force in the plane of the wheel and F_{nk} is the normal ground reaction force in the same plane. \vec{A}_k and \vec{N}_k are vectors which map the traction, frictional and the reaction forces into the Cartesian x - y - z coordinate system defined in Figure 4.1.

In addition to the traction and normal reaction forces, there are wheel rolling resistance forces and lateral forces acting on the wheel. The magnitude of these forces is a function of the normal reaction force, the friction properties of the ground surface, as well as that of the wheel, and are given in tyre-mechanics literature [58] as:

$$F_{rk} = \mu_{rk} F_{nk} \quad F_{lk} = \mu_{lk} F_{nk} \quad (4.4)$$

where μ_{rk} is the coefficient of rolling resistance friction, μ_{lk} is the coefficient of lateral friction. Thus the mapping vectors of the wheel forces \vec{A}_k and \vec{N}_k are given by:

$$\begin{aligned} \vec{A}_k &= \begin{bmatrix} \cos(\gamma_k) \cos(\delta_k) \\ \cos(\gamma_k) \sin(\delta_k) \\ \sin(\gamma_k) \end{bmatrix}, \\ \vec{N}_k &= \begin{bmatrix} -\mu_{rk} \cos(\gamma_k) \cos(\delta_k) + \mu_{lk} \sin(\delta_k) - \sin(\gamma_k) \cos(\delta_k) \\ -\mu_{rk} \cos(\gamma_k) \sin(\delta_k) - \mu_{lk} \cos(\delta_k) - \sin(\gamma_k) \sin(\delta_k) \\ -\mu_{rk} \sin(\gamma_k) + \cos(\gamma_k) \end{bmatrix} \end{aligned} \quad (4.5)$$

where δ_k is the steering angle and γ_k is the profile angle of the obstacle at wheel k .

The resultant force \vec{F} acting on the WMR is composed of all the wheel forces and other external forces including the gravitational force. It can be written as,

$$\vec{F} = A\vec{F}_a + N\vec{F}_n + \vec{C}F_e \quad (4.6)$$

where, $A = [A_1 \ . \ . \ . \ A_w]$, $N = [N_1 \ . \ . \ . \ N_w]$ and \vec{C} is a vector that projects external forces except the wheel forces onto the frame of reference x - y - z , w is the number of wheels of the vehicle currently in contact with the working surface, \vec{F}_a and \vec{F}_n are vectors of length w , and F_e is magnitude of the external force.

The acceleration \vec{a}_c of the centre of mass of the platform is found from Equation (4.1) as:

$$\vec{a}_c = M^{-1} \vec{F} \quad (4.7)$$

Substituting for \vec{F} from Equation (4.6),

$$\vec{a}_c = M^{-1} (A\vec{F}_a + N\vec{F}_n + \vec{C}F_e) \quad (4.8)$$

At a point P where the k^{th} wheel makes contact with the ground (Figure 4.2), the acceleration is given by:

$$\vec{a}_k = \vec{a}_c + \vec{\omega} \times \vec{\omega} \times \vec{r}_k + \vec{\alpha} \times \vec{r}_k \quad (4.9)$$

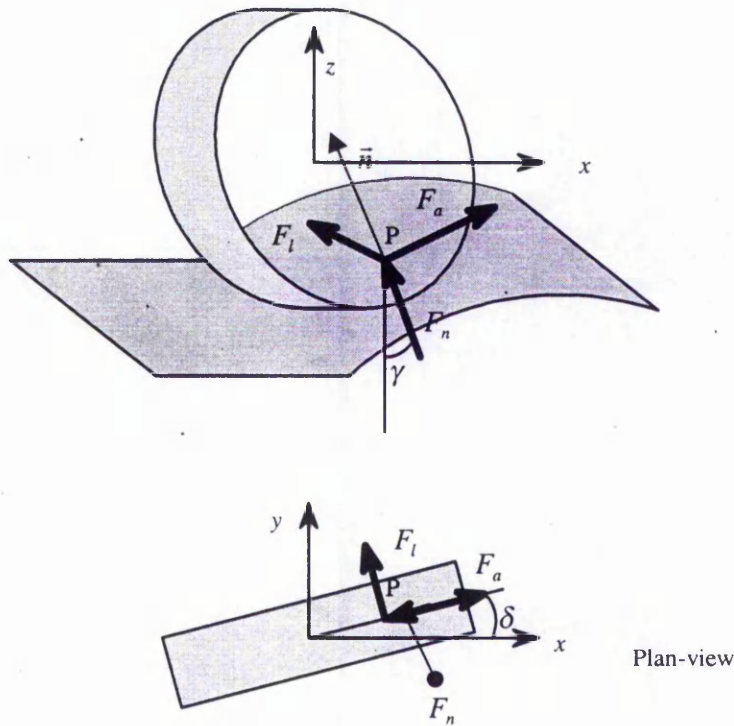


Figure 4.2 The free-body diagram of a steered wheel in contact with uneven ground surface. The x - y - z axes are parallel to the WMR coordinate axes.

where \vec{r}_k is the position vector of the contact point, $\vec{\alpha}$ is the angular acceleration vector of the platform, and $k = 1 \dots w$.

A normal vector, \vec{n}_k , can be introduced to define the shape of the surface at the contact point with wheel k ,

$$\vec{n}_k = \begin{bmatrix} \sin(\gamma_k) \cos(\delta_k) \\ \sin(\gamma_k) \sin(\delta_k) \\ -\cos(\gamma_k) \end{bmatrix} \quad (4.10)$$

The scalar component a_{nk} of the acceleration \vec{a}_k along the normal direction \vec{n}_k can be found by a vector dot product of the two quantities, i.e.,

$$a_{nk} = \vec{a}_k \bullet \vec{n}_k \quad (4.11)$$

Substituting for \vec{a}_k from Equation (4.9) into Equation (4.11),

$$a_{nk} = (\vec{a}_c + \vec{\omega} \times \vec{\omega} \times \vec{r}_k + \vec{\alpha} \times \vec{r}_k) \bullet \vec{n}_k = \vec{a}_c \bullet \vec{n}_k + (\vec{\omega} \times \vec{\omega} \times \vec{r}_k) \bullet \vec{n}_k + (\vec{\alpha} \times \vec{r}_k) \bullet \vec{n}_k \quad (4.12)$$

Substituting for \vec{a}_c from Equation (4.8) the term $\vec{a}_c \bullet \vec{n}_k$ in Equation (4.12) can be written as,

$$\vec{a}_c \bullet \vec{n}_k = (M^{-1}(A\vec{F}_a + N\vec{F}_n + \vec{C}\vec{F}_e)) \bullet \vec{n}_k = H_k \vec{F}_a + Q_k \vec{F}_n + G_k \quad (4.13)$$

where

$$H_k = (M^{-1}A)^T \bullet \vec{n}_k; \quad Q_k = (M^{-1}N)^T \bullet \vec{n}_k; \quad G_k = (M^{-1}\vec{C}\vec{F}_e) \bullet \vec{n}_k \quad (4.14)$$

Defining the normal components of the contact point acceleration vector \vec{a}_N as:

$$\vec{a}_N = \begin{bmatrix} a_{n1} \\ \vdots \\ a_{nw} \end{bmatrix} \quad (4.15)$$

Substituting for a_{nk} from Equation (4.12) Equation (4.15) now becomes:

$$\vec{a}_N = \begin{bmatrix} \vec{a}_c \bullet \vec{n}_1 + (\vec{\omega} \times \vec{\omega} \times \vec{r}_1) \bullet \vec{n}_1 + (\vec{\alpha} \times \vec{r}_1) \bullet \vec{n}_1 \\ \vdots \\ \vec{a}_c \bullet \vec{n}_w + (\vec{\omega} \times \vec{\omega} \times \vec{r}_w) \bullet \vec{n}_w + (\vec{\alpha} \times \vec{r}_w) \bullet \vec{n}_w \end{bmatrix} \quad (4.16)$$

or,

$$\vec{a}_N = \vec{a}_{Nc} + \vec{a}_{N\omega} + \vec{a}_{N\alpha} \quad (4.17)$$

where \vec{a}_{Nc} , $\vec{a}_{N\omega}$ and $\vec{a}_{N\alpha}$ are defined as:

$$\vec{a}_{Nc} = \begin{bmatrix} \vec{a}_c \bullet \vec{n}_1 \\ \vdots \\ \vec{a}_c \bullet \vec{n}_w \end{bmatrix}; \quad \vec{a}_{N\omega} = \begin{bmatrix} (\vec{\omega} \times \vec{\omega} \times \vec{r}_1) \bullet \vec{n}_1 \\ \vdots \\ (\vec{\omega} \times \vec{\omega} \times \vec{r}_w) \bullet \vec{n}_w \end{bmatrix}; \quad \vec{a}_{N\alpha} = \begin{bmatrix} (\vec{\alpha} \times \vec{r}_1) \bullet \vec{n}_1 \\ \vdots \\ (\vec{\alpha} \times \vec{r}_w) \bullet \vec{n}_w \end{bmatrix} \quad (4.18)$$

Thus the normal components of the contact point acceleration vector \vec{a}_N can be found by summing the contributions from the translational acceleration term \vec{a}_{Nc} , the centrifugal acceleration term $\vec{a}_{N\omega}$ and the angular acceleration term $\vec{a}_{N\alpha}$.

4.2.1 Translational Acceleration

Applying Equation (12) to each row of the vector \vec{a}_{Nc} one can write,

$$\vec{a}_{Nc} = \begin{bmatrix} \vec{a}_c \bullet \vec{n}_1 \\ \vdots \\ \vec{a}_c \bullet \vec{n}_w \end{bmatrix} = H\vec{F}_a + Q\vec{F}_n + \vec{G} \quad (4.19)$$

where H and Q are $w \times w$ matrices whose k^{th} rows are H_k and Q_k , respectively. \vec{G} is a vector of length w whose k^{th} element is given by G_k .

4.2.2 Centrifugal Acceleration

$\vec{a}_{N\omega}$ can easily be computed since the instantaneous angular velocity $\vec{\omega}$ of the platform is known.

4.2.3 Angular Acceleration

The vector $\vec{a}_{N\alpha}$ can be calculated as follows.

The angular acceleration $\vec{\alpha}$ is given by:

$$\vec{\alpha} = I^{-1} \vec{T} \quad (4.20)$$

where I is the moment of inertia matrix. \vec{T} is the total moment produced by wheel forces and external forces/moment.

If it is assumed that all external forces except the wheel forces are applied to the platform through the centre of mass (which is the case for the gravitational force), then only the wheel forces contribute to the total moment. Thus,

$$\vec{T} = \sum_1^w \vec{T}_k \quad (4.21)$$

where

$$\vec{T}_k = \vec{r}_k \times \vec{F}_{Rk} \quad (4.22)$$

Substituting Equation (4.3) for \vec{F}_{Rk} in Equation (4.22), one has

$$\vec{T}_k = \vec{r}_k \times (\vec{A}_k F_{ak} + \vec{N}_k F_{nk}) = (\vec{r}_k \times \vec{A}_k) F_{ak} + (\vec{r}_k \times \vec{N}_k) F_{nk} \quad (4.23)$$

The total moment can be written as:

$$\vec{T} = R_a \vec{F}_a + R_n \vec{F}_n \quad (4.24)$$

where R_a and R_n are $w \times w$ matrices whose k^{th} columns are given by:

$$\vec{R}_{ak} = \vec{r}_k \times \vec{A}_k \text{ and } \vec{R}_{nk} = \vec{r}_k \times \vec{N}_k \quad (4.25)$$

Substituting for the moment \vec{T} from Equation (4.24) into Equation (4.20),

$$\vec{\alpha} = I^{-1} (R_a \vec{F}_a + R_n \vec{F}_n) \quad (4.26)$$

Now,

$$(\vec{\alpha} \times \vec{r}_k) \bullet \vec{n}_k = (I^{-1} \vec{T}) \times \vec{r}_k \bullet \vec{n}_k = I^{-1} (R_a \vec{F}_a + R_n \vec{F}_n) \times \vec{r}_k \bullet \vec{n}_k \quad (4.27)$$

or

$$(\vec{\alpha} \times \vec{r}_k) \bullet \vec{n}_k = J_k \vec{F}_a + S_k \vec{F}_n \quad (4.28)$$

where J_k and S_k are row vectors whose j^{th} elements are given by $(I^{-1} \vec{R}_{aj} \times \vec{r}_k) \bullet \vec{n}_k$ and $(I^{-1} \vec{R}_{nj} \times \vec{r}_k) \bullet \vec{n}_k$, respectively.

Hence, the contribution of the angular acceleration, $\vec{a}_{N\alpha}$ is given by:

$$\vec{a}_{N\alpha} = \begin{bmatrix} (\vec{\alpha} \times \vec{r}_1) \bullet \vec{n}_1 \\ \vdots \\ (\vec{\alpha} \times \vec{r}_{nw}) \bullet \vec{n}_{nw} \end{bmatrix} = J \vec{F}_a + S \vec{F}_n \quad (4.29)$$

where J and S are $w \times w$ matrices whose k^{th} columns are given by \vec{J}_k and \vec{S}_k , respectively.

4.2.4 The Normal Components of Acceleration

Substituting Equations (4.19) and (4.29) into Equation (4.17), one can write:

$$\vec{a}_N = (H + J)\vec{F}_a + (Q + S)\vec{F}_n + \vec{G} + \vec{a}_{N\omega}$$

Substituting $H + J = U$ and $Q + S = P$

$$\vec{a}_N = U\vec{F}_a + P\vec{F}_n + \vec{G} + \vec{a}_{N\omega} \quad (4.30)$$

or

$$\vec{a}_N = P\vec{F}_n + \vec{b} \quad (4.31)$$

where

$$\vec{b} = U\vec{F}_a + \vec{G} + \vec{a}_{N\omega} \quad (4.32)$$

4.2.5 Wheel Unilateral Constraints

The three-dimensional equations of motion, Equations 4.1-4.2, are subject to unilateral constraints that are implied by the reaction forces at the wheel-ground interface. Unilateral constraints are non-adhesive and are liable to failure if the relative motion of the contacting bodies is such that the bodies are getting separated. This type of constraints can generate only compressive reaction forces. This is in contrast to bilateral constraints that are bi-directional and can generate both tensile or compressive reaction forces at the contact point of the two bodies. An example of a unilateral constraint is the contact point between a wheel and a road surface that the wheel is rolling on, whereas an example of a bilateral constraint can be found at the hinge of an arm of a robot.

Generally, accelerations and constraint forces on the body are determined simultaneously while solving the equations of motion of a rigid body. This is a relatively straightforward process for a bilaterally constrained dynamic system. However, for a wheeled mobile robot traversing an uneven surface, the dynamic system at hand has unilateral constraints where the solutions need to satisfy extra

conditions. The first condition is that the normal components of the accelerations of the wheel contact points are always directed away from the road surface in order to comply with the physical constraint of non-interpenetration between the wheel and the ground, which are considered as rigid bodies. In addition the solution must satisfy the condition that the constraint forces are not adhesive.

This requirement complicates the analysis of the dynamics and it has been a topic for many research works [61-67]. The problem was first addressed by Lotstedt [61] who suggested a formulation of the analysis as a Linear Complementary Problem.

The physical constraint that the k^{th} wheel can not penetrate into the ground, but is in loose contact with the surface can be expressed mathematically as follows:

$$a_{nk} \geq 0$$

It is also known from the physical conditions that the wheel normal forces F_{nk} can not be adhesive (tensile), that is, $F_{nk} \geq 0$. An important observation is that if $a_{nk} > 0$ contact is immediately lost at the k^{th} wheel which implies that $F_{nk} = 0$. For contact to be maintained $a_{nk} = 0$. Hence, the relationship $a_{nk}F_{nk} = 0$ always holds.

Thus the problem of calculating the normal reactions and hence the accelerations can be stated as determining the value of \vec{F}_n which satisfies the following relationships.

$$a_{nk}F_{nk} = 0, \quad k = 1 \dots w$$

In generalised form,

$$\vec{a}_N \vec{F}_n^T = 0 \quad . \quad (4.33)$$

After substituting Equation (4.31) for \vec{a}_N into Equation (4.33) and applying the unilaterality conditions of force and acceleration, the problem of determining the unknown variable \vec{F}_n can be stated as:

Find \vec{F}_n such that,

$$\left. \begin{array}{l} (P\vec{F}_n + b)\vec{F}_n^T = 0 \\ (P\vec{F}_n + \vec{b}) \geq 0 \\ \vec{F}_n \geq 0 \end{array} \right\} \quad (4.34)$$

This is a class of mathematical problems known as the Linear Complementary Problem (LCP), which can be solved by means of Quadratic Programming techniques [68-69].

Writing in the form of a Quadratic Programming problem Equation (4.34) appears as a minimisation problem:

$$\begin{aligned} & \min[(P\vec{F}_n + \vec{b})\vec{F}_n^T] \\ & \text{subject_to} \begin{cases} P\vec{F}_n \geq -\vec{b} \\ \vec{F}_n \geq 0 \end{cases} \end{aligned} \quad (4.33b)$$

If the wheels do not lose contact, that is if $F_n > 0$, the problem is easily solved by considering the wheel-ground contact point as a bilateral constraint. Since the wheels can not penetrate into the ground, the normal component of the contact point acceleration must be zero, i.e.

$$\begin{aligned} a_{nk} &= 0 \\ \vec{a}_N &= P\vec{F}_n + \vec{b} = 0 \end{aligned} \quad (4.34)$$

or

$$\vec{F}_n = -P^{-1}\vec{b} \quad (4.35)$$

4.3 Dynamics of a WMR Climbing a Ramp

Consider a four-wheeled rigid WMR travelling along a straight path when its front wheels encounter a laterally symmetrical road obstacle, as shown in Figure 4.3. As a result, the robotic vehicle is subjected to motion in the x - z plane, namely: pitching motion about the lateral (y) axis, a normal translational motion due to the road obstacle (z -axis) and longitudinal motion in the direction of travel. Since only rigid-body dynamics is considered we also assume that the contact between the obstacle and the wheels occurs without collision. This is the case if the geometry of the ground irregularity does not have discontinuity and that the radius of the wheels is small compared with the radius of curvature of the ground profile.

In Equation (4.3) a description of the contact forces for the general case of a steered wheel attached to a platform travelling along a curved trajectory in a three-dimensional space was given. However, simplification can be achieved by limiting the investigation to the case of a laterally symmetric surface and assuming that there is no lateral movement of the vehicle (i.e. $\delta_k = 0$). It is known from tyre mechanics that a non-steered wheel of a WMR that travels along a straight path generates no lateral tyre force. Thus the lateral friction coefficient on

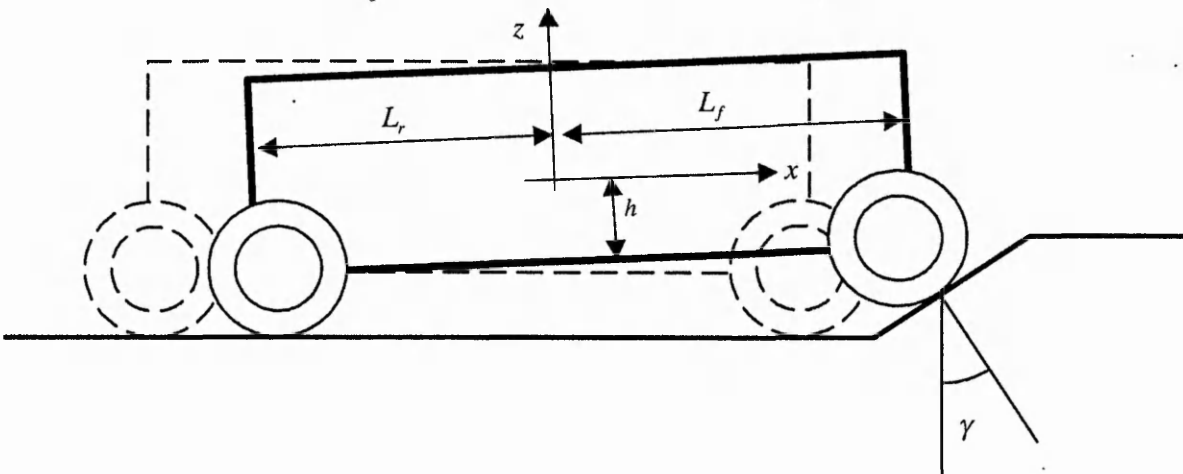


Figure 4.3 A WMR traversing a ramp front obstacle (laterally symmetrical).

all wheels of this WMR travelling along a straight path is equal to zero. That is, $\mu_{lk} = 0$. Further it is assumed that the wheel rolling resistance is negligibly small, i.e. $\mu_{nk} = 0$.

The derivation approach outlined in the previous section will be employed to obtain the relevant expressions for the case of a WMR that traverses the laterally symmetric obstacle. It is assumed that the height of the obstacle is very small in comparison to the dimensions of the WMR, hence the angle of inclination of the WMR relative to the horizontal is very small in comparison to the profile angle of the obstacle γ .

Thus, Equation (4.5) reduces to:

$$\vec{A}_1 = \begin{bmatrix} 1 \\ 0 \\ 0 \end{bmatrix}; \quad \vec{A}_2 = \begin{bmatrix} \cos(\gamma) \\ 0 \\ \sin(\gamma) \end{bmatrix} \quad (4.36)$$

where the subscripts 1 and 2 refer to the rear and front wheel pairs, respectively.

Similarly the \vec{N}_k terms can be written as

$$\vec{N}_1 = \begin{bmatrix} 0 \\ 0 \\ 1 \end{bmatrix}; \quad \vec{N}_2 = \begin{bmatrix} -\sin(\gamma) \\ 0 \\ \cos(\gamma) \end{bmatrix} \quad (4.37)$$

The normal vectors of the surface profile at the rear and front wheel contact points are respectively given as:

$$\vec{n}_1 = \begin{bmatrix} 0 \\ 0 \\ 1 \end{bmatrix}; \quad \vec{n}_2 = \begin{bmatrix} -\sin(\gamma) \\ 0 \\ \cos(\gamma) \end{bmatrix} \quad (4.38)$$

The position vectors of the contact points are:

$$\vec{r}_1 = \begin{bmatrix} -L_r \\ 0 \\ -h \end{bmatrix}; \quad \vec{r}_2 = \begin{bmatrix} L_f \\ 0 \\ -h \end{bmatrix} \quad (4.39)$$

Equation (4.25) allows the terms R_a and R_n to be evaluated for the rear and front wheels:

$$\vec{R}_{a1} = \begin{bmatrix} 0 \\ -h \\ 0 \end{bmatrix}; \quad \vec{R}_{a2} = \begin{bmatrix} 0 \\ -h\cos(\gamma) - L_f \sin(\gamma) \\ 0 \end{bmatrix} \quad (4.40)$$

$$\vec{R}_{n1} = \begin{bmatrix} 0 \\ L_r \\ 0 \end{bmatrix}; \quad \vec{R}_{n2} = \begin{bmatrix} 0 \\ h\sin(\gamma) - L_f \cos(\gamma) \\ 0 \end{bmatrix} \quad (4.41)$$

For the vehicle the matrix A is given by:

$$A = [\vec{A}_1 \quad \vec{A}_2] = \begin{bmatrix} 1 & \cos(\gamma) \\ 0 & 0 \\ 0 & \sin(\gamma) \end{bmatrix}$$

Similarly,

$$N = [\vec{N}_1 \quad \vec{N}_2] = \begin{bmatrix} 0 & -\sin(\gamma) \\ 0 & 0 \\ 1 & \cos(\gamma) \end{bmatrix}$$

$$n = [\vec{n}_1 \quad \vec{n}_2] = \begin{bmatrix} 0 & -\sin(\gamma) \\ 0 & 0 \\ 1 & \cos(\gamma) \end{bmatrix}$$

$$R_a = [\vec{R}_{a1} \quad \vec{R}_{a2}] = \begin{bmatrix} 0 & 0 \\ -h & -h\cos(\gamma) - Lf\sin(\gamma) \\ 0 & 0 \end{bmatrix}$$

$$R_n = [\vec{R}_{n1} \quad \vec{R}_{n2}] = \begin{bmatrix} 0 & 0 \\ Lr & h\sin(\gamma) - Lf\cos(\gamma) \\ 0 & 0 \end{bmatrix}$$

The inertia matrices M and I are given by:

$$M = m \begin{bmatrix} 1 & 0 & 0 \\ 0 & 1 & 0 \\ 0 & 0 & 1 \end{bmatrix}; \quad I = \begin{bmatrix} I_x & 0 & 0 \\ 0 & I_y & 0 \\ 0 & 0 & I_z \end{bmatrix} \quad (4.42)$$

where m is the total mass of the platform and payload, and I_x , I_y and I_z are the total mass moments of inertia of the platform and payload about the respective axes indicated by the suffices.

The U , P and \vec{b} matrices are derived using the methods outlined in the previous section. Thus,

$$U = \begin{bmatrix} U_{11} & U_{12} \\ U_{21} & U_{22} \end{bmatrix} \quad (4.43)$$

where,

$$U_{11} = \frac{-hLr}{I_y}$$

$$U_{21} = \frac{-\sin(\gamma)}{m} + \frac{-h^2\sin(\gamma) + hLf\cos(\gamma)}{I_y}$$

$$U_{12} = \frac{\sin(\gamma)}{m} + \frac{-(h\cos(\gamma) + Lf\sin(\gamma))Lr}{I_y}$$

$$U_{22} = \frac{(-h\cos(\gamma) - Lf\sin(\gamma))h\sin(\gamma) + (h\cos(\gamma) + Lf\sin(\gamma))Lf\cos(\gamma)}{I_y}$$

The P matrix is given as:

$$P = \begin{bmatrix} P_{11} & P_{12} \\ P_{21} & P_{22} \end{bmatrix} \quad (4.44)$$

where

$$P_{11} = \frac{1}{m} + \frac{Lr^2}{I_y}$$

$$P_{21} = -\frac{\sin(\gamma)}{m} + \frac{(h\sin(\gamma) - Lf\cos(\gamma))h\sin(\gamma) - (h\sin(\gamma) - Lf\cos(\gamma))Lf\cos(\gamma)}{I_y}$$

$$P_{12} = -\frac{\sin(\gamma)}{m} + \frac{Lr^2}{I_y}$$

$$P_{22} = \frac{1}{m} + \frac{(h\sin(\gamma) - Lf\cos(\gamma))h\sin(\gamma) - (h\sin(\gamma) - Lf\cos(\gamma))Lf\cos(\gamma)}{I_y}$$

The only external force considered is the body force, which is given by:

$$\vec{CF}_e = \begin{bmatrix} 0 \\ 0 \\ -1 \end{bmatrix} mg \quad (4.45)$$

where g is the acceleration due to gravity.

Thus the acceleration due to body forces, \vec{G} , is given by:

$$\vec{G} = g \begin{bmatrix} -1 \\ -\cos(\gamma) \end{bmatrix} \quad (4.46)$$

The contribution of the centrifugal acceleration term $\vec{a}_{n\omega}$ is given by,

$$\vec{a}_{n\omega} = \omega_p^2 \begin{bmatrix} h \\ Lf\sin(\gamma) + h\cos(\gamma) \end{bmatrix} \quad (4.47)$$

where ω_p is the pitch angular velocity of the platform.

The vector \vec{b} defined in Equation (4.32) is found as:

$$\vec{b} = U \begin{bmatrix} F_r \\ F_f \end{bmatrix} + g \begin{bmatrix} -1 \\ -\cos(\gamma) \end{bmatrix} + \omega_p^2 \begin{bmatrix} h \\ Lf\sin(\gamma) + h\cos(\gamma) \end{bmatrix} \quad (4.48)$$

where F_r and F_f are the rear and front-wheel traction forces, respectively.

The acceleration \vec{a}_c can be found from Equation (4.8) as:

$$\vec{a}_c = M^{-1}(A\vec{F}_a + N\vec{F}_n + \vec{CF}_e)$$

Assuming that there is no wheel contact loss we treat the constraints as bilateral one. The regime in which this assumption is justified will be discussed in the following section. Thus Equations (4.34-4.35) are valid for this case.

That is,

$$\vec{F}_n = -P^{-1}\vec{b}$$

Substituting for \vec{F}_n and $\vec{C}F_e$ into the expression for \vec{a}_c :

$$\vec{a}_c = M^{-1}(A\vec{F}_a + N(-P^{-1}\vec{b})) + \begin{bmatrix} 0 \\ 0 \\ -1 \end{bmatrix} mg \quad (4.49)$$

For the evaluation of jerk, the equation of the pitch angular acceleration is required, which can be found from Equation (4.26) as:

$$\vec{\alpha} = I^{-1}(R_a\vec{F}_a + R_n\vec{F}_n)$$

For a WMR moving on a straight course across a laterally symmetrical obstacle, both the rolling and the yaw angular accelerations are zero. Thus,

$$\vec{\alpha} = \begin{bmatrix} 0 \\ \alpha_p \\ 0 \end{bmatrix} = I^{-1}(R_a \begin{bmatrix} F_{tr} \\ F_{tf} \end{bmatrix} + R_n(-P^{-1}\vec{b})) \quad (4.50)$$

In the above derivation it was assumed that the constraints were bilateral. The effects of obstacle geometry and traction on the validity of this assumption is discussed in the following section.

4.4 Sensitivity of the Unilateral Constraint

The validity of the assumption of no-loss of contact (i.e., the assumption that allows us to treat the unilateral wheel constraints as bilateral ones) depends on:

- the relative magnitude of the elements of the matrix P , which depend on the dimensions and inertia of the WMR, the geometry of the ground profile and the orientation of the WMR with respect to the gravitational force direction;
- the relative magnitude of the elements of vector \vec{b} , which depend on the magnitude of the traction forces and the mode of actuation (i.e. whether the

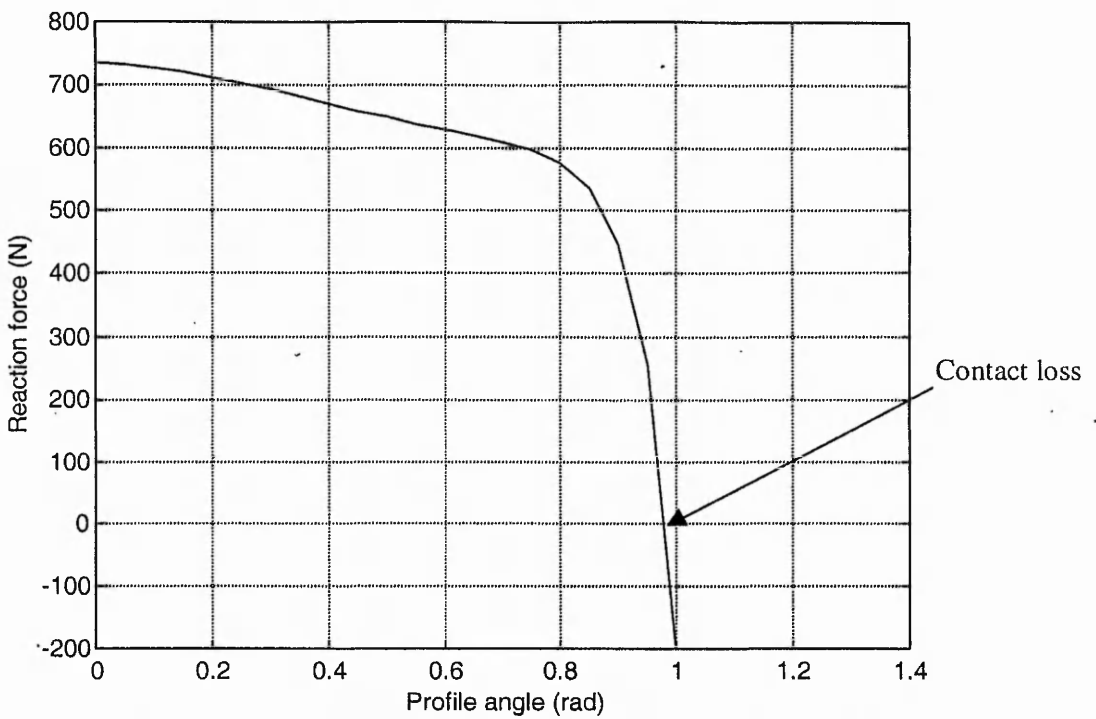


Figure 4.4 The effect of the profile angle γ on the front wheel contact.

WMR is front drive, rear drive or all-wheel drive) and the velocity of the WMR.

To determine the influences of the road profile geometry, the magnitude of the traction force and the driving mode on the integrity of the wheel-ground contact, a series of simulation studies have been carried out on a given WMR by varying each of the above listed parameters in turn. The WMR under consideration is a laboratory robot which is owned by the Nottingham Trent University, Mechanical and Manufacturing Department. A picture of the robot is shown in Figure 4.6. The dimensions of the WMR are given in Table 4.1. The front wheels of the WMR are traversing an obstacle with lateral symmetry. The results are summarised in Figures 4.4 and 4.5. Figure 4.4 shows the effect of the road profile angle, γ , on the condition of the contact between the front wheels and the ground surface. Since unilateral constraints can not sustain tensile reaction forces (represented by negative magnitude), the point where the curve crosses the zero value of the reaction force corresponds to contact loss. The negative reaction forces are not achievable by a unilateral constraint. In this simulation the WMR is

travelling at 2 m/s and there are no wheel-drive torque inputs. Thus for the given WMR travelling at the given condition, the range of profile angle γ within which the unilateral constraint can be treated as a bilateral one is less than 0.98 radians (56°).

Table 4.1. Dimension of the WMR used in the simulation

Symbol	Description	Value
L_f	Longitudinal distance of front axle from the vehicle centre of mass	0.6 m
L_r	Longitudinal distance of rear axle from the vehicle centre of mass	0.46 m
h	Height of centre of mass from the wheel centres	0.4 m
R	Radius of wheels	0.1 m
I_y	Pitch moment of inertia of the platform	47 kg-m^2
m	Mass of the platform and payload	170 kg

Figure 4.5 shows the simulation results of the same WMR traversing a ramp obstacle of $\gamma = 0.3$. The vehicle was driven with a range of traction forces and different traction modes at an initial velocity of 2 m/s. It can be observed that rear wheel traction can be applied at the widest range without causing contact

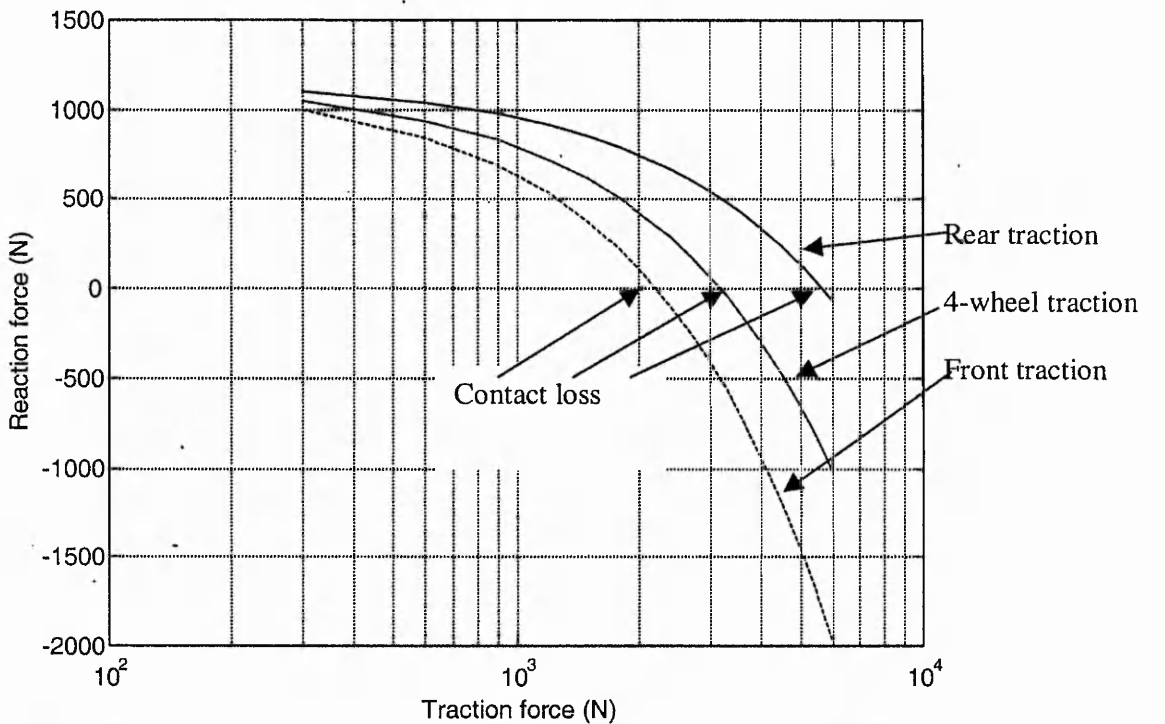


Figure 4.5 The effect of the magnitude and mode of traction on wheel contact loss. ($\gamma = 0.3$)

loss, since the curve corresponding to this mode of traction crosses the zero reaction at the furthest to the right. This is followed by 4-wheel traction. In this simulation it is assumed that the traction forces are equally distributed between the front and the rear axles for the 4-wheel traction. Front-wheel traction causes the earliest wheel-ground contact loss.

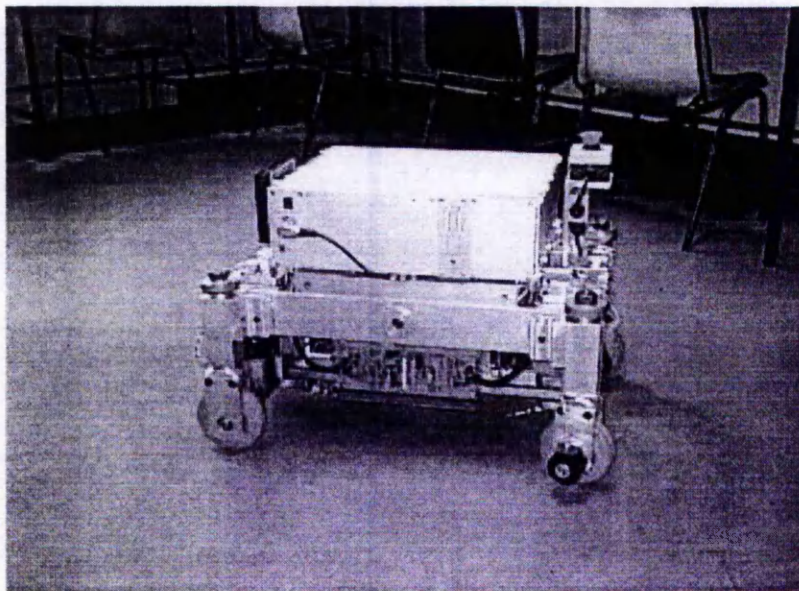


Figure 4.6 The Laboratory robot used in the case study. (Courtesy of the Mechanical and Manufacturing Department, The Nottingham Trent University)

4.5 Smoothness of Manoeuvre

Two vibration problems are identified in modern vehicle dynamics. One is the whole body vibration problem, which is related to rigid body motion, while the other is structural vibration problem which is due to a stress wave that propagates through material medium. The rigid body motion of the WMR over an obstacle can be thought of as a whole body vibration problem, such as that experienced by occupants of an automobile travelling on an uneven surface. The similarity allows us to derive a quantity which is a measure of smoothness of manoeuvre.

In automotive literature peak acceleration is commonly used as a measure of performance of suspension systems [59]. The reason for the choice of

acceleration as a measure of passenger comfort is rather ambiguous. In the oldest record of the definition of the quantity, Hartog [60] argued that an appropriate measure for passenger comfort should in fact be jerk, the rate of change of acceleration, because smooth changes in displacement or velocity have not been observed to cause much discomfort. Hartog [60] elaborated the argument by means of an example of passengers in a car. The responses of the occupants to small and large quasi-static displacement, small and large constant velocity, and small and large constant accelerations was assessed. It was argued that passenger comfort is not as much influenced by the magnitude of the quasi-static displacement, the constant velocity nor the constant acceleration as by the rate at which the acceleration changes (jerk). Apart from the fact that large accelerations are accompanied by large inertia forces which might cause structural stress, they are not directly related to the fatigue felt by passengers who experience a “*rough ride*”.

By drawing a parallel to the above argument the harshness, at which a payload on the platform of a WMR is handled, is proportional to the jerk experienced by it during the transportation. In order for the WMR to transport its payload smoothly it must as well be driven smoothly. The normal jerk is mainly related to the ‘*lifting-off*’ effect of any payload placed on the platform. In the analysis that follows we aim to derive the normal jerk to which the WMR is subjected while its wheels traverse a ramp obstacle.

The acceleration of a WMR can be written in terms of the rates of changes of speed with respect to a coordinate system attached to the WMR. Thus

$$\begin{aligned} a_{cx} &= \frac{d v_x}{dt} + v_z \omega_y - v_y \omega_z \\ a_{cy} &= \frac{d v_y}{dt} + v_x \omega_z - v_z \omega_x \\ a_{cz} &= \frac{d v_z}{dt} + v_y \omega_x - v_x \omega_y \end{aligned} \quad (4.51)$$

where v_x, v_y, v_z are the translational speeds ω_x , ω_y , and ω_z are the angular speeds (roll, pitch and yaw) of the WMR. It should be noted that the $v\omega$ terms arise as a consequence of using a coordinate system attached to the robotic vehicle. The equations of motion for a WMR traversing a laterally symmetric ground obstacle are thus:

$$\begin{aligned}\sum F_x &= m(\dot{v}_x + v_z \omega_y) \\ \sum F_z &= m(\dot{v}_z - v_x \omega_y) \\ \sum M_y &= I_y \alpha_y\end{aligned}\quad (4.52)$$

where m is the mass and I_y is the pitch moment of inertia of the vehicle; v_x and v_z are respectively the longitudinal and the normal speed; ω_y is the pitch angular velocity and α_y is the pitch angular acceleration of the platform.

Since, $a_{cx} = \dot{v}_x + v_z \omega_y$ and $a_{cz} = \dot{v}_z - v_x \omega_y$ the rates of changes of the longitudinal and the normal speeds are:

$$\begin{aligned}\dot{v}_x &= a_{cx} - v_z \omega_y \\ \dot{v}_z &= a_{cz} + v_x \omega_y\end{aligned}$$

Thus the translational jerk along z (normal jerk) is given by:

$$\begin{aligned}J_{cz} &= \frac{d\dot{v}_z}{dt} = \frac{d}{dt}(a_{cz} + v_x \omega_y) = \frac{da_{cz}}{dt} + v_x \frac{d\omega_y}{dt} + \omega_y \frac{dv_x}{dt} \\ J_{cz} &= \frac{da_{cz}}{dt} + v_x \alpha_y + \omega_y \dot{v}_x\end{aligned}$$

Substituting

$$\begin{aligned}\dot{v}_x &= a_{cx} - v_z \omega_y \\ J_{cz} &= \frac{da_{cz}}{dt} + v_x \alpha_y + \omega_y(a_{cx} - v_z \omega_y)\end{aligned}$$

Since the accelerations a_{cx} and a_{cz} are functions of the profile angle γ the following relationships are used to determine their respective time derivatives.

$$\frac{da_{cx}}{dt} = \frac{\partial a_{cx}}{\partial \gamma} \frac{d\gamma}{dt}$$

$$\frac{da_{cz}}{dt} = \frac{\partial a_{cz}}{\partial \gamma} \frac{d\gamma}{dt}$$

The following transformation is used for the time rate of the profile angle γ :

$$\frac{d\gamma}{dt} = \frac{dy}{dx} \frac{dx}{dt} = \frac{dy}{dx} v_x \quad (4.53)$$

Thus the jerk in the normal direction is given by:

$$J_{cz} = \frac{\partial a_{cz}}{\partial \gamma} \frac{dy}{dx} v_x + v_x \alpha_y + \omega_y(a_{cx} - v_z \omega_y) \quad (4.54)$$

The term $\frac{d\gamma}{dx}$ is the curvature of the road profile at the point of contact, which can be estimated for a continuous, smooth profile by differentiating the profile angle γ with respect to the longitudinal displacement x .

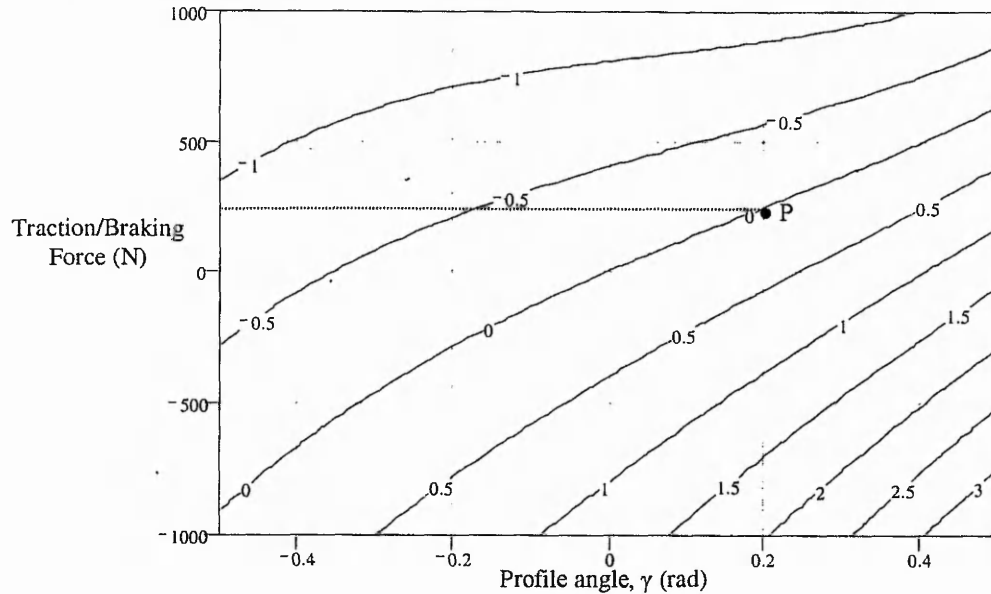


Figure 4.7 Contour plot of normal jerk of vehicle driven/braked by rear wheels.

4.6 Case Study

Equation (4.54) shows that the normal jerk caused by the manoeuvre of the WMR traversing a ramp type obstacle depends mainly on two parameters:

- the geometry of the road profile and
- the acceleration of the platform which in turn depends on the traction/braking force and the vehicle's inertial and geometric dimensions.

Substituting the appropriate expressions and the values of the vehicle dimensions, mass and inertia, into Equation (4.54) the normal jerk of a WMR can be obtained as a function of the profile angle and traction forces. The symbolic expression for the evaluation of the normal jerk for a generic WMR has been obtained by using

the Mathcad® software (Appendix A). The relationship between normal jerk, traction forces and road profile angle be represented as:

$$J_{cz} = f(\vec{F}_t, \gamma) \quad (4.55)$$

where \vec{F}_t is a vector of the traction forces and f is a function.

The results of a case study that has been carried out to compute the normal jerk response of a WMR whose dimensions are given in Table 4.1 is presented as follows. The contour plot in Figure 4.7 shows the relationship between the profile angle γ , the traction force F_t and the jerk response. Each contour line has a constant jerk value. The contour line with zero jerk value is of particular interest as it represents the functional relationship between the road profile geometry and

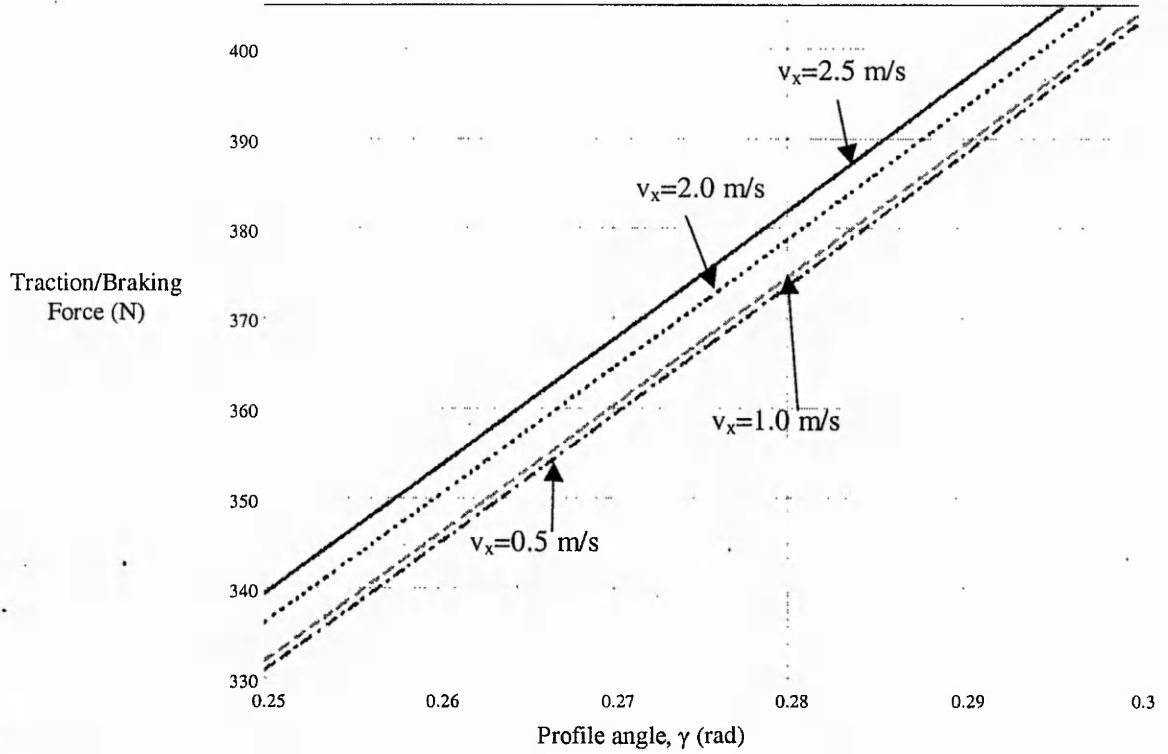


Figure 4.8 The relationship between of the ideal traction force and the longitudinal velocity of the vehicle.

an ideal traction force that will result in a jerk-free motion. The nominal longitudinal speed of the WMR used in the computation was 2 m/s.

The usefulness of Figure 4.7 for determining the traction force needed to avoid the onset of jerk can be demonstrated by means of the following example. Consider an instance when the vehicle is required to traverse a surface whose

profile gradient γ has a value of 0.2 (the abscissa of point P in Figure 4.6), an ideal rear traction force of 367 N (the ordinate of point P) is needed to avoid the onset of normal jerk.

As the velocity of the platform changes the demand for the traction force needed to eliminate jerk also changes. In Figure 4.8 this relationship between the ideal traction force and the velocity of the WMR has been plotted for velocities ranging from 0.5 m/s to 2.5 m/s. It is evident that as the velocity increases the ideal traction force increases in magnitude, even though not by a substantial amount.

The above consideration has been based on the assumption that the normal component of a jerk is the most important parameter in determining the smoothness of motion for payload handling purposes. In practice the vehicle is subjected to longitudinal jerk as well as normal jerk. The magnitude of the resultant jerk could be found by a vector of sum of the two components. That is,

$$J_c = \sqrt{J_{cx}^2 + J_{cz}^2}$$

where J_c is the magnitude of the resultant jerk, J_{cx} is the longitudinal jerk which can be derived in a similar manner to J_{cz} as shown in Equations 4.52 to 4.55.

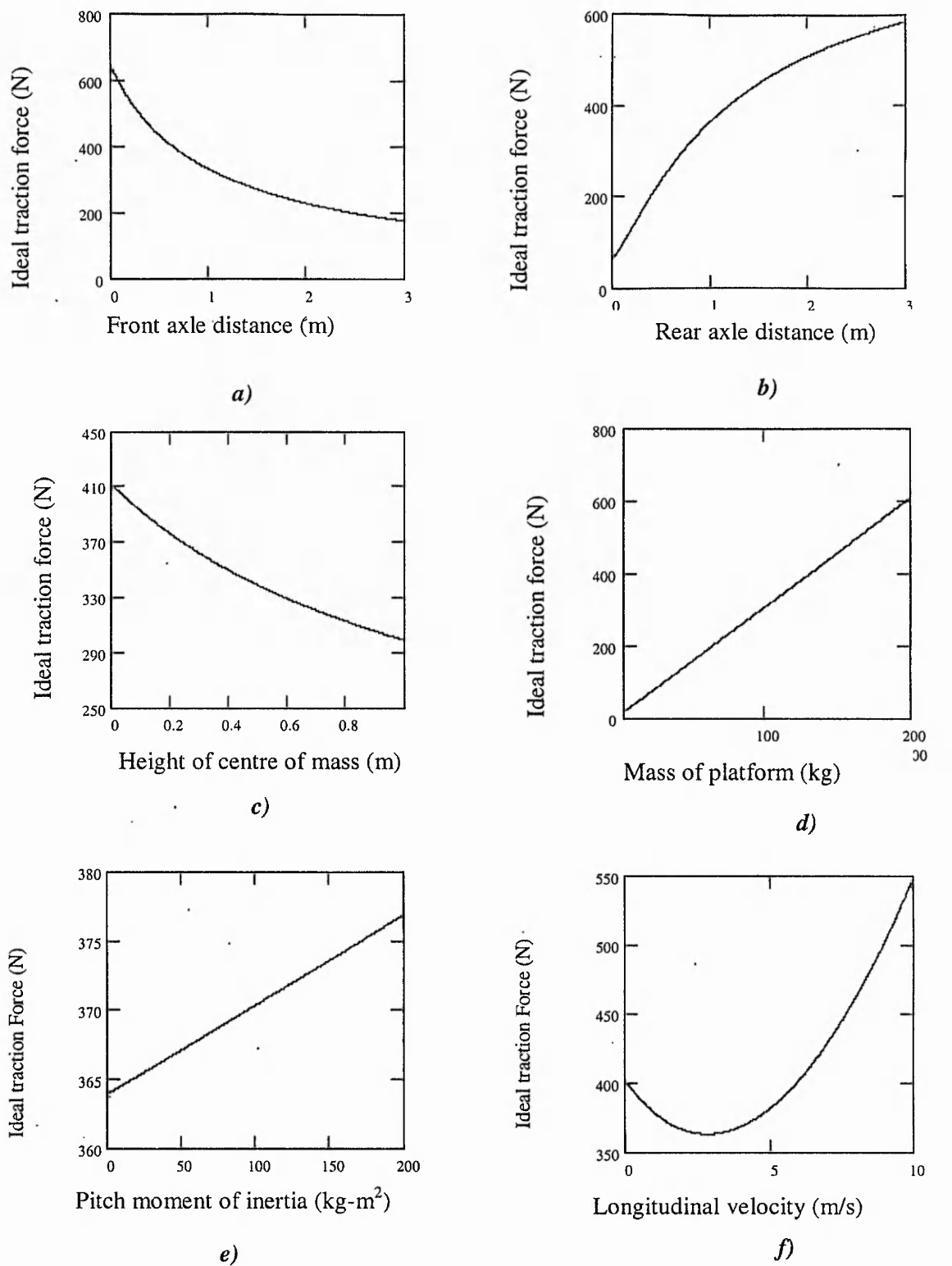


Figure 4.8 Dependence of the ideal traction force needed for a zero normal jerk motion, with respect to vehicle dimensions and speed.

The ideal traction force required to minimise the jerk depends not only on the surface profile angle but also on the vehicle speed and other geometric parameters of the vehicle including the axle length, height of the centre of mass, mass and pitch moment of inertia. The effects of these parameters on the requirements of the ideal rear traction force needed to maintain minimum jerk have been investigated for a profile angle of obstacle of 17° and the results are shown in Figure 4.8. Comparison of Figure 4.8a and 4.8b suggests that a better load distribution (one that would require less rear traction force to minimise normal jerk) can be achieved by positioning the centre of mass as close as possible to the rear axle. Furthermore, the lower the height of the centre of mass of a vehicle, the smaller is the requirement of the ideal traction force (Figure 4.8c). The ideal traction force varies relatively little with the value of pitch moment of inertia (Figure 4.8e). Figure 4.8f shows the dependency of the ideal rear traction force on the velocity of the platform, where the traction force decreases slightly until it reaches a minimum and increases monotonously afterwards.

The above scheme of reducing jerk requires the knowledge of the profile angle, which needs to be measured unless it is known *a priori*. One possible way of deducing the profile angle is by indirectly measuring the reaction force of the wheels which interact with the obstacle. Assuming the light wheels facing the obstacle, which are acted up on wheel-ground forces and axle forces from the vehicle's chassis, to be in static equilibrium an expression for the angle γ can be derived based on knowledge of the axle forces as follows:

$$\gamma = 2 \arctan \left[\frac{1}{R_x + F_a} \left(R_y \pm \sqrt{R_y^2 + R_x^2 - F_t^2} \right) \right] \quad (4.56)$$

where R_x and R_y are respectively the longitudinal and vertical axle forces, which may be measured by suitable load cells; F_t is the instantaneous traction force applied during the measurement.

4.7 Summary Comments

A modelling technique for the rigid body dynamics of a WMR traversing obstacles of generic geometry has been presented. The jerk response has been identified as a measure of manoeuvre harshness and an analytical technique for determining this quantity for WMRs has been developed. Computation of the jerk response has revealed that this quantity can be minimised by a proper choice of traction forces depending on the geometry of the profile, velocity and dimensions of the WMR.

One way of utilising the minimum jerk principle laid out in this work is to devise a scheme (Figure 4.9) for regulating the motor torque applied at the wheels in order to minimise the vehicle jerk. In this scheme, an ideal traction force is calculated using input values of vehicle mass, inertia, dimensions and velocity. Also needed is knowledge of the surface profile angle, which can be determined from Equation (4.56), based on measurements of axle load and a feedback measurement of the traction force (driving torque). The ideal traction force can be used as an input to a drive torque controller, which in turn regulates the power supply to the motor.

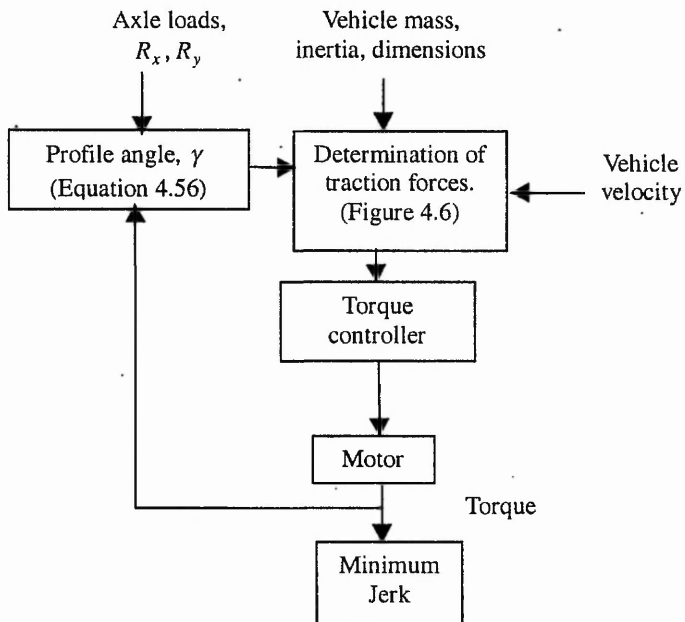


Figure 4.9 Implementation of the control scheme.

Chapter 5

Trajectory Planning and Control of WMR Pitch Dynamics

5.1 Introduction

In the previous chapter a technique for determining the equations of motion of WMRs that traverse obstacles was devised. One area of application of dynamic models is for planning feasible trajectories of mechanical systems. In this chapter we aim to introduce a new trajectory planning scheme for the pitching dynamics of WMRs.

Wheeled Mobile Robot motion planning problem generally consists of three major tasks:

- Path planning - the task of finding a feasible path satisfying all the constraints of the system.
- Trajectory planning - time parametrisation of the planned path in order to satisfy certain criteria, such as minimum jerk, minimum time or minimum energy.
- Trajectory tracking - designing a controller which is able to follow the planned trajectory.

The major area of research in WMR motion planning has so far been limited to path planning [31, 55-57]. These works on path planning are often based on inadequate, oversimplified models that do not take into account the important parameters such as: inertia, ground friction or rotational dynamics. There are few published research works on trajectory planning of mobile robots moving on smooth planar surface. For road vehicles Sledge et al [23] proposed trajectories defined by an elliptic function to achieve minimum energy, minimum jerk and minimum radius of curvature during emergency lane-change manoeuvre. The trajectories were, however, parametrised with longitudinal displacement, which makes them unsuitable for variable-velocity path planning.

Unlike the case of WMRs, the methodology for path and trajectory planning of stationary robots (manipulators) is well developed. The models employed are often

based on a more complete dynamics that accommodate inertia and gravity loads, as well as considering rotational and translational dynamics [70-72]. In the robotic manipulator literature, time parametrised trajectories are designed to satisfy various constraints. One of these constraints is the minimisation of jerk. Piazz and Visioli [11] used optimisation techniques to obtain minimum jerk cubic-spline trajectories of manipulator joints that enhance the path tracking capability of the mobile manipulator arms. It was also claimed that such trajectories elongate the service life of the manipulator by reducing the level of vibration which induces fatigue stress.

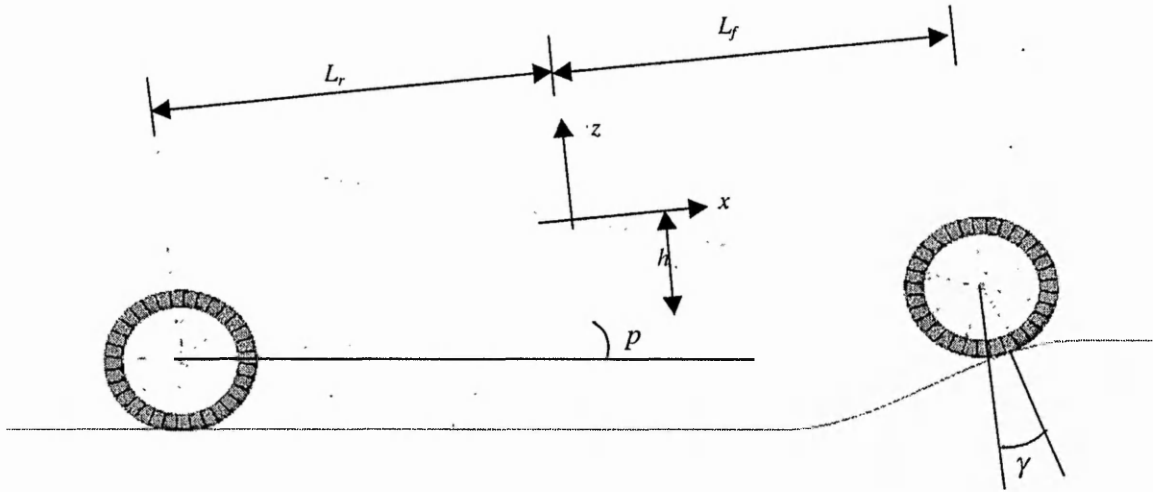


Figure 5.1 A mobile platform with front obstacle (laterally symmetrical).

In uneven terrain navigation of WMRs no previous research work, to the best of the author's knowledge, has addressed the problem of trajectory planning. It is important to consider a new approach for trajectory planning of mobile platforms which need to travel over localised surface irregularities. It is assumed that the WMR's, its wheels and the ground surface are rigid. The trajectory planning task will be based on the dynamics model derived in the previous chapter for a WMR that traverses a laterally symmetrical obstacle where all forces including inertia and gravitational forces are taken into consideration in the modelling process.

Assuming that the WMR is a rear wheel driven, the pitching motion dynamics will be considered for the trajectory planning. A single, continuous polynomial function is proposed as the time parametrised trajectory with zero jerk values at the starting and the ending points of the manoeuvre of obstacle traversing, because it guarantees velocity and acceleration continuity. The traction force required to complete the manoeuvre is then computed using the dynamics model.

5.2 Derivation of the Equations of Motion

In this section the pitch dynamics equations of motion are extracted from the generalised equations of motion of a WMR derived in the previous chapter. The robot is assumed to be driven by the rear-wheels while the front wheels encounter an obstacle of arbitrary profile. In this formulation the profile angle γ does not necessarily have to be constant. Also the assumption on the magnitude of the pitch angular displacement, a magnitude assumed to be small in the formulation of the minimum jerk principle for ramp obstacles, is relaxed. Assuming lateral symmetry the robotic vehicle can be represented by a *bicycle model* (Figure 5.1). In this case the steering angles of the front and rear wheels (δ_1 and δ_2) and the lateral friction coefficients on both axles (μ_{l1} and μ_{l2}) are zero. The relevant expressions are derived in a similar manner to the case study in the previous chapter but taking into account, the pitch displacement and the pitch angular velocity.

Thus, the \vec{A} matrix is:

$$\vec{A} = \begin{bmatrix} \cos(p) & \cos(\gamma) \\ 0 & 0 \\ -\sin(p) & \sin(\gamma) \end{bmatrix}; \quad (5.1)$$

The \vec{N} matrix is:

$$N = \begin{bmatrix} \sin(p) & -\sin(\gamma) \\ 0 & 0 \\ \cos(p) & \cos(\gamma) \end{bmatrix} \quad (5.2)$$

The normal vectors of the surface profile at the rear and front wheel contact points are respectively given as:

$$\vec{n}_1 = \begin{bmatrix} \sin(p) \\ 0 \\ \cos(p) \end{bmatrix}; \quad \vec{n}_2 = \begin{bmatrix} -\sin(\gamma) \\ 0 \\ \cos(\gamma) \end{bmatrix} \quad (5.3)$$

The position vectors at the contact points are:

$$\vec{r}_1 = \begin{bmatrix} -L_r \\ 0 \\ -h \end{bmatrix}; \quad \vec{r}_2 = \begin{bmatrix} L_f \\ 0 \\ -h \end{bmatrix} \quad (5.2)$$

$$R_{a1} = \begin{bmatrix} 0 & 0 \\ -h\cos(p) - Lr\sin(p) & -h\cos(\gamma) - Lf\sin(\gamma) \\ 0 & 0 \end{bmatrix} \quad (5.3)$$

$$R_{n1} = \begin{bmatrix} 0 & 0 \\ -h\sin(p) + Lr\cos(p) & h\sin(\gamma) - Lf\cos(\gamma) \\ 0 & 0 \end{bmatrix} \quad (5.4)$$

The U , P and b matrices are derived using the methods outlined in the previous chapter.

$$U = \begin{bmatrix} U_{11} & U_{12} \\ U_{21} & U_{22} \end{bmatrix} \quad (5.5)$$

where,

$$U_{11} = \frac{(h\cos(p) + Lr\sin(p))h\sin(p) - (h\cos(p) + Lr\sin(p))Lr\cos(p)}{I_y}$$

$$U_{21} = \frac{-\cos(\gamma)\sin(p) - \sin(\gamma)\cos(p)}{m} + \frac{(-h\cos(p) - Lr\sin(p))h\sin(\gamma) + (h\cos(p) + Lr\sin(p))Lf\cos(\gamma)}{I_y}$$

$$U_{12} = \frac{\cos(\gamma) \sin(p) + \sin(\gamma) \cos(p)}{m} + \frac{(h \cos(\gamma) + Lf \sin(\gamma)) h \sin(p) - (h \cos(\gamma) + Lf \sin(\gamma)) Lr \cos(p)}{I_y}$$

$$U_{22} = \frac{(-h \cos(\gamma) - Lf \sin(\gamma)) h \sin(\gamma) + (h \cos(\gamma) + Lf \sin(\gamma)) Lf \cos(\gamma)}{I_y}$$

The P matrix is given as:

$$P = \begin{bmatrix} P_{11} & P_{12} \\ P_{21} & P_{22} \end{bmatrix} \quad (5.6)$$

where

$$P_{11} = \frac{1}{m} + \frac{(-h \sin(p) + Lr \cos(p)) h \sin(p) + (-h \sin(p) + Lr \cos(p)) Lr \cos(p)}{I_y}$$

$$P_{21} = \frac{\sin(p - \gamma)}{m} + \frac{(h \sin(\gamma) - Lf \cos(\gamma)) h \sin(\gamma) - (h \sin(\gamma) - Lf \cos(\gamma)) Lf \cos(\gamma)}{I_y}$$

$$P_{12} = \frac{\sin(p - \gamma)}{m} - \frac{(-h \sin(p) + Lr \cos(p)) h \sin(p) - (-h \sin(p) + Lr \cos(p)) Lr \cos(p)}{I_y}$$

$$P_{22} = \frac{1}{m} + \frac{(h \sin(\gamma) - Lf \cos(\gamma)) h \sin(\gamma) - (h \sin(\gamma) - Lf \cos(\gamma)) Lf \cos(\gamma)}{I_y}$$

The body force vector \vec{G} is given by:

$$\vec{G} = g \begin{bmatrix} -1 \\ \sin(p) \sin(\gamma) - \cos(p) \cos(\gamma) \end{bmatrix} \quad (5.7)$$

where g is the acceleration due to gravity.

The contribution of the centrifugal acceleration term \vec{a}_{nw} is given by,

$$\vec{a}_{nw} = \omega_p^2 \begin{bmatrix} Lr \sin(p) + h \cos(p) \\ Lf \sin(\gamma) + h \cos(\gamma) \end{bmatrix} \quad (5.8)$$

where ω_p is the pitch angular velocity of the platform.

The vector \vec{b} is given by:

$$\vec{b} = U \begin{bmatrix} F_r \\ 0 \end{bmatrix} + g \begin{bmatrix} -1 \\ \sin(p)\sin(\gamma) - \cos(p)\cos(\gamma) \end{bmatrix} + \omega_p^2 \begin{bmatrix} Lr \sin(p) + h \cos(p) \\ Lf \sin(\gamma) + h \cos(\gamma) \end{bmatrix} \quad (5.9)$$

where F_r is the rear-wheel traction force.

The pitch angular equation of motion is found from Equation (3.26) where the roll and yaw angular accelerations are zero (because it is assumed that there is lateral symmetry):

$$\begin{bmatrix} 0 \\ \alpha_p \\ 0 \end{bmatrix} = I^{-1} (R_a \vec{F}_a + R_n \vec{F}_n) \quad (5.10)$$

where $\vec{F}_n = -P^{-1} \vec{b}$

Since \vec{F}_n is determinable as a function of p , γ and F_r Equation (5.10) can be solved to obtain the expression for α_p . The actual symbolic expression for the angular acceleration of the pitch motion α_p will be given in Appendix B for the sake of brevity. It can be shown that α_p has the following form:

$$\alpha_p = \Phi(p, \gamma) F_r + \Gamma(p, \gamma) \omega_p^2 + \Lambda(p, \gamma) \quad (5.11)$$

where $\Phi(p, \gamma)$, $\Gamma(p, \gamma)$ and $\Lambda(p, \gamma)$ are non-linear functions of the pitch angular displacement p and the profile angle γ .

5.3 Localised Trajectory Planning

In the previous section the equation of the pitch angular motion of a WMR that traverses a laterally symmetrical obstacle of arbitrary geometry (Equation 5.11) has been established. This result will be used in a case study to compute the traction force requirement of a WMR which follows a planned trajectory. Firstly, however, a

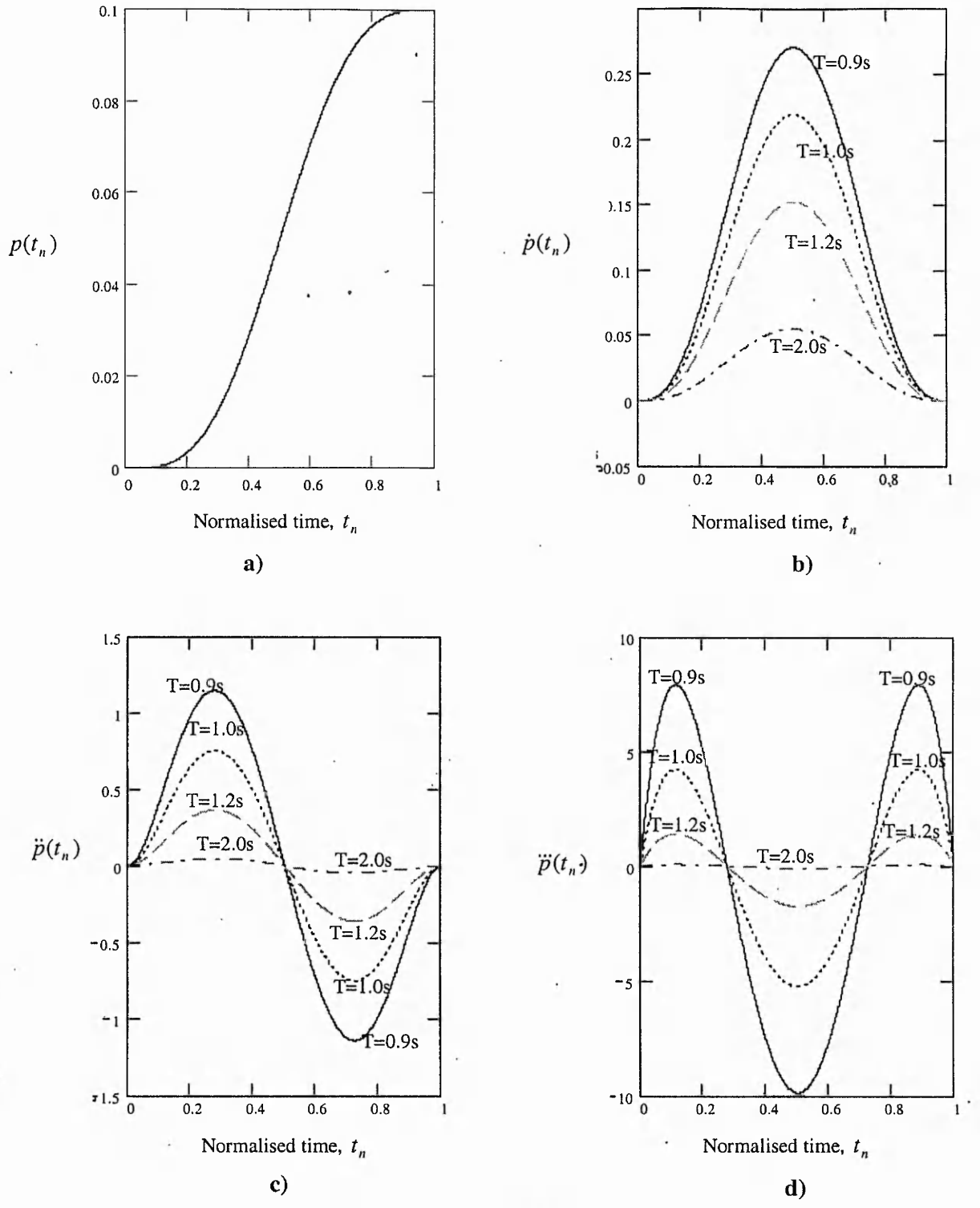


Figure 5.2 a) Displacement b) velocity c) acceleration d) jerk versus time plots of a polynomial trajectory function.

scheme for generating a localised trajectory for the pitching motion will be introduced. A localised trajectory is a curve parametrised with respect to time that provides the magnitude of the angular pitch displacement for the period of time during which the front wheels of the platform are in contact with the obstacle. The successive derivatives of the localised trajectory provide the velocity, acceleration and jerk of the pitching motion.

Let $p(t_n)$ be a polynomial trajectory function for the pitch angular displacement, where $t_n = \frac{t}{T}$ is a normalised time, t is the actual time variable, and T is the total time it takes the robotic vehicle to complete the obstacle-traversing manoeuvre. If the pitch angular jerks at the initial and final conditions of the manoeuvre are included in addition to the displacement, velocity, and acceleration, then there are eight conditions in total to be satisfied by the polynomial trajectory function $p(t_n)$ and its derivatives. Hence, $p(t_n)$ can be devised to be a polynomial of degree seven. That is,

$$p(t_n) = \sum_{i=0}^7 C_i t_n^i \quad (5.12)$$

from which the pitch angular velocity, acceleration and jerk of the WMR can be determined by successive differentiation with respect to time, i.e.,

$$\dot{p}(t_n) = \sum_{i=1}^7 i C_i t_n^{i-1} \quad (5.13)$$

$$\ddot{p}(t_n) = \sum_{i=2}^7 i(i-1) C_i t_n^{i-2} \quad (5.14)$$

$$\dddot{p}(t_n) = \sum_{i=3}^7 i(i-1)(i-2) C_i t_n^{i-3} \quad (5.15)$$

For front wheel obstacles the initial (i.e. at $t_n = 0$) and final (i.e. at $t_n = 1$) conditions of the platform are:

$$p(0) = 0 \quad p(1) = \beta$$

$$\dot{p}(0) = 0 \quad \dot{p}(1) = 0$$

$$\ddot{p}(0) = 0 \quad \ddot{p}(1) = 0$$

$$\ddot{p}(0) = 0 \quad \ddot{p}(1) = 0$$

where β is the pitch angular displacement of the platform at the end of the localised manoeuvre. By using these conditions the coefficients C_i where $i = 0 \dots 7$ in Equations (5.12-5.15) can be obtained. The following vector is the solution for the case being considered here:

$$C = [-20 \ 70 \ -84 \ 35 \ 0 \ 0 \ 0 \ 0] \beta$$

The planned trajectory function and its derivatives are plotted in Figure 5.2 as a function of normalised time. As can be seen in the Figure 5.2-d an intermediate jerk exists when a single polynomial function is used for the entire trajectory. However, the jerk at the start and end of manoeuvre are zero. This has a practical benefit from the point of view of actuation because the actuators that drive the wheels engage and disengage smoothly, i.e. with minimum jerk. It can also be observed that the peak value of the intermediate jerk can be reduced if a longer time span is allowed for the platform to complete the manoeuvre, which can also lead to a reduction in the peak velocities and accelerations. Any arbitrary profile angle corresponding to an arbitrary

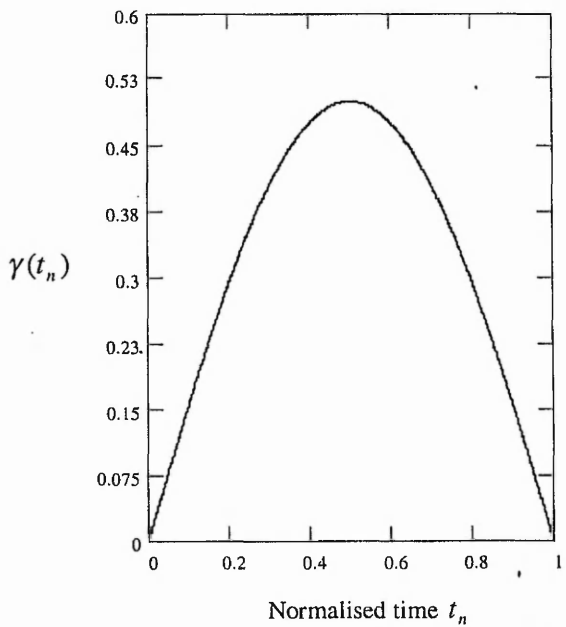


Figure 5.3 The time parametrised ramp profile angle considered in the simulation.

geometry of the front wheel obstacle can also be parametrised with the same time variable t_n to obtain $\gamma(t_n)$. An example is shown in Figure 5.3.

Once the trajectory has been planned, the rear wheel traction force needed to complete the manoeuvre can be computed as follows. Substituting the planned angular pitch displacement $p(t_n)$, velocity $\dot{p}(t_n)$, acceleration $\ddot{p}(t_n)$, and the profile angle $\gamma(t_n)$ in place of p , ω_p , α_p and γ , respectively, in Equation (5.11), then:

$$\ddot{p}(t_n) = \Phi(p(t_n), \gamma(t_n))F_{tr} + \Gamma(p(t_n), \gamma(t_n))\dot{p}(t_n)^2 + \Lambda(p(t_n), \gamma(t_n)) \quad (5.16)$$

from which the rear wheel traction force F_{tr} can be obtained as:

$$F_{tr} = \Phi(p(t_n), \gamma(t_n))^{-1}(\ddot{p}(t_n) - \Gamma(p(t_n), \gamma(t_n))\dot{p}(t_n)^2 - \Lambda(p(t_n), \gamma(t_n))) \quad (5.17)$$

Table 5.1 Dimensions of the mobile platform for used in the case study.

Symbol	Description	Value
L_f	Longitudinal distance of front axle from the vehicle centre of mass	0.6 m
L_r	Longitudinal distance of rear axle from the vehicle centre of mass	0.46 m
h	Height of centre of mass from the wheel centres	0.4 m
R	Radius of wheels	0.1 m
I_y	Pitch moment of inertia of the platform	47 kg·m ²
m	Mass of the platform and payload	270 kg

The dimensions, mass and inertia of the platform used in the case study are summarised in Table 5.1. The same robot used in the case study in the previous chapter has again been employed here. The only difference is that a 100kg payload has been added about the centre of mass of the WMR to highlight the fact the case study under consideration is for payload transfer applications. For a simulation study the profile of an obstacle with an arbitrary continuous function can be chosen. In this case the following function has been used.

$$\gamma(t_n) = \xi \sin(\alpha t_n + \delta) \quad (5.18)$$

The values for the parameters ξ , α , and δ are $\xi = 0.5$, $\alpha = \pi$, $\delta = 0$. The time parametrised profile angle of the obstacle is shown in Figure 5.3.

The traction effort needed to complete the manoeuvre of the platform over the obstacle whose geometry is specified by Equation (5.18) is computed by using Equation (5.17) for different time spans of manoeuvre T . The results are shown in Figures 5.4 and 5.5 on a normalised time scale. Figure 5.4 shows the traction force requirement when the total time required to complete the manoeuvre is less than or equal to 1.38 seconds, while Figure 5.5 shows the traction force requirement when the manoeuvre time is greater than or equal to 1.38 seconds. It can be seen in Figure 5.4 that the sign of the traction force may change for fast manoeuvres (i.e. with small values of T). A negative traction force corresponds to a braking action. From Figure 5.5, it is evident that a shift from the traction mode to a braking mode can be avoided if the manoeuvre time is increased so that the velocity of the platform is kept low. In

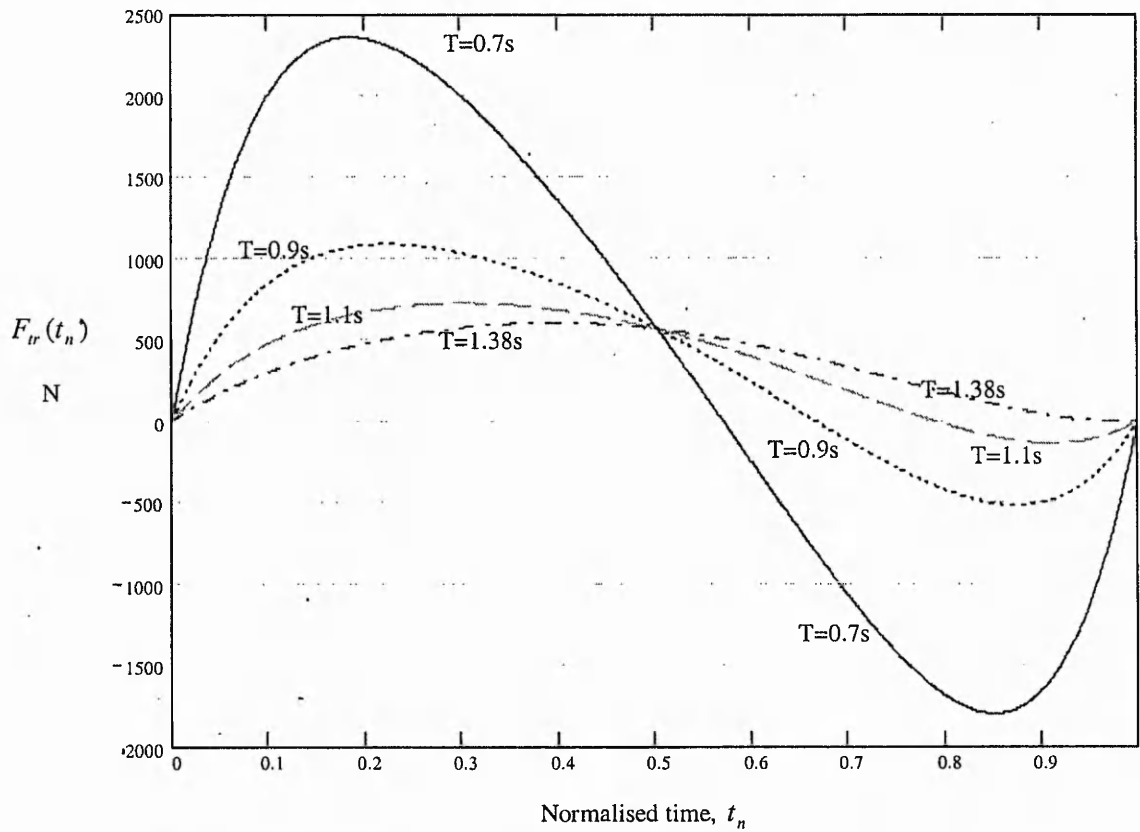


Figure 5.4 Traction force requirement when manoeuvre time span $T \leq 1.38s$.

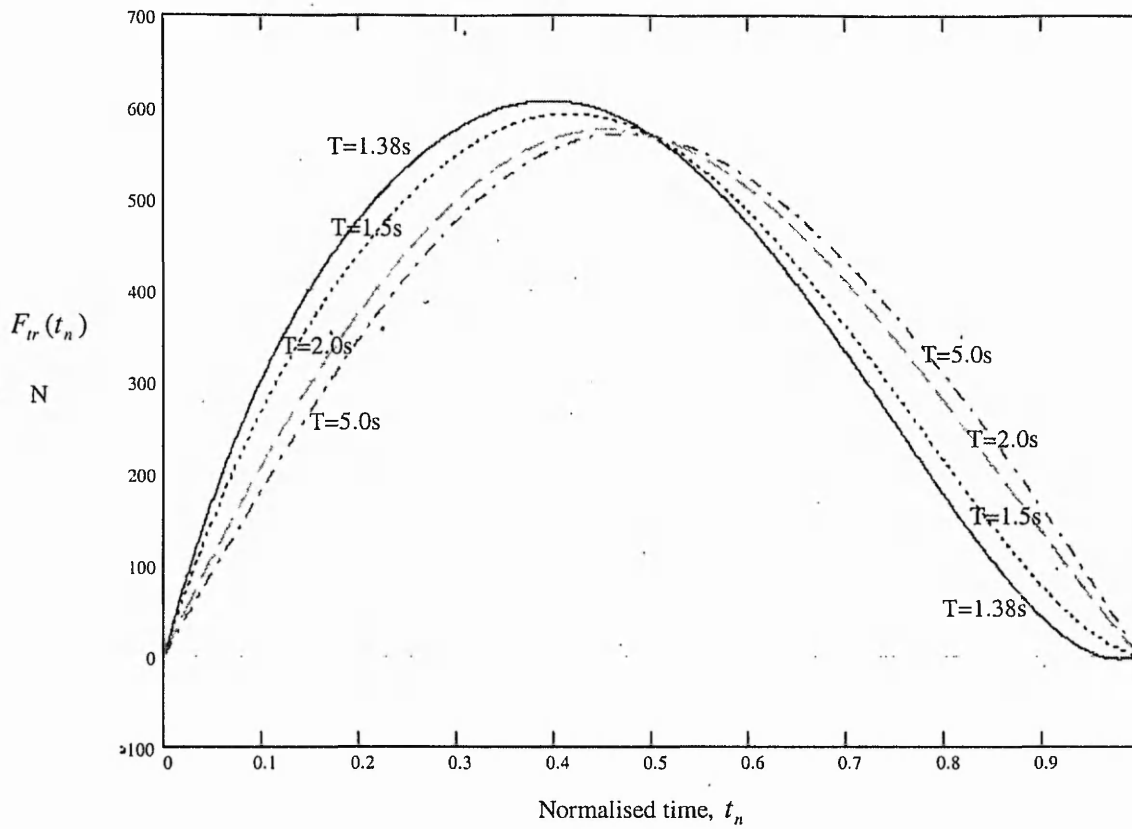


Figure 5.5 Traction force requirement when manoeuvre time span $T \geq 1.38\text{s}$.

in this case study, a minimum manoeuvre time of 1.38 seconds is needed to ensure that there is no change in the traction mode.

As is known from traction control literature [73-74], there is a limitation to the maximum traction force that can be generated by a wheel-ground interface due to friction force saturation. Consequently, the maximum traction force requirement in Figures 5.4 and 5.5 may not exceed the saturation friction force, which is determined by the property and condition of the traction surface. For example, a dry pavement has a larger saturation friction force than a wet pavement, providing all other conditions remain the same. The results also show that the maximum traction force requirement decreases as the manoeuvre time increases. In order to achieve an effective motion control for the WMR crossing an obstacle, an appropriate manoeuvre time should be

selected based on a prior knowledge of the friction characteristics associated with the traction surface.

5.4 Summary Comments

A novel approach to trajectory planning of WMRs traversing localised obstacles has been presented. The method, which is based on a dynamic model of the robotic vehicle, takes into account all forces including translational as well as rotational inertia forces. It has been demonstrated that, during obstacle traversing a compromise can be achieved between the minimal time of manoeuvre and each of the following parameters: vehicle traction force, inertia load and jerk. The shift between the traction mode and braking mode of the actuators can be avoided by an appropriate choice of a minimum time of manoeuvre, and hence the velocity of the platform. A basis for the selection of an appropriate manoeuvre time based on a prior knowledge of the friction characteristics of a traction surface has also been provided. The maximum traction force requirement decreases as the manoeuvre time increases resulting in the reduction of the maximum load on the actuators.

Chapter 6

Wheel Impact Control

6.1 Introduction

When a WMR navigates an uneven terrain or is involved in complex manoeuvres over obstacles in a generally smooth terrain such as shown in Figure 6.1, collisions between the wheels and the surface irregularities are almost always inevitable giving rise to impact dynamics problems. This problem had not been

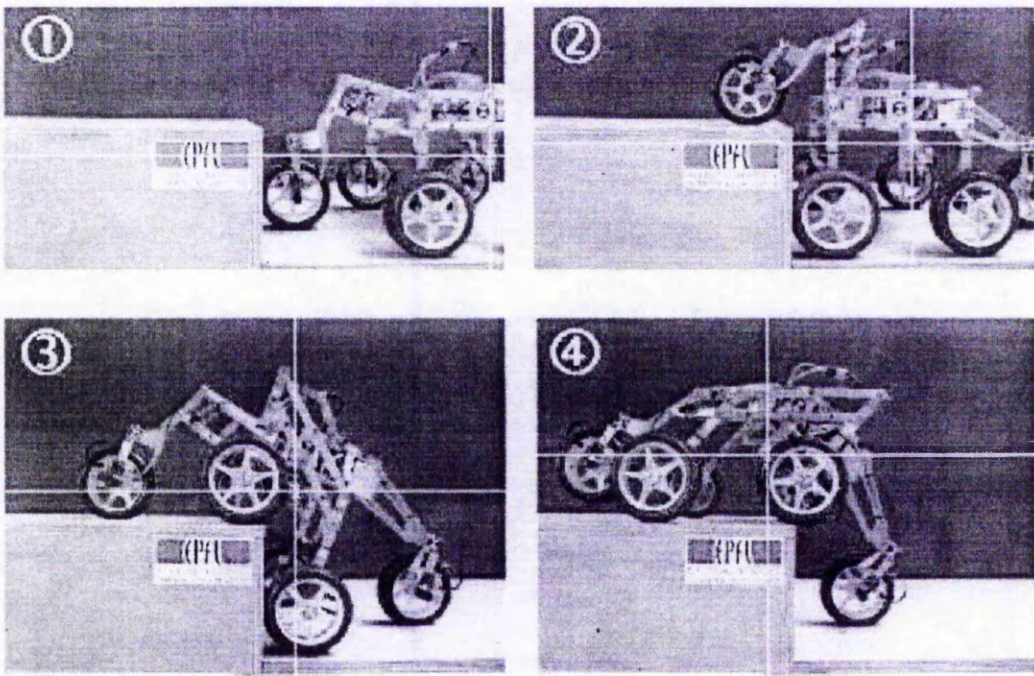


Figure 6.1 An application of a mobile robot climbing a step obstacle [17].

considered during rigid body dynamics formulations given in earlier Chapters 4 and 5 for the purpose of simplifications. Assumptions were made that the obstacles had smooth geometry that allows the steady contact interaction between the ground surface and the wheels. This assumption will now be relaxed to analyse the effect of the interaction of the WMR's wheels with a ground surface that has an abruptly changing geometry.

Wheel-ground impact of WMRs has adverse effects on the payload stability, safety, accuracy and proper functioning of delicate sensors and computational hardware aboard the robot. It also adversely affects the wheel-ground grip capability of the WMR. The wheel-ground grip is essential to maintain the WMR's handling controllability, because traction and steering forces can only be generated if there is contact between the wheels and the ground. There is thus a potential for functional hazards caused by wheel-ground collisions which may occur during a manoeuvre on an uneven surface. It is intended here to model the problem and to propose a remedying technique that addresses some of the problems related to wheel-ground impact.

An established contact between a wheel and a ground surface persists either until a geometric discontinuity arises or the velocity of the contact point on the wheel is directed away from the contact surface [68,75]. The later type of contact loss occurs due to the time history of the acceleration of the wheel that may eventually lead to the breaking of the contact. Any subsequent reestablishment of contact following a previous contact loss occurs, in general, with impact that induces structural vibrations, operational noise and harshness in payload handling.

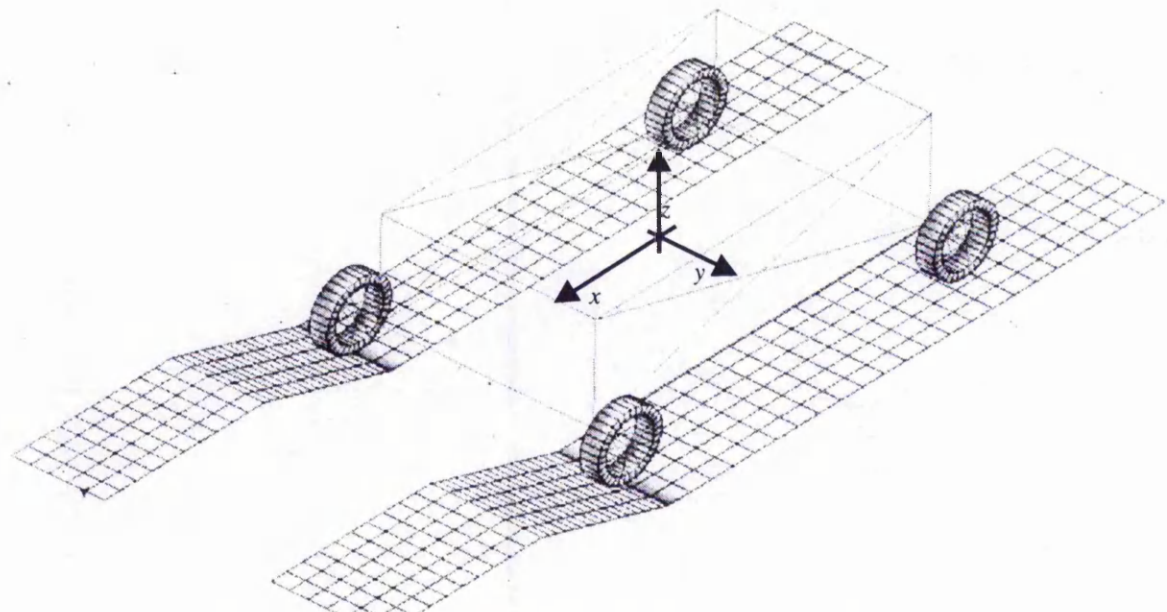


Figure 6.2 A WMR colliding with a ramp obstacle.

Consider the straight path motion of a mobile platform on a planar surface as shown in Figure 6.2 when its wheels encounter a surface irregularity that imposes a new constraint on the planar motion of the WMR. The WMR has a single degree of freedom, i.e. a longitudinal motion along its x -axis, just before encountering the obstacle. Assuming that the wheels will strictly follow the new constraint imposed by the surface irregularity new degrees of freedom of motion of the WMR are born due to the interaction between the road surface and the wheels. These new degrees of freedom are the pitching (rotational motion about the WMR's y -axis) and translational motion in the normal direction (along the WMR's z -axis). The transition between the single degree-of-freedom motion and the three-degree-of-freedom motion over the obstacle is marked by discontinuities in the pitching rotational velocity and in the velocity along the WMR's normal direction. Just before encountering the obstacle the platform has zero pitch angular velocity and zero normal velocity, whereas right after coming into contact with the ground obstacle it will have non-zero pitch angular and non-zero normal translational velocities. Theoretically the rates of change of velocities of the respective motions, which are the pitching and normal accelerations, are infinite at the discontinuities. These 'infinite' accelerations are accompanied by impulsive forces that are large in magnitude and which act in a differentially small time span. These impulsive forces come from the environment by means of reaction forces that are transmitted from the ground surface through the wheels and then to the chassis.

In actual cases transition between plane motion and pitching motion differs from the theoretical consideration described above for the following reasons.

- In reality both the impulsive reaction forces and their time duration are finite. This implies that the transition between the planar motion and the pitching motion occurs in a finite period of time, which is equal to the duration of the impulsive forces.
- The locality of the wheel where the contact takes place has a finite stiffness and deforms due to the impulsive reaction forces generated by the environment. The deformation is a function of the material property as well as the impulsive forces, which are in turn dependent on the velocity of approach

at the locality of collision. This localised deformation can be viewed as a contact vibration with stiffness, damping and an inertia matrix.

- Multiple collisions between the wheel and the ground may follow especially if the impact zone is stiff, if the damping is low and if the approach velocity is high. Thus the transition between the planar motion and the pitching motion could be the result of multiple events of impact rather than a single one.

Several ways of modelling impact have been proposed in the literature. The most common approach is the Newton relationship. In this approach impact is characterised by a constant called the coefficient of restitution which is a function of the material properties of the colliding bodies. The coefficient of restitution, which is defined as the ratio between the relative velocity of separation of the colliding bodies to the relative velocity of approach, is a measure of kinetic energy dissipation due to impact. Hence a coefficient of restitution of 1.0 is for a completely elastic collision where kinetic energy loss is minimum and a value of 0 is used for a completely plastic collision where kinetic energy loss is maximum and the impacting bodies move with the same velocity after collision. This method, although suitable for rigid-body dynamic simulations, relies on a prior knowledge of the coefficient of restitution, a parameter difficult to measure except for very simple cases such as bouncing of spherical balls. This modelling technique is not suited to devising an impact control technique based on contact deformations.

Another approach of evaluating impact forces often used in the stress computation literature is the empirical approximation of the contact forces [76]. In this method the impact forces are given as functions of the elastic properties of the colliding bodies and the deformation in the localised geometry of the impact. In most cases the deformation is measured as a scalar, one-dimensional elastic compression that is used to approximate the rather complex deformation at the contact region. The contact force is related to the contact deformation by an expression of the form:

$$F = C x^n \quad (6.1)$$

where F is the contact force, C is a constant depending on the elastic properties of the bodies in contact, and n is an empirical constant. A common value for n in elastic collisions with small deformations is 1, whereas $n = 1.5$ is employed for

modelling Hertzian elastic collisions. This approach is claimed to be a reasonably accurate way of evaluating contact and impact forces when the localised deformations are quasi-static, i.e. when the contact deformation dynamics is negligible [76].

The penalty formulation has been successfully used in rigid body dynamics simulations to predict impact-contact constraint forces [80]. In this method the contact regions are replaced by linear springs and dash-pots and the resulting contact dynamic equations will be linear as long as contact is maintained. Hence, the contact force is related to the deformation by the relationship:

$$F = k x + c \dot{x} \quad (6.2)$$

where k is a contact stiffness and the c is a damping constant. This approach best represents the actual physical interaction of colliding bodies. This is because the effect of contact is to generate local deformations while the reaction forces (and the associated impulse) generated will be transmitted to the rest of the structure to induce both stress waves as well as rigid body impulsive motions.

In this work it is assumed that while the rigid-body motion of the WMR is the source and sink of the energy transferred during impact, the states (position, orientations and their corresponding velocities) of the WMR are independent of the localised deformations at the contact points. The reaction forces at the contact points are assumed to be the only links that connect the rigid body motion of the WMR and the deformation at the wheel-ground contact points. For this purpose the results of the contact dynamics equations developed for rigid body analysis will be modified in order to take account of the deformations at wheel-ground contact points. While the deformation pattern at the area of the wheel-ground contact is very complex in this work it is approximated by a one-dimensional elastic compression. It is also assumed that at a given instant each wheel of the WMR makes contact with the ground surface only in one contact-area as opposed to multiple contacts.

6.2 Modelling and Control of Impact for WMRs

While the impact/contact of stationary manipulators has been a subject of several recent research work there is no similar reported work on mobile robots

interacting with wheel obstacles, to the best of the knowledge of the author. Wheeled mobile robots are essentially different both in structure and application from stationary manipulators. WMRs exert actuation effort through the contact points by means of traction, while robot manipulators often exert actuation effort through joints. This means for WMRs it is necessary that physical contacts be maintained with the environment (i.e. with the ground surface) in order that actuation is possible. Whereas for stationary manipulators actuation is possible even if the end-effector of the manipulator is not in contact with the environment. Another important distinction

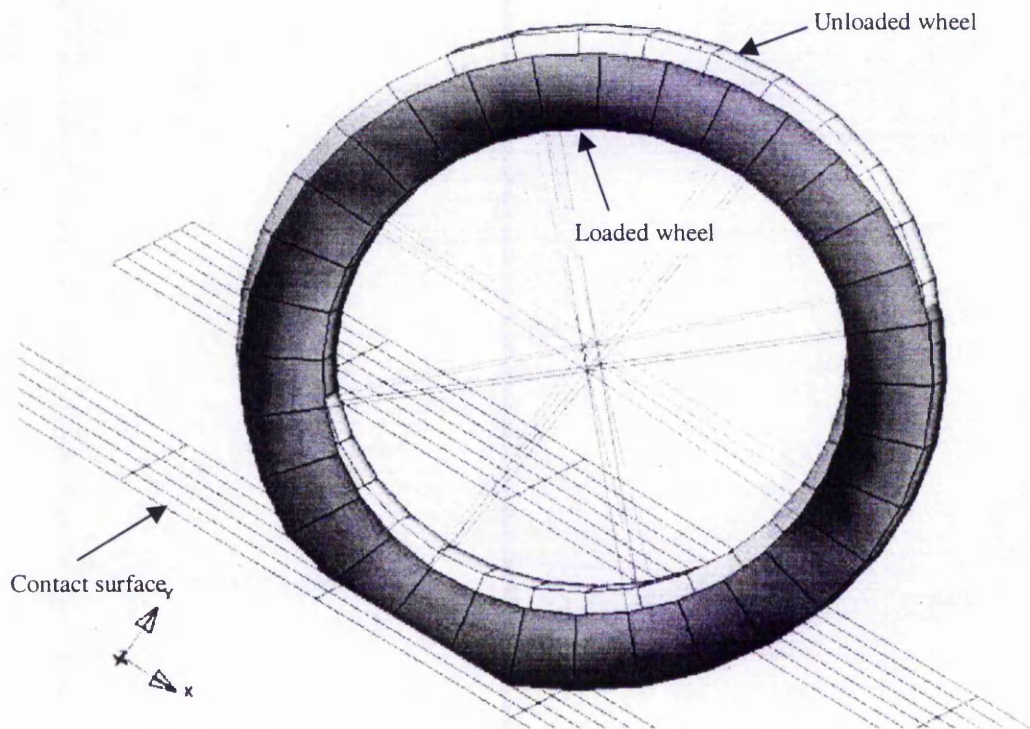


Figure 6.3 Deformation of a cylindrical wheel due to central load and contact reaction.

exists in the structure of the equations of motion of stationary manipulators and WMRs. Kinematic constraints are determined relatively in a straightforward manner in the case of stationary manipulators, which are often holonomic. Kinematic constraints for WMRs are non-holonomic in nature, which are less straightforward to handle. This problem is further compounded for WMRs navigating an uneven terrain due to the extra geometric complexity brought about by the shape of the ground

profile. In addition most manipulator tasks involve single-point contact with the environment and previous research work has been concerned on this special case. Whereas WMRs in general make multiple contacts with the environment, the maximum number of simultaneous contacts being equal to the number of wheels the robot consists. Therefore WMR impact/contact dynamics is a multivariable system.

In robotic manipulators systems kinematic constraint equations are employed to solve the equations of motion. Such kinematic constraint equations are difficult to formulate for a WMR travelling on uneven terrain. An alternative way modelling the contact-impact dynamics problem can be obtained through an implicit expression that relates the contact point deformations to the reaction forces from the environment. It has been shown in the treatment of rigid body dynamics of WMRs in earlier chapters (see Chapters 4 and 5) that it is possible to find an expression for the wheel-ground contact point acceleration. This contact point acceleration (\vec{a}_n) has been described in Equations (4.31) and (4.32) in terms of a characteristic matrix (P) of the WMR, a vector (\vec{b}) and a reaction force vector \vec{F}_n from the environment. It has also been shown in Chapter 4 that the P matrix depends on the geometrical and inertial properties of the WMR and on the wheel-ground contact geometry. The vector \vec{b} depends on the wheel traction forces, velocity and configuration of the WMR, the

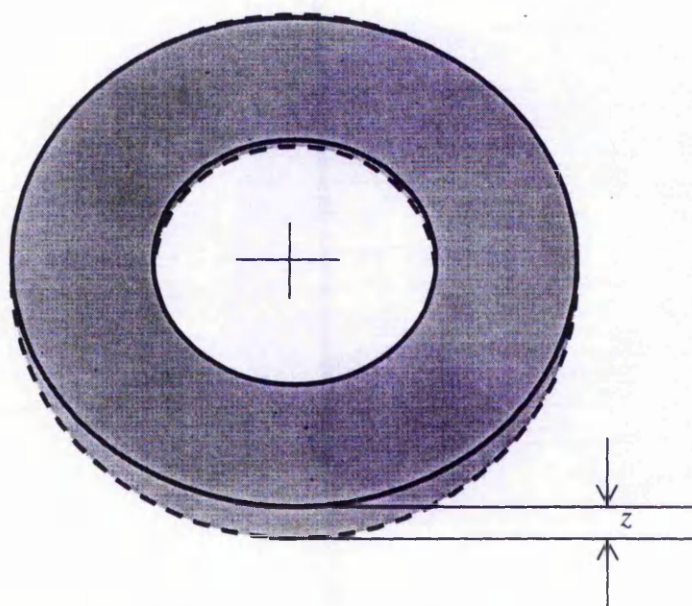


Figure 6.4 Definition of wheel deformation coordinate.

wheel-ground contact angle and gravity. Namely the relationship was written as:

$$\vec{a}_N = P\vec{F}_n + \vec{b} \quad (6.3)$$

For rigid body analysis purposes of a WMR the acceleration vector \vec{a}_N had been equated to zero in order to satisfy the non-interpenetration constraint of rigid bodies. The solution for \vec{F}_n was then found by matrix inversion as $\vec{F}_n = -P^{-1}\vec{b}$. The rigid body assumption needs however to be relaxed in order to account of the wheel deformation that takes place during wheel-obstacle impact/contact. The assumption that the ground surface is a rigid body will be retained because the flexibility of rubber wheels of WMRs is much higher than most hard ground surfaces. Thus the normal acceleration vector now represents the deformations of the wheels along the normal (radial) direction of each wheel of the WMR in contact with the ground surface.

A loaded cylindrical wheel contacting a ground surface will distort as shown in Figure 6.3 because of contact asperities. The radial deformation z is a function of the load and the elastic properties of the rubber wheel. This radial deformation has been shown in Figure 6.4 that has been sketched so that the geometric centres of the loaded and unloaded wheel coincide. It is assumed that the wheel deformations are very small in comparison to the size of the wheel so that the relationship between the load, the elastic modulus of the wheel material and the radial deformation is linear.

Defining an elastic deformation vector, \vec{z} , of length N at the wheel-ground contact points, the contact point acceleration vector \vec{a}_N can be written as:

$$\vec{a}_N = \vec{z} \quad (6.4)$$

where N is the number of wheels of the WMR in contact with the ground.

Substituting for \vec{z} into Equation (6.3) from Equation (6.4) we have,

$$\vec{z} = P\vec{F}_n + \vec{b} \quad (6.5)$$

Equation (6.5) is the dynamics model of the WMR, which takes into account wheel deformations. The aim is to control the wheel deformations \vec{z} during impact so that a permanent grip of the deformation, without any rebound, can be achieved.

In previous impact control strategies employed in the robotic manipulator literature, such as impedance control, it is assumed that the task space displacements which are equivalent to the wheel radial displacements of WMRs, z , the velocity \dot{z} are assumed to be accessible for measurement. In stationary manipulators these variables can be obtained indirectly from joint coordinate measurements which can be transformed into task space coordinates (end-effector position) thanks to kinematic equations relating the task displacement to the joint displacement. However, in WMRs that navigate uneven terrain it is very difficult to obtain these measurements for the following reasons:

- It is difficult to implement kinematic relationships which can be used to transform joint coordinate measurements to task space displacements where these task space displacements corresponds to the wheel contact point motions. If such a scheme could successfully be implemented it would be possible to measure the deformation of the wheel (and its derivatives) from wheel encoder measurements which measure wheel rotations. Surely this is a difficult task.
- It is not practical to obtain wheel deformation measurements directly by using sensors such as strain gages because the deformations are very small and they occur at a rather high rate.

An alternative approach to alleviating this problem can be found by recognising the fact that for robotic wheels rolling on a stiff environment the stiffness term is much higher than the inertia and the damping terms in the wheel deformation dynamics. Thus, instead of monitoring the deformations the reaction forces can be used to characterise the impact dynamics. The stiffness of the wheel that relates the wheel deformations to the reaction forces can be measured by experimental means quite accurately. Hence for a single wheel, if the contact force is measurable the contact deformation can easily be computed from the relationship:

$$z = \frac{F_n}{k_w} \quad (6.6)$$

where F_n is the measurable reaction force and k_w is the experimentally determinable wheel radial stiffness. The time rates of changes of z , namely \dot{z} and \ddot{z} , can be estimated by successive differentiation of z .

In order to regulate the contact deformation, and thus the reaction force, during and after wheel-ground impact it is proposed here to devise a controller with the wheel deformation vector \vec{z} as the control variable. Thus, substituting for F_n into Equation (6.5) from Equation (6.6) for each wheel we have:

$$\ddot{\vec{z}} = P k_w \vec{z} + \vec{b} \quad (6.7)$$

or substituting $K = -P k_w$ and $\vec{v} = \vec{b}$ into Equation (6.7),

$$\ddot{\vec{z}} + K \vec{z} = \vec{v} \quad (6.8)$$

Therefore a control law:

$$\vec{v} = -h_0(\vec{z} - \vec{z}_R) - h_1(\dot{\vec{z}} - \dot{\vec{z}}_R) + \ddot{\vec{z}}_R - K z \quad (6.9)$$

stabilises Equation (6.8) about a desired reference \vec{z}_R , where \vec{z}_R is a twice-differentiable reference trajectory tracked by the contact point deformation vector \vec{z} . h_1 and h_0 are positive constants chosen so that the desired transient behaviour can be achieved. A similar control law has been used by Tornambe [78] to control a one-dimensional, head-on impact between two flat objects. Under the control law Equation (6.8) becomes:

$$(\ddot{\vec{z}} - \ddot{\vec{z}}_R) + h_1(\dot{\vec{z}} - \dot{\vec{z}}_R) + h_0(\vec{z} - \vec{z}_R) = 0 \quad (6.10)$$

or substituting a tracking error, $\vec{e} = \vec{z} - \vec{z}_R$, in Equation (6.10)

$$\ddot{\vec{e}} + h_1\dot{\vec{e}} + h_0\vec{e} = 0 \quad (6.11)$$

where \vec{e} is the error vector.

As defined in Chapter 4 (Equation 4.32), the vector \vec{b} in Equations (6.5) and (6.7) consists of terms dependent on the wheel traction forces, on the velocity of the WMR and on the body forces. Thus \vec{b} can be written as a sum of its components. That is,

$$\vec{b} = U \vec{F}_a + \vec{b}_g \quad (6.12)$$

where \vec{F}_a is the vector of wheel traction forces, U is the matrix which projects the traction forces into the wheel-deformation coordinates, and \vec{b}_g is the sum of body force and velocity dependent terms.

Thus the traction force at the wheels corresponding to the vector \vec{v} can be obtained as follows. Since,

$$\vec{v} = \vec{b} = U \vec{F}_a + \vec{b}_g \quad (6.13)$$

solving for \vec{F}_a ,

$$\vec{F}_a = U^{-1}(\vec{v} - \vec{b}_g) \quad (6.14)$$

Equation (6.14) describes the traction force \vec{F}_a needed to be generated by the wheels in order to stabilise the wheel deformations about the desired reference trajectory \vec{z}_R according to the control law specified by Equation (6.9).

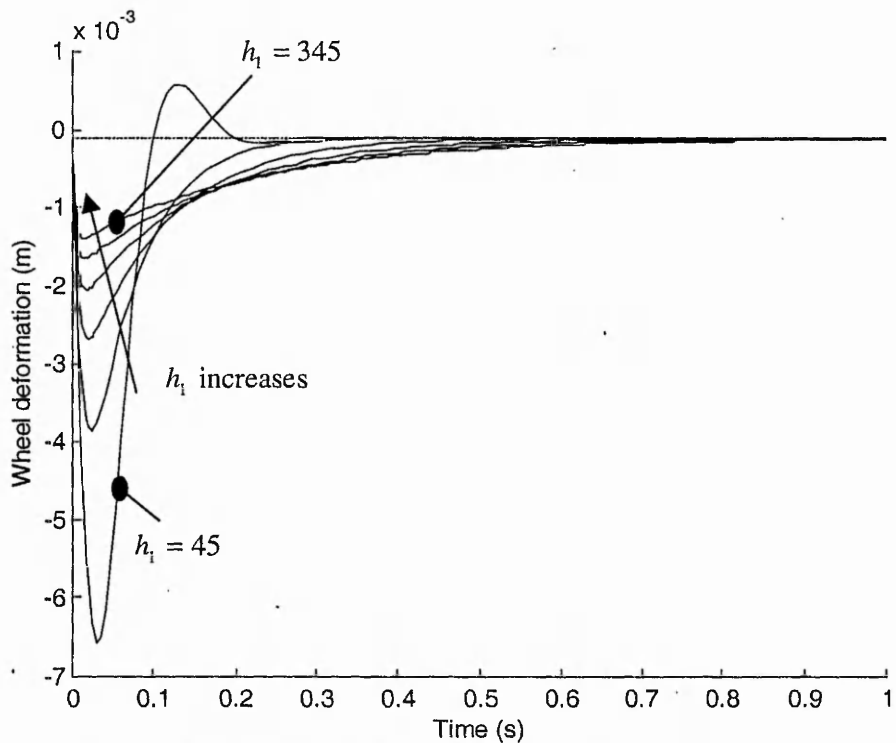


Figure 6.5 The effect of variation of h_1 on the settling time after impact at the front wheels ($h_0 = 1500$).

6.3 Case Study

A WMR colliding with a ramp obstacle while travelling along a straight path has been considered. The vehicle dimensions are given in Table 6.1, which are similar to the cases considered in Chapters 4 and 5. The parameters P and U derived earlier in Chapter 4 are employed here. We seek to control the deformations (and thus the wheel-ground reaction forces) on all wheels of the WMR in such a way that wheel-ground grip is attained immediately after impact on all wheels. The rear wheels are on a flat surface, while the front wheels collide with a ramp obstacle of inclination $\gamma = 0.3 \text{ rad}$ (17°) from the horizontal (Figure 6.2).

In order to investigate the effects of the proportional and the damping gains (h_0 and h_1 in the control law Equation 6.9) on the control system a series of simulations of the system given by Equation (6.7) have been carried out by using the MATLAB® software. A step trajectory has been employed as the desired deformation

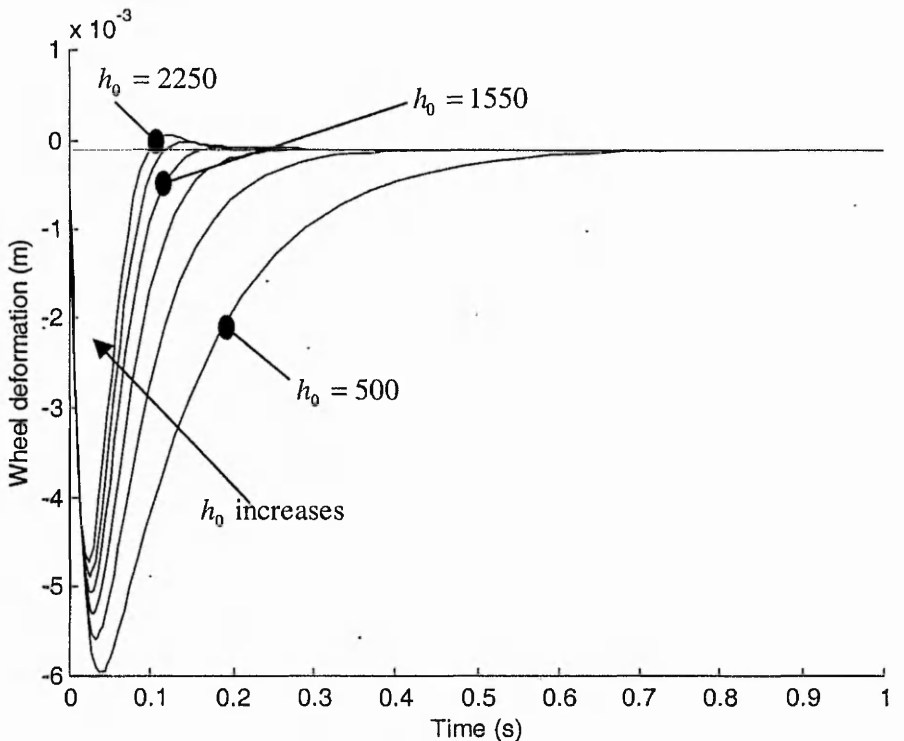


Figure 6.6 The effect of variation of h_0 on the settling time after impact at the front wheels ($h_1 = 70$).

of the wheels. Figure 6.5 shows the time histories of the wheel deformations of the impacting front wheel for increasing values of the damping gains h_1 . It is evident from Figure 6.5 that as the damping gain increases the desired wheel deformation is attained slower. If h_1 is below a critical value of 65.0 for this plant then oscillatory behaviour is observed, which corresponds to wheel rebound immediately after impact. The effect of the proportional gain, h_0 , on the system dynamics is illustrated in Figure 6.6. It is seen that as h_0 increases the settling time decreases, higher values causing the system to oscillate which corresponds to rebound of the impact. This observation is similar to the behaviour of PD controlled systems where a proportional controller has the effect of reducing the rise time and will reduce the steady state error. A derivative control has the effect of increasing the stability of the system, reducing the overshoot, and improving the transient response [81]. An integral control makes the transient response worse even if it has an effect of eliminating the steady-state error. In impact control the most important performance is the transient response hence in this work an integral term has not been considered.

In Figures 6.7 and 6.8 the wheel deformations and the corresponding actuator (traction) forces are plotted for an optimal set of control parameters $h_0 = 70.0$ and $h_1 = 1500$. It is assumed that both the front and the rear wheels are undeformed just before impact ($z_{0f} = 0.0$, $z_{0r} = 0.0$). The initial velocity at which rate the rear wheels deform is assumed to be zero. The front wheels initially deform at the rate equal to the velocity of approach of the wheel contact point to the surface of the obstacle along a direction normal to the surface. The velocity at which the front-wheel contact point approaches the ramp obstacle, which is inclined at an angle of 0.3 rad (17°), is found to be 0.6 m/s when the WMR's horizontal velocity is 2 m/s. Thus $\dot{z}_{0f} = -0.6$ and $\dot{z}_{0r} = 0.0$. The final deformations of the wheels are chosen to be $z_{Rr} = -0.01$ for the rear wheels and $z_{Rf} = -0.02$ for the front wheels. The total time of simulation is 0.2 seconds. The radial stiffness of the wheels of the WMR is $k_w = 5.6E6 \text{ N/m}$. It is seen from Figure 6.8 that the desired wheel deformations are attained in relatively small period of time of about one tenth of a second. The rear

wheels, which are not directly involved in the impact, approach the desired deformation slower than the front wheels. This can be attributed to the initial rate of deformation the rear wheels which is zero. The front wheels having an initial rate of deformation equal to the normal velocity of impact approach the final deformation at a faster rate.

The effect of the wheel stiffness on the actuation effort needed to control the impact has been analysed by computing the traction forces for two different types of wheels, one hard and a soft wheel. The soft wheel has a stiffness of 75% of the hard one. The results have been plotted in Figure 6.9. It can be seen that the soft wheels demand a lower magnitude of traction forces, and thus a lower power demand on the actuators. This is an indication that from the point of view of impact control soft wheels are more favourable than hard wheels.

Table 6.1 Dimensions of the WMR used in the simulation.

Symbol	Description	Value
L_f	Longitudinal distance of front axle from the vehicle centre of mass	0.6 m
L_r	Longitudinal distance of rear axle from the vehicle centre of mass	0.46 m
h	Height of centre of mass from the wheel centres	0.4 m
R	Radius of wheels	0.1 m
I_y	Pitch moment of inertia of the platform	$47 \text{ kg}\cdot\text{m}^2$
m	Mass of the platform	170 kg

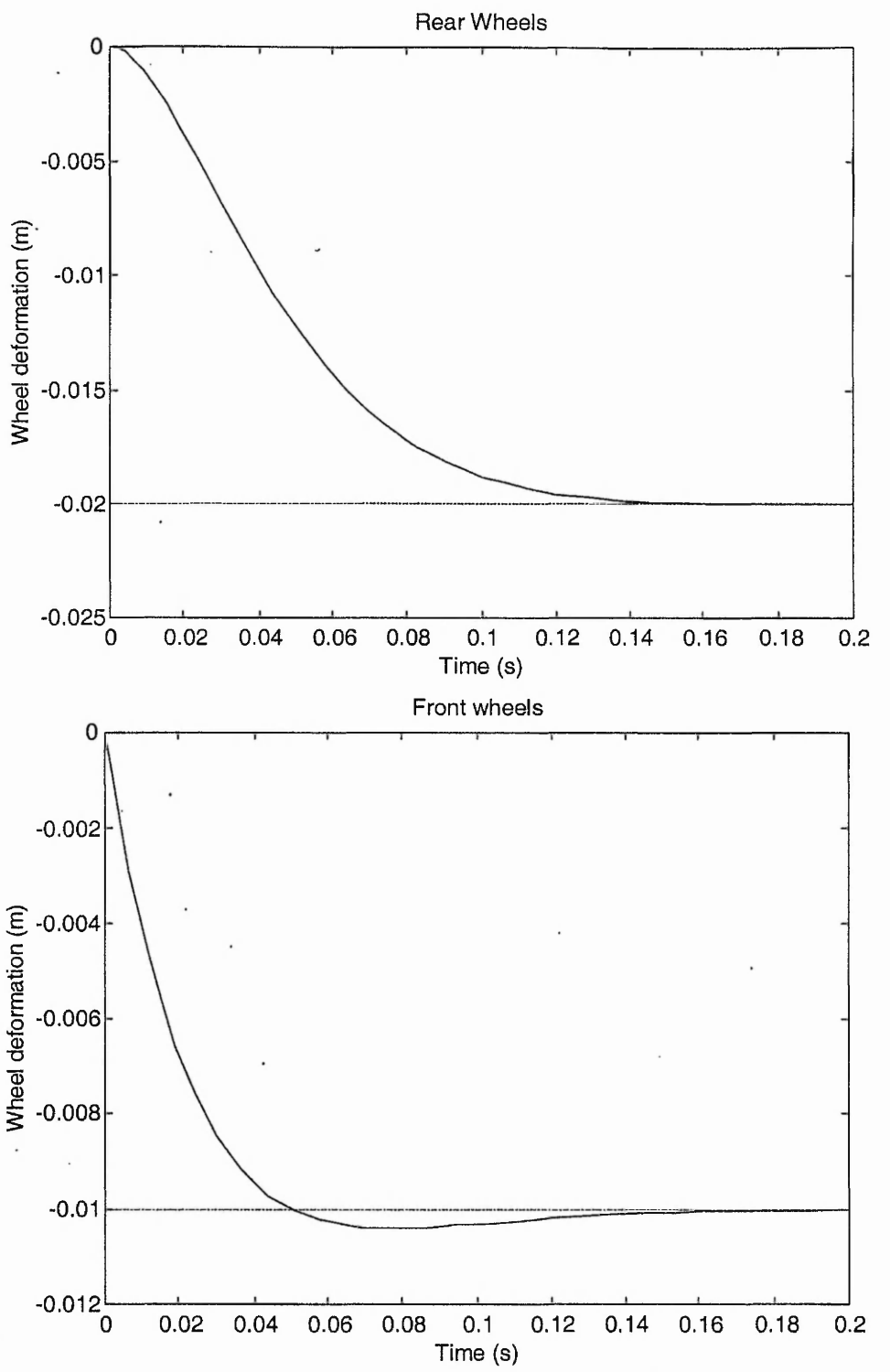


Figure 6.7 Variation of the wheel deformations.

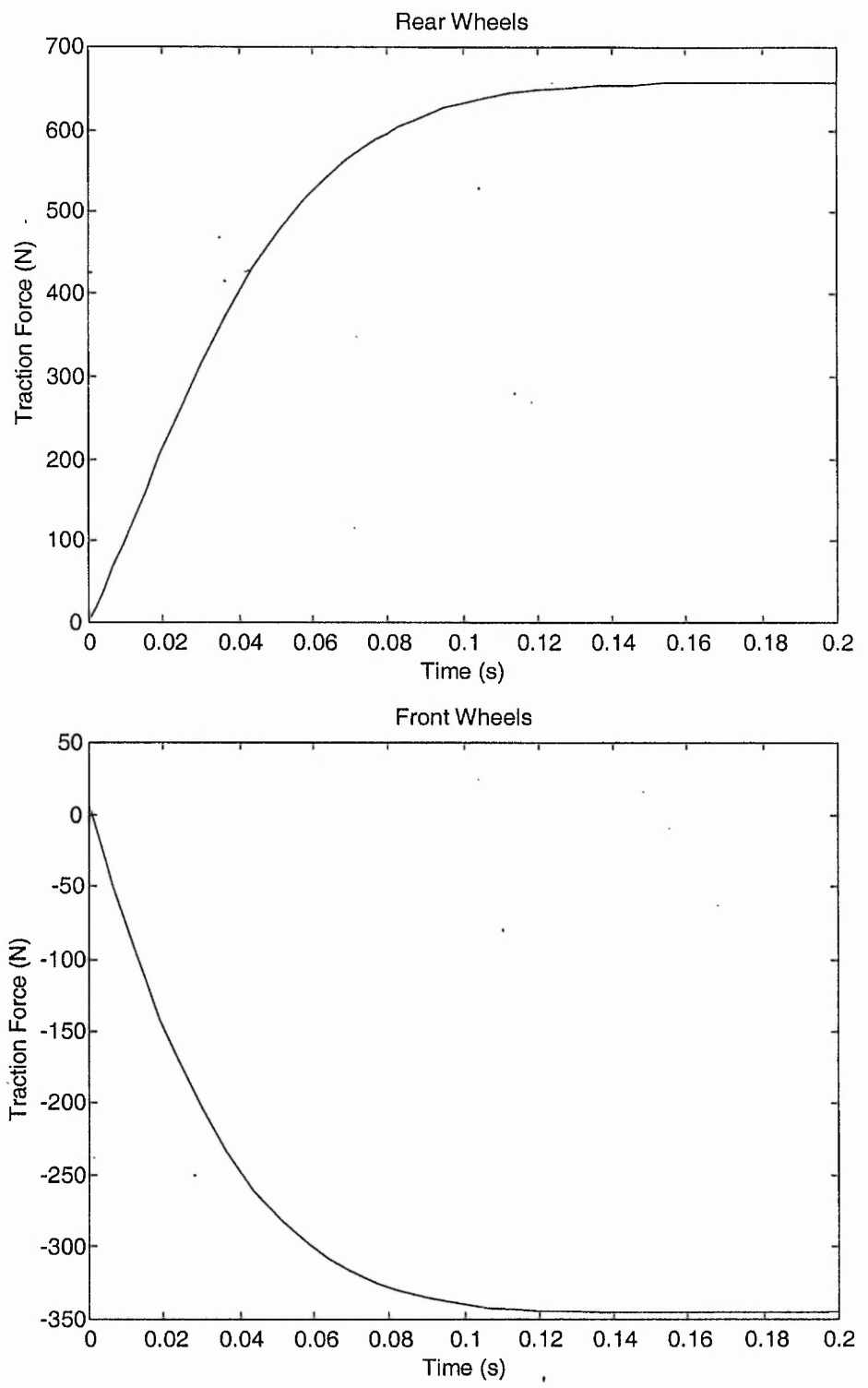


Figure 6.8 Variation of the actuation forces.

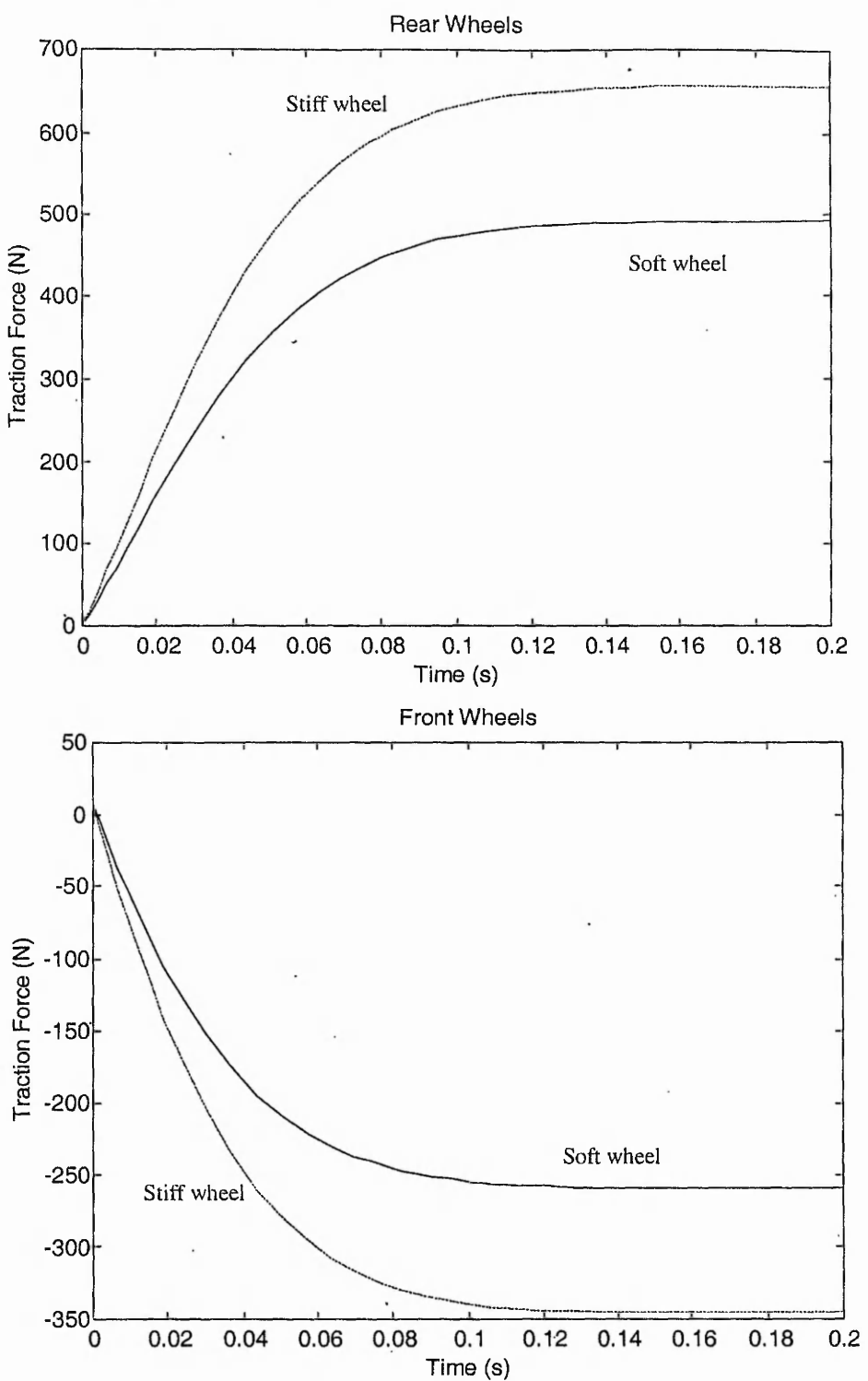


Figure 6.9 The dependency of the actuation effort on the stiffness of the wheel, k .

Stiff wheel $k = 5.6E6 \text{ N/m}$, **soft wheel** $k = 4.1E6 \text{ N/m}$.

of the profile. It has also been that an identical zero-jerk contour line is present in both components of the translational motions (vertical and longitudinal), as well as the pitch angular rotation. Hence, it can be concluded that for a given profile gradient, an appropriate traction force can be determined and applied to the wheels in order to ensure that the jerk in all motions is instantaneously zero. It should be noted that the longitudinal jerk and the longitudinal acceleration can not be simultaneously zero. The desired state is for the jerk to remain at zero throughout the duration of the motion of the mobile robot. This requires that the robot's longitudinal acceleration be positive.

4. Conclusions

A technique has been presented for the minimisation of jerk during longitudinal manoeuvre of a wheeled mobile robot traversing fixed road obstacles, which have positive gradient geometry. This can be accomplished by controlling the traction forces applied at the wheels. The traction force requirement for a given application can be determined from knowledge of the geometry of the road profile and vehicle dimensions.

5. References

1. Z. Deng and M. Brady, "Dynamics and Control of a Wheeled Robot," *Proceedings of the American Control Conference*.
2. M. G. Mehrabi and A. Hemami, "Dynamic Modelling of Wheeled Mobile Robots. Theory and Experiment," *Second IEEE Conference on Control Applications*. September 1993.
3. J.C. Alexander and J.H. Maddocks, "On The Kinematics of Wheeled Mobile Robots," *The International Journal of Robotics Research*. Vol. 8, No. 5. Oct 1989.
4. T. Simeon, "Motion Planning for a Non-holonomic Mobile Robot on 3-dimensional Terrain," *IEEE/RSJ International Workshop on Intelligent Robots and Systems, IROS'91*.
5. A. Hait and T. Simeon, "Motion Planning on Rough Terrain for an Articulated Vehicle in Presence of Uncertainties," *IEEE International Conference on Intelligent Robots and Systems, 1996*.
6. F. Ben Amar, Ph. Bidaud and F. Ben Ouezdou, "On Modelling and Motion planning of Planetary Vehicles," *Proceedings of the 1993 IEEE/RSJ International Conference on Intelligent Robots and Systems*.
7. R. Featherstone. Robot Dynamics Algorithms, *Kluwer Academic Publishers*. 1987.
8. D. Baraff, "Issues in Computing Contact Forces for Non-penetrating Rigid Bodies," *Algorithmica*, 1993.
9. Z. Shiller and Y. Gwo, "Dynamic Motion Planning of Autonomous Vehicles," *IEEE Transactions on Robotics and Automation*. 1991

6.4 State-Space Formulation

The system in Equation (6.7) can be represented in the conventional state-space form after defining state variables. Let the deformation at the rear wheels be $x_1 = z_1$, the deformation at the front wheels be $x_2 = z_2$. Two more state variables x_3 and x_4 are defined so that $\dot{x}_1 = x_3$ and $\dot{x}_2 = x_4$. We assume that the body forces and the vehicle velocity are independent of the states (i.e. of the wheel deformation) and hence the term \bar{b}_g in Equation (6.12) that is a function of the body forces and the vehicle velocity, can be left out of the state-space formulation. Hence Equation (6.7) can now be written as:

$$\begin{bmatrix} \dot{x}_3 \\ \dot{x}_4 \end{bmatrix} = P k_w \begin{bmatrix} x_1 \\ x_2 \end{bmatrix} + U \begin{bmatrix} F_{tr} \\ F_{tf} \end{bmatrix} \quad (6.15)$$

This equation can be extended to contain all the states. Hence after defining

$$A = \begin{bmatrix} 0 & I \\ P k_w & 0 \end{bmatrix}, \quad B = \begin{bmatrix} 0 \\ U \end{bmatrix}, \quad C = \begin{bmatrix} 1 & 0 & 0 & 0 \\ 0 & 1 & 0 & 0 \end{bmatrix} \text{ and } D = 0, \text{ where } I \text{ is the identity matrix.}$$

The state space representation of the dynamic system (Equation 6.7) is obtained as:

$$\begin{bmatrix} \dot{x}_1 \\ \dot{x}_2 \\ \dot{x}_3 \\ \dot{x}_4 \end{bmatrix} = A \begin{bmatrix} x_1 \\ x_2 \\ x_3 \\ x_4 \end{bmatrix} + B \begin{bmatrix} F_{tr} \\ F_{tf} \end{bmatrix}; \quad Y = C \begin{bmatrix} x_1 \\ x_2 \\ x_3 \\ x_4 \end{bmatrix} + D \begin{bmatrix} F_{tr} \\ F_{tf} \end{bmatrix} \quad (6.16)$$

The pole-placement technique can be applied on this state space form in order to achieve a desired controlled behaviour. In this technique the poles of the dynamic system are chosen in order to satisfy a specified performance criteria. Alternatively a feedback gain can be determined by applying one of the many control design techniques available in the control literature.

6.5 Control with Trajectory Planning

In Chapter 5 a polynomial trajectory planning technique has been devised to control the pitch dynamics of a WMR traversing an obstacle. This technique can also be used to control the wheel-ground impact dynamics after some modifications on the boundary conditions. In the context of the impact dynamics the trajectory-planning problem can be stated as follows. Given the dynamic system Equation (6.7), a control law Equation (6.8), initial conditions \vec{z}_o , $\dot{\vec{z}}_o$, $\ddot{\vec{z}}_o$ and steady state (final) conditions \vec{z}_R , $\dot{\vec{z}}_R$, $\ddot{\vec{z}}_R$ find a feasible trajectory \vec{z}_r , $\dot{\vec{z}}_r$, $\ddot{\vec{z}}_r$ to be tracked by the controller. The feasibility will depend on certain criteria that will result in a favourable performance of the controlled system.

For the impact control system devised earlier the following performance criteria can be considered.

- The trajectory needs to be smooth in order to avoid jerky actuation efforts.
- The maximum actuation effort should not exceed the value that can be generated taking into account the power of the drive motor and the saturation of friction forces between the wheels and the ground.
- The task of stabilising the contact point deformation must be accomplished in as small period of time as possible. It must be noted that the robot is mobile and the geometry of the road surface may be constantly changing therefore it is essential that steady state is achieved in as short period of time as possible.

As the time needed to complete the desired trajectory is inversely proportional to the required control effort, a compromise is often needed between the second and the third criteria mentioned above. Therefore there is a lower bound on the duration of the time in which the task of stabilising the contact point deformation can be completed.

Let $p(t_n)$ be a polynomial trajectory function for the contact point deformation where $t_n = \frac{t}{T}$ is a normalised time scale. t is actual time variable and T

is the total time it takes to complete the stabilisation of the contact point deformation. The initial and final conditions are designed to satisfy four initial conditions and four final conditions with respect to jerk, acceleration, velocity and displacement specified by the polynomial trajectory function $p(t_n)$ and its derivatives. Hence $p(t_n)$ can be devised to be a polynomial of degree seven. That is,

$$p(t_n) = \sum_{i=0}^7 C_i t_n^i \quad (6.17)$$

which has been stated in Chapter 5 as Equation 5.12.

The velocity, acceleration and jerk are subsequent time derivatives of Equation (6.17).

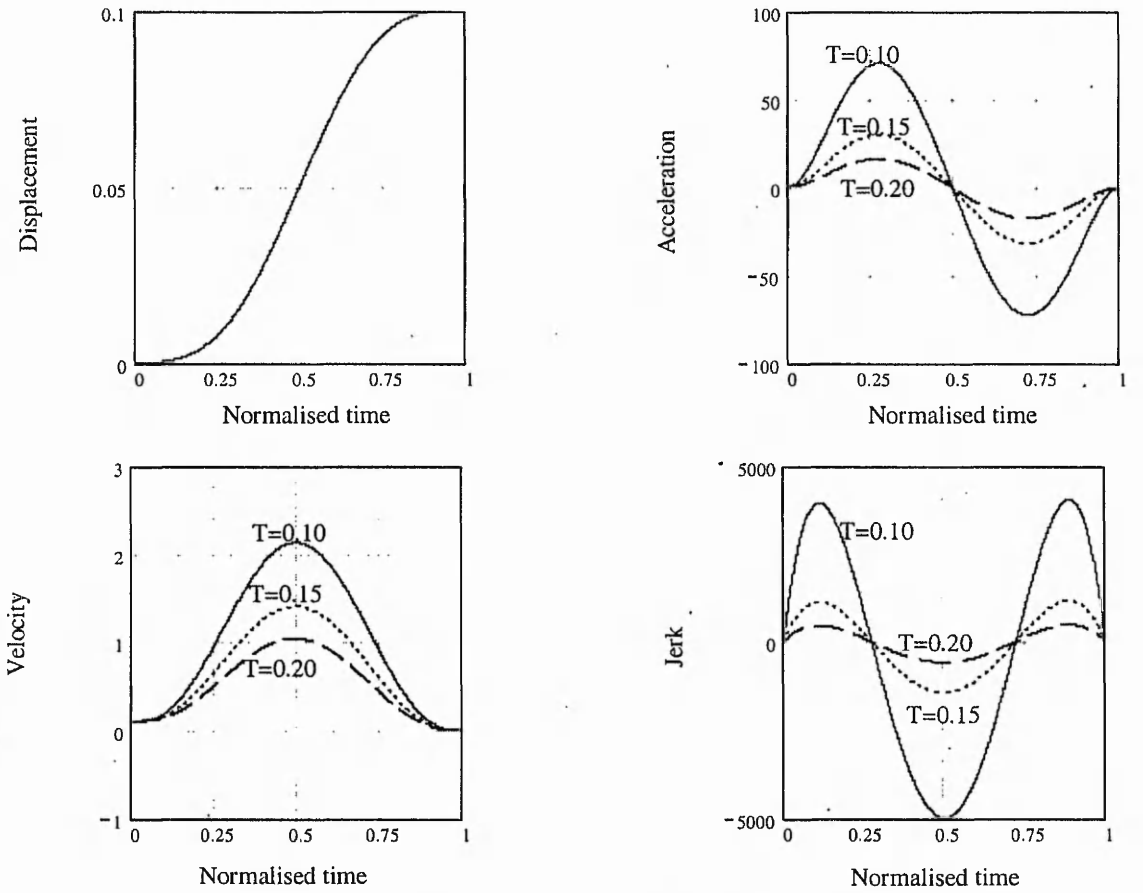


Figure 6.10 The planned trajectory for the front wheel deformations for differing durations of the control.

$$\begin{aligned}
 \dot{p}(t_n) &= \sum_{i=0}^7 i C_i t_n^{i-1} \\
 \ddot{p}(t_n) &= \sum_{i=0}^7 i(i-1) C_i t_n^{i-2} \\
 \dddot{p}(t_n) &= \sum_{i=0}^7 i(i-1)(i-2) C_i t_n^{i-3}
 \end{aligned} \tag{6.18}$$

The initial and final conditions for a deformation at a wheel impact point can be given as:

$$\begin{aligned}
 p(0) &= 0 & p(1) &= d \\
 \dot{p}(0) &= v_0 & \dot{p}(1) &= 0 \\
 \ddot{p}(0) &= 0 & \ddot{p}(1) &= 0 \\
 \dddot{p}(0) &= 0 & \dddot{p}(1) &= 0
 \end{aligned}$$

where d is the final wheel deformation at the contact point and v_0 is the approach velocity of impact between the wheel and the road surface at the contact point. By using these conditions one can solve for C_i , $i = 0..7$ and for the case being considered here they are obtained as:

$$\begin{bmatrix} C_7 & C_6 & C_5 & C_4 & C_3 & C_2 & C_1 & C_0 \end{bmatrix} = \begin{bmatrix} -10 \frac{v_0 T + 2d}{T^7} & 2 \frac{-18v_0 T + 35d}{T^6} & -3 \frac{-15v_0 T + 28d}{T^5} & 5 \frac{-4v_0 T + 7d}{T^4} \\ 0 & 0 & v_0 & 0 \end{bmatrix} \tag{6.19}$$

The displacement, velocity, acceleration and jerk curves have been plotted in Figure 6.10 on a normalised time scale $t_n = \frac{t}{T}$ where t is actual time and T is the duration of the task. As can be seen from this figure the overall jerk decreases as the time allowed for the task of reaching steady state, T , increases.

The trajectory planning process needs to be carried out for all contact points, i.e. for all elements of the vector \bar{z} in Equation (6.7). However the initial conditions may be different for each contact point. For a bicycle model of a platform approaching a front axle obstacle as shown in Figure 6.2 it is reasonable to assume that the contact points at the front have an initial velocity v_0 different from zero and

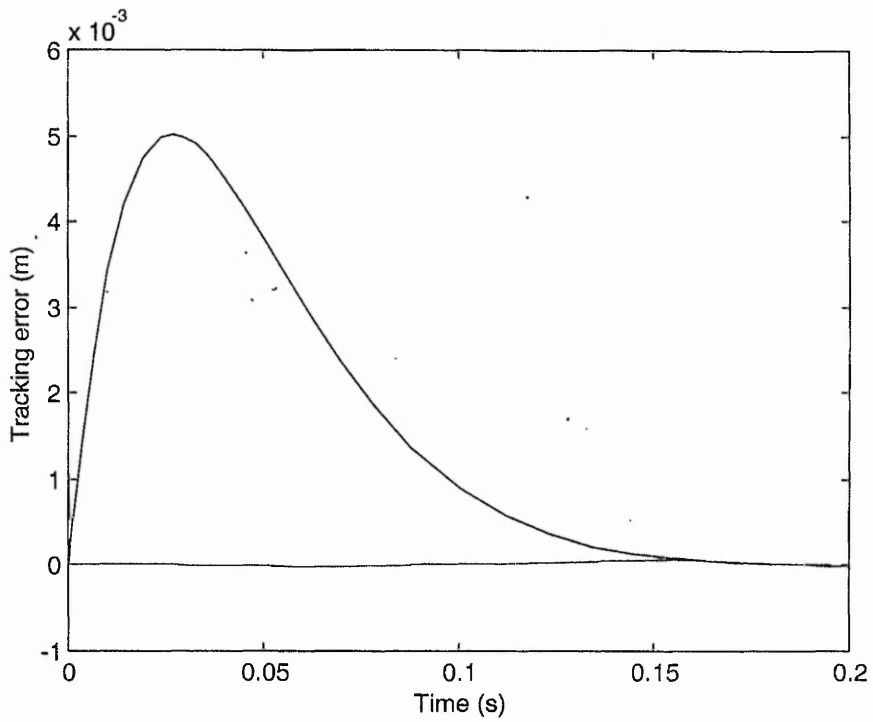


Figure 6.11 Comparison of the tracking errors between a step input and planned trajectory input.

have no initial deformation. This velocity v_0 can be estimated by resolving the longitudinal velocity of the vehicle along the normal direction of the obstacle surface. The rear wheels may have an initial deformation d_0 different from zero and no initial velocity. The final conditions will be equated to a desired steady state condition.

Hence applying the planned trajectory in the control law Equation (6.8) the simulated responses have been obtained. In Figure 6.11 the tracking errors due to step input trajectory and the devised polynomial trajectory have been compared. As can be seen the planned trajectory greatly reduces the tracking error. Also since the trajectory was planned to result in a zero initial and final jerk the actuators will engage and disengage smoothly.

6.6 Implementation Issues

The impact control activity is a transition task that starts with impact dynamics culminating in a desired condition of the wheel deformation without rebound. The work done by the control forces is mainly in damping the transient oscillations at the wheel-ground interface due to the deformations of the wheel.

The impact control strategy can be implemented either in an online, real time, control system where one needs to have deformation sensors, rate of deformation estimator and a trajectory planner or in an off-line scheme. An off-line control approach allows computation of actuation forces *a priori*, which is much more practical, as the phenomenon of impact is too fast for real-time implementations. Off-line computation of input forces eliminates the need for installation of expensive measuring devices for the measurements of the control variables. However, off-line implementation requires accurate modelling of the system. Reasonably accurate information regarding the system parameters, namely, the vehicle dimensions, the

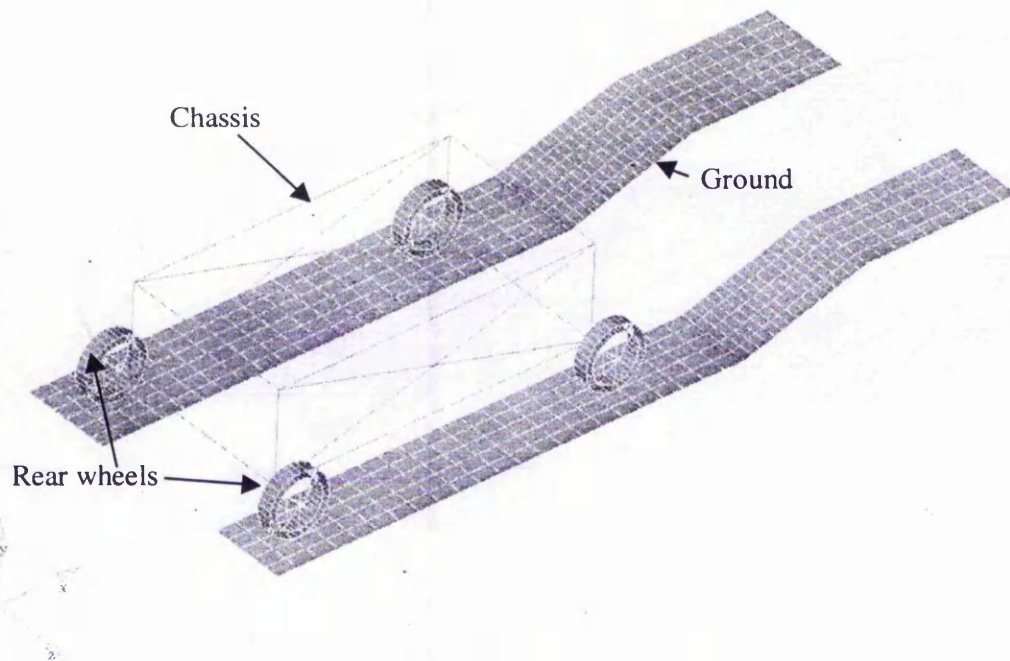


Figure 6.12 A finite model of the WMR used in the case study.

elastic properties of the wheel and the geometry of the obstacle are needed for a good performance of the system. One major advantage of an online implementation is that it can react to errors due to uncertainties in the model and magnitudes of system parameters. In this work the effectiveness of an off-line implementation of the proposed control scheme has been assessed by means a finite element (FE) simulation which is discussed below.

6.7 Finite Element Simulation

Finite element (FE) simulation of the control of the WMR has been used as a validation tool for the performance of the proposed methodology in an off-line control scheme. The advantage of finite simulation over the use of analytically formulated model for the simulation is that it is more realistic because simplifying

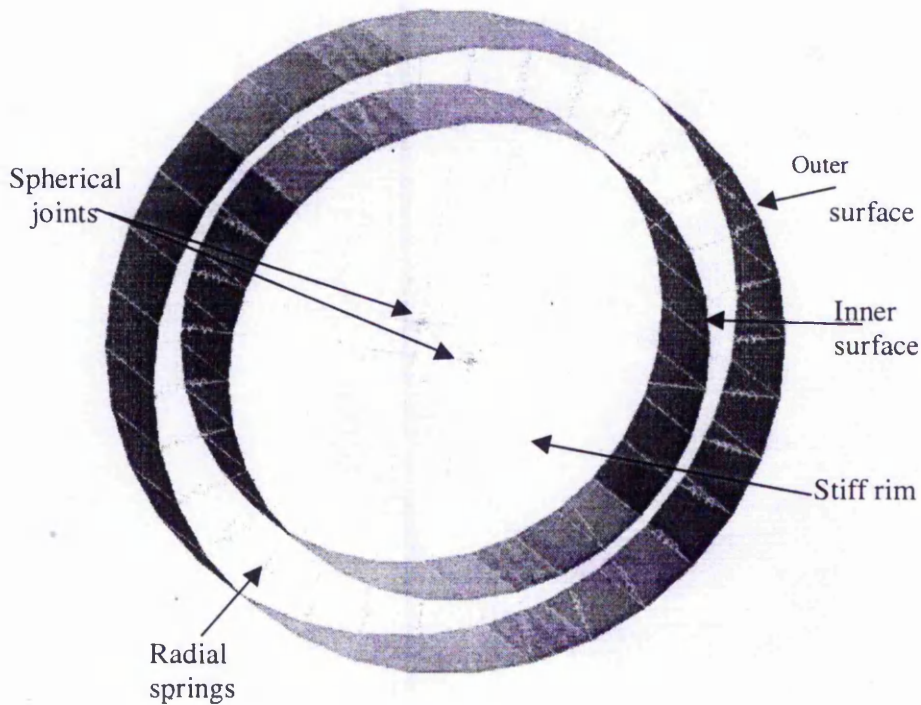


Figure 6.13 A finite element model of one wheel of the WMR.

assumptions are minimal. Both the chassis of the WMR and its wheels now have a distributed inertia and stiffness which is more realistic than they were depicted in the contact dynamics modelling, where simple linear springs (and dashpots) were used to represent the localised wheel deformations. The full-order finite element model has also an advantage in that it allows the gross-motion (rigid-body) dynamics and the structural dynamics problem to be handled simultaneously, a task extremely difficult to handle with analytical modelling. In summary the following points could be noted about differences in the devised analytical model and the full-order FE model used for validation:

- In the FE model the wheel deformation is distributed over the entire wheel disc as opposed to the simplifying assumption that the deformation is localised at a wheel-ground contact point.
- In the FE model the chassis deformation contributes to the overall structural dynamics of the platform as opposed to the assumption made in the analytical modelling process that the deformations are concentrated only at the wheels.
- In the FE model the wheel inertia is not zero and it has a finite rotational as well as translational dynamics.

The state-of-the art nonlinear dynamics finite element software LS-Dyna® has been employed in this work for the simulation. A finite element model of the WMR used in the simulation has been shown in Figure 6.12. To model the floor surface a total of 539 shell elements made of a rigid material have been used. The choice of the shell elements is based on the fact that in LS-Dyna® they are most suited for simulating contact with other entities, especially contact with other shell elements. Each wheel is made up of 64 shell elements, 32 of which are used to model an inside surface and the remaining 32 to model the outer surface of the wheel which makes contact with the ground surface. As shown in Figure 6.13 the outer surface of each wheel and the inside surface are connected by 64 spring (discrete) elements. The choice of spring elements to connect the inner and outer surfaces of the wheel provides the advantage of being able to change the radial stiffness of the wheel by simply altering the stiffness of the spring elements for either parametric study or model correlation.

Table 6.2 Summary of the characteristics of the finite element model of the WMR.

Part	Property	Material	Mass (kg)	Thickness (mm)	Number	Remark
Ground Surface	Shell	Rigid	203	15	539	-
Wheel	Shell	Rubber	0.83	15	64	For each wheel
Wheel	Spring	Spring	-	-	64	For each wheel
Rim	Beam	Rigid	-	-	32	For each wheel
Axle	Beam	Rigid	-	-	2	For each wheel
Chassis	Beam	Rigid	-	-	40	-
Payload	Mass	-	170	-	4	-
Accelerometer	-	-	-	-	1	-
Joints	-	-	-	-	2	For each wheel
Total	-	-	377	-	1240	-

Each wheel is connected to axle bearings by 32 stiff (rigid) beams which simulate the rim of the wheel. The rim is then connected to the rigid axle through two spherical joints on each side of the wheel in order to allow the rotation of the wheel around the axis of the axle (Figure 6.13). The axles are connected to the chassis of the platform by rigid beam elements while the chassis itself is made up of 40 rigid beam elements. A discrete accelerometer element (not shown in the figure) has also been defined at the centre of mass of the platform in order to monitor the rigid body motion of the WMR. The number of elements and their characteristics are summarised in Table 6.2.

In order to simulate the contact between the wheels of the WMR and the ground surface a surface-to-surface contact interface has been defined by using the outer wheel surface elements and the shell elements of the ground surface. The friction characteristic parameters between an ordinary pavement and rubber wheel have been used. Thus, a static friction coefficient of 0.8 and a dynamic friction coefficient of 0.3 have been applied.

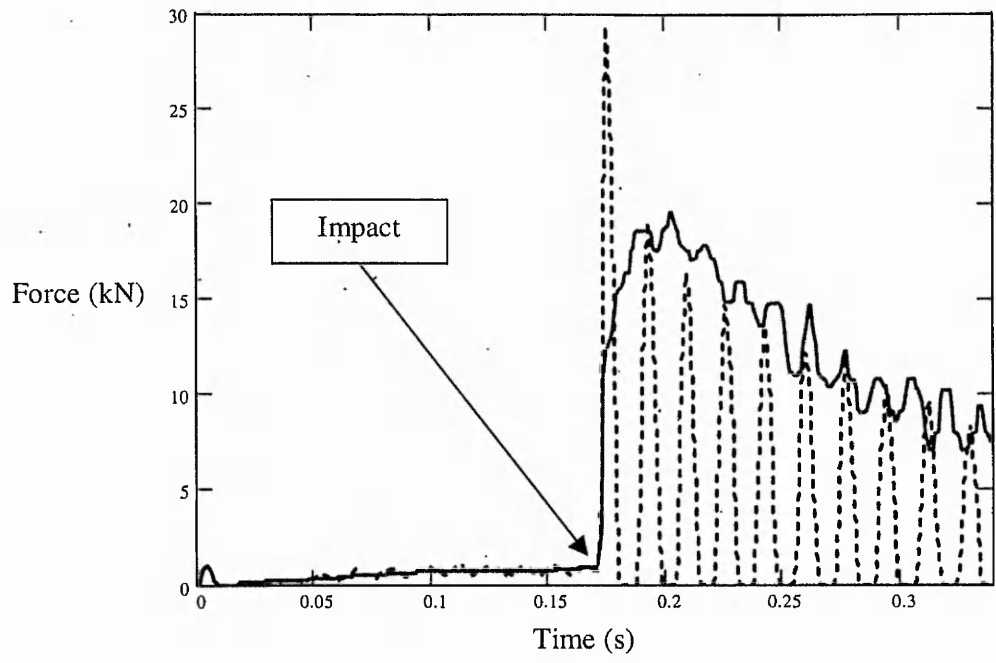


Figure 6.14 Variation of the front wheel reaction force from finite element simulations of uncontrolled impact (dashed curve) and controlled impact (solid curve).

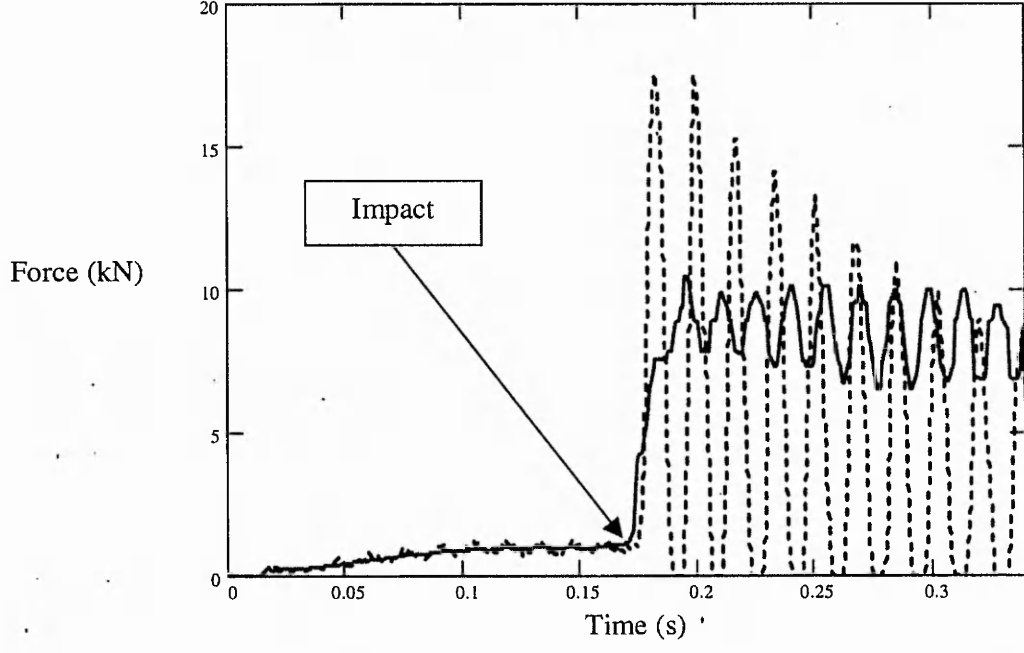


Figure 6.15 Variation of the rear wheel reaction force from finite element simulations of uncontrolled impact (dashed curve) and controlled impact (solid curve).

reaction force. Zero reaction force represents a lost contact. The results of the FE simulation have been summarised in Figures 6.14 and 6.15 where the time histories of the reaction forces of the front and the rear wheels have been plotted both for controlled and uncontrolled impact of the front wheels with a ramp obstacle. For the purpose of the FE simulation the gravitational preload has been ramped up slowly until just before impact. This avoids the artificial excitation of the structure that would occur if the gravitational preload is applied suddenly at time is equal to zero.

During an uncontrolled impact, shown by the dashed curves in Figures 6.14 and 6.15, the contact forces drop to zero several times which indicates that contact has been lost at these instances. A controlled impact is hence one that results in a normal contact force approaching the steady state contact force asymptotically that enables permanent wheel grip with the ground after impact. As can be seen from the solid curves in Figures 6.14 and 6.15 the proposed control has been able to maintain the wheel-ground contact immediately after collision which is an indication that the specified objective of attaining wheel-ground contact has been achieved.

6.8 Summary Comments

The impact modelling and control of a WMR whose front wheels collide with a ramp obstacle has been discussed. The traction forces are used as a means of actuation. Simulation results carried out using an approximate model in the MATLAB[®] environment have indicated the effectiveness of the proposed control scheme. It has been found out that soft wheels make the impact control easier by demanding less actuation effort. Finally an off-line control scheme has been simulated by using a full-order finite element model. By using the proposed control scheme it has been possible to prevent the rebound of the wheels of the WMR after impacting with a ramp obstacle.

Chapter 7

Shock Response Analysis of WMRs - Modelling

7.1 Introduction

The derivation of the dynamics model of the WMR in Chapter 4 was based on a critical assumption that the WMR's chassis and wheels as well as the manoeuvring surface are so stiff that they can be represented by rigid bodies. Although in reality there are no perfectly rigid bodies, however the rigid body assumption was essential to decouple the large displacement, gross motion dynamics of the WMR to the small deformations of its body related to structural dynamics. While the rigid body assumption was useful in simplifying the large displacement dynamics problem arising from wheel-obstacle interaction it was inadequate for describing the fast dynamics response due to the impact between the wheels and ground obstacles. In Chapter 6 the rigid body assumption was relaxed for the wheels in order to devise an impact control mechanism that enables the contact-grip control of the wheels of the WMR.

This chapter will focus on modelling the problem of wheel induced structural excitations on the chassis, which are the consequences of WMR-ground obstacle collisions. By modelling the structural dynamics of the WMR whose wheels are subjected to shock loads, a simple analytical scheme that enables the estimation of the acceleration response at various point on the platform will be provided. The model thus introduced will then be used in a case study, which is provided in the next chapter.

Vibration analysis of vehicles fitted with a suspension system has been explored extensively due to the high motivation stimulated by the automotive industry. The advent of passive and active suspension systems has greatly improved ride-comfort, road holding and vehicle stability of passenger cars [82]. However, there is a lack of good understanding of vibration problems related to vehicles that can not take advantage of such advances in suspension systems.

Wheeled Mobile Robots (WMRs) are commonly designed without a well-defined suspension system, mainly for simplifying motion control problems that often are based on rigid-body kinematics or dynamics models. These vehicles are, however,

vulnerable to the effects of vibration because they often carry delicate sensors and computing hardware, in addition to loose payloads on the platform.

Safe path and trajectory planning of a WMR navigating on an uneven terrain requires a good understanding of the shock response of the platform when it comes into contact with an obstacle. One criterion for selecting a feasible path and trajectory could be based on an acceptable magnitude of the dynamic load on the platform that would minimise payload instability or damage to instrumentation on the WMR. A mathematical framework that would assist the controller of the robot to estimate the potential damage is thus essential. The controller could use the information regarding the potential damage to decide on appropriate actions that could minimise any adverse effects that might result from excessive dynamic loading.

A limited amount of literature is available in the area of robotics research that gives consideration to vibrations caused by WMR interaction with ground surface obstacles. Stochastic vibration of manipulators mounted on mobile robots has been discussed in [83], which considered only the structural dynamics of the manipulator. The displacement of the manipulator tip resulting from stochastic vibration inputs at the wheel of the mobile robot was analysed. The work recommended the application of a suspension system with significant damping in order to minimise error in manipulator control. The work was based on continuous random excitation and did not address the shock response of the mobile platform to suddenly applied loads that are more relevant for a WMR navigating in an environment cluttered with wheel-level obstacles.

The vibration problem of mobile systems, such as WMRs, is more difficult than stationary structures such as buildings or anchored machinery. This is because of the fact that two types of dynamics are manifested simultaneously in the case of mobile systems. The first is the gross-motion dynamics (also referred to as rigid-body dynamics) which is related to the large displacement that a mobile structure undergoes with respect to its surrounding. The second dynamics involves the structural deformations of the system, which is caused by the stress wave that travels through the chassis at the speed of sound in the continuum. For practical purposes, however, these two dynamics problems are often analysed and dealt with separately.

The excitation forces are more of a result of the gross-motion dynamics than the structural dynamics. It will be assumed through out this chapter that the temporal and spectral distribution of the external forces is not affected by the structural dynamics of the mobile robot. In other words, the gross-motion dynamics and the structural dynamics have a cause and effect relationship, in that the gross-motion dynamics is responsible for generating the structural excitation forces, while the structural deformation dynamics passively responds to these excitations. A similar assumption was made by Dupont and Yamajako [64] who carried out a rigid body analysis where it was assumed that structural deformations took place in a fast time scale, thus only having perturbation effects on the gross-motion dynamics.

To determine the structural response to impact forces a temporal or spectral distribution of the forces is needed. The acquisition of temporal distribution of impact forces is a rather difficult task for the reason that such events take place in a very small period of time, thus making accurate measurements impractical. Various theoretical formulations have been proposed to describe the phenomenon of impact but with little success in experimental validation [84]. Fortunately, structural dynamics response is more sensitive to the spectral content of an excitation than its temporal shape, even if the two are intrinsically related, and information regarding the spectral contents of most shock load forms can easily be extracted. One area of application of shock loading is in industrial verification of the structural integrity of delicate components. For this purpose some form of shock pulse is applied to the component or assembly of interest in order to verify whether it satisfies a specified acceptable level of acceleration response [85]. The most common forms of shock pulses used for such purposes are rectangular, triangular, half-sine and versed-sine curves shown Figure 7.1. These shock loads have been used to simulate pyrotechnique excitations in spacecraft electronic components and delicate military hardware [86]. In [87] the author examined rectangular, half-sine and triangular forms of excitation to assess the relative severity of the structural response of WMR chassis. It has been found that rectangular inputs cause the highest dynamic loading. Hence a cautious and a safest approach to estimating structural response due to this little understood phenomenon of impact is one that is based on a rectangular temporal

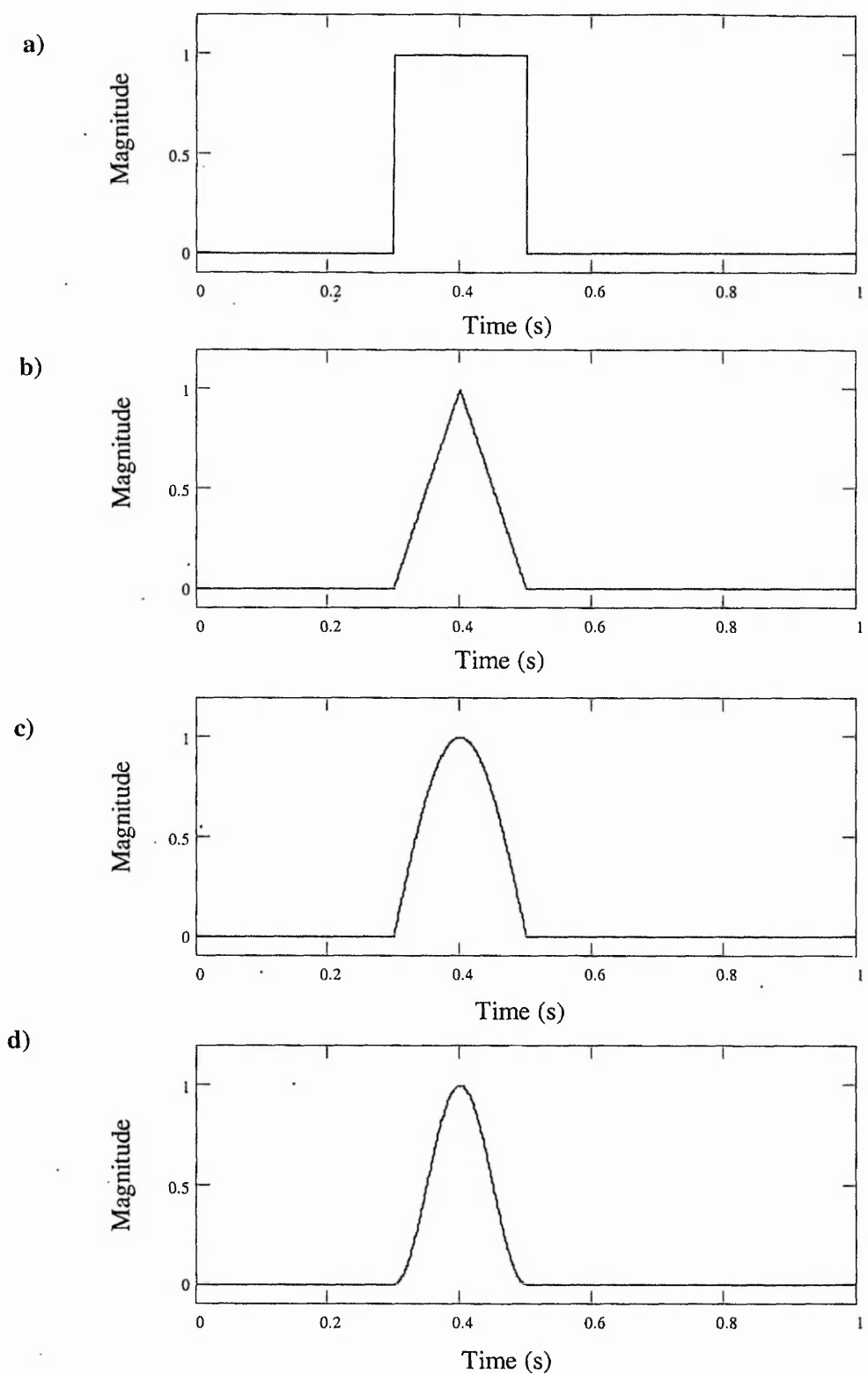


Figure 7.1 Common forms of shock pulses,
a) Rectangular b) Triangular c) Half-sine d) Versed-sine.

shape of the excitation forces. The fact that rectangular pulses are more sever is consistent with the observation that their spectral content is stronger than any other forms of excitation mentioned above. Through out this chapter the shock loads are assumed to have a rectangular temporal shape.

7.2 Modelling

The common modelling approach for vibration analysis of passenger vehicles is the quarter car model (Figure 7.2). This simple model, which is used for ride comfort and road holding assessments, contains two mass elements, referred to as sprung and unsprung masses, and two spring-damper systems [88]. The limitation of this model is that it does not take into account vibrations due to chassis deformation. This, however, may be acceptable for road vehicles whose chassis deforms much less than the suspension springs. Since suspension systems are virtually non-existent in WMRs, the chassis deformation is an important parameter in describing the structural response of the platform to external shock inputs.

Based on the theory of structural mechanics, a continuum has infinite modes of vibration. However, during a certain application, only those modes of vibration whose natural frequencies are close to the frequencies of the excitation forces, make

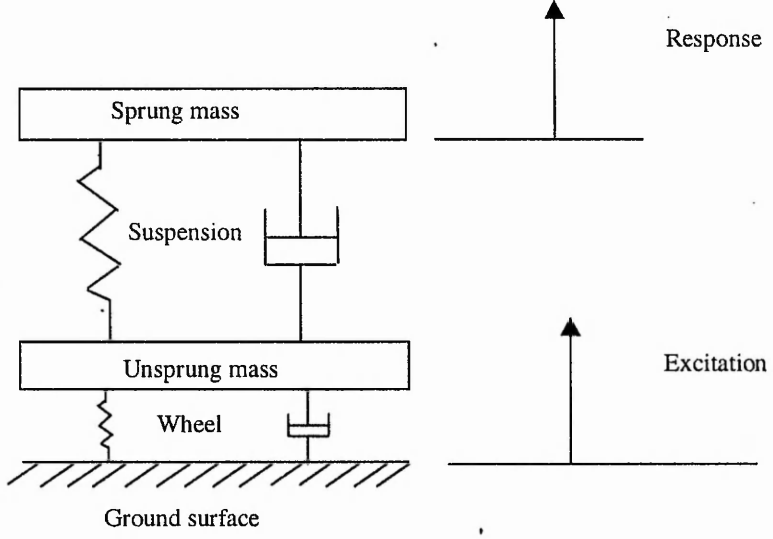


Figure 7.2 Quarter car model.

significant contribution to the overall response. This fact is well exploited in dealing with vibration problems with periodic excitations, such as that caused by unbalanced rotary drives, in order to assess whether resonance will occur in the structure. In this case the interest in the analysis may be limited to a small range of natural frequencies which can be excited significantly. In the case of shock loading, however, the spectral content of the excitation is relatively wide and thus the natural frequencies of interest are larger than those of periodic excitations.

The structural excitation caused by wheels colliding with stationary obstacles is identified as a transient excitation as distinguished from continuous (periodic or random) vibration excitations normally encountered in passenger cars and rotating machinery. The intensity and frequency range of impact-type structural excitations are dependent on the impact velocity, the inertia of the colliding bodies and the elasto-plastic material properties of the colliding bodies, particularly in the locality of the impact. For shop floor applications WMRs are normally operated at low speeds (in the range of 1.0 - 3.0 m/s) on generally smooth working surfaces. Applications on uneven terrain tend to have a slower travelling speed. The low working speed combined with the fact that common wheel materials tend to be soft rather than stiff means that the excitation frequency range of interest is on the lower bound [89]. In addition if the platform at hand is used for the purposes of material handling it is likely to be heavy which generally contributes to the lowering of the natural frequency. From these observations it is evident that the lower modes of vibration of a WMR are more likely to be excited by wheel obstacle impact loads. Hence it is reasonable to concentrate on the lowest natural frequencies and their associated modes of vibration.

Common WMR chassis designs can be structurally identified as thick rectangular plates with reinforcement beams of various configurations. Analytical solutions for the natural frequencies and modes of vibrations of uniform rectangular plates are easily obtained by solving the following partial differential equation of elasticity [90]:

$$-K \nabla^4 w = \rho \frac{\partial^2 w}{\partial t^2} \quad (7.1)$$

where w is the deformation variable.

$$K = \frac{E h^3}{12(1-\nu^2)} \quad (7.2)$$

K is the plate's flexural rigidity, E the elastic modulus, ρ is the density of the material, ν is Poisson's ratio, h is the uniform thickness of the rectangular plate and t is time. However, the analytical solutions for a variable section, beam reinforced, thick plates are quite involved and will not be attempted here. An alternative approach to solving this problem is the use of finite element method that involves the approximation of the continuum by a discretised model. In the present study a finite element model of the platform has been built and the natural frequencies of the platform are to be determined from this model. Attempts have also been made to keep the method of analysis simple and analytically orientated so that the resulting expressions are suitable for integration with mobile-robot motion control systems.

Finite element formulation of the structural dynamics assumes that the platform is discretised into n points. The equations of motion of the structure due to a system of external forces \vec{R} is given by:

$$M\ddot{\vec{U}} + C\dot{\vec{U}} + K\vec{U} = \vec{R} \quad (7.3)$$

where M , C and K are $n \times n$ mass, damping and stiffness matrices, respectively. \vec{U} is an n -length nodal displacement vector in the global coordinate system. In the following section the procedure to extract the natural frequencies is described by first formulating the eigenvalue problem for the chassis of the WMR.

7.3 Eigenvalue Problem Formulation

The damping in metallic structures, such as the chassis of a WMR, is due to structural hysteresis, and is relatively small compared to viscous damping. Therefore, undamped natural frequencies of a WMR are good approximations to the natural frequencies of the chassis when characterising the vibration behaviour of the structure. In general, for the determination of the natural frequencies of a given

structure the damping and the excitation forces are ignored, so Equation (7.3) reduces to:

$$M\ddot{\vec{U}} + K\vec{U} = 0 \quad (7.4)$$

The solution of the simplified differential Equation (7.4) can be obtained by considering:

$$\vec{U} = \vec{\Phi} \sin(\omega t) \quad (7.5)$$

where $\vec{\Phi}$ is an arbitrary vector of amplitudes and ω is a frequency variable.

Substituting Equation (7.5) and its second derivative with respect to time in Equation (7.4) results in:

$$K\vec{\Phi} = \omega^2 M\vec{\Phi} \quad (7.6)$$

which is the *eigenvalue problem*. In finite element analysis Equation (7.6) is solved by various methods such as vector iteration, transformation, polynomial iteration or the Sturm sequence to obtain the solutions Λ and Φ , the matrices of eigenvalues λ_i and eigenvectors ϕ_i respectively [91]. That is,

$$\Lambda = \begin{bmatrix} \lambda_1 & & & \\ & \ddots & & \\ & & \ddots & \\ & & & \lambda_n \end{bmatrix} \text{ and } \Phi = [\phi_1 \quad \bullet \quad \bullet \quad \bullet \quad \phi_n] \quad (7.7)$$

where $\lambda_i = \omega_i^2$, ω_i is the angular natural frequency of the i^{th} mode of vibration which has a an eigenvector (i.e. a modal shape vector) specified by the vector ϕ_i .

7.4 Response Computation

There are two methods available to determine the response of the structure of a WMR to external excitations based on Equation (7.3). The first method involves the direct integration of the equation. This method, which is based on a time-stepping integration of a system of equations, does not directly expose the frequency domain

relationship between the excitation and the response and will not be pursued in the present analysis. The second method, known as the 'modal superposition principle', involves the determination of the responses of each mode of vibration of the structure to external inputs separately, and then combining them to obtain a total response, providing that the deformations can be considered elastic and thus the system is linear. The relationships between dynamic response, natural frequency and excitation frequency in this second method is more obvious. Another advantage of this method is that a reasonably accurate response can be obtained by considering only a few natural frequencies and their corresponding modal shapes, which may save computational effort relative to a time stepping integration [91]. Since the aim here is to devise an efficient shock response assessment tool for future on-line implementation aboard the WMRs computer, the speed of the computation is as important as the accuracy. Because of these advantages the response computation model will be formulated based on the modal superposition technique.

A system of decoupled equations of motion can be obtained by transforming Equation (7.3) into a convenient coordinate system. One such coordinate system is that of the modal coordinates \vec{X} related to the nodal displacement \vec{U} by:

$$\vec{U} = \Phi \vec{X} \quad (7.8)$$

where Φ is the matrix formed by assembling the eigenvectors. Thus the undamped, forced equation of motion of the system is given by:

$$M \ddot{\vec{U}} + K \vec{U} = \vec{R} \quad (7.9)$$

where \vec{R} is the vector of the external forces. In terms of the modal coordinates \vec{X} , the equation of motion, Equation (7.9), can be written as:

$$\ddot{\vec{X}} + \Lambda \vec{X} = \Phi^T \vec{R} \quad (7.10)$$

The system of decoupled equations in Equation (7.10) can be solved by treating each individual equation as a system of single-degree-of-freedom motions. The convolution integral can be used to obtain the modal responses in the modal coordinates. In a multi-degree-of-freedom system it is customary to define the damping in terms of modal parameters so that the damped system of equations of

motion also remain decoupled by the use of the coordinate transformation employed for the undamped system, i.e. $U = \Phi X$.

The convolution integral for the i^{th} modal response x_i is given by:

$$x_i(t) = \frac{1}{\bar{\omega}_i} \int_0^t f_i(\tau) e^{-\zeta_i \omega_i(t-\tau)} \sin(\bar{\omega}_i(t-\tau)) d\tau + (a_i \sin(\omega_i t) + b_i \cos(\omega_i t)) \quad (7.11)$$

where

$$\bar{\omega}_i = \omega_i \sqrt{1 - \zeta_i^2} \quad (7.12)$$

$$f_i(t) = \phi_i^T \bar{R} \quad (7.13)$$

ω_i is the undamped angular natural frequency of the i^{th} mode of vibration and $\bar{\omega}_i$ is the damped angular natural frequency of the same mode. $f_i(t)$ is the projection of the external excitation forces \bar{R} into the i^{th} modal coordinate. ζ_i is the damping ratio of the i^{th} mode, a_i and b_i are constants depending on the initial conditions.

In Equation (7.11) the term which is convoluted with the excitation is called the impulse response of a single-degree-of-freedom mass-spring-damper system. That is,

$$h(t) = \frac{1}{\bar{\omega}_i} e^{-\zeta_i \omega_i t} \sin(\bar{\omega}_i t) \quad (7.14)$$

The frequency response function, $H(\omega)$, of the system is given by the Fourier transform of the impulse response as:

$$H(\omega) = \int_{-\infty}^{\infty} h(t) e^{-j\omega t} dt = \frac{1}{\bar{\omega}_i} \int_{-\infty}^{\infty} e^{-\zeta_i \omega_i(t)} \sin(\bar{\omega}_i t) e^{-j\omega t} dt$$

$$H(\omega) = \frac{1}{(\omega + \zeta_i \omega_i)^2 + \bar{\omega}_i^2} \quad (7.15)$$

7.5 Projection of the Excitation Force

Arbitrary periodic excitation forces or base accelerations can be decomposed into simple harmonic components by means of the Fourier series expansion. Each harmonic component of the excitation force excites the structure separately. The

responses of the structure to each individual harmonic component can be superimposed on one another to obtain the total response, providing that the structural deformations are elastic so that the dynamic system remains linear. The analytical evaluation of the convolution integral Equation (7.11) is relatively straightforward if the excitation force $f_i(t)$ is composed of harmonic components only.

However, shock loads are not periodic and theoretically they can not be represented by a finite Fourier series. The alternative is to use Fourier integrals to represent them. The Fourier integral results in complex expressions for such simple shock loads as the rectangular pulse. For example the following is the Fourier integral transform of a rectangular pulse:

$$f(t) = \begin{cases} 1 & 0 \leq t \leq T \\ 0 & \text{otherwise} \end{cases} \quad (7.16)$$

$F(\omega)$, the Fourier integral of $f(t)$ is given by,

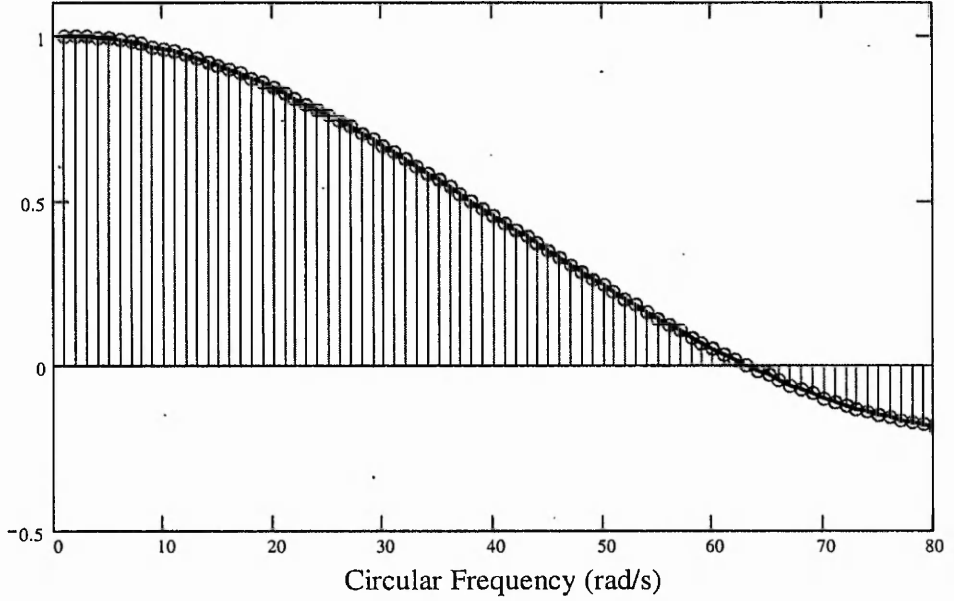


Figure 7.3 Comparison between the amplitudes of a Fourier series of a rectangular pulse of period 3s (bars) and the Fourier integral of a rectangular pulse (solid curve).

$$\begin{aligned}
 F(\omega) &= \int_{-\infty}^{\infty} f(t) e^{-j\omega t} dt = \int_0^T e^{-j\omega t} dt \\
 F(\omega) &= -\frac{e^{-j\omega T}}{j\omega} \Big|_0^T = \frac{1}{j\omega} (1 - e^{j\omega T}) \\
 F(\omega) &= -\frac{\sin(\omega T)}{\omega}
 \end{aligned} \tag{7.17}$$

In the frequency domain the modal response can be computed as:

$$X_i(\omega) = F(\omega)H(\omega) \tag{7.18}$$

where $H(\omega)$ is the modal frequency response function (Equation 7.15). And the time domain response can be computed back by using the Fourier integral expression:

$$x_i(t) = \frac{1}{2\pi} \int_{-\infty}^{\infty} X(\omega) d\omega = \frac{1}{2\pi} \int_{-\infty}^{\infty} F(\omega)H(\omega) d\omega \tag{7.19}$$

Transformation of the type performed in Equation (7.19) is straightforward if $F(\omega)$ is the Fourier transform of harmonic functions. However, there are no simple analytical solutions for Equation (7.19) if $F(\omega)$ is the Fourier integral of a non-periodic function such as a rectangular shock pulse, as given in Equation (7.17).

In common WMR applications, where the vehicle is travelling at a low speed, it is expected that the frequency at which the wheels encounter one road obstacle after another is low. In addition this frequency can be controlled by carefully planning the path and the speed of the WMR. This fact may be utilised to overcome the problem associated with the Fourier integral. In the present work the following procedure has been devised to replace the Fourier integral by the Fourier series.

The rectangular shock pulse can be thought of as a periodic signal but with an infinite period, or can be approximated by a signal having a long finite period. The theoretical shock pulse takes place only once and never repeats itself. However, if the shock pulse is repeated after a long duration, so that the transient response caused by the initial pulse has died out before the second pulse acts, the two shock loads can be thought of as separate events. Still they remain two peaks of the same periodic wave. In the frequency domain this approximation corresponds to approximating the continuous frequency spectrum of the excitation forces by a discrete frequency

spectrum. In Figure 7.3 a comparison between the frequency spectrum of a theoretical shock pulse and an approximated shock pulse of 3 seconds period has been plotted. The solid curve indicates the spectrum of a theoretical pulse with infinite period. The discrete frequencies of the approximated rectangular pulse which repeats itself after 3 seconds are shown as bars. It can be seen that even for a period as short as 3 seconds, the approximation of a theoretical shock pulse (of an infinite period) by a periodic one can provide a reasonable representation.

Now that the shock loading is assumed to be periodic, it can be represented by a Fourier series with harmonic components, the responses to which can be obtained as outlined below.

The Fourier expansion of a periodic external force $r(t)$, a component of $R(t)$, truncated after s terms is given by:

$$r(t) = \sum_{j=1}^s (a_j \cos(p_j t) + b_j \sin(p_j t)) \quad (7.20)$$

where a and b are vectors of Fourier's cosinusoidal and sinusoidal coefficients, respectively, and p is the vector of frequencies of the excitation.

Equation (7.11) allows the determination of the total response that is generally composed of a transient response and a steady-state response. The transient response is the term that dies out in time provided that the system is damped (as is generally the case) and has a frequency equal to the natural frequency of the corresponding mode. The steady state response, also known as the forced response, has the frequency of the forcing function and is the response observed after the transient response has died out. Most vibration problems are concerned with the steady state response because it may result in large amplitudes if the frequency of excitation is close to any of the natural frequencies of the structure, a phenomenon known as *resonance*. For this reason transient responses are often left out of the consideration. For the present study, however, the aim is to determine the immediate response of the platform to external excitations which are impulsive type. Consequently, we

investigate both the transient and the steady state responses with equal interest and their arithmetic sum constitutes the total response.

The solution of Equation (7.11) will be determined for sinusoidal and cosinusoidal excitations separately as these constitute the Fourier components of a generic excitation force. The total response is the sum of the responses of the structure to both sinusoidal and cosinusoidal excitations.

The modal response, $x(t)$, of a sinusoidal excitation $s(t) = f \sin(pt)$ is found by substituting $f_i(t) = s(t)$ in Equation (7.11). (For the sake of brevity the suffix referring to the modal number i (Equation 7.19) will be dropped from now on). Thus,

$$x(t) = \frac{1}{\omega} \int_0^t f \sin(p\tau) e^{-\zeta\omega(t-\tau)} \sin(\bar{\omega}(t-\tau)) d\tau + e^{-\zeta\omega t} (a \sin(\omega t) + b \cos(\omega t)) \quad (7.21)$$

After integrating Equation (7.21), substituting the initial conditions and simplifying the response $x(t)$ is found as:

$$x(t) = x_t(t) + x_s(t) \quad (7.22)$$

where the transient response $x_t(t)$ and the steady state response $x_s(t)$ are given by:

$$x_t(t) = f e^{(-\zeta\omega t)} (A_t \sin(\bar{\omega}t) + B_t \cos(\bar{\omega}t)) \quad (7.23)$$

$$x_s(t) = f (A_s \sin(pt) + B_s \cos(pt)) \quad (7.24)$$

where

$$\begin{aligned} A_t &= \frac{-p}{\omega} \frac{(-\zeta^2\omega^2 - p^2 + \bar{\omega}^2)}{\Psi} & B_t &= \frac{2p\zeta\bar{\omega}}{\Psi} \\ A_s &= \frac{(\zeta^2\omega^2 - p^2 + \bar{\omega}^2)\sqrt{1-\zeta^2}}{\Psi} & B_s &= -\frac{2p\zeta\bar{\omega}}{\Psi} \end{aligned} \quad (7.25)$$

$$\Psi = (p^4 - 2p^2\omega^2 + 4\zeta^2 p^2\omega^2 + \omega^4)$$

Similarly the modal response, $y(t)$, for a cosinusoidal excitation can be obtained by substituting $f(t) = f \cos(pt)$ in Equation (7.11):

$$y(t) = \frac{1}{\omega} \int_0^t f \cos(p\tau) e^{-\zeta\omega(t-\tau)} \sin(\bar{\omega}(t-\tau)) d\tau + e^{-\zeta\omega t} (a \sin(\omega t) + b \cos(\omega t)) \quad (7.26)$$

which results in a response:

$$y(t) = y_t(t) + y_s(t)$$

where

$$y_t(t) = f e^{(-\zeta\omega t)} (C_t \sin(\bar{\omega} t) + D_t \cos(\bar{\omega} t)) \quad (7.27)$$

$$y_s(t) = f (C_s \sin(pt) + D_s \cos(pt)) \quad (7.28)$$

$$\begin{aligned} C_t &= \frac{-\zeta(p^2 + \omega^2)}{\Psi} & D_t &= \frac{p^2 \sqrt{1 - \zeta^2} - \omega^2 \zeta^2 \sqrt{1 - \zeta^2} - \omega^2 (1 - \zeta^2)^{3/2}}{\Psi} \\ C_s &= \frac{2p\zeta\bar{\omega}}{\Psi} & D_s &= \frac{(\zeta^2\omega^2 - p^2 + \bar{\omega}^2)\sqrt{1 - \zeta^2}}{\Psi} \end{aligned} \quad (7.29)$$

Thus, the total modal response, $z(t)$, due to sinusoidal and cosinusoidal excitations is:

$$z(t) = x(t) + y(t) \quad (7.30)$$

The modal response needs to be transformed into the global coordinate system before physical interpretation of the response can be made. Noting that the excitation forces may only act through the four wheel-ground contact points of the wheeled

mobile robot, a transformation matrix that relates the modal response to a response in the global coordinate system at a point on the platform can be obtained as follows.

Let n_1 , n_2 , n_3 , and n_4 be the points on the bed of the platform connecting the wheel structure to the chassis (Figure 7.4). If the chassis is discretised into k nodes then the $k \times m$ matrix of eigenvectors composed of the m modes of vibration, Φ , is given by:

$$\Phi = [\vec{\phi}_1 \quad \vec{\phi}_2 \quad \vec{\phi}_3 \quad \vec{\phi}_4 \quad \dots \quad \vec{\phi}_m] \quad (7.31)$$

where $\vec{\phi}_i$ is a k -length eigenvector of the i^{th} mode of vibration.

The k -length nodal excitation force vector \vec{R} is given by:

$$\vec{R}^T = [r_1(t) \quad r_2(t) \quad r_3(t) \quad r_4(t) \quad 0 \quad \dots \quad 0] \quad (7.32)$$

The modal excitation force vector, $f(t)$, is found from the right hand side of Equation (7.13).

That is,

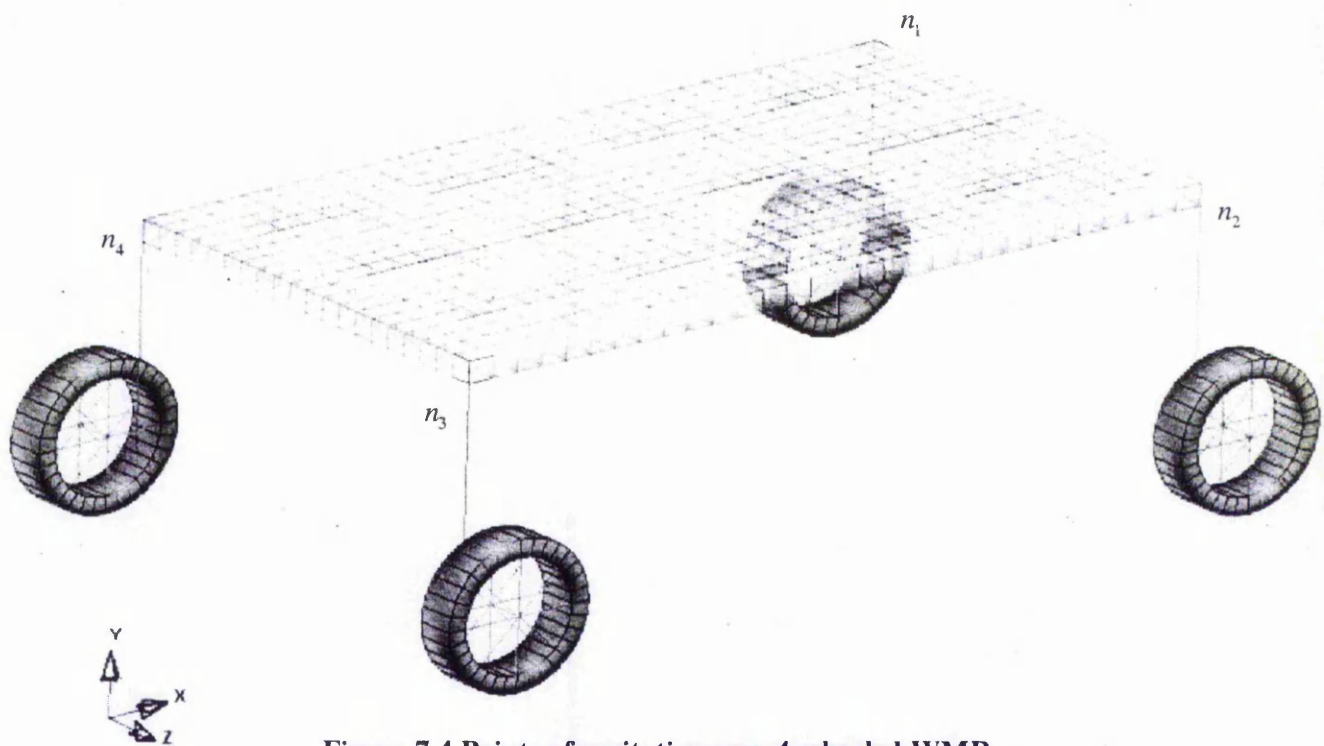


Figure 7.4 Points of excitation on a 4-wheeled WMR.

$$f(t) = \Phi^T R(t)$$

or

$$f(t) = [\phi_1 \quad \phi_2 \quad \phi_3 \quad \phi_4 \quad \dots \quad \phi_m]^T \begin{bmatrix} r_1(t) \\ r_2(t) \\ r_3(t) \\ r_4(t) \\ 0 \\ \vdots \\ 0 \end{bmatrix} \quad (7.33)$$

The modal response needs to be projected onto the global coordinate system to obtain the nodal displacements. These nodal displacements are computed by using the relationship described by Equation (7.8) where the extracted m modes are utilised to approximate the total response by using the principle of *modal superposition*. Therefore,

$$U = \begin{bmatrix} v_{11} & v_{21} & v_{31} & \dots & v_{m1} & | & z_1 \\ v_{12} & v_{22} & v_{32} & \dots & v_{m2} & | & z_2 \\ v_{13} & v_{23} & v_{33} & \dots & v_{m3} & | & z_3 \\ \vdots & \vdots & \vdots & \ddots & \vdots & | & \vdots \\ \vdots & \vdots & \vdots & \ddots & \ddots & | & \vdots \\ \vdots & \vdots & \vdots & \ddots & \ddots & | & \vdots \\ v_{1n} & \dots & \dots & \dots & v_{mn} & | & z_m \end{bmatrix} \quad (7.34)$$

where U is the nodal displacement vector and v_{ij} is the j^{th} component of the i^{th} eigenvector and z_i are the modal response of the i^{th} mode obtained by using Equation (7.30).

The acceleration response can be considered as a measure of potential damage to delicate instrumentation aboard the robot. This is because as a direct consequence of Newton's second law the acceleration response generates inertial forces that in turn induce dynamic stresses in the structure. The acceleration response can be computed by differentiating the displacement response, Equation (7.34), twice with respect to time.

Thus,

$$A = \frac{d^2U}{dt^2} \quad (7.35)$$

Symbolic implementation of the above algorithm to compute the acceleration response has been carried out by using the Mathcad® programme, which is given in Appendix C.

7.6 Summary Comments

An analytical framework for estimating the chassis acceleration response of a WMR subjected to obstacle induced shock excitations has been presented. The proposed approach involves the extraction of the modal shapes and frequencies of the platform by using a finite element method. The rectangular shock pulses used in the investigation have been approximated by Fourier series representation. The extracted modes of vibration are then excited independently by each of the harmonic components of the shock load to obtain modal responses. The modal responses thus obtained have been superimposed and transformed to the global coordinate system to determine the nodal displacements.

Acceleration response, which is obtained by successive differentiation of the nodal displacements, has been used as measure of potential damage and a symbolic algorithm to compute the response has been developed. The results of this chapter will be used in a case study to be presented in the following chapter.

Chapter 8

Shock Response Analysis of WMRs - Application

8.1 Introduction

A modelling approach which enables the estimation of the acceleration response at various stations on the platform of a WMR, when the wheels are excited by shock loads resulting from wheel-obstacle collision, has been given in Chapter 7. The developed model will be applied in this chapter in case studies to analyse the responses of a WMR subjected to various forms of collision with ground level obstacles.

In the case studies presented here a WMR whose dimensional and material characteristics are summarised in Table 8.1 has been considered. The platform, which is shown in Figure 8.1, has a longitudinal and lateral dimensional symmetry. It is intended to study the shock responses of the given WMR when the wheels are excited by rectangular shock loads. The following three cases are considered:

- i. One of the wheels is excited while the WMR is assumed to be suspended freely in space. This analysis allows the examination of the structural response when

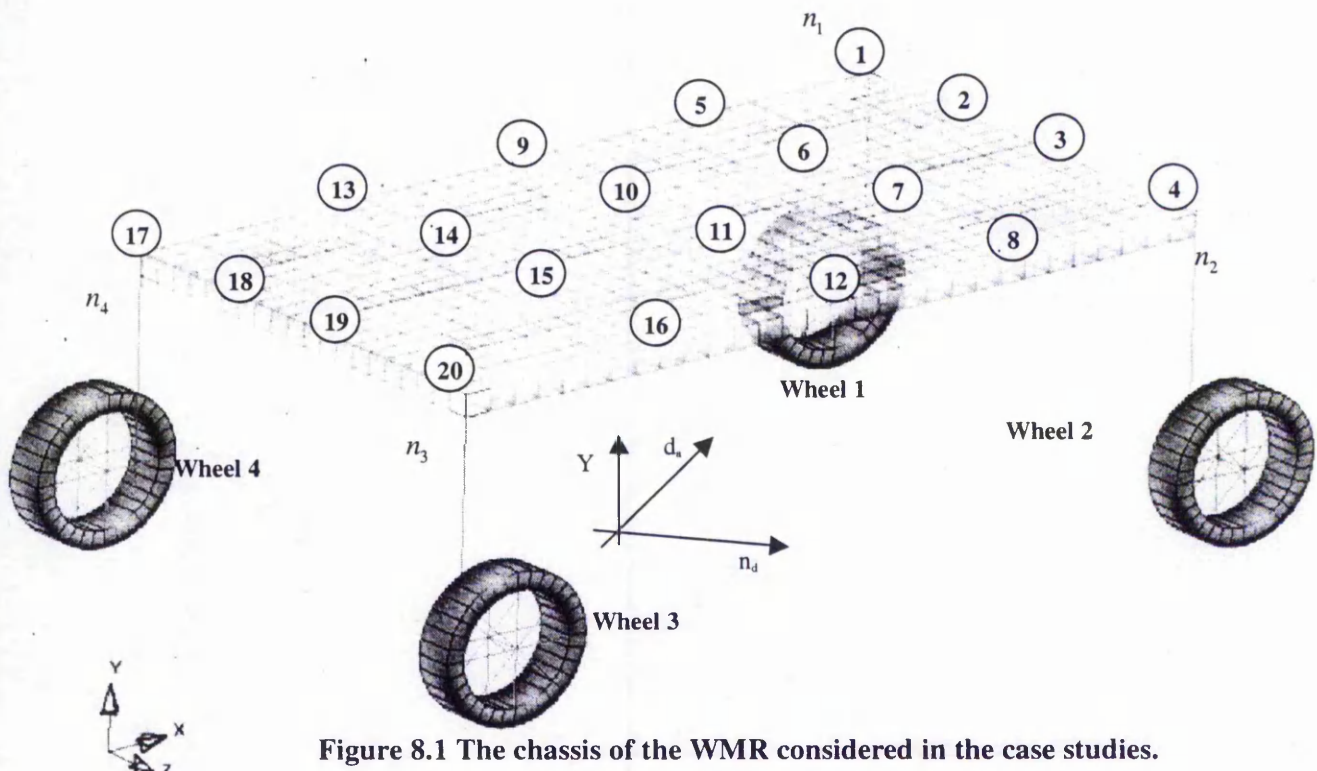


Figure 8.1 The chassis of the WMR considered in the case studies.

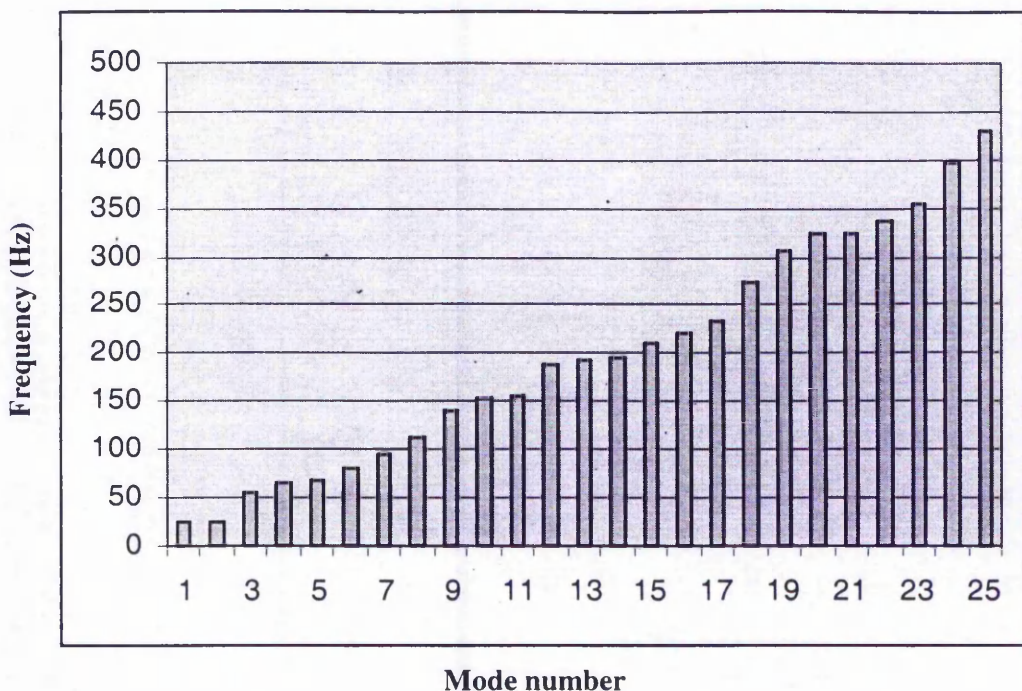


Figure 8.2 The first 25 natural frequencies of the chassis of the WMR considered for the shock response analysis.

the excitation of one wheel causes the other three wheels to lose contact with the ground.

- ii. Diagonally opposite wheels are excited while the rest of the wheels are assumed to have lost contact. This is a scenario observed when a single wheel hits a stationary road obstacle. When a wheel hits an obstacle the rigid-body dynamics of the platform dictates that the diagonally opposite wheel produce a counteracting reaction.
- iii. All four wheels are excited simultaneously. This scenario corresponds to the collision of two wheels on the same axle (the front wheels, for example) with an obstacle while the other two wheels (the rear wheels, for example) produce a reactive force.

In the case studies it will be assumed that the front wheels are colliding with obstacles. However, since the rigid-body motion is not considered the choice of either front wheel or rear wheel collision does not introduce any loss of generality.

Therefore, similar results are expected if the rear wheels collide with obstacles as in, for example, a reversing manoeuvre.

Table 8.1 Dimensions and structural properties of a WMR used in the case study.

Symbol	Description	Value
L_f	Longitudinal distance of front axle from the vehicle centre of mass	0.6 m
L_r	Longitudinal distance of rear axle from the vehicle centre of mass	0.46 m
L_w	Width of platform	0.58m
h	Height of centre of mass from the wheel centres	0.4 m
R	Radius of wheels	0.1 m
I_y	Pitch moment of inertia of the platform	47 kg-m ²
m	Mass of the platform and payload	270 kg
E	Modulus of Elasticity of the chassis (Aluminium)	72 GPa
ν	Poisson's ratio for the chassis' material (Aluminium)	0.33
ρ	Density of the chassis material (Aluminium)	2700 kg/m ³
η	Flexural loss factor for Aluminium [92] ($\eta = 2\zeta$, where ζ is the ratio of viscous damping)	1.0e-4

8.2 Modes of Vibration

As discussed in the previous chapter, in order to estimate the acceleration response of a given WMR information regarding the modal shapes of vibration and their corresponding natural frequencies is needed. In the present work this information is obtained by carrying out a finite element analysis of the WMR being considered. For this purpose the ANSYS® software has been employed and the first 25 modes of vibration and their natural frequencies have been extracted.

The finite element mesh of the WMR is given in Figure 8.1. The chassis of the platform has been meshed with solid elements. In addition 9 payload boxes distributed over the platform have been modelled in solid. Solid elements have been chosen by taking into consideration the fact that such elements provide a better

representation of the degrees of freedom of motion in a solid continuum. Past experience suggests that ANSYS® is considered to be more suited to work with solid elements than with shell elements, which is the case with the LS-Dyna® programme. A total of 600 solid elements are used to represent the platform and 30 solid elements have been used to model each payload box. The total number of nodes in the model is 1299 of which 651 are used to model the chassis and 72 nodes are used to discretise each of the 9 payload boxes.

All modes of vibration of interest have been found to be of 'bending' type with the corresponding frequencies ranging from 24 Hz to 430 Hz, which are summarised in Figure 8.2. The first 12 modal shapes of the platform have also been plotted in Figures 8.3 - 8.5.

As seen in Figure 8.3 the first mode of vibration, which is associated with the lowest natural frequency of 24 Hz, is a longitudinal bending about a mid-length lateral axis. The deformations associated with this mode are mainly on the front and rear edges of the WMR. The second mode of vibration is very close to the first mode in terms of frequency, which is equal to 26 Hz. The shape of this second mode of vibration is an alternate bending about the two diagonal axes, which contributes largely to the deformations at the corners. The third mode with a frequency of 54.5 Hz is an out of phase bending of the lateral edges about the mid-length axis, mainly deforming the front and the rear corners alternately. The fourth mode is a bending about a longitudinal axis that passes through the mid-width point.

The fifth mode (Figure 8.4) is a vibration about a symmetric longitudinal axis. This is a second order mode of vibration with respect to the first mode. It bends the platform about a lateral axis that passes through the mid-length at a frequency of 68.7 Hz and is in phase with the first mode of vibration at the front edge and out of phase at the rear edge. The sixth mode, vibrating at a frequency of 80.3 Hz, is an out of phase longitudinal bending of the front and rear edges about a longitudinal axis and is in phase with the fourth mode at the front edge and out of phase at the rear edge of the WMR. Mode 7 represents an out of phase, vibration of the two lateral edges of the WMR at a frequency of 95.1 Hz. This mode is a second order mode of vibration with respect to the third mode. Mode 8 is an out of phase second order bending of the

platform about the longitudinal axis, vibrating about three longitudinal axes which lie at the side edges and along the mid-width line.

The next mode is 9 (Figure 8.5) which is vibrating at a frequency of 140.2 Hz. This mode is a third order mode of vibration with respect to mode 1. Mode 10 vibrates the lateral edges of the WMR in a similar fashion to modes 3 and 7 but with a higher order, namely it is a third order mode with respect to mode 3. Mode 11 is a higher order of vibration with respect to mode 8. Similarly, mode 12 follows mode 9 as its higher order longitudinal bending.

At the front left corner of the WMR all of the considered modes except modes 8, 10 and 12 are in phase and their contribution to the overall deformation at this corner is additive. Where as at the front right corner only modes 1, 4, 5, 6 and 11 contribute to the deformation at this corner in an additive sense. At the rear left corner modes 1, 3, 4, 10 and 12 are in phase, while at the rear right corner of the WMR modes 1, 2, 4, and 12 are in phase and will contribute to an additive deformation at this corner. As will be shown later from the frequency domain analysis of the excitation forces, the low frequency modes of vibration are excited more severely because the amplitude of rectangular shock loads is highest at low frequency. Thus it is expected that the response is mainly influenced by the first few modes of vibration

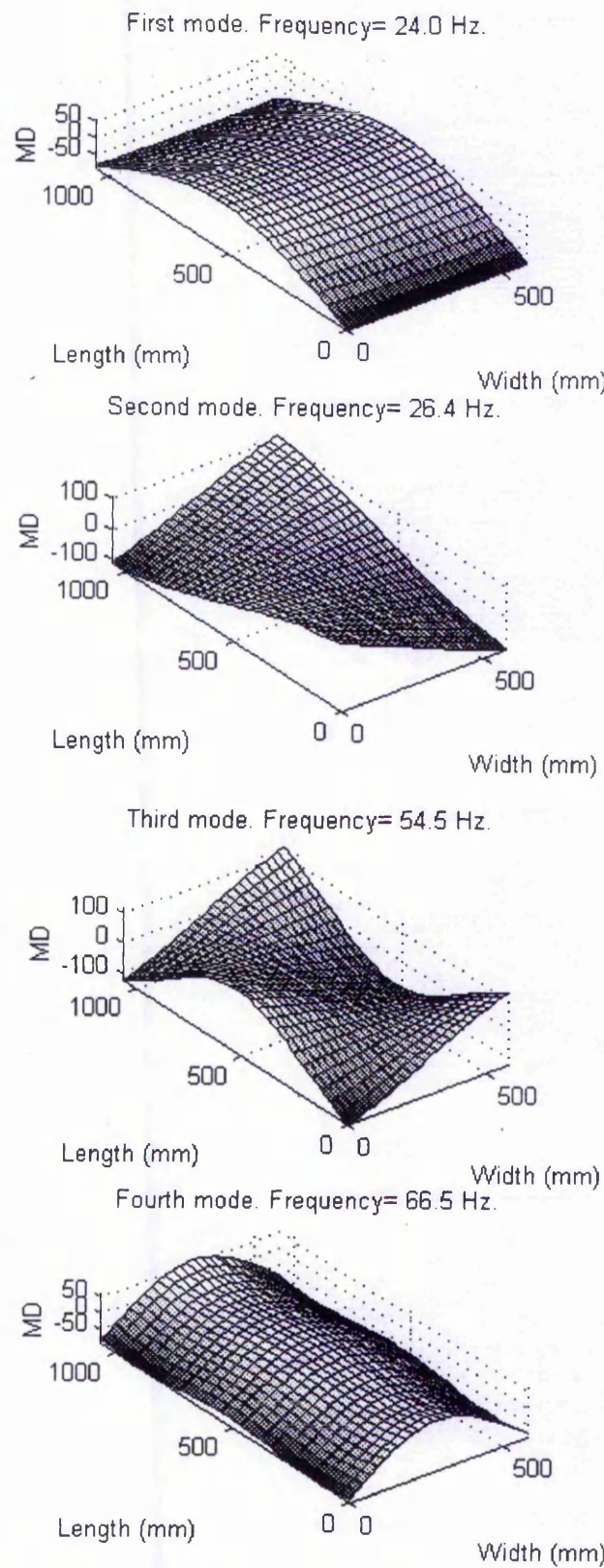


Figure 8.3 Modes of vibration 1 to 4. Vehicle coordinate is measured from rear to front along the length and from left to right along the width.

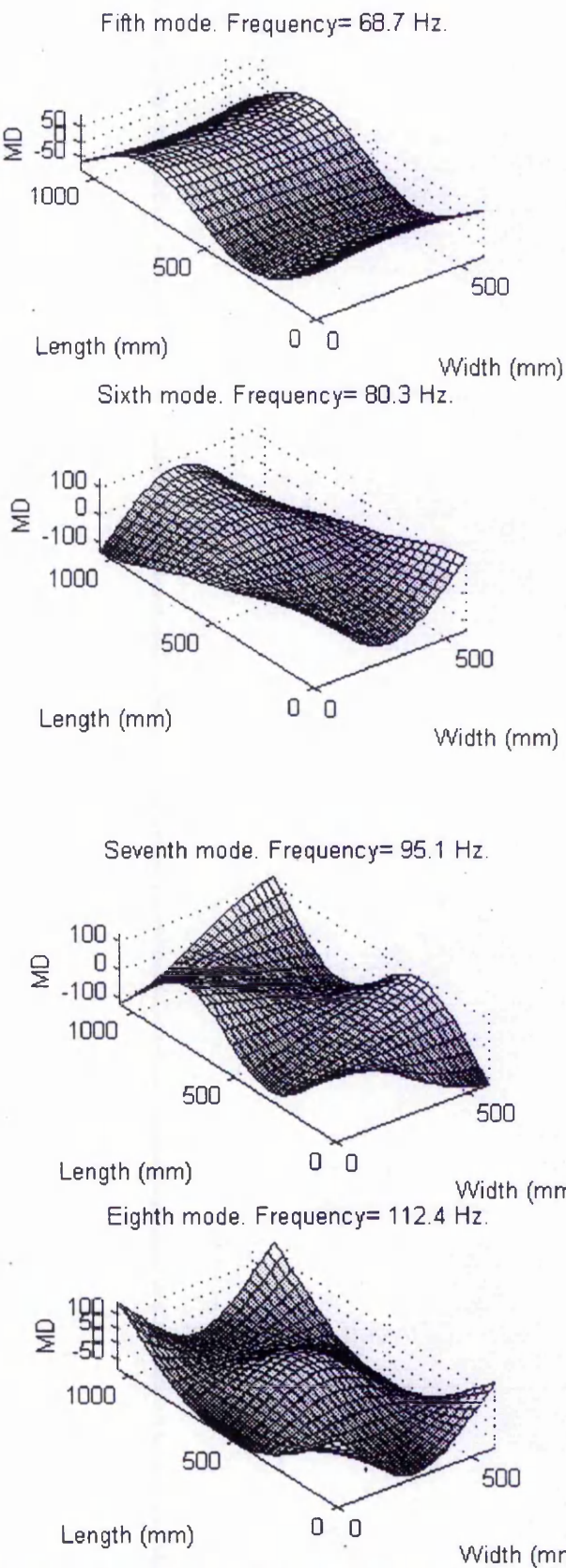
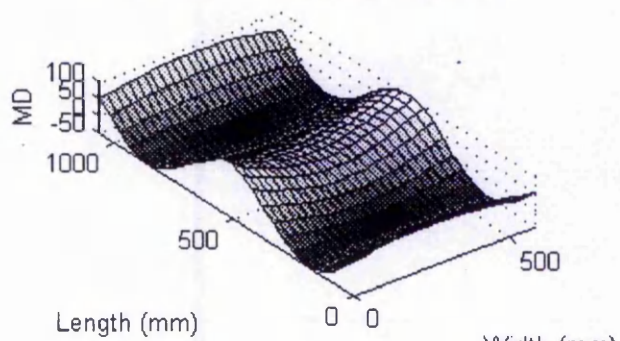
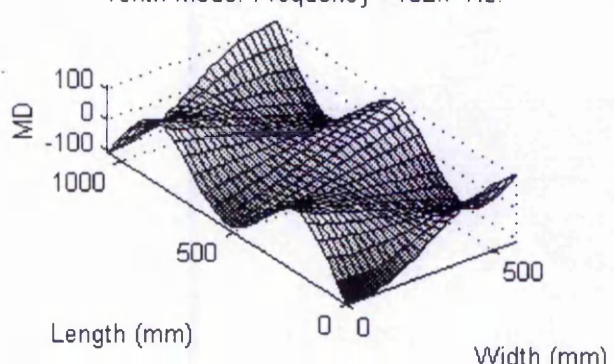


Figure 8.4 Modes of vibration 5 to 8. Vehicle coordinate is measured from rear to front along the length and from left to right along the width.

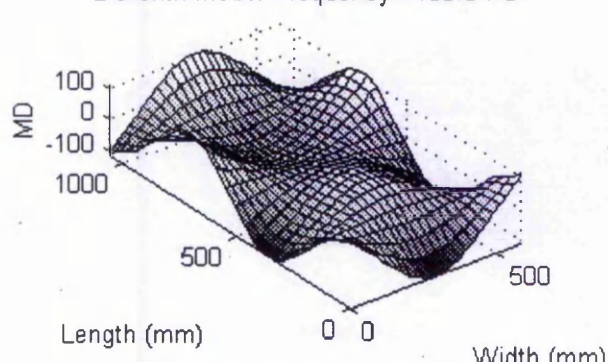
Nineth mode. Frequency= 140.2 Hz.



Tenth mode. Frequency= 152.7 Hz.



Eleventh mode. Frequency= 156.3 Hz.



Twelfth mode. Frequency= 189.5 Hz.

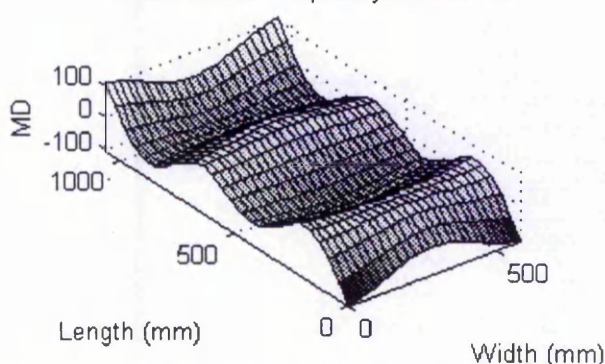


Figure 8.5 Modes of vibration 9 to 12. Vehicle coordinate is measured from rear to front along the length and from left to right along the width.

8.3 Analysis of the Shock Load

The Fourier expansion of a shock load, $r(t)$, at a single wheel, for example at wheel 1 in Figure 8.1, is given by:

$$r(t) = \sum_{k=1}^s a_k \sin(p_k t) + b_k \cos(p_k t) \quad (8.1)$$

The temporal shapes of two rectangular pulses, chosen for a comparative study, and having different time duration, i.e. 0.05s and 0.08s have been plotted in Figure 8.6. These pulses have a unit magnitude. In the actual simulations this unit magnitude was multiplied by 1000N in order to obtain a shock load of maximum value 1000N. As discussed in the previous chapter theoretical shock loads can be approximated by periodic pulses of long period. In this case both of the 0.05s and 0.08s rectangular pulses have been approximated by periodic waves of period equal to 3 seconds. These shock pulses will be used to excite the wheels of the WMR whose dimensions and structural properties have been summarised in Table 8.1 and whose natural frequencies have been plotted in Figure 8.2.

The periodic approximation was needed to use the Fourier series instead of

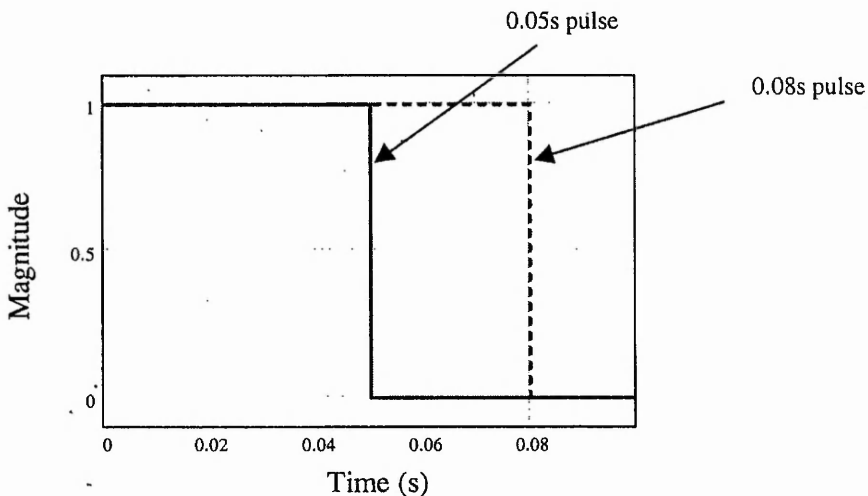


Figure 8.6 Plot of two rectangular pulses employed in the simulations.

the Fourier integral. The Fourier coefficients of the two rectangular pulses of duration 0.05s and 0.08s have been evaluated by using the Fast Fourier Transform (FFT) utility of the MATLAB® software. The coefficients obtained from the FFT analysis have been plotted in Figures 8.7 and 8.8. These coefficients represent the amplitudes of the excitation force corresponding to the frequency in the abscissa. As can be seen from these figures, in general, for both the sinusoidal and the cosinusoidal components of the excitation forces the amplitudes diminish as the frequency increases from zero, even though not monotonously. This is an indication that in general the most severe excitations occur at low frequency. The considered spectrum of the two loads lies in the range of 0-1250 rad/s (0-200 Hz).

The next step is the evaluation of the time domain modal responses by utilising Equations (7.22-7.29) given in the previous chapter. The transformation of the modal responses into the global coordinate system is then carried out by using Equation (7.34). A total of 20 stations on the chassis, evenly distributed over the rectangular platform, as shown in Figure 8.1, have been chosen for the response assessment. The acceleration responses at selected points on the platform will then be

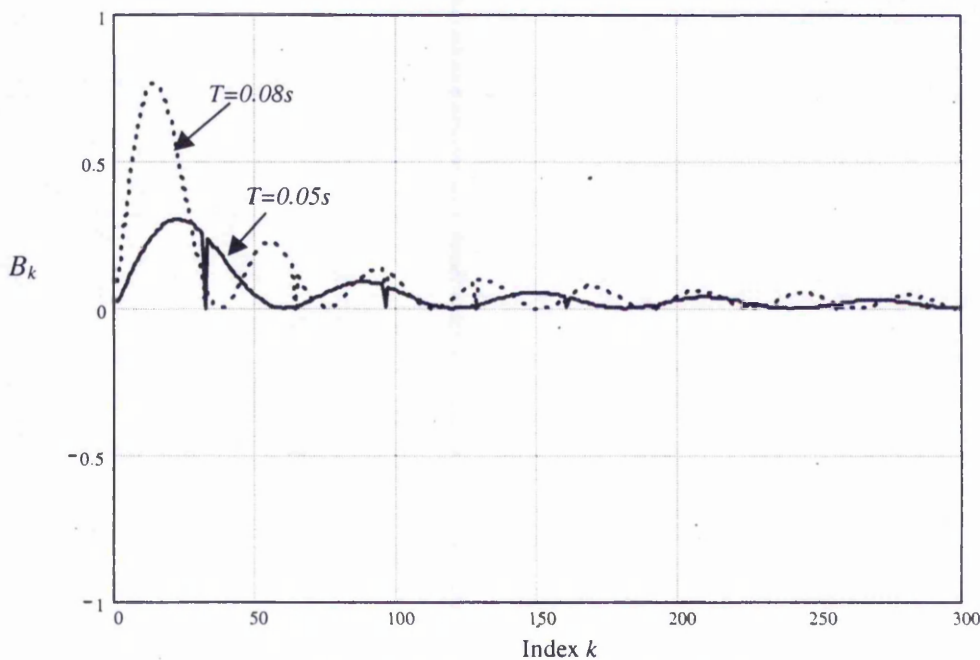


Figure 8.7 The sinusoidal Fourier coefficients of two rectangular pulses of different durations.

computed by differentiating the displacement response twice with respect to time as indicated in Equation (7.35). The algorithm used for computing the acceleration response has been given in Appendix C.

A total of three scenarios of wheel-obstacle collisions will be considered. In the first scenario it will be assumed that only one wheel is involved in the collision while the remaining three wheels are unaffected. This is a theoretical consideration and may not generally occur in practice, as there will almost always be a reactive impulse by any or all of the remaining wheels of the 4-wheeled WMR. Consideration will be given to multi-wheel excitations in the other two scenarios where diagonal and all-wheel excitations will be analysed.

8.4 Single Wheel Excitation

For the first case study only wheel-1 (Figure 8.1) is subjected to a shock load. The excitation force in the global coordinates is given by:

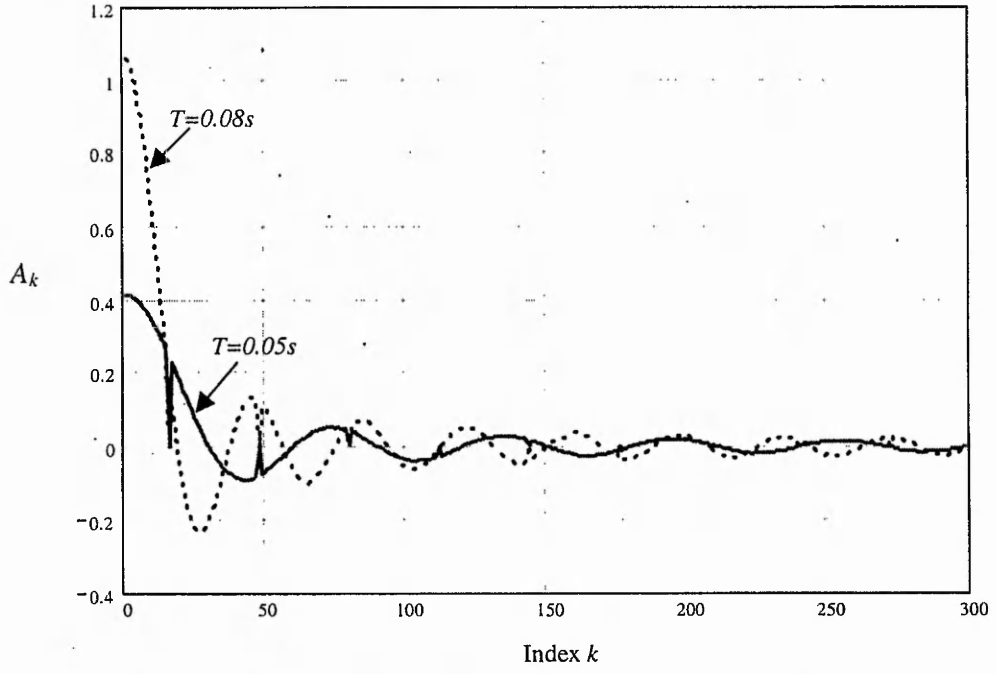


Figure 8.8 The cosinusoidal Fourier coefficients of two rectangular pulses of different durations.

$$\bar{R}^T = [r_1(t) \ 0 \ 0 \ 0 \ 0 \ \dots \ 0] \quad (8.2)$$

where $r_1(t)$ is the shock load function to which wheel 1 is subjected. The modal excitation forces are found from Equation (7.32) as:

$$f(t) = r_1(t)\phi_1^T$$

The modal responses of the structure to step loads with durations of 0.05 s and 0.08 s have been computed. The results of this computation have been plotted in Figures 8.9 and 8.10, which show the maps of the acceleration response for the corresponding points specified in Figure 8.1. Figure 8.9 shows the response due to a rectangular pulse of duration 0.05 seconds while in Figure 8.10 the response to a 0.08 pulse has been plotted.

In Figure 8.9 it is seen that station 1, which is on top of the colliding wheel 1, sustains the largest peak acceleration response. Going across the front edge of the WMR, intermediate stations 2 and 3 experience lower peak accelerations while station 4 is excited significantly with peak acceleration of about 5g. The stations on the second row are excited with less severity than the front edge stations with the most significant excitation being on the edges at stations 5 and 8. In a similar trend to the first row stations 2 and 3, the intermediate stations 6 and 7 experience a lower acceleration response. The middle row stations of the symmetrical rectangular platform under consideration are excited relatively less severely. Again in a similar trend to the first two rows the excitation is more considerable at the edges than at the intermediate stations.

As one goes to the rear of the WMR the peak acceleration response at the edges increase (stations 13 and 16), while the middle stations respond the least of all of the considered stations. The rear edge, despite being furthest away from the colliding wheel, is excited significantly, with the rear corner stations 17 and 20 having an acceleration peak value of about 5g.

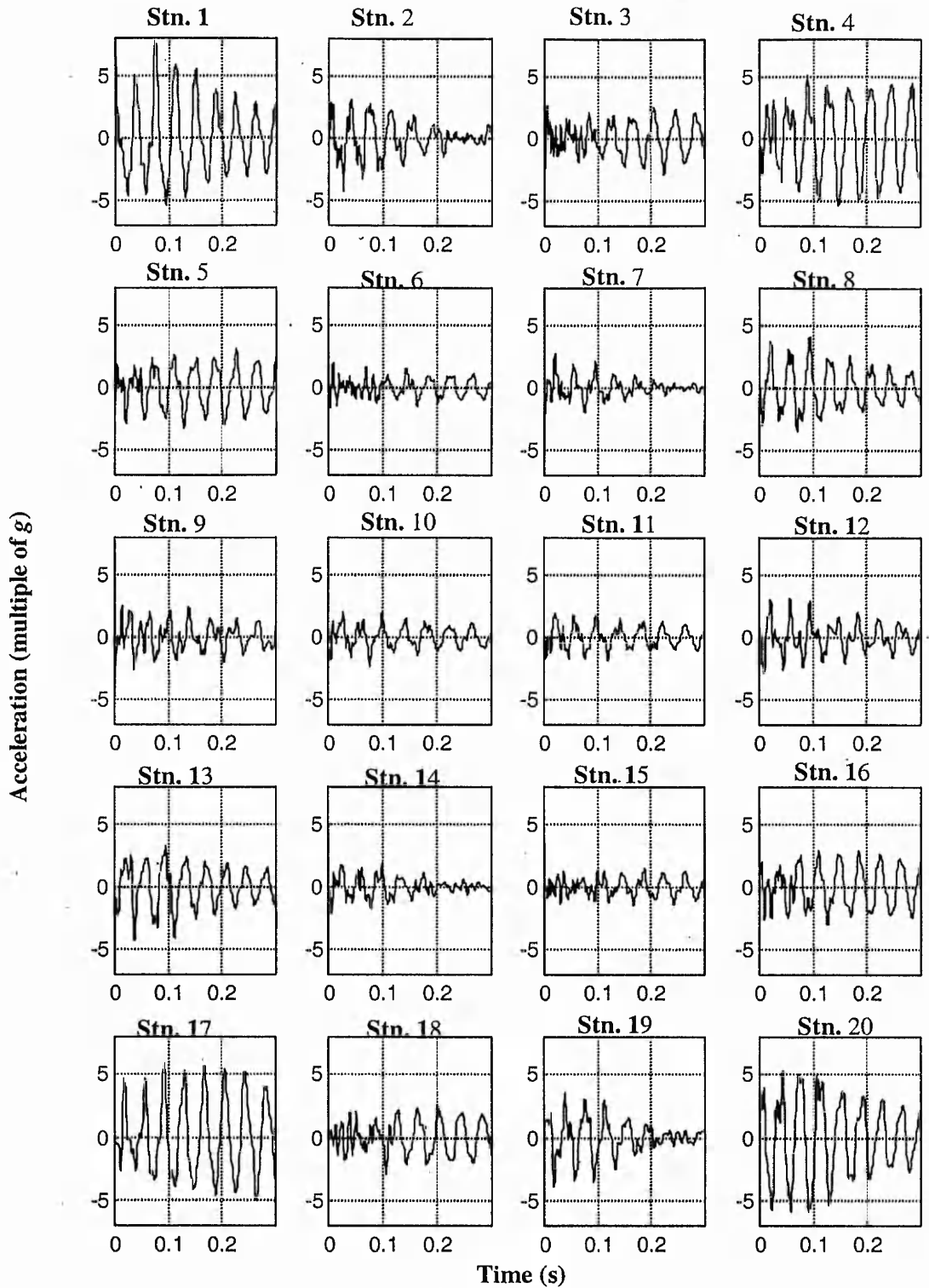


Figure 8.9 Acceleration response map of a rectangular platform to one front wheel excitation with 0.05s rectangular pulse

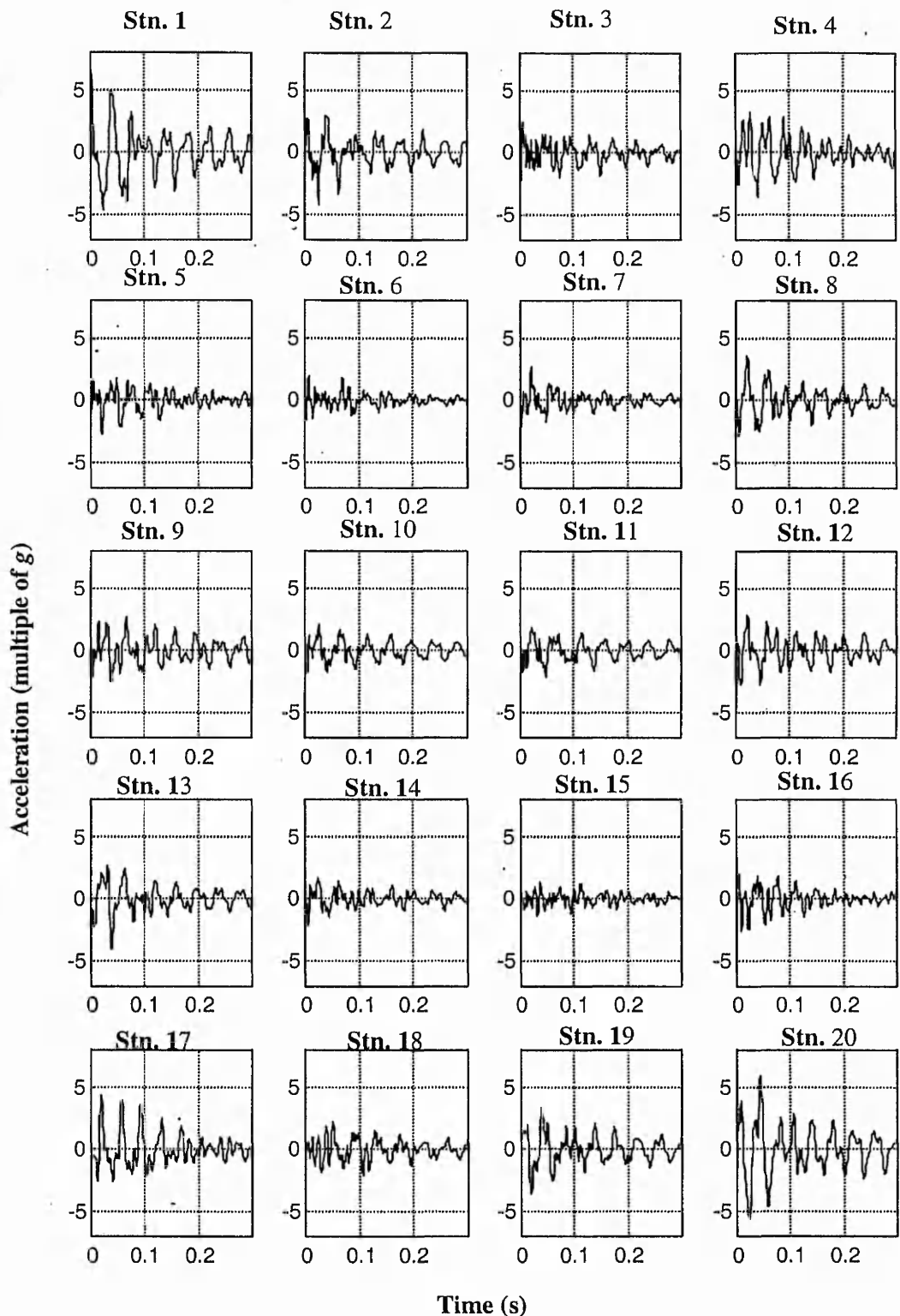


Figure 8.10 Acceleration response map of a rectangular platform to one front wheel excitation with 0.08s rectangular pulse

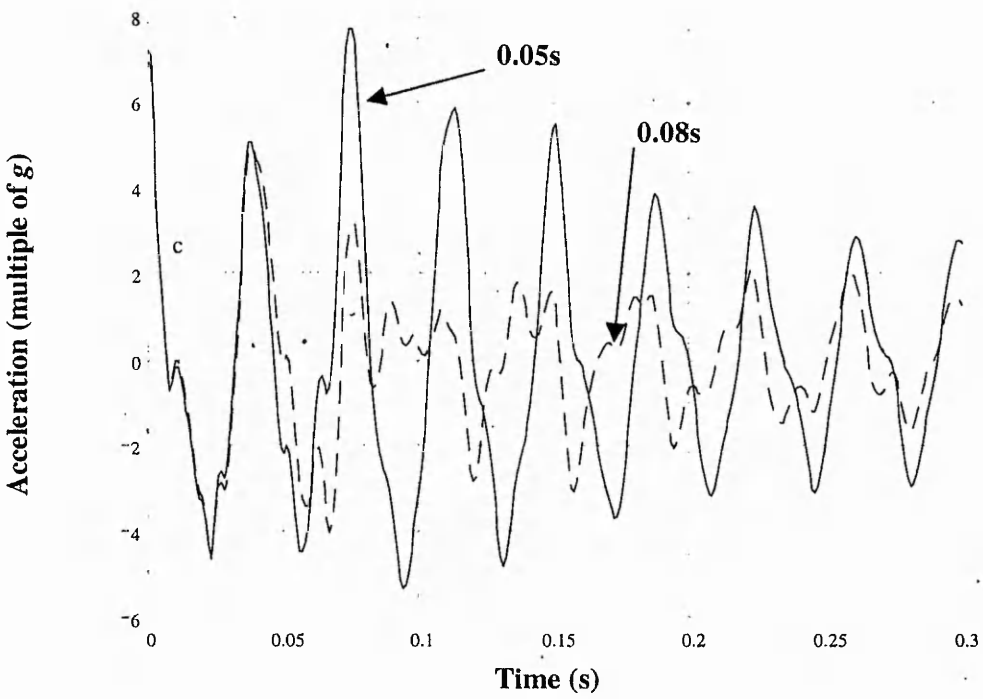


Figure 8.11 Comparison of acceleration responses between 0.05 s pulse (solid) and 0.08 s pulse (dashed) excitations at station 1.

The overall trend is that the corner stations experience large excitations, followed by the intermediate stations at the front, rear, right and left edges of the platform. The central zone of the WMR is excited relatively low with the peak acceleration at the central station 10 23% less than that at the corner station 1. The practical implications of this observation is that any vibration sensitive hardware aboard the robot should not be mounted near the corners and the edges as the peak accelerations are highest in these zones.

To see the effect of the duration of the impact on the response a comparison has been given in Figure 8.11. The figure shows the acceleration responses at station 1 as generated by a 0.05s pulse and a 0.08s pulse. While the overall trend of peak acceleration distribution over the platform remains the same it is seen that the 0.05s pulse generates peak accelerations that are consistently higher than those generated by the 0.08s pulse for a more sustained duration of time. Since impact duration is directly related to stiffness [89], softer wheel materials provide a better performance by enabling longer duration of impact forces which in turn results in a less sustained

excitation with respect to time. However soft wheels are not generally a welcome choice from motion control perspective as they are subject to large deformations which can introduce positioning errors. Odometric techniques for estimating the position of a WMR depend on wheel rotation counts whose, the accuracy of which can be adversely affected by the deformation of the wheels. Therefore, when choosing a material for the wheels a compromise is needed to satisfy the need to reduce sensitivity to impact as well as maintaining an acceptable odometric accuracy.

8.5 Diagonal Wheel Excitation

For the second case study the structural response of the platform to excitations due to the impact of diagonal wheels has been computed. This scenario corresponds to the mode of excitation observed while any one of the wheels hit a fixed obstacle. This causes the diagonally opposite wheel (to that hitting the obstacle) to react in such a way that the total angular momentum with respect to the rigid body dynamics of the platform is a minimum.

Assuming that the front-left wheel (wheel-1 in Figure 8.1) collides with an obstacle, the diagonally opposite rear-right wheel will generate a reactive force. The magnitude of the reactive force can be computed as follows.

Equating the change in the angular momentum of the platform about an axis perpendicular to the diagonal axis and to the vehicle's z-axis (axis n_d in Figure 8.1), to the total angular impulse generated by the reaction forces at the wheels we have:

$$I_d \Delta\omega = M \Delta t \quad (8.3)$$

where I_d is the mass moment of inertia of the platform about the n_d axis, $\Delta\omega$ is the change in the angular velocity of the WMR, M is the sum of moments and Δt is the duration of impact. The total diagonal moment of the two wheel forces is:

$$M = r_1(t)d_f - r_3(t)d_r \quad (8.4)$$

from which the rear wheel reaction force can be found as:

$$r_3(t) = -\frac{I_d \Delta\omega}{d_r \Delta t} + r_1(t) \frac{d_f}{d_r} \quad (8.5)$$

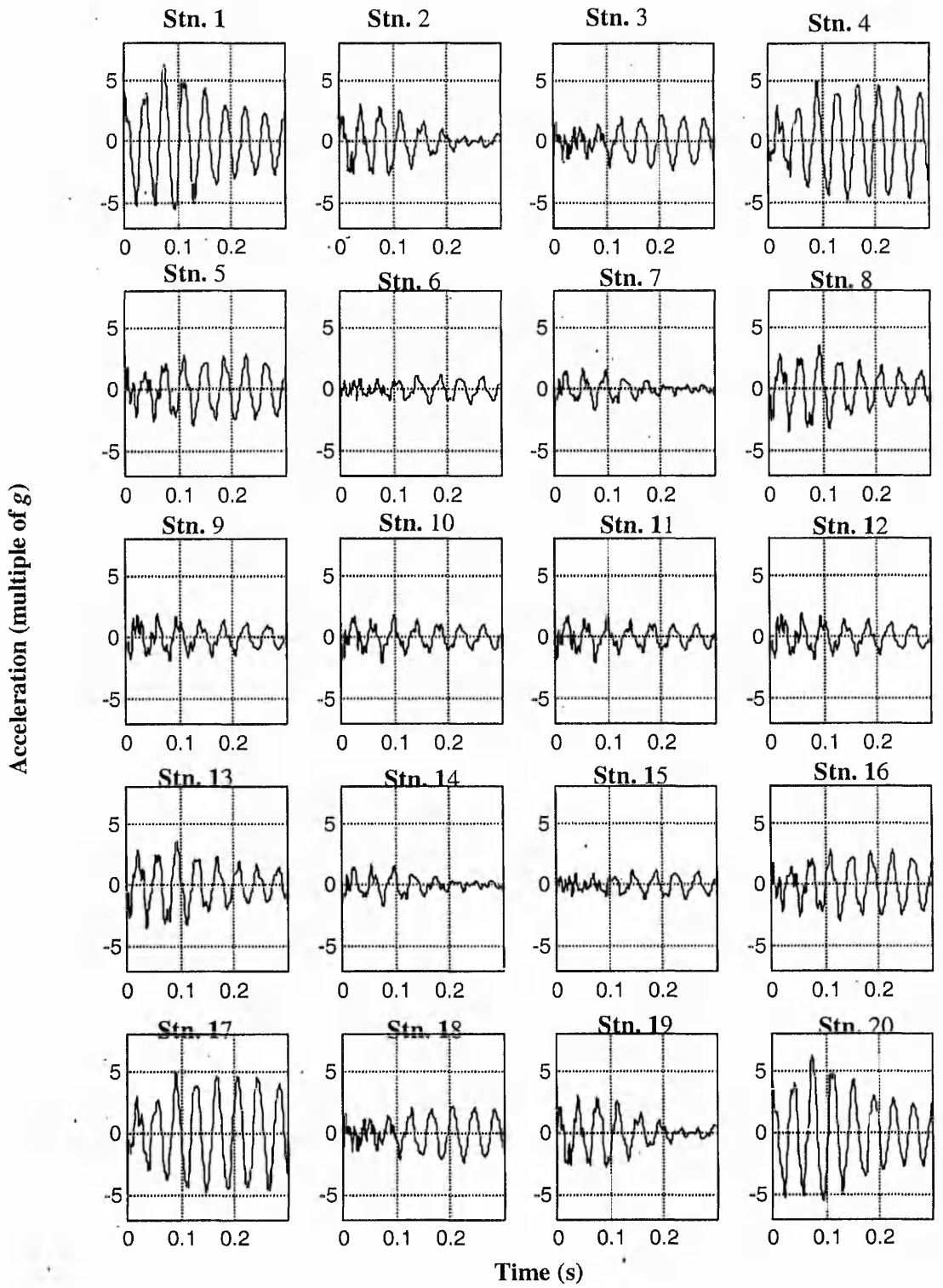


Figure 8.12 Acceleration response map of a rectangular platform to diagonal wheel excitations with 0.05s rectangular pulse.

In the above expression the impulsive force at the front wheel, $r_1(t)$, is assumed to be known, which for the purpose of this analysis will be given as a step input having a duration of Δt equal to 0.05s. Hence the global excitation vector can be written as:

$$\vec{R}^T = [r_1(t) \ 0 \ r_3(t) \ 0 \ 0 \ . . . \ 0] \quad (8.6)$$

The acceleration responses for all the stations (Figure 8.12) are similar to those of the single wheel excitation with a 0.05s pulse (Figure 8.9) which has been discussed in the previous section. The similarity is not a coincidence but is due to the fact that both the single-wheel and diagonal-wheel modes of loading excite similar set of modes. This can be demonstrated by comparing the modal participation factor for the two forms of loading.

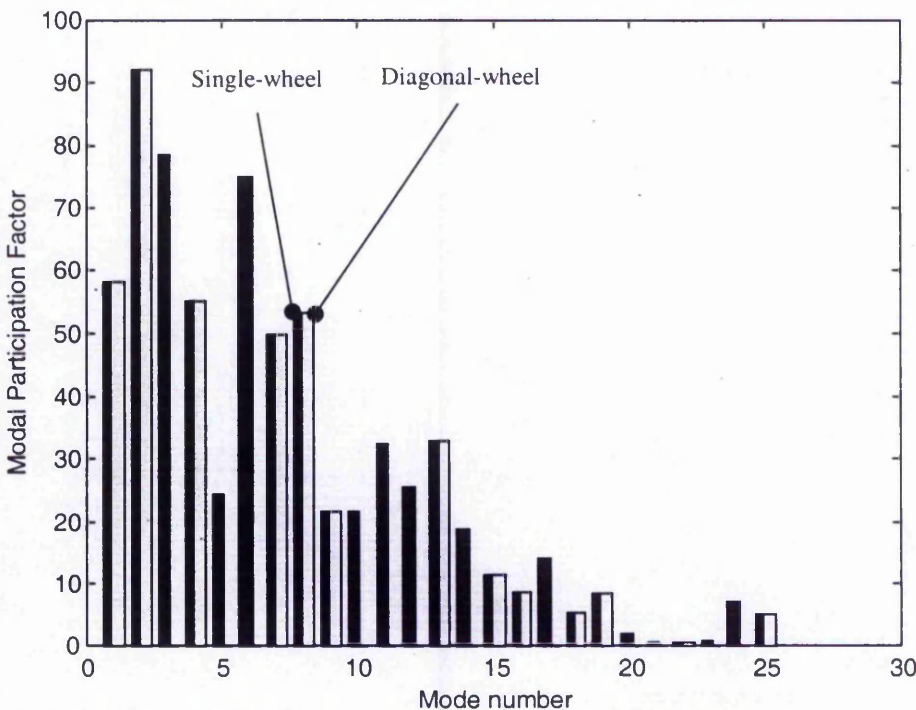


Figure 8.13 Comparison of modal participation factor between single-wheel and diagonal-wheel excitations.

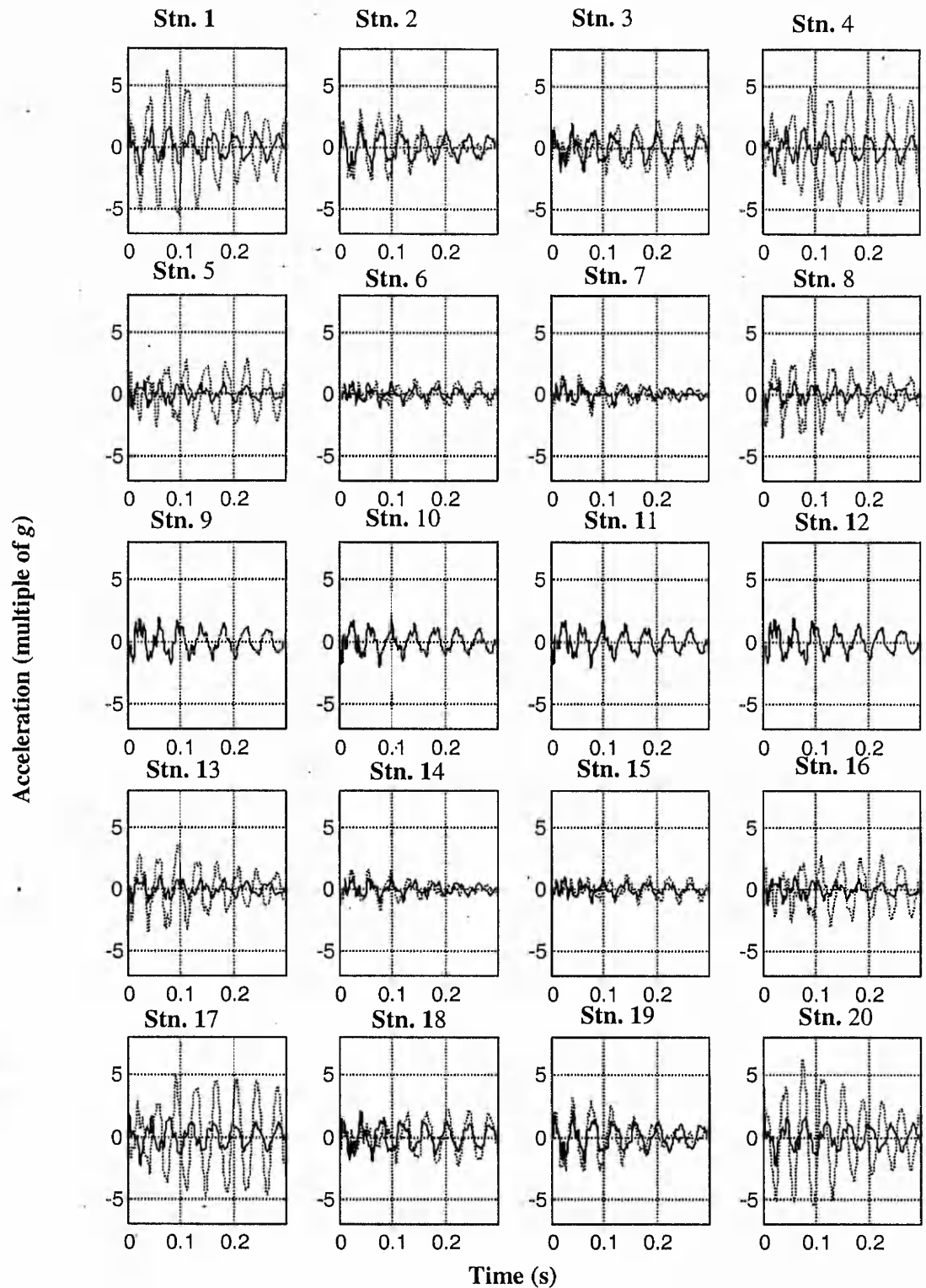


Figure 8.14 Comparison of acceleration response between 4-wheel excitations (solid) and diagonal-wheels excitations (dotted).

The modal participation factor, γ , is a measure of the contribution of a particular mode of vibration to the total response and is defined for the i^{th} mode as:

$$\gamma_i = \phi_i \vec{R} \quad (8.7)$$

where ϕ_i is the eigenvector of the i^{th} mode of vibration and \vec{R} is the global excitation force vector [91]. This parameter has been computed for the first 25 modes and the results have been plotted for the single-wheel and diagonal-wheel excitations in Figure 8.13. It is seen that for most of the modes the two excitations generate equal modal participation factors. However, the single-wheel excitation has non-zero modal participation factors in all the 25 modes considered, thus resulting in a higher response. Whereas in the diagonal-wheel excitation only a few modes including modes 1 and 2 are excited. The excitation of mode 2 is particularly important as it corresponds to diagonal corner deformations which are in phase with this second mode of loading (i.e. diagonal-wheel excitation). Also since most of the vibration energy is contained in the first few modes this contributes to the similarity between the acceleration responses of the two types of excitation.

The diagonal-wheel form of excitation is a more realistic form of loading that represents the most common scenario in uneven terrain navigation. It is seen that this loading induces significant acceleration in the zones close to the wheels that are involved in the excitation.

8.6 Four-wheel Excitation

Another familiar scenario of excitation is when the wheels on the same axle hit a fixed obstacle simultaneously. The wheels on the other axle will produce a reactive impulse in order to generate a counteracting angular impulse. This case represents a four-wheel excitation such that the excitation force vector in the global coordinates is given by:

$$R(t)^T = [r_1(t) \ r_2(t) \ r_3(t) \ r_4(t) \ 0 \ \dots \ 0] \quad (8.8)$$

A case where the wheels on the front axle collide to produce a step excitation force has been considered. The rear wheels are subjected to a reactive impulse whose

value can be computed in a manner similar to the case of the diagonal excitation. Thus,

$$I_y \Delta\omega = M \Delta t \quad (8.9)$$

I_y is the pitch moment of inertia and $\Delta\omega$ is the change in pitch angular velocity. The total moment produced by the rear and the front wheels is given by:

$$M = (r_1(t) + r_2(t))l_f - (r_3(t) + r_4(t))l_r \quad (8.10)$$

Assuming uniform force distribution on the wheels that are lying on the same axle we have:

$$r_1(t) = r_2(t) \text{ and } r_3(t) = r_4(t)$$

Thus,

$$r_3(t) = -\frac{I_y \Delta\omega}{l_r \Delta t} + r_1(t) \frac{l_f}{l_r} \quad (8.11)$$

The acceleration response map for the four-wheel loading has been plotted in

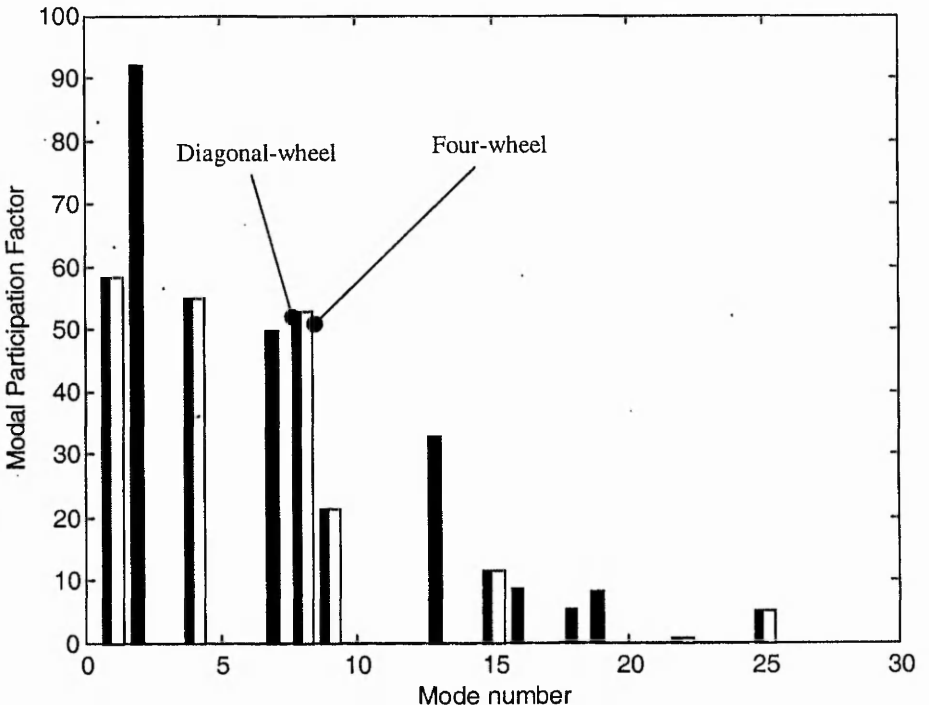


Figure 8.15 Comparison of modal participation factors between diagonal and 4-wheel wheel excitations.

Figure 8.14. Also shown are the responses due to diagonal-wheel excitations. Again the distribution of the acceleration response is quite similar to the previous two cases considered, i.e. single-wheel and diagonal-wheel excitations. However, it is noted that the four-wheel excitation induces peak acceleration responses which are less severe than the case of diagonal-wheel loading. This can be explained by examining the modal participation factors for the two forms of loading, which is given in Figure 8.15. It is seen from this figure that the modal participation factor for the second mode of vibration corresponding to the four-wheel mode of excitation is zero. This means that the second mode of excitation is not excited by this form of loading thus not contributing to the total response. On the other hand the diagonal-wheel form of loading excites this mode with a strong intensity. This makes the total response due to diagonal-wheel excitation stronger than that due to 4-wheel excitations.

The fact that the diagonal mode excites the second mode can be deduced by inspecting the shape of the second mode of vibration as given in Figure 8.3. This mode is a vibration about the diagonal axes which is in phase with the diagonal-wheel form of loading.

Having noticed the importance of the second mode of vibration to the acceleration response it can be deduced that a better design of WMR chassis should provide a higher natural frequency for this mode which helps to decrease the sensitivity of the response to the 2nd mode of vibration. One possible solution to achieve this is by stiffening the platform in the diagonal directions. This can be done, for example, by introducing two diagonal stiffening bars welded at the corners of the platform. It is also noted that the mid-span stations (stations 9 to 12 in Figure 8.1) respond with identical intensity to both 4-wheel and diagonal-wheel forms of loading. The reason is that due to symmetry the modes of vibrations excited by the diagonal-wheel form of loading alone are stationary, i.e. they have zero modal response.

8.7 Summary Comments

The analytical approach for estimating the shock response of WMRs provided in the previous chapter has been applied to three case studies. It has been found that

an unsymmetrical collision, which involves a diagonal-wheel excitation, generates larger acceleration responses than a symmetrical collision that involves a 4-wheel excitation. This has a practical implication for path planning of WMRs. If a collision between the wheels and a ground obstacle is unavoidable then it is preferable to steer the robot in such a way to achieve a full frontal collision instead of having a non-symmetrical one. The full frontal collision results in a 4-wheel excitation while the unsymmetrical collision brings about a diagonal-wheel form of loading.

Chapter 9

Discussion

9.1 Discussion

This project has been undertaken at a time when very little work existed on the three dimensional dynamics of WMRs, at a time even when there are several open questions regarding the two dimensional dynamics of WMRs. It has been the aim of this project to provide a mathematical basis for understanding the dynamics of WMRs navigating on uneven terrain, identify the undesired dynamic effects of uneven terrain dynamics, propose and validate remedying techniques.

The problems related to dynamic responses of WMR navigating unstructured ground surface were tackled in this work. It was found convenient to divide the modelling task into two considerations, namely, rigid body dynamics and non-rigid body dynamics. In the rigid body dynamics the effect of the structural flexibility of the chassis and the wheels has been ignored. This model is reasonably justified for navigating conditions where the geometry of the ground is smoothly varying, with no abrupt changes that may otherwise cause severe collisions between the wheels and the discontinuous ground surface. It was found more convenient to deal with the problem by the Newton-Euler modelling approach as this method provides a means to deal with the forces directly rather than implicitly, as is the case in the Lagrangian modelling approach. Furthermore, during an uneven terrain manoeuvre it is more practical to measure the wheel forces rather than the geometry of the terrain itself.

In the rigid-body dynamics consideration the problem of wheel-ground contact loss has been depicted as a linear complementary problem. A method to predict such contact loss has been presented in Section (3.2.6). Such a method is useful for path and trajectory planning of WMRs navigating an uneven ground surface with smoothly varying geometry. It was noted in particular that, for a given WMR, wheel-ground contact loss is dependent on the profile angle of the ground surface, the magnitude of the traction force and the mode of traction (i.e. front, rear or four-wheel traction).

The jerk response of mobile structures has been found to be a useful quantifier of the harshness of motion. It is thought that human beings intuitively handle objects with minimum jerk. In the context of WMRs, the higher the jerk the greater is the potential of dropping loose payloads from the platform of the WMR. A mathematical technique that can be used to compute the rigid-body jerk response of a WMR that traverses ground surface unevenness has been developed. A methodology based on the regulation of the traction forces to reduce the jerk response has also been proposed.

The normal jerk on the platform is an important parameter in estimating the potential to which unrestrained payload is subjected to a '*lifting off*' effect during an obstacle traversing manoeuvre. By means of a simplified model, extracted from the generic mathematical model of WMRs navigating a terrain of arbitrary geometry, it has been shown that this parameter is a function of the velocity of the WMR, the geometry of the terrain, and the traction force on the wheels. In the derivation of the model it has been assumed that:

- the WMR undergoes a straight line motion,
- the front wheels encounter a laterally symmetric obstacle,
- the WMR undergoes a smooth transition between planar and motion over the obstacle.

The relationship between the normal jerk response, the road profile angle and the traction forces has been exploited to the benefit of reducing the jerk for a given geometry. While this scenario represents an ideal situation, because smooth transition between planar motion and motion over obstacles is not always possible, the analytical relationship between actuation forces, geometry of obstacle and jerk can be used where the above assumptions are reasonably satisfied. Although it is not expected to completely nullify jerk, mainly due to uncertainty in dimensional and geometric parameters involved in the model, this technique should provide a starting point for enhancing the smoothness of WMR manoeuvres in the presence of obstacles. Also as the approach is not based on state-feedback it does not require complex control systems.

Traditionally in WMR control, wheel rotations (displacement based control) have been used as the controlling inputs. The traction forces are not normally computed nor monitored. This is a setback, as important issues such as the availability of friction forces could not be addressed. One advantage of the approach followed in the present work is that such forces are explicitly available either for motion control purposes or motion planning assessments. Thus using the model developed in Chapter 4 one can plan motion knowing that the ground surface (and the wheels) can generate the required traction forces without causing the wheels to skid because of friction saturation. Requiring the driving motors of the wheels to generate a required torque, as opposed to displacement, needs an underlying torque control scheme. However, torque control is not a well developed discipline at the moment and the author hopes there will be significant progress in this area so that efficient traction force control systems could be developed.

The pitching-motion of a WMR has also been considered for defining the smoothness of manoeuvre over a front-wheel obstacle. A single, polynomial smooth trajectory has been chosen to plan this pitching motion. Such a trajectory, which is defined by a single continuous function, is advantageous from the computational point of view, as it requires less computational effort. However, a series of interconnected polynomial curves, i.e. *splines*, could have given more flexibility for satisfying more constraints on the maximum actuation forces, maximum manoeuvre time and maximum velocity, maximum acceleration and maximum intermediate jerk. This in turn would have led to a formulation of an optimisation problem. Taking into account that obstacle-traversing manoeuvres are accompanied by fast motions, online solutions of the optimisation problem using the processor aboard the robot may not be a feasible option. Nonetheless such a technique of solving optimisation problems may be useful for off-line programming technique and further investigations will be needed.

The polynomial trajectory-planning technique is a convenient way of specifying the manoeuvre time, peak velocity, peak acceleration, peak jerk and guaranteeing minimum jerk engagement and disengagement of actuation. This method in conjunction with the analytical model for the dynamics of the WMR is used to

compute a wheel traction force needed to achieve the set objectives. The computed traction force is supplied as a command to another level of traction control system. Traction control is a fairly well treated topic and discussions highlighting the state-of-the art of traction control have been given in the background theory.

The second part of this work attempted to answer the question: what happens if the geometry of the ground surface contains discontinuities? In this case a collision between the wheels and the ground surface irregularity is imminent. The consequences in the event of an impact are twofold:

- The impact causes wheel-ground contact loss, thus adversely affecting the controllability of the WMR.
- Shock loads are generated at the wheel-ground interface causing structural vibration of the chassis with adverse effects on the safety of the WMR's delicate instrumentation and payload.

To assess the effect of the wheel-ground impact on the wheel contact loss, the problem has been modelled by extending the rigid body dynamics model of the WMR to incorporate the deformations of the wheel. The model has been used to devise a control scheme in order to minimise wheel-ground contact loss during wheel collisions with ramp obstacles. As in the case of the rigid-body dynamics the traction forces are used as a means of actuation. The analytical control scheme has been tested by means of simulation in MATLAB®. The effectiveness of the model was evident from the results of the simulations. However, several simplifying assumptions were made in the analytical model. In particular the inertia of the wheels were assumed negligible, the flexibility of the chassis was ignored, the deformations of the wheels were assumed to be radial and concentrated at the locality of wheel-ground contact points. By means of finite element simulation the robustness of the control scheme was also assessed using a more realistic, full-order model. The finite element model was constructed in an attempt to fully represent the actual WMR, with all its structural details, and its working conditions. The evaluation of the control system in this full-order, finite element simulation was found to be satisfactory. Another benefit of the finite element simulation has been that it was possible to apply the control forces that had been

predetermined. This corresponds to an off-line implementation of the proposed control scheme. The achievement of the desired wheel-grip effect by applying predetermined control forces has been a noteworthy good performance of the control system.

The elasticity property of the wheels has been an important parameter in determining the magnitude of the traction forces. In particular it is found that the stiffer the wheel the greater is the magnitude of the traction forces required to maintain wheel-ground grip after an impact. However, it is also known that the softer the wheel the larger is the wheel-rolling resistance. Large deformations of the wheels are also undesirable from the point of view of odometry (the technique used to estimate the distance travelled by a WMR based on wheel rotation counts) as larger radial deformations can cause larger error when computing the displacement of the wheel centre. The choice of the material for the wheels needs to be based on a compromise between the need to achieve lower demand for traction control forces, and the reduction of wheel rolling resistance forces as well as the reduction of odometric error.

Regarding the problems associated with the shock-induced vibration, the approach in this work has been to devise an analytical tool for estimating the acceleration response at various stations on the chassis of the WMR. The method relies on structural characteristic data especially modal properties such as natural frequencies and modal shapes of the platform, parameters that can be determined experimentally or by carrying out a finite element analysis on the design of the WMR's chassis. Also needed are the estimates of the peak shock forces. The acceleration response was taken as a measure of the potential damage to delicate instrumentation and payload aboard the WMR.

As ideal, smooth and flat ground surfaces are available only in very limited applications, the successful development of wheeled mobile robots hinges on their capability to cope with the adverse effects of ground surface unevenness. Notwithstanding the simplifying assumptions used in the formulation of the equations of motion and in subsequent case studies the work presented here should provide a basis for engineers to assess the adverse effects of uneven ground surface navigation.

In the treatment of the shock response analysis only the flexibility of the chassis has been considered, and the wheel vibrations were ignored. This is justified because in a typical WMR the wheels have much less inertia than the combined value of the chassis and the payloads. Three case studies representing a theoretical scenario with a single-wheel excitation and two practical scenarios with diagonal-wheel and 4-wheel excitations were investigated. It was noted that the diagonal-wheel excitation, often a consequence of unsymmetrical wheel-ground collision, resulted in larger acceleration responses over a wide area of the platform than those observed in the 4-wheel collision. Regarding the distribution of the potential damage that might be caused by large peak acceleration responses across the platform, the corners and edges of the rectangular platform considered were found to be high risk zones for placing vibration sensitive instrument or payload. Similar to the problem of minimising traction control effort during wheel-ground impact problem it was found that soft wheels provide a less sustained acceleration response than rigid wheels.

The author believes that the objectives set out in this research program have been satisfactorily completed with the following major contributions:

- A three-dimensional, analytical, rigid-body, dynamics model of WMRs navigating uneven ground surface has been developed.
- The problem of wheel-ground contact loss due to rigid body dynamics of WMRs has been analytically represented and the parameters that affect it have been identified. These parameters are the profile angle of the obstacle, the magnitude of the traction force and the mode of traction (front/rear/4-wheel traction).
- Jerk associated with the rigid body dynamics of the WMRs has been identified as a measure of the non-smoothness of manoeuvre of WMRs over obstacles. Analytical relationships that enable the computation of the normal jerk have been developed. By employing the relationship between traction forces and the normal jerk a method that enables the minimisation of normal jerk by using a traction control scheme has been proposed and evaluated by means of simulations.

- A polynomial trajectory planning technique that is used to conveniently specify the manoeuvre time over obstacles based on a prescribed peak jerk, acceleration, velocity or maximum traction forces has been proposed. The method has been used in conjunction with the pitching motion of a WMR that travels over a frontal obstacle of an arbitrary geometry.
- An extended dynamics model of WMRs that takes account of wheel deformations has been devised.
- By using the extended dynamics model an impact control scheme that prevents wheel rebounding during a collision between the wheels and stationary ground obstacles has been proposed. Simulation results have shown the effectiveness of the proposed control scheme to control impact.
- An analytical tool that enables the estimation of acceleration response at various points on the platform of WMRs that are subject to shock loading due to wheel-obstacle collision has been developed.

Chapter 10

Conclusions and Further Work

10.1 Conclusions

The aim of this investigation was to carry out dynamics analysis of Wheeled Mobile Robots navigating uneven terrain to enable a better understanding of their behaviour while working in a non-ideal environment. The adverse effects of uneven terrain manoeuvre on a WMR are found to be:

- jerk associated with the rigid body dynamics.
- wheel-ground contact loss, both due to rigid body dynamics and wheel-ground impact.
- chassis vibration induced by shock loading of wheel-ground impact.

The normal jerk associated with rigid body dynamics of a WMR traversing a fixed ground obstacle is the cause of the '*lifting off*' effect of loose payloads aboard the WMR. It has been shown that this quantity can be reduced by a proper choice of traction forces that drive the WMR across an obstacle. There is a potential risk of wheel-ground contact loss associated to the rigid body dynamics. This risk is a function of the modes of traction, namely, front/rear/4-wheel traction. It has been found that for a WMR negotiating a front axle obstacle rear wheel traction provides a better performance by allowing larger traction forces to be generated without causing wheel-ground contact loss.

Motion planning is another important way of minimising the rigid body dynamics jerk. This method, which has been investigated in relation to the pitching dynamics of a WMR traversing an obstacle of known geometry, has been shown to be a convenient way of specifying peak jerk, peak acceleration, peak velocity. The traction forces needed to achieve the above specified quantities can easily be computed by means of the tools presented in Chapter 5.

Wheel-ground impact is a major problem inherent in uneven terrain navigation of WMRs. This phenomenon has been observed to cause wheel-ground contact loss

due to the structural dynamics localised in the region of wheel-ground contact points. It has been found that this problem can be minimised by using a traction control system that takes into account the material properties of the wheels, the dimensions and inertia of the WMR, and the velocity of the vehicle. It has been observed that soft wheels provide a better choice for minimising wheel-ground contact loss due to wheel-ground impact by demanding lower magnitude of traction forces.

Another major problem intrinsic to WMRs navigating an uneven terrain is the shock loading of the platform due to collisions between wheels and obstacles. The approach followed in this work is to devise an analytical tool that enables the estimation of the acceleration responses and their distribution across the platform. By means of a case study it has been shown that some areas of a rectangular chassis, namely, the edges and the corners, are susceptible to large peak acceleration responses making them unsuitable for placement of vibration sensitive instrumentation and payload. It has also been shown that unsymmetrical collision between wheels and obstacles causes larger peak acceleration responses than symmetrical collision.

10.2 Further Work

The author believes that the objective set out to be accomplished in this project, which is to contribute to the understanding of WMR dynamic behaviour during uneven ground surface navigation, has been achieved successfully. However several areas are still open for future research in this topic. Including:

- Devising measuring techniques for ground profile geometry.
- Development of jerk measuring techniques.
- Extension of the trajectory planning technique.
- Extension of the dynamics model for multiple contacts of wheel and ground surface.

10.2.1 Ground Profile Measurement

Most of the analysis work presented in this relies on the knowledge of the geometry of the geometry of the obstacle. It has been assumed that such an information would be available for use in the dynamics model presented. In practice the acquisition of this parameter is not easy and further research is needed to develop an appropriate technique for use with WMRs. In the literature several ways of

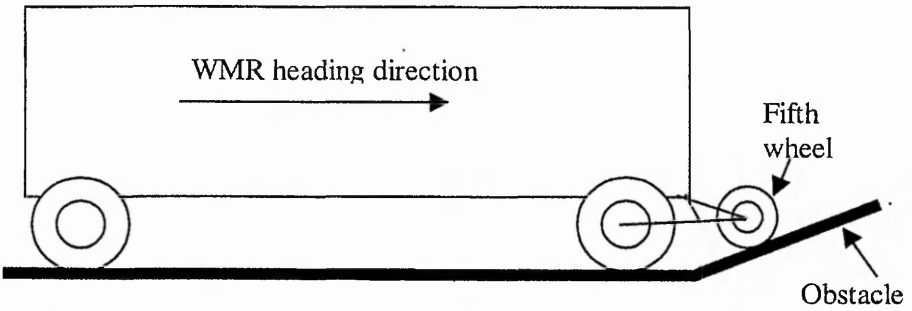


Figure 10.1 Fifth-wheel technique for measuring obstacle geometry.

obtaining obstacle geometry have been sited including optical techniques. The author believes the fifth-wheel technique as used by vehicle handling researchers to measure wheel forces can be adapted to the purpose of measuring wheel obstacle geometry. Such a technique could work by attaching a dummy wheel to the chassis of the WMR which traverses the obstacle ahead of the wheels of the WMR as shown in Figure 9.1. The profile geometry can be obtained by measuring the displacement of the centre of the fifth-wheel from a reference plane. This can be achieved either by mechanical means, which requires some mechanism or an electrical means by attaching a potentiometer that transforms the displacement of the centre of the fifth-wheel to an electrical signal which can then be fed to the WMR's microprocessor.

10.2.2 Measuring Jerk

Jerk is an important parameter that quantifies the smoothness of WMR manoeuvre over obstacles. To date there has been no technique that enables the direct

measurement of this high order quantity, to the best of the knowledge of the author. This is partly because jerk is not governed by similar physical relationships governing acceleration, which thanks to Newton's law, can be directly measured by means of accelerometers. Other quantities such as displacement and velocity can be estimated by successive integration of acceleration measurements. Theoretically jerk can be obtained by differentiating acceleration response with respect to time. Unfortunately, acceleration response as measured by accelerometers is quite noisy and the differentiation of such a noisy signal degrades the quality of the data even further. This problem could be overcome if a technique could be developed that measures jerk directly rather than relying on acceleration measurements.

10.2.3 Trajectory Planning

A simple polynomial trajectory planning technique has been proposed in Chapter 5. The simplicity of the proposed technique means it is suitable for real-time implementations. However the technique can be used to optimise only one parameter at a time. In the present work only jerk has been used as a quantity to be reduced. In practice one may want to obtain a feasible trajectory based on multiple criteria including minimum jerk, minimum traction force, minimum acceleration, minimum task time and minimum power. Such a consideration needs a formulation of an optimisation problem based on the constraints such as maximum allowable jerk, available traction force, maximum acceleration available drive power and maximum time for completing the desired task. The solution of the optimisation problem then results in a feasible trajectory that satisfies the above stated constraints.

10.2.4 Multiple Wheel-Ground Contact

For the purpose of simplicity in the work presented it has been assumed that each wheel makes a single contact with the ground surface at a given instant. However, in practice a wheel may make several contacts with the surface as shown in Figure 9.2. The dynamics model needs to be extended in order to investigate the effect

of the distribution of the reaction forces as well as the traction forces on the dynamic behaviour of the WMR.

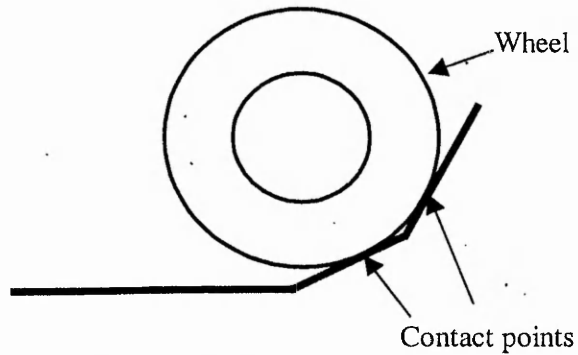


Figure 10.2 A wheel that makes multiple contacts with the ground surface.

References

- 1 Holland, J., "Basic Robotics Concepts," Howard W. Sams & Co., Indianapolis, 1983.
- 2 Muir P, Neuman, C., "Kinematic Modelling of Wheeled Mobile Robots," Journal of Robotic Systems, Vol. 4, 1987.
- 3 Gould, L., "Europe 1996: The drive for new technologies continues," Modern Materials Handling, Cahners Business Information, A Division of Reed Elsevier, Inc., No. 4, 1996.
- 4 Scheding S., Dissanayake G., Nebot E. M. and Durrant-Whyte H, "Experiment in Autonomous Navigation of an Underground Mining Vehicle," IEEE Transactions on Robotics and Automation, Vol.15, No.1, 1999.
- 5 Hollingum, J., "Robots for Dangerous Tasks," DERA, Defence Evaluation and Research Agency, Industrial Robot, Vol. 26, No. 3, 1999.
- 6 Salichs, M., Moreno, L., "Navigation of Mobile Robots: Open questions," Robotica, Vol.18, No.3, 2000.
- 7 Popa, D., "Path-Planning and Feedback Stabilization of Nonholonomic Control Systems," PhD Thesis, Rensselaer Polytechnic Institute, 1998.
- 8 Zhang Y., Velinsky S. and Feng X., "On the Tracking Control of Differentially Steered Wheeled Mobile Robots," Journal of Dynamic Systems, Measurement, and Control, Vol.119, No.3, 1997.
- 9 Alexander, C. and Maddocks, H., "On The Kinematics of Wheeled Mobile Robots," The International Journal of Robotics Research, Vol. 8, No. 5, 1989.
- 10 Tounsi, M., Corre, J., "Trajectory Generation for Mobile Robots," Mathematics and Computers in Simulation, Vol. 41, 1996.
- 11 Piazzì A., Visioli A., "An Interval Algorithm for Minimum-Jerk Trajectory Planning of Robot Manipulators," Proceedings of the 36th IEEE Conference on Decision and Control, 1997.

- 12 Egerstedt. M., Hu, X., Stotsky, A., " Control of a Car-Like Robot Using a Virtual Vehicle Appraoch," Proceedings of the IEEE Conference on Decision and Control, Florida, USA, 1998.
- 13 Shiller, Z., and Gwo, Y., "Dynamic Motion Planning of Autonomous Vehicles," IEEE Transactions on Robotics and Automation, 1991.
- 14 Choi, J., Sreenivasan, V., "Gross motion characteristics of articulated mobile robots with pure rolling capability on smooth uneven surfaces," IEEE Transactions on Robotics and Automation, Vol.15, No.2, Austin, USA, 1999.
- 15 Matsumoto, O., Kajita, S., Tani, K., Oooto, M., "A four-wheeled robot to pass over steps by changing running control modes," IEEE International conference on Robotics and automation, 1995.
- 16 T. Estier, Y. Crasaz, B. Merminod, M. Lauria, R.Piguet, R. Siegwart," An innovative Space Rover with Extended Climbing Abilities", Proceedings of *Space and Robotics 2000*, Albuquerque, USA, 2000.
- 17 Guntur R. and Sankar S., "A friction circle concept for Dugoff's tyre friction model," International Journal of Vehicle Design, Vol 1, No 4, 1980.
- 18 Wang, Y, Linnet, J., Roberts, J., " A Unified Approach to Inverse and Direct Kinematics for Four Kinds of Wheeled Mobile Robots and its Application," Proceedings of the IEEE International Conference on Robotics and Automation, Minnesota, 1996.
- 19 Scheding S., Dissanayake G., Nebot E., Durrant-Whyte H., "Slip Modelling and Aided Inertial Navigation of an LHD," Proceedings of IEEE International Conference on Robotics and Automation.
- 20 D'Andrea Novel B., Campion G, Bastin G., "Control of wheeled mobile robots not satisfying ideal velocity constraints: a singular perturbation approach," International Journal of Robust and Nonlinear Control, Vol. 5, No.4, 1995.
- 21 Agullo J., Cardona S, Vivancos J., "Kinematics of Vehicles with Directional Sliding Wheels," Journal of Mechanism and Machine Theory, Vol. 22, No. 4, 1987.

- 22 Deng, Z., Brady, M., "Dynamics and Control of a Wheeled Robot," Proceedings, The American Control Conference, San Francisco, 1993.
- 23 Boyden F., Demick and Velinsky, Steven A., "Dynamic Modelling of Wheeled Mobile Robots for High Load Applications," Proceedings of IEEE International Conference on Robotics and Automation, No 4, 1994.
- 24 Mehrabi M. G., and Hemami, A., "Dynamic Modelling of Wheeled Mobile Robots", Second IEEE Conference on Control Applications, Vancouver, 1993.
- 25 Thanjavur K., Rajagopalan, R., "Ease of Dynamic Modeling of Wheeled Mobile Robots (WMRs) using Kane's Approach," Proceedings of the 1997 IEEE International Conference on Robotics and Automation, New Mexico, 1997.
- 26 Kane R., "Dynamics: theory and applications," McGraw-Hill Series in Mechanical Engineering, New York: McGraw-Hill, 1985.
- 27 Pilutti, T., Ulsoy, G., Hrovat, D, "Vehicle Steering Intervention Through Differential Braking," Transactions of ASME. Journal of Dynamic Systems, Measurement, and Control, Vol. 120, 1998.
- 28 Sledge Jr, N., Marshek, K., "Development and Validation of an Optimized Emergency Lane-Change Trajectory," SAE Special Publications, Vol. 1361.
- 29 Matsumoto N., Tomizuka M., "Vehicle Lateral Velocity and Yaw rate Control with Two Independent Control Inputs," Journal of Dynamic Systems, Measurement and Control, Transactions of the ASME, Vol.114, No.4, 1992.
- 30 Ben Amar, F., Bidaud, P., Ben Ouezdou, F., "On Modelling and Motion planning of Planetary Vehicles," Proceeding of the 1993 IEEE/RSJ International Conference on Intelligent Robots and Systems, 1993.
- 31 Siméon, T., Dacre-Wright, B, "A Practical Motion Planner for All-Terrain Mobile Robots," IEEE International Conference On Intelligent Robots and Systems, Yokohama, Japan, 1993.
- 32 Cherif, M., Laugier, C., "Motion planing of Autonomous Off-Road Vehicles Under Physical Interaction Constraints," Proceedings of IEEE International Conference on Robotics and Automation, 1995.

- 33 Necsulescu D., Lonmo V., Kim, B., Vukovich G., "Autonomous mobile robot control in operational space with torque saturation, slippage and tip-over avoidance," IECON Proceedings (Industrial Electronics Conference), Vol.2, 1995.
- 34 Borenstein J., Feng L., "Gyrodometry: a new method for combining data from gyros and odometry in mobile robots," Proceedings of IEEE International Conference on Robotics and Automation, Vol.1, 1996.
- 35 Volpe, R., Khosla, P., " On The Equivalence of Second Order Impedance Control and Proportional Gain Explicit Force Control," The International Journal of Robotics research, 1994.
- 36 Schutter, J., Bruyninckx, H., Spong, M., " Force Control: A Bird's Eye View," IEEE CSS/RAS International Workshop on Control Problems in Robotics and Automation: Future Directions, San Diego, USA, 1997.
- 37 Sarkar, N., Yun, X., " Design of a Continuos Controller for Contact Transition Task based on Impulsive Constraint Analysis," Proceedings of the IEEE International Conference on Robotics and Automation, Minnesota, 1996.
- 38 Seraji, H., Colbaugh, R., "Force Tracking in Impedance Control," The International Journal of Robotics Research, Vol. 16, No. 1, 1997.
- 39 Milliken, F., Milliken, D., "Race Car Vehicle Dynamics," Warrendale, SAE International, 1995.
- 40 Dugoff, H., Fancher, P., Segel, L., "An Analysis of Tire Traction Properties and Their Influence on Vehicle Dynamic Performance, " SAE Paper No. 700377, 1970.
- 41 Palkovics, L. El-Gindiy, M., Pacejka, H., " Application of Neural Networks to Tyre Modelling for Vehicle Simulation," International Journal of Vehicle Design, Heavy Vehicle Systems, Vol. 3, Nos. 1-4, 1996.
- 42 Genta, G., "Motor Vehicle Dynamics: Modelling and Simulation," Singapore: World Scientific, 1997.

- 43 Sakai, S., Sado, H., Hori, Y., " Motion Control in an Electric Vehicle with Four Independently Driven In-Wheel Motors," IEEE/ASME Transactions on Mechatronics, Vol. 4, No. 1, 1999.
- 44 Makki, A.; Siy, P. "A robust traction controller design using the theory of variable structure systems," Proceedings of the 36th Midwest Symposium on Circuits and Systems, vol.1, 1993..
- 45 Sarkar, N., Yun, X., "Traction Control of Wheeled Vehicles Using Dynamic Feedback Approach," Proceedings of IEEE/SRJ International conference On Intelligent Robots and Systems, Victoria, 1998.
- 46 Hori, Y., Toyoda, Y., Tsuruoka, Y., "Traction Control of Electric Vehicle: basic Experimental Results Using The Test EV 'UOT Electric March'," IEEE Transactions on Industry Applications, Vol. 34, No. 5, 1998.
- 47 Kim R, Lee J., Kim, J., "Dead-reckoning of a Two-Wheeled Mobile Robot on Curved Surfaces," Proceedings of the IEEE International Conference on Robotics and Automation, Minneapolis, 1996.
- 48 Zhao, Y., BeMent, S., "Kinematics, Dynamics and Control of Wheeled Mobile Robots," Proceedings of the IEEE International Conference on Robotics and Automation, nice, France, 1992.
- 49 Necsulescu, D., Lonmo, V., Kim, B., Droguet, E., "Autonomous Mobile Control Using Kinematics and Dynamics Based Approaches," IEEE, 1996.
- 50 Alicja Mazur, "A New Adaptive Tracking Control Law for Nonholonomic Wheeled Mobile Robots Moving in R^3 Space," IEEE.
- 51 Cheng, R., Hemami, A Mehrabi, M, " Control of A Wheeled Mobile Robot with Double Steering," IEEE/RSJ, International Workshop on Intelligent Robots and Systems, Osaka, Japan, 1991.
- 52 Shekhar, S. " Wheel Rolling Constraints and Slip in Mobile Robots," Proceedings of the IEEE International Conference on Robotics and Automation, New Mexico, 1997.
- 53 Marth, G., Tarn, T., Bejczy, A., " An Event Based Approach to Impact Control: Theory and Experiments," IEEE, 1994.

- 54 Allotta, B., Buttazzo, G., " Impact Handling by Proximity and Force Sensing," Proceedings of IEEE International Conference on Robotics and Automation, France, 1992.
- 55 Siméon, T., "Motion Planning for a Non-holonomic Mobile Robot on 3-dimensional Terrain," *IEEE/RSJ International Workshop on Intelligent Robots and Systems, IROS'91*, Osaka, Japan, 1991.
- 56 Hait, A., and Siméon, T., " Motion Planning on Rough Terrain for an Articulated Vehicle in Presence of Uncertainties," *IEEE International Conference on Intelligent Robots and Systems*, Vol.3, 1996.
- 57 Moez Cherif, Christian Laugier, " Motion planning of Autonomous off-road vehicles under physical interaction constraints," IEEE International Conference On Robotics and Automation, 1995.
- 58 J.R. Ellis, "Vehicle handling dynamics," Mechanical Engineering Publications Limited, London, 1994.
- 59 T. Tseng, D. Hrovat, " Some characteristics of optima vehicle suspensions based on quarter-car models", IEEE Proceedings of the 29th conference on decision and control, Honolulu, 1990.
- 60 J. P., Den Hartog, "Mechanical vibrations," McGraw-Hill, London, 1956.
- 61 Lotstedt P., "Mechanical Systems of Rigid Bodies Subject to Unilateral Constraints," *SIAM Journal on Applied Mathematics*, Vol.42, No.2, 1982.
- 62 Kraus R., Kumar V., Dupont P., "Analysis of frictional contact models for dynamic simulation," *Proceedings of IEEE International Conference on Robotics and Automation*, Vol.2, 1998.
- 63 Trinkle C. and Pang S., "Dynamic multi-rigid-body systems with concurrent distributed contacts," *Proceedings of IEEE International Conference on Robotics and Automation*, Vol.3, 1997.
- 64 Dupont E. and Yamajako P., "Stability of frictional contact in constrained rigid-body dynamics," *IEEE Transactions on Robotics and Automation*, Vol.13, No.2, 1997.

- 65 Dupont E. and Bapna D., "Perturbation stability of frictional sliding with varying normal force," *Journal of Vibration and Acoustics, Transactions of the ASME*, Vol.118, No.3, 1996.
- 66 Pang S. and Trinkle C. and Lo G., "Complementarity approach to a quasistatic multi-rigid-body contact problem," *Computational Optimisation Applications*, Vol.5, No.2, 1996.
- 67 Baiardi P., Cannata G., Casalino G. and Pagano P., "Modelling contact phenomena within the dynamic simulation of advanced robotic structures," Proceedings – IEEE.
- 68 Baraff, D., "Issues in Computing Contact Forces for Non-penetrating Rigid Bodies," *Algorithmica*, 1993, pp. 292-352.
- 69 R. Cottle, J. Pang and R. Stone. "The Linear Complementarity Problem," *Series on Computer Science and Scientific Computing*, Academic Press, Boston, 1992.
- 70 Serna, M., Bayo, E., "Trajectory Planning for Flexible Manipulators," Proceedings 1990 IEEE International Conference on Robotics and Automation, Vol.2. Los Alamitos, USA, 1990.
- 71 Suzuki, T., Nagai, J., Okuma, S., "A Realtime Trajectory Planning Method for Manipulators Based on Kinetic Energy," IEEE International Workshop ON Intelligent Robots and Systems, Okata, Japan, 1991.
- 72 Won, J., Choi, B. and Chung, J., "Smooth Joint Trajectory Planning for a Point-To-Point Task," IEEE International Workshop on Intelligent Robots and Systems, Okata, Japan, 1991.
- 73 Burg, Jan van der and Blazevic, P., "Anti-lock braking and Traction Control Concept for All-terrain Robotic Vehicle," Proceedings of IEEE International Conference on Robotics and Automation, Vol.2, 1997.
- 74 Hori, Y., Yasushi, T. and Tsuruoka, Y., "Traction Control of Electric Vehicles: Basic Experimental Results Using the Test EV, UOT Electric March.," IEEE Transactions on Industry Applications, 1998.

References

- 75 Featherstone, R., "Robot Dynamics Algorithms," Kluwer Academic Press, 1987.
- 76 Goldsmith, W., "Impact - The Theory and Physical Behaviour of Colliding Solids," Edward Arnold Publishers Ltd., London, 1960.
- 77 Engel, P., "Impact Wear of Materials," Elsevier Scientific Publishing Company, The Netherlands, 1978.
- 78 Tornambe, A., "Modelling and Controlling One-Degree-of-Freedom Impacts," IEE Proceedings on Control Theory Applications, Vol. 143, No. 1, 1996.
- 79 Volpe, R., Khosla, P., "A Theoretical and Experimental Investigation of Impact Control for Manipulators," The International Journal of Robotics Research, Vol. 12, No. 4, 1993.
- 80 Horacio, M., Felippa, C., "Ephemeral Penalty Functions for Contact-Impact Dynamics," Finite Elements and Design, Elsevier Science Publishers, Vol. 9, 1991.
- 81 Shinners, S., "Modern Control System Theory and Design," John Wiley & Sons, Inc., 1998.
- 82 Hac, A., Youn I., Chen, H., "Control of suspensions for vehicles with flexible bodies-Part 1: active suspensions," Transactions of ASME, Journal of Dynamic Systems, Measurement and Control, Vol. 118, 1996.
- 83 Akpan, U., Kujath, M., "Stochastic vibration of a mobile manipulator.. Journal of applied mechanics," Vol. 64, No.3, 1997.
- 84 Stoianovici, D., Hurmuzulu, Y., "A Critical Study of the Applicability of Rigid-Body Collision Theory," Journal of Applied Mechanics, Vol. 63, 1996.
- 85 Eriksson, J., Hansson, M, "Measuring and Analysis of Pyrotechnic Shock," Thesis, Chalmers University of Technology, 1999.
- 86 Department of the Army, "Transportability Criteria of the Shock and Vibration," Department of the Army Technical Bulletin," TB 55-100, Washington D. C., 1964.

References

- 87 Ayalew, A., E. Lai, E., Oyadji, S.O., "Shock Response Analysis of WMRs," Proceedings of the International Conference on Gearing, Transmissions and Mechanical Systems, 2000, Nottingham, UK.
- 88 Narayanan, S., Senthil, S., "Stochastic Optimal Active Control of a 2-DOF Quarter Car Model with Nonlinear Passive Suspension Elements, Journal of Sound and Vibration, Vol. 211, 1998.
- 89 Ewins, D., "Modal testing : Theory and Practice," Taunton Research Studies Press, 1995
- 90 Meirovitch, L., "Analytical methods in vibrations," Collier-Macmillan, London 1967.
- 91 Bathe, K., "Finite element procedures in engineering analysis," Englewood Cliffs, Prentice-Hall, London, 1982.
- 92 L. Cremer, L., Heckl, M., "Structure-Borne Sound," Springer-Verlag, New York, 1988.
- 93 Yun, X., Srakar, N. "Dynamic feedback control of vehicles with two steerable wheels," Proceedings of the IEEE International Conference on Robotics and Automation, Minneapolis, USA, Vol 4, 1996.
- 94 Dugoff, H, Brown, B, " Measurement of Tire Shear Forces," Journal of SAE, Paper 700092, 1970.

Appendix A

Computation of Normal Jerk

Let

$$\begin{aligned}\Psi &= m[-2h(L_r + L_f)\sin(\gamma)\cos(\gamma) + (h^2 - 2L_rL_f - L_f^2)\sin^2(\gamma) + 2L_rL_f + L_f^2 + L_r^2] + I_y \sin^2(\gamma) \\ \xi_1 &= F_{fr}[(L_r^2 + L_f^2 + 2L_rL_f)\cos(\gamma) - h(L_r + L_f)\sin(\gamma)] \\ \xi_2 &= F_{tr}[-h(L_r + L_f)\sin(\gamma)\cos(\gamma) + (L_r + L_f)^2 \cos^2(\gamma)] \\ \xi_3 &= m \sin(\gamma)\cos(\gamma)[2v_z\omega_y h(L_r + L_f) - L_r g(L_r + L_f) + h\omega_y^2(L_f L_r + L_r^2)] \\ \xi_4 &= m \sin^2(\gamma)[hL_r g + L_r \omega_y^2(L_r L_f - h^2) + v_z \omega_y(L_f^2 + L_r L_f - h^2)] \\ \xi_5 &= -I_y \sin^2(\gamma)(v_z \omega_y + L_f \omega_y^2) \\ \xi_6 &= -m v_z \omega_y (L_r + L_f) \\ \xi &= \xi_1 + \xi_2 + \xi_3 + \xi_4 + \xi_5 + \xi_6\end{aligned}$$

The rate of change of longitudinal speed is given by:

$$\frac{d}{dt} v_x = \frac{\xi}{\Psi} \quad (\text{A.1})$$

Let

$$\eta = \eta_1 + \eta_2 + \eta_3 + \eta_4 + \eta_5 + \eta_6$$

$$\eta_1 = F_{fr}(L_r + L_f)\sin(\gamma)$$

$$\eta_2 = F_{tr}(L_r L_f + L_r^2)\sin(\gamma)\cos(\gamma)$$

$$\eta_3 = m(-2v_x\omega_y h(L_f + L_r) + \omega_y^2(2h^2 L_f + 2h^2 L_r - L_r L_f^2 - L_f L_r^2))\sin(\gamma)\cos(\gamma)$$

$$\eta_4 = I_y(v_x \omega_y - \omega_y^2 h) \sin^2(\gamma)$$

$$\eta_5 = m(v_x \omega_y(h^2 - L_f^2 - 2L_r L_f) - L_r^2 g + h\omega_y^2(3L_f L_r + L_r^2 + L_f^2 - h^2))\sin^2(\gamma)$$

$$\eta_6 = m(-h\omega_y^2 + v_x \omega_y)(L_r + L_f)^2$$

The rate of change of normal speed is given by:

$$\frac{d}{dt} v_z = \frac{\eta}{\Psi} \quad (\text{A.2})$$

Let

$$\rho = \rho_1 + \rho_2 + \rho_3$$

$$\rho_1 = F_{rf}(L_r + L_f) \sin(\gamma)$$

$$\rho_2 = F_{rf}(L_r + L_f) \sin(\gamma) \cos(\gamma)$$

$$\rho_3 = m(\omega_y^2(-L_f(L_r + L_f) \sin(\gamma) \cos(\gamma) + h(L_r + L_f) \sin^2(\gamma)) - L_r g)$$

The rate of change of pitch angular speed is given by:

$$\frac{d}{dt} \omega_y = \frac{\rho}{\Psi} \quad (\text{A.3})$$

Since,

$$a_{cx} = \frac{d}{dt} v_x + v_z \omega_y$$

then from Equation (A.1) we have

$$a_{cx} = \frac{\xi}{\Psi} + v_z \omega_y \quad (\text{A.4})$$

Similarly since

$$a_{cz} = \frac{d}{dt} v_z - v_x \omega_y$$

from Equation (A.2) we have

$$a_{cz} = \frac{\rho}{\Psi} - v_x \omega_y \quad (\text{A.5})$$

The normal jerk is given by:

$$J_{cz} = \left(\frac{d}{d\gamma} (a_{cz}) \right) \frac{d}{dx} \gamma v_x + v_x \left(\frac{d}{dt} \omega_y \right) + \omega_y (a_{cx} - v_z \omega_y)$$

Substituting from Equations (A.4-A.5) a_{cx} and a_{cz} we have:

$$J_{cz} = \left(\frac{d}{d\gamma} \left(\frac{\eta}{\Psi} - v_x \omega_y \right) \right) \frac{d}{dx} \gamma v_x + v_x \frac{\rho}{\Psi} + \omega_y \frac{\xi}{\Psi}$$

Simplifying

$$J_{cz} = \frac{\Psi \frac{d}{d\gamma} \eta - \eta \frac{d}{d\gamma} \Psi}{\Psi^2} \frac{d}{dx} \gamma v_x + v_x \frac{\rho}{\Psi} + \omega_y \frac{\xi}{\Psi} \quad (\text{A.6})$$

where

Appendix A – Computation of Normal Jerk

$$\frac{d}{d\gamma} \Psi = m(2h(L_r + L_f)(2\sin^2(\gamma) - 1) + 2(h^2 - 2L_rL_f - L_f^2)\sin(\lambda)\cos(\gamma)) + 2I_y\sin(\gamma)\cos(\gamma)$$

$$\frac{d}{d\gamma} \eta = \frac{d}{d\gamma} \eta_1 + \frac{d}{d\gamma} \eta_2 + \frac{d}{d\gamma} \eta_3 + \frac{d}{d\gamma} \eta_4 + \frac{d}{d\gamma} \eta_5 + \frac{d}{d\gamma} \eta_6$$

$$\frac{d}{d\gamma} \eta_1 = F_f(L_rL_f + L_r^2)$$

$$\frac{d}{d\gamma} \eta_2 = F_r(L_rL_f + L_r^2)(\cos^2(\gamma) - \sin^2(\gamma))$$

$$\frac{d}{d\gamma} \eta_3 = m(-2v_x\omega_y h(L_f + L_r) + \omega_y^2(2h^2L_f + 2h^2L_r - L_rL_f^2 - L_fL_r^2))(\cos^2(\gamma) - \sin^2(\gamma))$$

$$\frac{d}{d\gamma} \eta_4 = 2I_y(v_x\omega_y - \omega_y^2h)\sin(\gamma)\cos(\gamma)$$

$$\frac{d}{d\gamma} \eta_5 = m(v_x\omega_y(h^2 - L_f^2 - 2L_rL_f) - L_r^2g + h\omega_y^2(3L_fL_r + L_r^2 + L_f^2 - h^2))\sin(\gamma)\cos(\gamma)$$

$$\frac{d}{d\gamma} \eta_6 = 0$$

Appendix B

Expression for the Pitch Angular Acceleration

The pitch angular acceleration of a WMR traversing a laterally symmetrical obstacle is given by:

$$\alpha_p = \Phi(p, \gamma) F_{tr} + \Gamma(p, \gamma) \omega_p^2 + \Lambda(p, \gamma) \quad (\text{B.1})$$

where

$$\Phi(p, \gamma) = \frac{\phi(p, \gamma)}{\Delta}, \quad \Gamma(p, \gamma) = \frac{\tau(p, \gamma)}{\Delta}, \quad \Lambda(p, \gamma) = \frac{\lambda(p, \gamma)}{\Delta}$$

$$\Delta = \delta_1 + m(\delta_2 + \delta_3 + \delta_4) \quad (\text{B.2})$$

where

$$\delta_1 = I_y \sin^2(\gamma)$$

$$\delta_2 = (2(L_f^2 + L_r L_f) \cos^2(\gamma) - 2h(L_r + L_f) \cos(\gamma) \sin(\gamma) + L_r^2 - L_f^2) \cos^2(p)$$

$$\delta_3 = (2(L_f^2 + L_r L_f) \cos(\gamma) \sin(\gamma) - 2h(L_r + L_f) \sin^2(\gamma)) \cos(p) \sin(p)$$

$$\delta_4 = (L_f^2 + h^2) \sin^2(\gamma)$$

$$\phi(p, \gamma) = (L_r + L_f)(\sin^2(\gamma) \sin(p) + \cos^2(\gamma) \sin(\gamma)) + R \sin^2(\gamma)$$

$$\tau(p, \gamma) = (\tau_1 + \tau_2)mR + (\tau_3 + \tau_4 + \tau_5)m \quad (\text{B.3})$$

where

$$\tau_1 = (L_f(\cos(\gamma) - 1) \sin(\gamma) - h \sin^2(\gamma)) \sin(p)$$

$$\tau_2 = (-(L_r + L_f) \cos(\gamma) + h(1 - \cos(\gamma)) \sin(\gamma) + L_f \cos^2(\gamma) + L_r) \cos(p)$$

$$\tau_3 = (2(L_f^2 + L_r L_f) \cos^2(\gamma) - 2h(L_r + L_f) \cos(\gamma) \sin(\gamma) + L_r^2 - L_f^2) \cos(p) \sin(p)$$

$$\tau_4 = (L_f^2 + L_r L_f) \cos(\gamma) \sin(\gamma) - h(L_f + L_r) \sin^2(\gamma)$$

$$\tau_5 = -(2(L_f^2 + L_r L_f) \cos(\gamma) \sin(\gamma) - 2h(L_r + L_f) \sin^2(\gamma)) \cos^2(p)$$

and

$$\lambda(p, \lambda) = \sin(p) \sin^2(\gamma) m g h - \cos(p) \sin^2(\gamma) m g L_r \quad (\text{B.4})$$

Appendix C

Shock Response Computation

The modal response due to sinusoidal excitation is given by:

$$x_t(t) = f_s e^{(-\xi \omega t)} (A_t \sin(\bar{\omega} t) + B_t \cos(\bar{\omega} t)) \quad (\text{C.1})$$

$$x_s(t) = f_s (A_s \sin(pt) + B_s \cos(pt)) \quad (\text{C.2})$$

$$\begin{aligned} A_t &= \frac{-\frac{p}{\omega} (-\xi^2 \omega^2 - p^2 + \bar{\omega}^2)}{\Psi} & B_t &= \frac{2p\xi\bar{\omega}}{\Psi} \\ A_s &= \frac{(\xi^2 \omega^2 - p^2 + \bar{\omega}^2)\sqrt{1-\xi^2}}{\Psi} & B_s &= -\frac{2p\xi\bar{\omega}}{\Psi} \end{aligned} \quad (\text{C.3})$$

where $\Psi = (p^4 - 2p^2\omega^2 + 4\xi^2p^2\omega^2 + \omega^4)$

The modal response due to cosinusoidal excitation is give by:

where

$$y_t(t) = f_c e^{(-\xi \omega t)} (C_t \sin(\bar{\omega} t) + D_t \cos(\bar{\omega} t)) \quad (\text{C.4})$$

$$y_s(t) = f_c (C_s \sin(pt) + D_s \cos(pt)) \quad (\text{C.5})$$

$$\begin{aligned} C_t &= \frac{-\xi(p^2 + \omega^2)}{\Psi} & D_t &= \frac{p^2\sqrt{1-\xi^2} - \omega^2\xi^2\sqrt{1-\xi^2} - \omega^2(1-\xi^2)^{\frac{3}{2}}}{\Psi} \\ C_s &= \frac{2p\xi\bar{\omega}}{\Psi} & D_s &= \frac{(\xi^2\omega^2 - p^2 + \bar{\omega}^2)\sqrt{1-\xi^2}}{\Psi} \end{aligned} \quad (\text{C.6})$$

Figure C.1 is a MATHCAD® algorithm for evaluating the acceleration response on the platform of WMR due to a shock load described by a function $f(t)$. The algorithm starts by evaluating the discrete frequencies of the forcing function according to a selected approximation order M . The period to which the theoretical shock load is approximated to is equal to twice the length L . After the Fourier Coefficients are obtained they are used to excite a total number of $N + 1$ modes (the first mode has a zero index). After the modal responses are superimposed and transformed to the global coordinates the acceleration response is obtained by double differentiation. Finally the acceleration response is scaled by g (acceleration due to gravity) to convert it to the usual units of measurement of shock responses.

$A(t) =$	$p \leftarrow$	for $j \in 1..M$	
		$r_j \leftarrow \frac{j \cdot \pi}{L}$	Discrete forcing frequencies.
	r		
	$F(p, M, L) \leftarrow$	$F^{<0>} \leftarrow \begin{bmatrix} \frac{1}{2 \cdot L} \cdot \int_0^L f(t) dt \\ 0 \end{bmatrix}$	
		for $0 \in 1..M$	
		$F^{<n>} \leftarrow \begin{bmatrix} \frac{1}{L} \cdot \int_0^L f(t) \cos\left(\frac{n \cdot \pi \cdot t}{L}\right) dt \\ \frac{1}{L} \cdot \int_0^L f(t) \sin\left(\frac{n \cdot \pi \cdot t}{L}\right) dt \end{bmatrix}$	Loop for evaluating the Fourier Coefficients corresponding to the discrete frequencies
		F^T	
	$f_s \leftarrow F^{<1>}$	The sinusoidal and cosinusoidal Fourier Coefficients	
	$f_c \leftarrow F^{<0>}$		
	$Rm(t, \omega) \leftarrow$	$\Sigma(t, \omega) \leftarrow 0$	
		for $i \in 0..N$	
		$r(t, \omega) \leftarrow f_s \cdot x(t, \omega) + f_c \cdot y(t, \omega)$	Loop for the definition of the modal displacement response
		$\Sigma(t, \omega) \leftarrow \Sigma(t, \omega) + r(t, \omega)$	
		$\Sigma(t, \omega)$	
	$Z(t) \leftarrow$	for $j \in 0..(n-1)$	Loop for evaluating the modal displacements of each mode of
		$R_j(t) \leftarrow \phi_j \cdot Rm(t, \omega_j)$	
		$R(t)$	
	$G(t) \leftarrow \frac{d^2}{dt^2} Z(t)$	Modal acceleration response.	
	$A_G \leftarrow (\Phi \cdot G(t))^T$	Global acceleration	
	$\frac{1}{9.81} \cdot A_G$	Scale by g (Acceleration due to gravity).	

Figure C.1. A MATHCAD® algorithm for evaluating the shock acceleration response on the chassis of a WMR

Appendix D

Publications

- A. Ayalew, E. Lai and S. O. Oyadji, "**Wheel impact control of a WMR colliding with an obstacle,**" IMECE Journal of Multibody Dynamics (submitted)
- A. Ayalew, E. Lai and S. O. Oyadji, "**Analytical Framework for the Smooth Manoeuvre of a Wheeled Mobile Robot (WMR) Traversing an Obstacle,**" Mathematical, Physical and Engineering Sciences, Proceedings of the Royal Society (submitted)
- A. Ayalew, E. Lai and S. O. Oyadji, "**Shock Response Analysis of WMRs,**" *Proc. Int. Conference on Gearing, Transmissions and Mechanical Systems*, 2000, Nottingham, UK.
- Ayalew A., Lai E. and S. O. Oyadji, "**Dynamic response of a Wheeled Mobile Robot navigating on an uneven surface,**" *Proc. DYMAC 1999, International Conference on the Integration of Dynamics, Monitoring and Control*, 1999, Manchester, UK.
- Ayalew A., Lai E. and Oyadji S. O., "**Minimum Jerk Traction Control of a Wheeled Mobile Robot Moving over a Hump,**" *Proc. ASME, DETC99 17TH Biennial Conference on Mechanical Vibration and Noise*, 1999, Las Vegas, USA.
- Ayalew A., Lai E. and, Oyadji S. O., "**Minimum jerk traction of a wheeled mobile robot passing over a hump,**" *Proc. TIMR 99-Towards Intelligent Mobile Robots*, 1999. Bristol, UK.

Wheel impact control of a WMR colliding with an obstacle

A. Ayalew, E. Lai*

Department of Mechanical & Manufacturing Engineering
The Nottingham Trent University
Nottingham, NG1 4BU, UK

S. O. Oyadji

Manchester School of Engineering
The University of Manchester
Manchester, M13 9PL, UK

Abstract

This paper presents a new approach for modelling and control of the impact of a wheeled mobile robot (WMR) after its wheels collide with stationary ground obstacles during a manoeuvre on an uneven ground surface. By using an extended rigid-body dynamics model of the WMR to account for wheel deformations and incorporating suitable trajectory planning, a control strategy is proposed that seeks to maintain permanent wheel-ground contact following a collision with a ground obstacle. The effectiveness of the strategy has been evaluated by means of a full-order finite element simulation. The results show that, with proper trajectory planning, the proposed control strategy can help to prevent the rebounding of a wheel after its collision with a ramp obstacle. This was achieved by generating active damping through the regulation of the wheel traction forces.

Keywords: Impact control, Wheeled Mobile Robot, Uneven terrain navigation, Traction control.

* To whom all correspondences should be sent. E-mail: eugene.lai@ntu.ac.uk.

List of symbols

\vec{a}_c	acceleration
F_a	traction/actuation force
F_{tr}	rear-wheels traction force
F_n	normal reaction force
g	acceleration due to gravity
I	moment of inertia matrix
I_y	pitch moment of inertia
k_w	wheel stiffness.
L_f, L_r	axle distances
M	mass matrix
m	mass
p	pitch angular displacement
R	wheel radius
x, y, z	coordinates
α_p	pitch angular acceleration
ω_p	pitch angular velocity
z	wheel radial deformation

1 Introduction

Impulsive structural excitation brought about by a collision between the wheel of a Wheeled Mobile Robot (WMR) and a ground surface irregularity has various adverse effects on the functional integrity of the robot. These include payload stability, safety and proper functioning of delicate sensors and computer hardware, wheel grip capability of the robot and hence the vehicle's handling control. Consequently, the potential safety and operational hazards brought about by wheel-ground collisions need to be minimised. A wheel will remain in contact with the ground surface until either a geometric discontinuity arises or the normal velocity of the wheel-ground contact point is directed away from the surface [1-2]. The latter type of contact loss is due to the time history of the acceleration of the wheel that may eventually lead to the breaking of the contact. Subsequent re-establishment often leads to impact-induced structural vibrations and repetitive collisions with decreasing amplitude. For this reason, it is important to develop a good understanding of the impact characteristics resulting from the collisions between rubber wheels and 'rigid' working surfaces.

Consider a straight path motion of a mobile platform on a plain surface (Figure 1), the platform initially has only a longitudinal translational motion. When it comes into contact with a surface obstacle, a new constraint is imposed on its motion leading to the generation of new degrees of freedom of motion. The sudden transition between the plane motion and the motion over the obstacle is marked by a non-zero pitch angular velocity and a translational velocity normal to the surface. Furthermore, their rates of change (i.e. pitch angular and normal accelerations) are theoretically infinite at the transition point. A theoretical 'infinite' force, referred to as an impulsive reaction force which acts over an infinitesimally small time span, accompanies these 'infinite' accelerations.

In practice, however, other factors need also to be taken into account when considering the transition between the plane motion and the pitching motion for the following reasons.

- The magnitude of the impulsive reaction force and the duration within which it occurs are finite. This implies that the vehicle undergoes a transition from planar motion to angular pitch motion in a finite time.
- The wheel material has a finite stiffness and will deform when it is subject to external impulsive reaction forces generated by collisions in the locality where the contact takes place. A function of the material property as well as the impulsive force, this localised deformation can be viewed as a contact vibration with stiffness and inertia.
- Multiple collisions may follow in cases where the impact zone is stiff, the damping is low and the approach velocity is high. Thus, the transition from planar motion to angular pitch motion may comprise multiple events of impact rather than a single one.

There are a number of ways of modelling impact dynamics. A traditional approach is the Newton relationship, in which the impact is characterised by a coefficient of restitution which is a function of the material properties of the colliding bodies. The coefficient of restitution is a measure of the kinetic energy dissipation during impact. A coefficient of restitution of 1.0 implies a completely elastic collision where there is minimal loss in kinetic energy and a value of 0 represents a completely plastic collision where maximum kinetic energy loss is experienced and the impacting bodies move together as a single entity after collision. For most collisions the coefficient of restitution lies between 0 and 1. The Newton approach is suitable for analysing

non-central collisions where impulse reaction forces may not pass through the mass centres of the colliding bodies. However, determination of the reaction forces require knowledge of the impact duration, which is usually very small and is very difficult to measure.

Hertzian method [3] is an empirical method where the impact force is given as a function of the elastic properties of the colliding bodies and of the resulting deformation in the localised geometry of the impact. The deformation is approximated by a scalar one-dimensional elastic indentation. Literature review suggests that the method appears to offer an accurate means of determining the level of impulsive reaction forces at collision interfaces and has been used in several stress analysis models [4-5].

2 Modelling and control of wheel-ground impact for a mobile robot

While the impact/contact of stationary robotic manipulators has been a subject of several recent investigations [6-8], there is no similar reported work known to the authors on wheeled mobile robots (WMRs). Unlike robotic manipulators where actuation is normally through joints, WMRs exert actuation effort through the contact points by means of traction and this requires that contacts must be maintained at all times. Furthermore, kinematic constraints for WMRs are non-holonomic in nature. When deriving the equations of motion for a mobile robot navigating an uneven terrain, consideration must be given to the number of contact points. The maximum number of simultaneous contacts is equal to the number of wheels. Consequently, WMR impact/contact control can be considered as a multi-input multi-output control problem.

In general, the equation of motion of a dynamic system can be written as:

$$M(q)\ddot{q} + \vec{h}(q, \dot{q}) = \vec{\tau} + \phi_q^T(q, t)\vec{F}_n \quad (1)$$

where $M(q)$ is a configuration dependent inertia matrix, q is a set of generalised coordinates specifying the configuration of the system, $\vec{h}(q, \dot{q})$ is a collection of position and velocity dependent forces, $\vec{\tau}$ is the actuation torque in the generalised coordinates, $\phi(q, t)$ is a matrix of constraints and \vec{F}_n is a vector of normal reaction (i.e. constraint) forces of the environment.

The wheels of a mobile robot are constrained by the environment - the concept of non-penetration in rigid body dynamics [2]. These constraints produce reaction forces that are generally the result of the gross motion dynamics of the WMR. The relationship between the contact point

acceleration, \vec{a}_N , and the normal reaction forces, \vec{F}_n , at the wheel-ground interface can be obtained as follows.

$$\vec{a}_N = P\vec{F}_n + \vec{b} \quad (2)$$

Where P is a matrix related to the geometry and inertia of the WMR, and to the geometry of the ground profile; \vec{b} is a vector related to the vehicle velocity and the wheel traction forces.

In situations where the dynamics associated with the deformation of a wheel is assumed to be negligibly small, the acceleration vector \vec{a}_N can be taken as zero and the solution for \vec{F}_n is simply given by $\vec{F}_n = -P^{-1}\vec{b}$. This is the solution for the rigid-body dynamics problem. For impact dynamics formulation, however, knowledge of the localised wheel contact deformation is important and must be included in the model. This will allow the contribution of impact dynamics of the WMR to be represented, this in turn enables a control strategy to be devised that will minimise any undesirable effects resulting from wheel-ground collisions. For a WMR fitted with rubber wheels, only the rubber material is assumed to undergo deformation when acted upon by external forces, while the rest of the vehicle structure and the ground are assumed to behave as rigid bodies.

Consider a cylindrical wheel that suddenly comes into contact with an inclined surface (Figure 1), it will be distorted as shown in Figure 2 because of contact asperities. The radial deformation \vec{z} is a function of the load \vec{F} and the elastic property of the rubber wheel (Figure 3). It is assumed that the wheel deformation is generally very small in comparison to the size of the wheel, so that a linear relationship exists between the load, the elastic modulus of the wheel material and the radial deformation.

Defining an elastic deformation vector of length N at the contact point between a wheel and the ground, \vec{z} , the contact point acceleration vector \vec{a}_N can be written as:

$$\vec{a}_N = \vec{z} \quad (3)$$

Combining Equations (2) and (3), we have

$$\vec{z} = P\vec{F}_n + \vec{b} \quad (4)$$

Since the vector \vec{b} is a function of the wheel traction forces, the vehicle velocity and the body forces, it can be written as:

$$\vec{b} = U \vec{F}_a + \vec{b}_s \quad (5)$$

where \vec{F}_a is a vector of wheel traction forces, U is a matrix which projects the traction forces into the wheel-deformation coordinates, and \vec{b}_s is the sum of body force and velocity dependent terms.

For WMRs navigating uneven terrain, it is very difficult to measure wheel deformation directly using sensors. However, it is reasonable to assume that the contribution of the stiffness term in the dynamic equation is much higher than either the inertia term or the damping term. As the stiffness of the wheel can be determined experimentally, the radial deformation can easily be computed from the relationship:

$$\vec{z} = \frac{\vec{F}_n}{k_w} \quad (6)$$

where k_w is the known wheel radial stiffness. Derivatives of \vec{z} (i.e. \vec{z}' and \vec{z}'') can be obtained by successive differentiation or by means of an estimator.

In order to achieve the desired reaction forces after impact it is proposed to devise a controller with the wheel deformation vector \vec{z} as the controlled variable. Substituting Equations (5) and (6) into (4) we have:

$$\vec{z} = P k_w \vec{z} + \vec{b} \quad (7)$$

$$\text{or } \vec{z} + K \vec{z} = \vec{b} \text{ where } K = -P k_w \quad (8)$$

Assuming that the control law proposed by Tornambe [5] can be extended to the present study, we can define

$$\vec{b} = -h_0(\vec{z} - \vec{z}_R) - h_1(\vec{z} - \vec{z}_R) + \vec{z}_R - K \vec{z} \quad (9)$$

where \vec{z}_R is the reference trajectory being tracked by the wheel contact point deformation \vec{z} . The coefficients h_1 and h_0 are positive constants so chosen to achieve the desired transient behaviour. Substitute Equation (9) into (8) and rearrange:

$$(\vec{\dot{z}} - \vec{\dot{z}_R}) + h_1(\vec{z} - \vec{z}_R) + h_0(\vec{z} - \vec{z}_R) = 0 \quad (10)$$

In terms of the tracking error vector, $\vec{e} = \vec{z} - \vec{z}_R$, Equation (10) can be written as:

$$\vec{\ddot{e}} + h_1\vec{\dot{e}} + h_0\vec{e} = 0 \quad (11)$$

The traction forces at the wheels can be obtained from Equation (5), where

$$\begin{aligned} \vec{b} &= U \vec{F}_a + \vec{b}_g \\ \therefore \vec{F}_a &= U^{-1}(\vec{b} - \vec{b}_g) \end{aligned} \quad (12)$$

3 Effects of varying the coefficients of the control law

An assessment has been made on the effects of varying in turn the coefficients h_0 (the proportional gain) and h_1 (the derivative gain) on the performance of the proposed control law (Equation (9)) on the wheel deformation. Simulation studies have been carried out within the MATLAB® environment with the following assumptions.

- The rear wheels remain on the flat surface before, during and after the collision.
- The front wheels have zero deformation before colliding with the ramp.
- The masses of the wheels are lumped with the vehicle body so that the MWR can be treated as a single rigid body and the dynamics of the wheels can be ignored.
- There is no vibration of the vehicle structure.
- The ramp has an inclination of 17° and the wheel approach velocity (normal to the surface of the ramp) is 0.6 m/s.

Figure 4 shows the effects of varying the derivative gain h_1 on front wheel deformation, while keeping h_0 constant (at 1500). A negative value of the deformation signifies a compression of the wheel material, while a positive value implies that the wheel is no longer in contact with the ground. It can be seen that as the amount of derivative gain increases, corresponding to higher values of h_1 , the settling time of (i.e. the time taken to stabilise the wheel deformation) increases. A critical value for h_1 is found to be about 65, below which oscillatory behaviour is observed, this corresponds to wheel rebound immediately after impact.

The effects of varying the proportional gain, h_0 , while keeping h_1 constant (at 70) have also been investigated and the results are shown in Figure 5. It can be seen that as h_0 increases, corresponding to higher values of the proportional gain h_0 , the settling time decreases. The critical value for h_0 is found to be about 1550, above which oscillatory behaviour is observed, corresponding to wheel rebound immediately after impact. The effects of varying the values of h_1 and h_0 on the transient response is similar to those of a PD control system.

4 Control with trajectory planning

The theoretical analysis described earlier can be applied to the problem of trajectory-planning. Consider a dynamic system represented by Equation (7) is subject to the control law defined by Equation (9) with known initial conditions \vec{z}_o , $\vec{\dot{z}}_o$, $\vec{\ddot{z}}_o$ and final (steady-state) conditions \vec{z}_f , $\vec{\dot{z}}_f$, $\vec{\ddot{z}}_f$. The task is to determine a feasible trajectory \vec{z}_r , $\vec{\dot{z}}_r$, $\vec{\ddot{z}}_r$ that will result in a favourable performance of the impact control methodology, subject to satisfying the following performance criteria.

- The trajectory should be smooth in order to avoid jerky actuation efforts.
- The required actuation forces must not exceed the maximum available traction force, taking into account of the power of the drive motor and the saturation of friction forces between the wheels and the ground.
- The task of stabilising the wheel deformation should be accomplished in the shortest possible time. This is because the platform is moving on a road surface whose geometry may be constantly changing, therefore it is essential that steady state is achieved as soon as possible.

As the time needed to complete the desired trajectory is inversely proportional to the required control efforts, a compromise is often needed between the second and the third criteria. Consequently, there is a minimum time required to complete the task of stabilising the wheel deformation following a collision.

We now examine the capability of the impact control methodology to track a polynomial trajectory by monitoring the wheel deformation. Let $p(t_n)$ be the desired polynomial trajectory function for the front wheel contact point deformation, where $t_n = \frac{t}{T}$ is a normalised time, t is actual time variable and T is the total time taken to complete the task of stabilising the wheel deformation. The function $p(t_n)$, and its derivatives are required to satisfy four initial and four final conditions with respect to displacement, velocity, acceleration and jerk. Hence $p(t_n)$ can be devised to be a polynomial of degree seven:

$$p(t_n) = \sum_{i=0}^7 C_i t_n^i \quad (13)$$

The velocity, acceleration and jerk are given by the time derivatives:

$$\dot{p}(t_n) = \sum_{i=1}^7 i C_i t_n^{i-1} \quad (14)$$

$$\ddot{p}(t_n) = \sum_{i=2}^7 i(i-1) C_i t_n^{i-2} \quad (15)$$

$$\dddot{p}(t_n) = \sum_{i=3}^7 i(i-1)(i-2) C_i t_n^{i-3} \quad (16)$$

The initial and final conditions are given by:

$$\begin{aligned} p(0) &= 0 & p(1) &= d \\ \dot{p}(0) &= v_0 & \dot{p}(1) &= 0 \\ \ddot{p}(0) &= 0 & \ddot{p}(1) &= 0 \\ \dddot{p}(0) &= 0 & \dddot{p}(1) &= 0 \end{aligned} \quad (17)$$

where d is the goal deformation of the wheel at the contact point and v_0 is the approach velocity of the wheel contact point immediately before impact. By applying these conditions to Equation (13), the coefficients C_i , where $i = 0 \dots 7$ can be determined as follows.

$$\begin{aligned} & (C_7 \ C_6 \ C_5 \ C_4 \ C_3 \ C_2 \ C_1 \ C_0) \\ &= \left(-10 \frac{v_0 T + 2d}{T^7} \ 2 \frac{-18v_0 T + 35d}{T^6} \ -3 \frac{-15v_0 T + 28d}{T^5} \ 5 \frac{-4v_0 T + 7d}{T^4} \ 0 \ 0 \ v_0 \ 0 \right) \end{aligned}$$

The planned trajectories with respect to displacement, velocity, acceleration and jerk for three control time intervals, namely $T = 0.1$, $T = 0.15$ and $T = 0.2$, are shown in Figure 6 using a normalised time scale.

The actuation forces needed to achieve the goal deformation have been determined for the specified planned trajectories and the results for both the front and rear wheels are shown in Figure 7. In this instance, the proportional gain h_0 and the derivative gain h_1 have been chosen as 1500 and 70 respectively.

With all the relevant information available, the effectiveness of the proposed control methodology has been evaluated within the MATLAB[®] environment using the analytically formulated dynamic model. The problem under consideration is depicted in Figure 1 where a bicycle model of a wheeled mobile robot is about to collide with an obstacle in the form of an inclined surface. The following assumptions have been made. First, the front wheel has no initial deformation before the impact. Second, the wheel contact point velocity v_0 can be estimated by considering the normal component of the longitudinal velocity of the vehicle at the obstacle surface. Third, the rear wheels have a non-zero initial deformation d_0 and no initial normal velocity. The final conditions are defined by the desired steady state performance.

The control actions can be considered as a means of enabling a smoother transition from impact dynamics of the wheel to a desired steady-state wheel deformation in the shortest possible time. The main function of the actuation forces is to minimise any transient oscillations of the wheel at the wheel-ground interface brought about by the wheel deformation.

Figure 8 shows the tracking error of the front-wheel deformation when it is subject to the planned trajectory input (solid line). For comparison, the corresponding tracking error for a step (i.e. unplanned) input is also computed (broken line). It can be seen that the availability of a planned trajectory has helped to reduce the tracking error significantly when compared with a step (i.e. unplanned) input. Furthermore, a planned trajectory also allows a smoother engagement and disengagement of actuators, which in turn should help to eliminate initial and final jerk.

5 Finite element simulation

So far, a number of assumptions have been made to simplify the analytical study within the MATLAB[®] environment. For a more realistic assessment of the proposed control methodology, finite element (FE) analysis has been carried out using the state-of-the-art nonlinear dynamics

finite element software LS-Dyna. Finite element simulation has an advantage over the use of an analytically formulated model in that it uses minimal simplifying assumptions. For example, a contact dynamic model often uses simple linear springs (and dashpots) to represent the localised wheel deformations. In contrast, the full order finite element model allows both the chassis of the WMR and its wheels to have a distributed inertia and stiffness. Furthermore, the problems associated with gross-motion (rigid-body) dynamics and structural dynamics can be handled simultaneously. In the present investigation, the full order FE model offers the following advantages:

- The wheel deformation is distributed over the entire disc, and is not just confined to the wheel contact point;
- The deformation of the chassis contributes to the overall structural dynamics of the platform, as opposed to the assumption that deformations are confined only to the wheels. This generates a disturbance against which the performance of the control scheme will be assessed.
- The wheel inertia is not zero so that its contribution can be taken into account in the analysis.
- The wheel has a finite rotational as well as translational dynamics.

A convenient measurable output parameter when considering wheel-ground interaction is the normal reaction force at the wheel contact point. Figure 9 shows the variation of the normal reaction force for the front wheels shortly after collision without, and with, the proposed impact control strategy. For the wheel to remain in contact with the ground surface, the normal reaction force is expected to have a positive value. A zero reaction force implies that the wheel is no longer in contact with the surface. Figure 10 shows the variation of the normal reaction force for the rear wheels shortly after collision with the ramp obstacle.

The broken line represents the uncontrolled impact of the wheel with the ramp. As can be seen the reaction force drops down to zero several times and with progressively reducing amplitude. This corresponds to a “bouncing” behaviour of the wheel after hitting the surface. The amplitude of each rebound is smaller than the previous one due to the natural damping provided by the material.

With the implementation of the impact control strategy a smoother transition to steady-state (represented by the solid line) is achieved that enables permanent wheel grip with the ground after impact.

6 Conclusions

A new technique for modelling and control of wheel-to-ground-obstacle impact has been presented. The rigid-body dynamics model of a wheeled mobile robot has been extended to include wheel deformations. Based on the extended model and incorporating suitable trajectory planning, a control law has been proposed that seeks to maintain permanent wheel-ground grip immediately after collision by regulating the wheel traction forces.

The proposed approach has been analysed by means of simulation studies using MATLAB® and encouraging results were obtained. Evaluation of the technique has been carried out by means of a full-order finite element simulation study by using the state-of-the-art dynamics software LS-Dyna®. The results show that, with proper trajectory planning, the proposed control strategy can help to prevent the rebounding of a wheel after its collision with a ramp obstacle. This was achieved by generating active damping through the regulation of the wheel traction forces.

References

1. Featherstone, R., "Robot Dynamics Algorithms," Kluwer Academic Press, 1987.
2. Baraff, D., "Issues in Computing Contact Forces for Non-penetrating Rigid Bodies," *Algorithmica*, 1993, pp. 292-352.
3. Goldsmith, W., "Impact - The Theory and Physical Behaviour of Colliding Solids," Edward Arnold Publishers Ltd., London, 1960.
4. Engel, P., "Impact Wear of Materials," Elsevier Scientific Publishing Company, The Netherlands, 1978.
5. Tornambe, A., "Modelling and Controlling One-Degree-of-Freedom Impacts," IEE Proceedings on Control Theory Applications, Vol. 143, No. 1, 1996.
6. Volpe, R., Khosla, P., "A Theoretical and Experimental Investigation of Impact Control for Manipulators," The International Journal of Robotics Research, Vol. 12, No. 4, 1993.
7. Sarkar N., Yun, X., "Design of a Continuous Controller for Contact Transition Task Based on Impulsive Constraint Analysis," Proceedings of the 1996 IEEE International Conference on Robotics and Automation, Minnesota, 1996.
8. Seraji, H., Colbaugh, R., "Force Tracking in Impedance Control," The International Journal of Robotics Research, Vol. 16, No. 1, 1997.

Table (1) The dimensions of the WMR used in the simulation.

Symbol	Description	Value
L_f	Longitudinal distance of front axle from the vehicle centre of mass	0.6 m
L_r	Longitudinal distance of rear axle from the vehicle centre of mass	0.46 m
h	Height of centre of mass from the wheel centres	0.4 m
R	Radius of wheels	0.1 m
I_y	Pitch moment of inertia of the platform	$47 \text{ kg}\cdot\text{m}^2$
m	Mass of the platform	170 kg

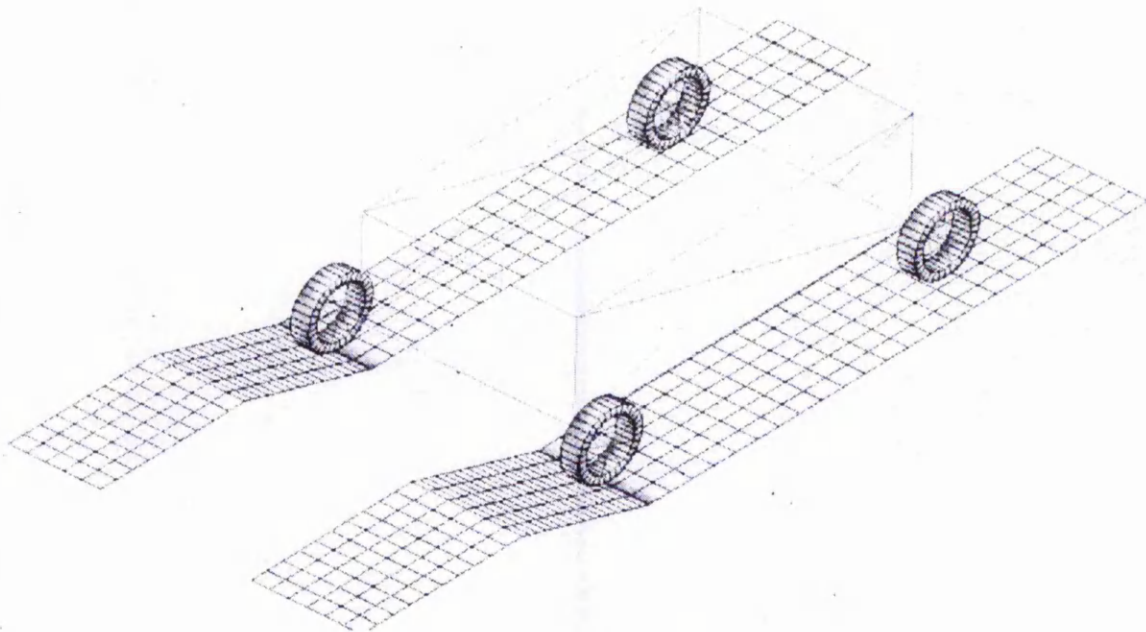


Figure 1 A Wheeled mobile robot colliding with a ramp obstacle.

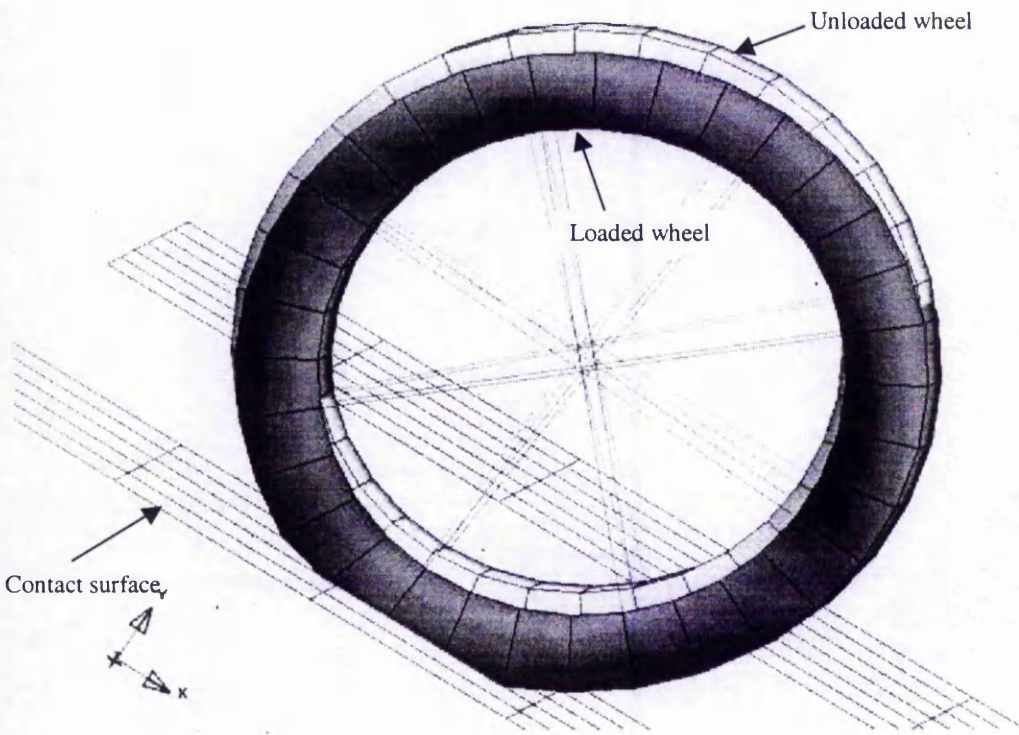


Figure 2 Deformation of a cylindrical wheel due to central load and contact reaction.

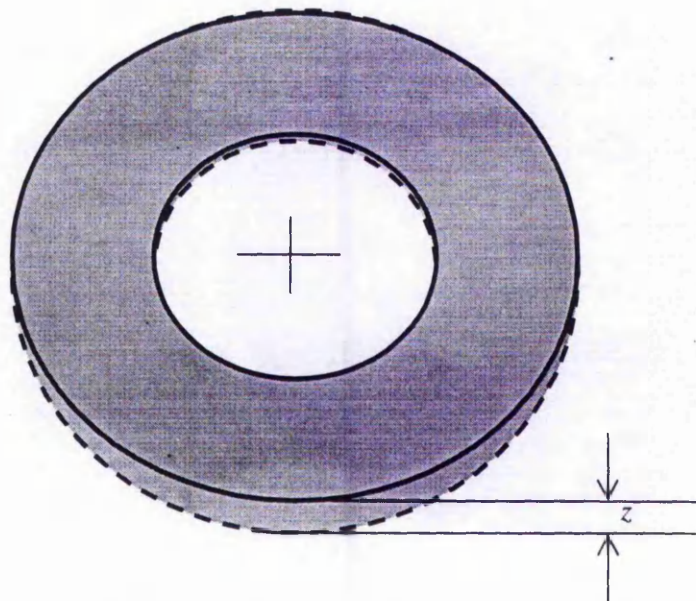


Figure 3 Definition of wheel deformation.

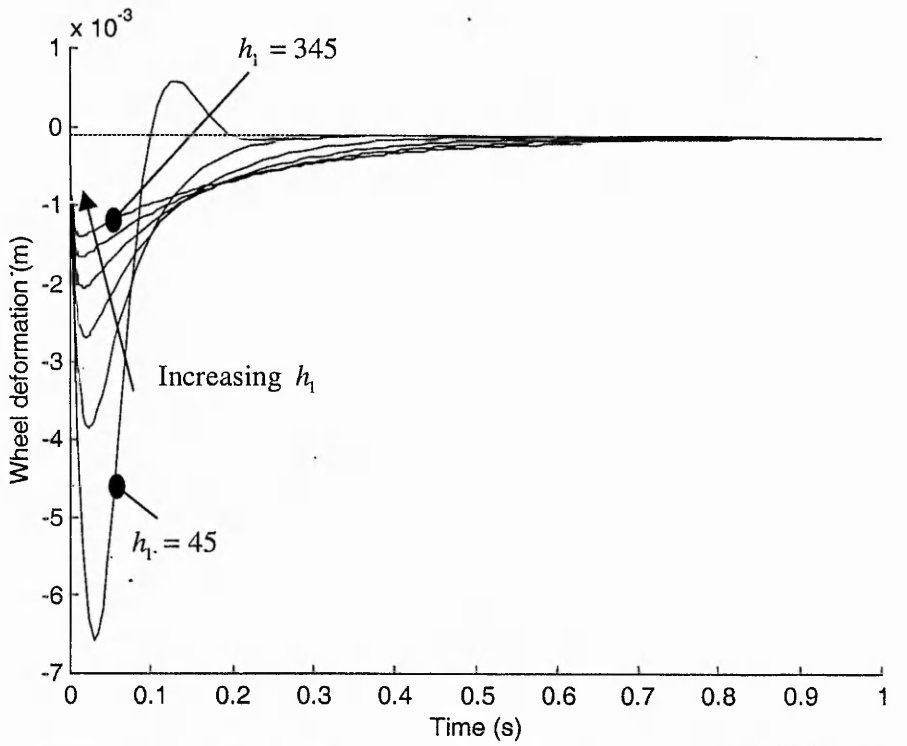


Figure 4 The effect of varying h_1 on the settling time ($h_0 = 1500$) of front wheel deformation.

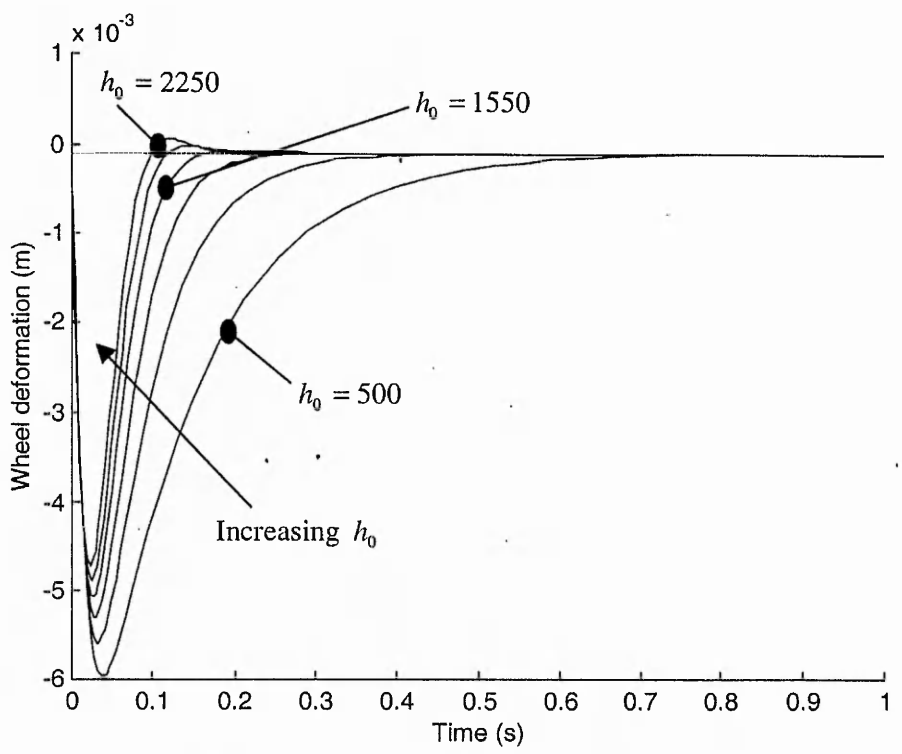


Figure 5 The effect of varying h_0 on the settling time ($h_1 = 70$) of front wheel deformation.

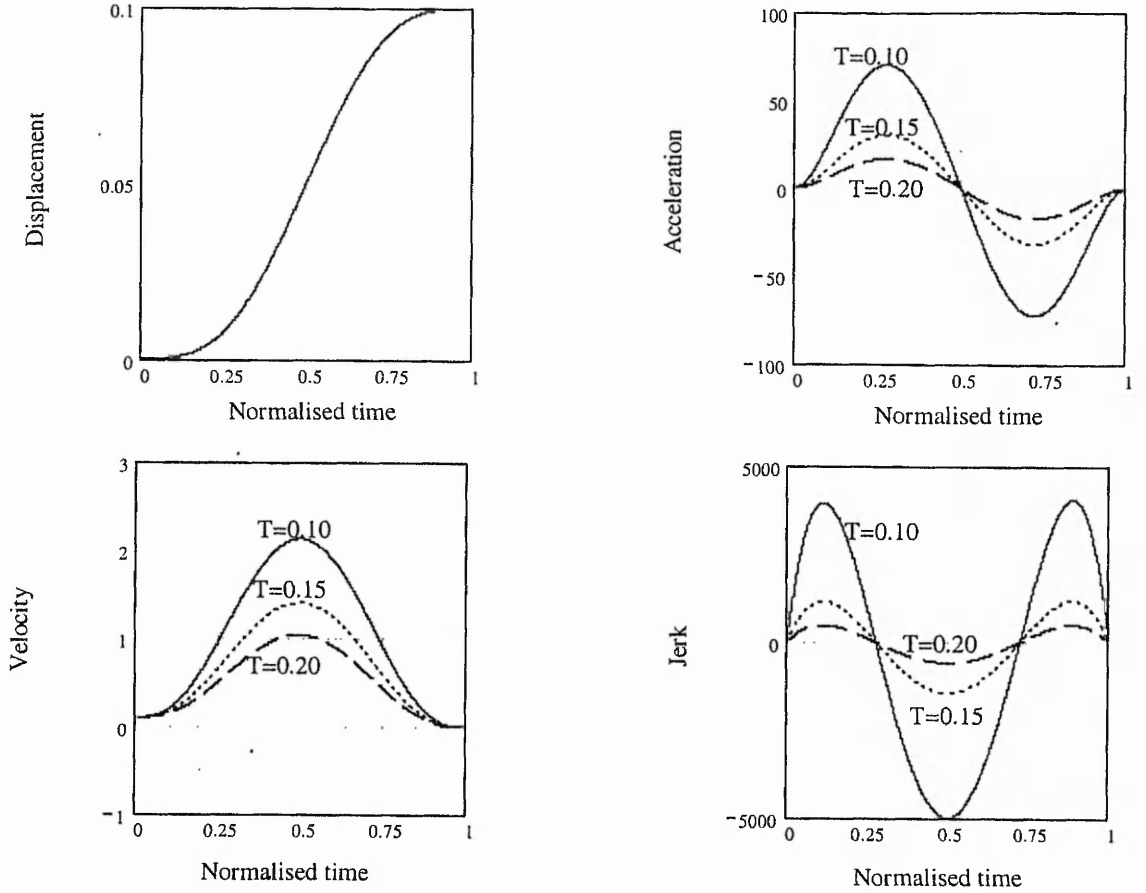


Figure 6 The planned trajectories of front wheel deformations for different control time intervals.

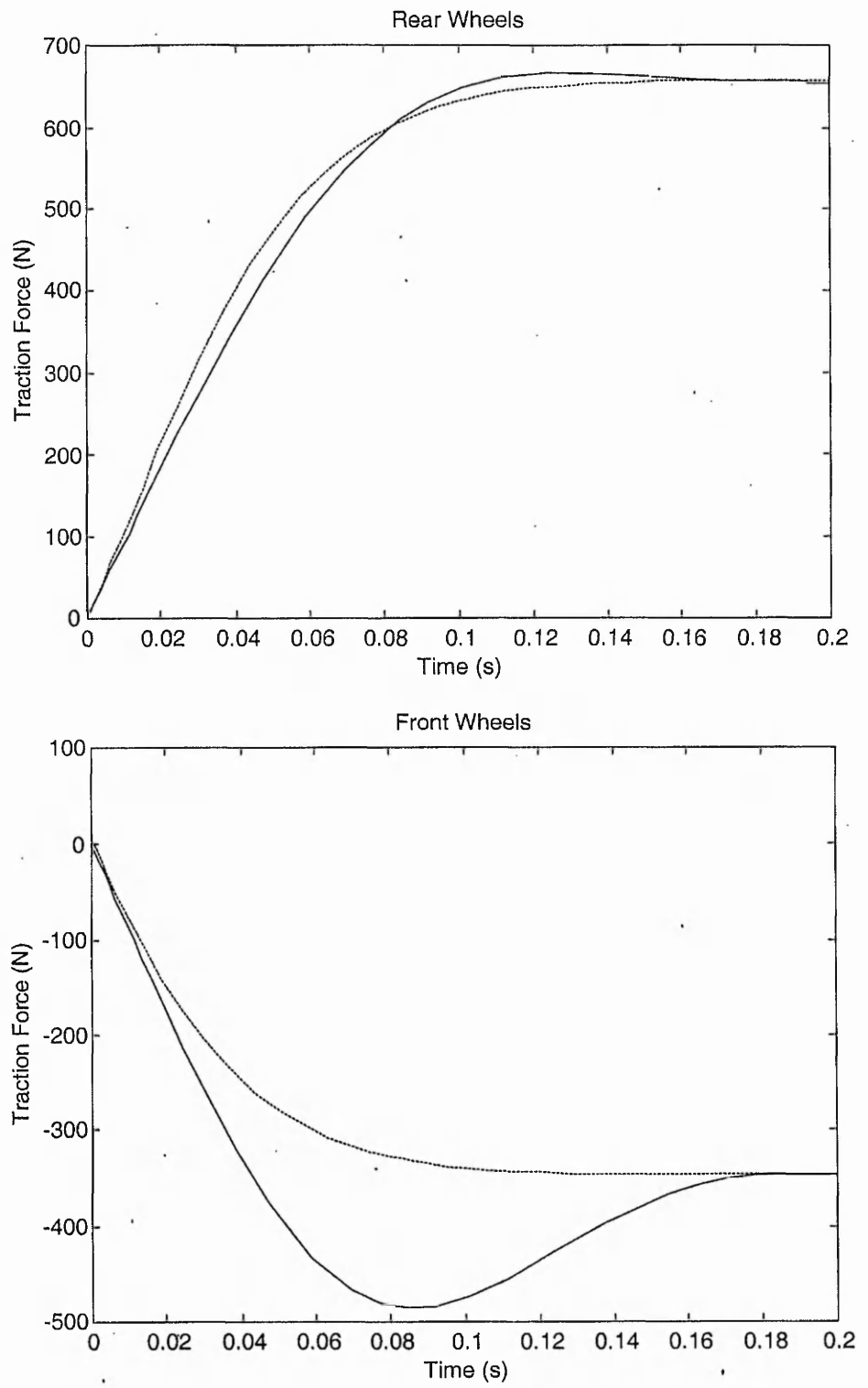


Figure (7) Variation of actuation forces: $h_1 = 70$, $h_0 = 1500$, $k = 5.6E6 \text{ N/m}$
 Planned trajectory reference (solid line); Step reference (broken line).

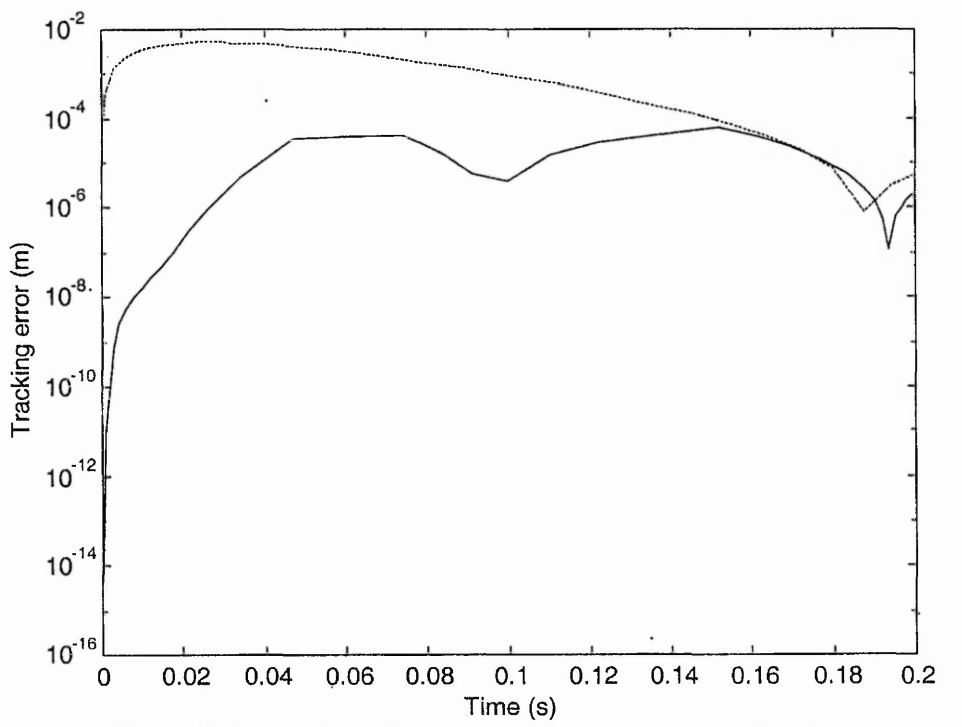


Figure 8 Comparison of the tracking errors for a step input (broken line) and planned trajectory input (solid line).

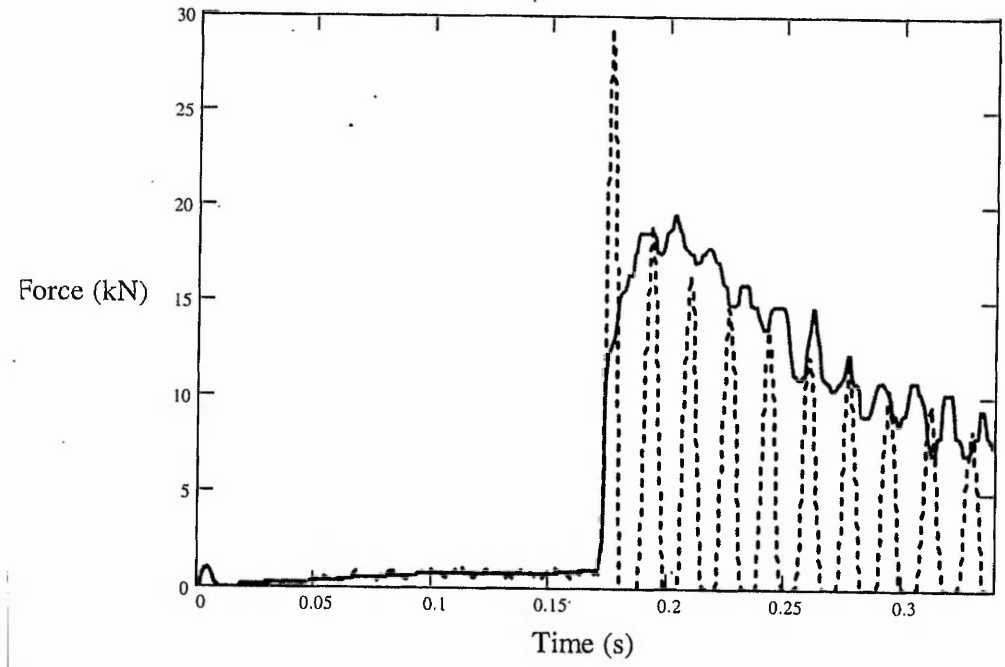


Figure 9 FE simulations of the front wheel reaction forces. Uncontrolled impact (broken line) and controlled impact (solid line) following a collision with a 17° inclined surface.

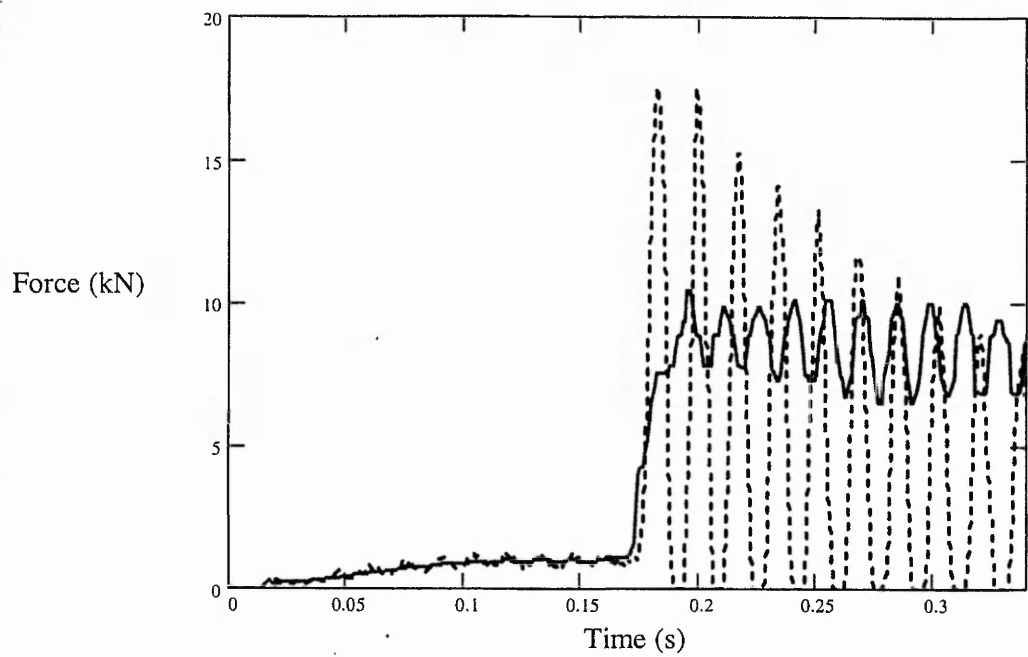


Figure 10 FE simulations of rear wheel reaction forces. Uncontrolled impact (broken line) and controlled impact (solid line) following a collision with a 17° inclined surface.

Analytical Framework for the Smooth Manoeuvre of a Wheeled Mobile Robot (WMR) Traversing an Obstacle

A. Ayalew, E. Lai*

Department of Mechanical & Manufacturing Engineering
The Nottingham Trent University
Nottingham, NG1 4BU, UK

S. O. Oyadji

Manchester School of Engineering
The University of Manchester
Manchester, M13 9PL, UK

Synopsis

The aim of this paper is to introduce a new approach for modelling the dynamics and for trajectory planning of mobile platforms which need to travel over localised surface irregularities. A dynamic model of a Wheeled Mobile Robot (WMR), which is also denoted as a mobile platform, that takes into account all forces including translational as well rotational inertia forces has been developed. The model has been used in a case study to devise a polynomial trajectory planning of the pitching motion of a mobile platform, driven by a controlled rear-wheel traction, moving over an obstacle of a known geometry. It has been demonstrated that, during obstacle traversing, a compromise can be achieved between the minimal time of manoeuvre on one hand and vehicle traction force, inertia load and jerk on the other hand. It has also been found that the traction force needed to complete the manoeuvre may change sign necessitating a switch to a braking action. This shift between the traction mode and braking mode of the actuators can be avoided by an appropriate choice of a minimum time of manoeuvre. This study also provides a basis for the selection of an appropriate manoeuvre time based on a prior knowledge of the friction characteristics of a traction surface.

* To whom all correspondences should be sent. E-mail: eugene.lai@ntu.ac.uk.

Keywords: mobile robots, trajectory planning, traction control, obstacle traversing.

List of symbols

\vec{a}_c	acceleration
F_a	traction/actuation force
F_{tr}	rear-wheels traction force
F_n	normal reaction force
\vec{F}_w	resultant wheel force
g	acceleration due to gravity
I	moment of inertia matrix
I_y	pitch moment of inertia
k	index
L_f, L_r	axle distances
M	mass matrix
\vec{T}	moment
m	mass
\vec{n}	normal vector
p	pitch angular displacement
\vec{r}	position vector
R	wheel radius
x, y, z	coordinates
$\vec{\alpha}$	angular acceleration
α_p	pitch angular acceleration
δ	steering angle
μ_l	coefficient of lateral friction
γ	road profile gradient angle
$\vec{\omega}$	angular velocity
ω_p	pitch angular velocity

1 Introduction

Kinematic and dynamic models of a Wheeled Mobile Robot (WMR) are often derived based on the assumption that the surface on which it manoeuvres is free from any irregularities. In practice, however, even for indoor applications, the wheels of a mobile platform are likely to encounter small but unavoidable obstacles. The interaction between stationary obstacles and the

wheels of the mobile robot can adversely affect the stability of the payload as well as the robot's handling control. The limited understanding of the mechanism of wheel-obstacle interaction and its implication to the overall dynamics of a mobile platform has hindered the development of control tools that may be used to limit the adverse effects of traversing surface irregularities.

Before trajectory tracking control systems can be implemented on a mobile robot travelling on an uneven surface, a feasible path must be planned and a trajectory generated. The path planning is often based on several criteria like obstacle avoidance, drive-torque saturation and tip-roll avoidance. The trajectory planning phase involves the time parametrisation of the path generated that defines the velocity and acceleration of the platform as well as the drive-torque necessary to accomplish the manoeuvre. Both path planning and trajectory planning should be based on a reasonably accurate model of the system in order that the trajectory tracking control will converge.

Global path-planning of WMRs travelling on uneven surfaces is often based on simplified criteria such as static stability, wheel-torque saturation based on static forces, and geometric obstacle avoidance [1-5]. In few investigations, attempts have been made to base the analysis on dynamic models of the platform. However, the models employed are often over-simplified and do not provide an accurate representation of the actual dynamics of the vehicle. A path planning approach based on a model that assumes the platform to be a point mass is provided by Shiller [3]. In Shiller's work, the rotational dynamics of the vehicle is entirely ignored which makes the model incomplete because rotational motion characteristics have not been taken into account. Another simplifying assumption often made in path planning literature of mobile platforms is the reduction of the dynamics problem to a quasi-static one. In the model developed by Ben-Amar et al [1] the inertia forces have been ignored and only gravitational forces have been taken into

consideration in the computation of reaction forces. This simplification restricts the relevance of the model to slow manoeuvring platforms with negligible dynamics.

Trajectory planning of mobile robots moving on smooth planar surfaces has been addressed in several works. For road vehicles Sledge et al [10] have introduced trajectories defined by an elliptic function to achieve minimum energy, minimum jerk and minimum radius of curvature for emergency lane-change manoeuvre. However, the trajectories are parametrised with longitudinal displacement, which makes them unsuitable for variable-velocity path planning.

In contrast to mobile platforms, path and trajectory planning of robotic manipulators is often based on a more complete dynamic model that accommodates inertia and gravity loads, as well as considering rotational and translational dynamics [6-8]. In the robotic manipulator literature, time parametrised trajectories are designed to satisfy various constraints. One of these constraints is the minimisation of jerk [9]. Optimisation techniques are used to obtain minimum jerk cubic-spline trajectories of manipulator joints that enhance the path tracking capability of the mobile manipulator arms as well as reducing the level of vibration.

The aim of this analytical work is to introduce a new approach for modelling the dynamics and for trajectory planning of mobile platforms which need to travel over localised surface irregularities. Both inertia and gravitational forces are taken into consideration in the modelling process. Also the model takes into account the rotational as well as the translational dynamics of the platform. To begin with, a modelling approach for obstacles of generic geometry applicable to all-wheel steered platforms is provided. This is followed by a case study of a mobile platform whose front wheels traverse a laterally symmetrical obstacle while its rear wheels are used for driving. The pitching motion of the platform will be used as a basis for the planning process. A single, continuous polynomial function is employed as the time parametrised

trajectory with zero jerk values at the start and the end of a manoeuvre of obstacle traversing.

The polynomial function used also guarantees velocity and acceleration continuity. The traction force required to complete the manoeuvre is computed using the model derived.

2 Modelling

The following simplifying assumptions have been made in the modelling of the WMR dynamics:

- i. The platform, its wheels and the surface are assumed to be rigid. This simplifies the modelling effort by ignoring the extra fast dynamics brought about by elastic deformations at wheel-ground contact points as well as in the structural members of the mobile platform.
- ii. Smooth geometry of obstacles is assumed. This helps to ensure that the wheel ground contact progresses without collisions that may generate impulsive forces and cause velocity discontinuities. For this assumption to be satisfied the contact surface geometry must be such that the loci of contact points have a radius of curvature greater than the wheel radius.
- iii. The contribution of the wheel dynamics relative to the overall vehicle dynamics is negligibly small. Consequently, the wheel mass and inertia are ignored in the formulation of the equations of motion.

The Newton-Euler equations of motion of the platform (Equations 1 and 2) are derived with respect to a Cartesian coordinate system attached to the vehicle's centre of mass (Figure 1).

The sum of forces and moments about the x - y - z axes are:

$$\sum \vec{F} = M \vec{a}_c \quad (1)$$

$$\sum \vec{M} = I \vec{\alpha} \quad (2)$$

where M and I are the mass and moment of inertia matrices of the platform respectively.

The wheel force \vec{F}_{wk} , at an arbitrary wheel k is given as:

$$\vec{F}_{wk} = \vec{A}_k F_{ak} + \vec{N}_k F_{nk} \quad (3)$$

where F_{ak} is the magnitude of the traction force acting in the plane of the wheel and F_{nk} is the magnitude of the normal reaction force from the ground. \vec{A}_k and \vec{N}_k are vectors which map the traction, frictional and reaction forces into the x - y - z coordinate system.

$$\vec{A}_k = \begin{bmatrix} \cos(\gamma_k) \cos(\delta_k) \\ \cos(\gamma_k) \sin(\delta_k) \\ \sin(\gamma_k) \end{bmatrix}; \quad \vec{N}_k = \begin{bmatrix} \mu_{lk} \sin(\delta_k) - \sin(\gamma_k) \cos(\delta_k) \\ -\mu_{lk} \cos(\delta_k) - \sin(\gamma_k) \sin(\delta_k) \\ -\mu_{rk} \sin(\gamma_k) + \cos(\gamma_k) \end{bmatrix} \quad (4)$$

where μ_l is the coefficient of lateral friction and δ_k is the steering angle of the k^{th} wheel.

The resultant force \vec{F} acting on the vehicle is composed of the wheel forces and other external forces including the gravitational force. It can be written as,

$$\vec{F} = A \vec{F}_a + N \vec{F}_n + \vec{C} F_e \quad (5)$$

where $A = \sum_1^w \vec{A}_k$, $N = \sum_1^w \vec{N}_k$ and \vec{C} is a vector that projects external forces except the wheel forces onto the frame of reference, x - y - z , and w is the number of wheels of the vehicle currently in contact with the working surface. \vec{F}_a and \vec{F}_n are vectors of length w , and F_e is magnitude of the external force.

The acceleration \vec{a}_c of the centre of mass of the platform is found from Equation (1) as:

$$\vec{a}_c = M^{-1} \vec{F} \quad (6)$$

substituting for \vec{F} from Equation (5),

$$\vec{a}_c = M^{-1} (A\vec{F}_a + N\vec{F}_n + \vec{C}F_e) \quad (7)$$

At a point P where the k^{th} wheel makes contact with the ground (Figure 2), the acceleration is given by:

$$\vec{a}_k = \vec{a}_c + \vec{\omega} \times \vec{\omega} \times \vec{r}_k + \vec{\alpha} \times \vec{r}_k \quad (8)$$

where \vec{r}_k is the position vector of the contact point, $\vec{\alpha}$ is the angular acceleration vector of the platform, and $k = 1 \dots w$.

A normal vector, \vec{n}_k , can be introduced to define the shape of the surface at the contact point with wheel k ,

$$\vec{n}_k = \begin{bmatrix} \sin(\gamma_k) \cos(\delta_k) \\ \sin(\gamma_k) \sin(\delta_k) \\ -\cos(\gamma_k) \end{bmatrix} \quad (9)$$

The scalar component a_{nk} of the acceleration \vec{a}_k along the normal direction \vec{n}_k can be found by a vector dot product of the two quantities, i.e.,

$$a_{nk} = \vec{a}_k \bullet \vec{n}_k \quad (10)$$

Substituting for \vec{a}_k from Equation (8),

$$a_{nk} = (\vec{a}_c + \vec{\omega} \times \vec{\omega} \times \vec{r}_k + \vec{\alpha} \times \vec{r}_k) \bullet \vec{n}_k = \vec{a}_c \bullet \vec{n}_k + (\vec{\omega} \times \vec{\omega} \times \vec{r}_k) \bullet \vec{n}_k + (\vec{\alpha} \times \vec{r}_k) \bullet \vec{n}_k \quad (11)$$

By using Equation (7) the term $\vec{a}_c \bullet \vec{n}_k$ can be written as,

$$\vec{a}_c \bullet \vec{n}_k = (M^{-1}(A\vec{F}_a + N\vec{F}_n + \vec{C}\vec{F}_e)) \bullet \vec{n}_k = H_k \vec{F}_a + Q_k \vec{F}_n + G_k \quad (12)$$

where

$$H_k = (M^{-1}A)^T \bullet \vec{n}_k; \quad Q_k = (M^{-1}N)^T \bullet \vec{n}_k; \quad G_k = (M^{-1}\vec{C}\vec{F}_e) \bullet \vec{n}_k \quad (13)$$

The normal components of the contact point acceleration vector \vec{a}_N is given by:

$$\vec{a}_N = \begin{bmatrix} a_{n1} \\ \vdots \\ a_{nw} \end{bmatrix} \quad (14)$$

Substituting for a_{nk} from Equation (11)

$$\vec{a}_N = \begin{bmatrix} \vec{a}_c \bullet \vec{n}_l + (\vec{\omega} \times \vec{\omega} \times \vec{r}_l) \bullet \vec{n}_l + (\vec{\alpha} \times \vec{r}_l) \bullet \vec{n}_l \\ \vdots \\ \vec{a}_c \bullet \vec{n}_w + (\vec{\omega} \times \vec{\omega} \times \vec{r}_w) \bullet \vec{n}_w + (\vec{\alpha} \times \vec{r}_w) \bullet \vec{n}_w \end{bmatrix} \quad (15)$$

or,

$$\vec{a}_N = \vec{a}_{Nc} + \vec{a}_{N\omega} + \vec{a}_{N\alpha} \quad (16)$$

where \vec{a}_{Nc} , $\vec{a}_{N\omega}$ and $\vec{a}_{N\alpha}$ are defined as:

$$\vec{a}_{Nc} = \begin{bmatrix} \vec{a}_c \bullet \vec{n}_l \\ \vdots \\ \vec{a}_c \bullet \vec{n}_w \end{bmatrix}; \quad \vec{a}_{N\omega} = \begin{bmatrix} (\vec{\omega} \times \vec{\omega} \times \vec{r}_l) \bullet \vec{n}_l \\ \vdots \\ (\vec{\omega} \times \vec{\omega} \times \vec{r}_w) \bullet \vec{n}_w \end{bmatrix}; \quad \vec{a}_{N\alpha} = \begin{bmatrix} (\vec{\alpha} \times \vec{r}_l) \bullet \vec{n}_l \\ \vdots \\ (\vec{\alpha} \times \vec{r}_w) \bullet \vec{n}_w \end{bmatrix} \quad (17)$$

Thus the normal components of the contact point acceleration vector \vec{a}_N can be found by summing the contributions from the translational acceleration term \vec{a}_{Nc} , the centrifugal acceleration term $\vec{a}_{N\omega}$ and the angular acceleration term $\vec{a}_{N\alpha}$.

2.1 Translational Acceleration

Applying Equation (12) to each row of the vector \vec{a}_{Nc} one can write,

$$\vec{a}_{Nc} = \begin{bmatrix} \vec{a}_c \bullet \vec{n}_1 \\ \vdots \\ \vec{a}_c \bullet \vec{n}_{nw} \end{bmatrix} = H\vec{F}_a + Q\vec{F}_n + \vec{G} \quad (18)$$

where H and Q are $w \times w$ matrices whose k^{th} rows are H_k and Q_k , respectively. \vec{G} is a vector of length w whose k^{th} element is given by G_k .

2.2 Centrifugal Acceleration

$\vec{a}_{N\omega}$ can easily be computed since the instantaneous angular velocity $\vec{\omega}$ of the platform is known.

2.3 Angular Acceleration

The vector $\vec{a}_{N\alpha}$ can be calculated as follows.

The angular acceleration $\vec{\alpha}$ is given by:

$$\vec{\alpha} = I^{-1}\vec{T} \quad (19)$$

where I is the moment of inertia matrix. \vec{T} is the total moment produced by wheel forces and external forces/momenta.

If it is assumed that all external forces except the wheel forces are applied to the platform through the centre of mass (which is the case for the gravitational force), then only the wheel forces contribute to the total moment. Thus,

$$\vec{T} = \sum_1^w \vec{T}_k \quad (20)$$

where

$$\vec{T}_k = \vec{r}_k \times \vec{F}_k \quad (21)$$

Substituting Equation (3) for \vec{F}_k in Equation (21), one has

$$\vec{T}_k = \vec{r}_k \times (\vec{A}_k F_{ak} + \vec{N}_k F_{nk}) = (\vec{r}_k \times \vec{A}_k) F_{ak} + (\vec{r}_k \times \vec{N}_k) F_{nk} \quad (22)$$

The total moment can be written as:

$$\vec{T} = R_a \vec{F}_a + R_n \vec{F}_n \quad (23)$$

where R_a and R_n are $w \times w$ matrices whose k^{th} columns are given by:

$$\vec{R}_{ak} = \vec{r}_k \times \vec{A}_k \text{ and } \vec{R}_{nk} = \vec{r}_k \times \vec{N}_k \quad (24)$$

Substituting for the moment \vec{T} from Equation (23) into Equation (19),

$$\vec{\alpha} = I^{-1}(R_a \vec{F}_a + R_n \vec{F}_n) \quad (25)$$

Now,

$$(\vec{\alpha} \times \vec{r}_k) \bullet \vec{n}_k = (I^{-1} \vec{T}) \times \vec{r}_k \bullet \vec{n}_k = I^{-1}(R_a \vec{F}_a + R_n \vec{F}_n) \times \vec{r}_k \bullet \vec{n}_k \quad (26)$$

or

$$(\vec{\alpha} \times \vec{r}_k) \bullet \vec{n}_k = J_k \vec{F}_a + S_k \vec{F}_n \quad (27)$$

where J_k and S_k are row vectors whose j^{th} elements are given by $(I^{-1} \vec{R}_{aj} \times \vec{r}_k) \bullet \vec{n}_k$ and $(I^{-1} \vec{R}_{nj} \times \vec{r}_k) \bullet \vec{n}_k$, respectively.

Hence, the contribution of the angular acceleration, $\vec{a}_{N\alpha}$ is given by:

$$\vec{a}_{N\alpha} = \begin{bmatrix} (\vec{\alpha} \times \vec{r}_1) \bullet \vec{n}_1 \\ \vdots \\ (\vec{\alpha} \times \vec{r}_{nw}) \bullet \vec{n}_{nw} \end{bmatrix} = J\vec{F}_a + S\vec{F}_n \quad (28)$$

where J and S are $w \times w$ matrices whose k^{th} columns are given by \vec{J}_k and \vec{S}_k , respectively.

2.4 The Normal Components of the Contact Point Acceleration Vector

Substituting Equations (17), (18) and (27) into Equation (16), one can write:

$$\vec{a}_N = (H + J)\vec{F}_a + (Q + S)\vec{F}_n + \vec{G} + \vec{a}_{N\omega}$$

Substituting $H + J = U$ and $Q + S = P$

$$\vec{a}_N = U\vec{F}_a + P\vec{F}_n + \vec{G} + \vec{a}_{N\omega} \quad (29)$$

or

$$\vec{a}_N = P\vec{F}_n + \vec{b} \quad (30)$$

$$\text{where } \vec{b} = U\vec{F}_a + \vec{G} + \vec{a}_{N\omega} \quad (31)$$

Since the wheels can not penetrate into the ground, the normal component of the contact point acceleration must be zero, i.e.

$$a_{nk} = 0$$

$$\vec{a}_N = P\vec{F}_n + \vec{b} = 0 \quad (32)$$

or

$$\vec{F}_n = -P^{-1}\vec{b} \quad (33)$$

The translation and angular acceleration components of the platform can be obtained by substituting Equation (33) for \vec{F}_n into Equations (7) and (25), respectively.

3 Case Study of a Laterally Symmetrical Vehicle Climbing a Ramp

In this section the equations of motion derived earlier are considered for a special case of a rear-wheel driven mobile platform whose front wheels encounter a ramp. Lateral symmetry is assumed and the mobile platform can be represented by a *bicycle model* (Figure 3). For this case the steering angles of the front and rear wheels (δ_1 and δ_2) and the lateral friction coefficients on both axles (μ_{l1} and μ_{l2}) are zero. The relevant expressions are given below.

For this case study, Equation (4) reduces to:

$$\vec{A}_1 = \begin{bmatrix} \cos(p) \\ 0 \\ -\sin(p) \end{bmatrix}; \quad \vec{A}_2 = \begin{bmatrix} \cos(\gamma) \\ 0 \\ \sin(\gamma) \end{bmatrix} \quad (34)$$

where the subscripts 1 and 2 refer to the rear and front wheel pairs, respectively. Similarly the \vec{N}_k terms can be written as

$$\vec{N}_1 = \begin{bmatrix} \sin(p) \\ 0 \\ \cos(p) \end{bmatrix}; \quad \vec{N}_2 = \begin{bmatrix} -\sin(\gamma) \\ 0 \\ \cos(\gamma) \end{bmatrix} \quad (35)$$

The normal vectors of the surface profile at the rear and front wheel contact points are respectively given as:

$$\vec{n}_1 = \begin{bmatrix} \sin(p) \\ 0 \\ \cos(p) \end{bmatrix}; \quad \vec{n}_2 = \begin{bmatrix} -\sin(\gamma) \\ 0 \\ \cos(\gamma) \end{bmatrix} \quad (36)$$

The position vectors of the contact points are:

$$\vec{r}_1 = \begin{bmatrix} -L_r \\ 0 \\ -h \end{bmatrix}; \quad \vec{r}_2 = \begin{bmatrix} L_f \\ 0 \\ -h \end{bmatrix} \quad (37)$$

Equation (23) allows the terms R_a and R_n to be evaluated for the rear and front wheels:

$$R_{a1} = \begin{bmatrix} 0 \\ -h \cos(p) - Lr \sin(p) \\ 0 \end{bmatrix}; \quad R_{a2} = \begin{bmatrix} 0 \\ -h \cos(\gamma) - Lf \sin(\gamma) \\ 0 \end{bmatrix} \quad (38)$$

$$R_{n1} = \begin{bmatrix} 0 \\ -h \sin(p) + Lr \cos(p) \\ 0 \end{bmatrix}; \quad R_{n2} = \begin{bmatrix} 0 \\ h \sin(\gamma) - Lf \cos(\gamma) \\ 0 \end{bmatrix} \quad (39)$$

The inertia matrices M and I are given by:

$$M = m \begin{bmatrix} 1 & 0 & 0 \\ 0 & 1 & 0 \\ 0 & 0 & 1 \end{bmatrix}; \quad I = \begin{bmatrix} I_x & 0 & 0 \\ 0 & I_y & 0 \\ 0 & 0 & I_z \end{bmatrix} \quad (40)$$

where m is the total mass of the platform and payload and I_x , I_y and I_z are the total mass moments of inertia of the platform and payload about the respective axes.

The U , P and b matrices are derived using the methods outlined in the previous section. Thus,

$$U = \begin{bmatrix} U_{11} & U_{12} \\ U_{21} & U_{22} \end{bmatrix} \quad (41)$$

where,

$$U_{11} = \frac{(h \cos(p) + Lr \sin(p))h \sin(p) - (h \cos(p) + Lr \sin(p))Lr \cos(p)}{I_y}$$

$$U_{21} = \frac{-\cos(\gamma)\sin(p) - \sin(\gamma)\cos(p)}{M} + \frac{(-h\cos(p) - Lr\sin(p))h\sin(\gamma) + (h\cos(p) + Lr\sin(p))Lf\cos(\gamma)}{I_y}$$

$$U_{12} = \frac{\cos(\gamma)\sin(p) + \sin(\gamma)\cos(p)}{M} + \frac{(h\cos(\gamma) + Lf\sin(\gamma))h\sin(p) - (h\cos(\gamma) + Lf\sin(\gamma))Lr\cos(p)}{I_y}$$

$$U_{22} = \frac{(-h\cos(\gamma) - Lf\sin(\gamma))h\sin(\gamma) + (h\cos(\gamma) + Lf\sin(\gamma))Lf\cos(\gamma)}{I_y}$$

The P matrix is given as:

$$P = \begin{bmatrix} P_{11} & P_{12} \\ P_{21} & P_{22} \end{bmatrix} \quad (42)$$

where

$$P_{11} = \frac{1}{M} + \frac{(-h\sin(p) + Lr\cos(p))h\sin(p) + (-h\sin(p) + Lr\cos(p))Lr\cos(p)}{I_y}$$

$$P_{21} = \frac{\sin(p - \gamma)}{M} + \frac{(h\sin(\gamma) - Lf\cos(\gamma))h\sin(\gamma) - (h\sin(\gamma) - Lf\cos(\gamma))Lf\cos(\gamma)}{I_y}$$

$$P_{12} = \frac{\sin(p - \gamma)}{M} - \frac{(-h\sin(p) + Lr\cos(p))h\sin(p) - (-h\sin(p) + Lr\cos(p))Lr\cos(p)}{I_y}$$

$$P_{22} = \frac{1}{M} + \frac{(h\sin(\gamma) - Lf\cos(\gamma))h\sin(\gamma) - (h\sin(\gamma) - Lf\cos(\gamma))Lf\cos(\gamma)}{I_y}$$

The body force vector \vec{G} is given by:

$$\vec{G} = g \begin{bmatrix} -1 \\ \sin(p)\sin(\gamma) - \cos(p)\cos(\gamma) \end{bmatrix} \quad (43)$$

where g is the acceleration due to gravity.

The contribution of the centrifugal acceleration term $\vec{a}_{n\omega}$ is given by,

$$\vec{a}_{n\omega} = \omega_p^2 \begin{bmatrix} Lr \sin(p) + h \cos(p) \\ Lf \sin(\gamma) + h \cos(\gamma) \end{bmatrix} \quad (44)$$

where ω_p is the pitch angular velocity of the platform.

The vector \vec{b} defined in Equation (31) is found as:

$$\vec{b} = U \begin{bmatrix} F_r \\ 0 \end{bmatrix} + g \begin{bmatrix} -1 \\ \sin(p)\sin(\gamma) - \cos(p)\cos(\gamma) \end{bmatrix} + \omega_p^2 \begin{bmatrix} Lr \sin(p) + h \cos(p) \\ Lf \sin(\gamma) + h \cos(\gamma) \end{bmatrix} \quad (45)$$

where F_r is the rear-wheel traction force.

It is necessary to obtain the equation of the pitch angular motion, which can be found from Equation (24) as:

$$\vec{\alpha} = I^{-1}(R_a \vec{F}_a + R_n \vec{F}_n), \quad \text{where } \vec{F}_n = -P^{-1} \vec{b}$$

For a laterally symmetrical obstacle, both the rolling and the yawing rotational accelerations are zero. Thus,

$$\vec{\alpha} = \begin{bmatrix} 0 \\ \alpha_p \\ 0 \end{bmatrix}$$

The actual expression for the angular acceleration of the pitch motion α_p has been derived by using the Mathcad® and is given in Appendix (A). It can be shown that α_p has a form as follows:

$$\alpha_p = \Phi(p, \gamma) F_r + \Gamma(p, \gamma) \omega_p^2 + \Lambda(p, \gamma) \quad (46)$$

where $\Phi(p, \gamma)$, $\Gamma(p, \gamma)$ and $\Lambda(p, \gamma)$ are non linear functions of the pitch angular displacement p and the profile angle γ .

3.1 Localised Trajectory Planning

In this section a trajectory is generated for the manoeuvre of the mobile platform in the locality of the obstacle where it needs to traverse. The localised trajectory is a time parametrised curve that provides the magnitude of the angular pitch for the period of time during which the front wheels of the platform are in contact with the obstacle. Let $p(t_n)$ be a polynomial trajectory function for the pitch angular displacement, where $t_n = \frac{t}{T}$ is a normalised time, t is the actual time variable, and T is the total time it takes the platform to complete the obstacle-traversing manoeuvre. If the pitch angular jerks at the initial and final conditions of the manoeuvre are included in addition to the displacement, velocity, and acceleration, then there are eight conditions in total to be satisfied by the polynomial trajectory function $p(t_n)$ and its derivatives. Hence, $p(t_n)$ can be devised to be a polynomial of degree seven. That is,

$$p(t_n) = \sum_{i=0}^7 C_i t_n^i \quad (47)$$

from which the velocity, acceleration and jerk of the platform can be determined by successive differentiation with respect to time, i.e.,

$$\dot{p}(t_n) = \sum_{i=1}^7 i C_i t_n^{i-1} \quad (48)$$

$$\ddot{p}(t_n) = \sum_{i=2}^7 i(i-1) C_i t_n^{i-2} \quad (49)$$

$$\ddot{p}(t_n) = \sum_{i=3}^7 i(i-1)(i-2)C_i t_n^{i-3} \quad (50)$$

For ramp obstacles (Figure 3), the initial ($t_n = 0$) and final ($t_n = 1$) conditions of the platform are:

$$p(0) = 0 \quad p(1) = \beta$$

$$\dot{p}(0) = 0 \quad \dot{p}(1) = 0$$

$$\ddot{p}(0) = 0 \quad \ddot{p}(1) = 0$$

$$\dddot{p}(0) = 0 \quad \dddot{p}(1) = 0$$

By using these conditions the coefficients C_i where $i = 0 \dots 7$ in Equations (47-50) can be obtained:

$$C = [-20 \quad 70 \quad -84 \quad 35 \quad 0 \quad 0 \quad 0 \quad 0] \beta$$

where β is the steady pitch angular displacement at the end of the localised manoeuvre.

The trajectory function and its derivatives are plotted in Figure 4 as a function of normalised time. As can be seen in the Figure 4(d) an intermediate jerk exists when a single polynomial function is used for the entire trajectory. However, the jerk at the start and end of manoeuvre are null which are essential from the point of view of actuation. It can also be observed that the peak value of the intermediate jerk can be reduced if a bigger time span is allowed for the platform to complete the manoeuvre as this helps to reduce the peak velocities and accelerations. With regards to the profile angle, it can be parametrised with the same time variable t_n to obtain $\gamma(t_n)$.

Once the trajectory has been planned, the rear wheel traction force needed to complete the manoeuvre can be computed as follows. Substituting the planned displacement $p(t_n)$,

velocity $\dot{p}(t_n)$, acceleration $\ddot{p}(t_n)$, and the profile angle $\gamma(t_n)$ in place of p , ω_p , α_p and γ , respectively, in Equation (46), then:

$$\ddot{p}(t_n) = \Phi(p(t_n), \gamma(t_n))F_{tr} + \Gamma(p(t_n), \gamma(t_n))\dot{p}(t_n)^2 + \Lambda(p(t_n), \gamma(t_n)) \quad (51)$$

from which the rear wheel traction force F_{tr} can be obtained as:

$$F_{tr} = \Phi(p(t_n), \gamma(t_n))^{-1}(\ddot{p}(t_n) - \Gamma(p(t_n), \gamma(t_n))\dot{p}(t_n)^2 - \Lambda(p(t_n), \gamma(t_n))) \quad (52)$$

The dimensions, mass and inertia of the platform used in the case study are summarised in Table 1. For the simulation, a ramp with the following profile angle has been chosen.

$$\gamma(t_n) = \xi \sin(\alpha t_n + \delta) \quad (53)$$

The values for the parameters ξ , α , and δ are $\xi = -0.2$, $\alpha = \pi$, $\delta = 0$. The time parametrised profile angle of the ramp is shown in Figure (5).

The traction effort needed to complete the manoeuvre of the platform over the ramp is computed by using Equation (52) for different time spans of manoeuvre (T). The results are shown in Figures 6 and 7 on a normalised time scale. Figure 6 shows the traction force requirement when the total time required to complete the manoeuvre is less than or equal to 1.38 seconds. Conversely, Figure 7 shows the traction force requirement when the manoeuvre time is greater than or equal to 1.38 seconds. It can be seen in Figure 6 that the sign of the traction force may change for fast manoeuvres (i.e. with small values of T). A negative traction force corresponds to a braking action. From Figure 7, it is evident that a shift from the traction mode to a braking mode can be avoided if the manoeuvre time is increased so that the velocity of the platform is kept low. In this example, a minimum manoeuvre time of 1.38 seconds is needed to ensure that there is no change in the traction mode.

As is known from traction control literature [11-12], there is a limitation to the maximum traction force that can be generated by a wheel-ground interface due to friction force saturation. Consequently, the maximum traction force requirement in Figures 6 and 7 can not exceed the saturation friction force, which is determined by the property and condition of the traction surface. For example a dry pavement has a larger saturation friction force than a wet pavement, providing all other conditions remain the same. Figures 6 and 7 also show that the maximum traction force requirement decreases as the manoeuvre time increases. In order to achieve an effective motion control for the WMR crossing an obstacle, an appropriate manoeuvre time should be selected based on a prior knowledge of the friction characteristics associated with the traction surface.

4 Conclusion

A novel approach to trajectory planning of mobile platforms traversing localised obstacles has been presented. The method, which is based on a dynamic model of the platform, takes into account all forces including translational as well as rotational inertia forces. The method has been used in a case study to devise a polynomial trajectory planning of the pitching motion of a mobile platform moving over an obstacle of a known geometry. It has been demonstrated that, during obstacle traversing a compromise can be achieved between the minimal time of manoeuvre and each of the following parameters, namely, vehicle traction force, inertia load and jerk. The shift between the traction mode and braking mode of the actuators can be avoided by an appropriate choice of a minimum time of manoeuvre, and hence the velocity of the platform. This study also provides a basis for the selection of an appropriate manoeuvre time based on a prior knowledge of the friction characteristics of a traction surface. The maximum

traction force requirement decreases as the manoeuvre time increases which helps to reduce the maximum load on the actuators.

REFERENCES

- 1 **Ben Amar, F., Bidaud, P., and Ben Ouezdou, F.**, On modeling and motion planning of planetary vehicles. *Proceeding of the 1993 IEEE/RSJ International Conference on Intelligent Robots and Systems*, 1993, pp. 1381-1386.
- 2 **Shiller, Z. and Gwo, Y.** Dynamic motion planning of autonomous vehicles. *IEEE Transactions on Robotics and Automation*, 1991, pp. 241-249.
- 3 **Siméon, T.** Motion planning for a non-holonomic mobile robot on 3-dimensional terrain. *Proceeding of the IEEE/RSJ International Workshop on Intelligent Robots and Systems, IROS'91*, Osaka, Japan, 1991, pp. 1455-1460.
- 4 **Hait, A. and Siméon, T.** Motion planning on rough terrain for an articulated vehicle in presence of uncertainties. *Proceeding of the IEEE International Conference on Intelligent Robots and Systems*, 1996, Vol.3, pp. 1126-1133.
- 5 **Siméon, T. and Dacre-Wright, B.** A practical motion planner for all-terrain mobile robots. *Proceeding of the IEEE International Conference On Intelligent Robots and Systems*, Yokohama, Japan, 1993, pp. 1357-1363.
- 6 **Serna, M. and Bayo, E.** Trajectory planning for flexible manipulators. *Proceedings 1990 IEEE International Conference on Robotics and Automation*, vol.2. Los Alamitos, USA, 1990, pp.910-15.
- 7 **Suzuki, T., Nagai, J. and Okuma, S.,** A realtime trajectory planning method for manipulators based on kinetic Energy. *IEEE International Workshop ON Intelligent Robots and Systems*, Okata, Japan, 1991.

- 8 **Won, J., Choi, B.** and **Chung, J.** Smooth joint trajectory planning for a point-to-point task.
IEEE International Workshop on Intelligent Robots and Systems, Okata, Japan, 1991.
- 9 **Piazz, A.** and **Visioli, A.** An interval algorithm for minimum-jerk trajectory planning of robot manipulators. *IEEE, Proceedings of the 36th. Conference on Decision and Control*, San Diego, California, 1997.
- 10 **Sledge; N. Jr., Marshek K.**, Development and validation of an optimised emergency lane-change trajectory. Vehicle dynamics and simulation, SAE International congress and exposition, Detroit, USA, Session, 1998.
- 11 **Burg, Jan van der** and **Blazevic, P.** Anti-lock braking and traction control concept for all-terrain robotic vehicle. *Proceedings - IEEE International Conference on Robotics and Automation*, 1997, Vol.2, pp.1400-1405.
- 12 **Hori, Y., Yasushi, T.** and **Tsuruoka, Y.** Traction control of electric vehicles: basic experimental results using the test EV, UOT Electric March. *IEEE Transactions on Industry Applications*, 1998, pp. 1131-1138.

Appendix A

The following is the expression for the pitch angular acceleration.

$$\alpha_p = \Phi(p, \gamma) \cdot F_{tr} + \Gamma(p, \gamma) \cdot (\omega_p)^2 + \Lambda(p, \gamma)$$

where

$$\Phi(p, \gamma) = \frac{\phi(p, \gamma)}{\Delta} \quad \Gamma(p, \gamma) = \frac{\tau(p, \gamma)}{\Delta} \quad \Lambda(p, \gamma) = \frac{\lambda(p, \gamma)}{\Delta}$$

$$\Delta = \delta_1 + m(\delta_2 + \delta_3 + \delta_4)$$

where

$$\delta_1 = (\sin(\gamma))^2 \cdot I_y$$

$$\delta_2 = [2(L_f^2 + L_r \cdot L_f) \cdot \cos(\gamma)^2 - 2 \cdot h \cdot (L_r + L_f) \cdot \cos(\gamma) \cdot \sin(\gamma) + L_r^2 - L_f^2] \cdot \cos(p)^2$$

$$\delta_3 = [2(L_f^2 + L_r \cdot L_f) \cdot \cos(\gamma) \cdot \sin(\gamma) - [2 \cdot h \cdot (L_r + L_f)] \cdot \sin(\gamma)^2] \cdot \cos(p) \cdot \sin(p)$$

$$\delta_4 = (L_f^2 + h^2) \cdot \sin(\gamma)^2$$

$$\phi(p, \gamma) = (L_r + L_f) \cdot [(1 - \cos(\gamma)^2) \cdot \sin(p) + \cos(\gamma) \cdot \sin(\gamma) \cdot \cos(\gamma)] + R \cdot (\sin(\gamma)^2)$$

$$\tau(p, \gamma) = [\tau_1 + \tau_2] \cdot m \cdot R + [\tau_3 + \tau_4 + \tau_6] \cdot m$$

where

$$\tau_1 = [L_f \cdot (\cos(\gamma) - 1) \cdot \sin(\gamma) - h \cdot \sin(\gamma)^2] \cdot \sin(p)$$

$$\tau_2 = [-(L_r + L_f) \cdot \cos(\gamma) + (-h \cdot \cos(\gamma) + h) \cdot \sin(\gamma) + L_f \cdot \cos(\gamma)^2 + L_r] \cdot \cos(p)$$

$$\tau_3 = [2 \cdot L_f^2 + 2 \cdot L_r \cdot L_f] \cdot \cos(\gamma)^2 - 2h \cdot (L_r + L_f) \cdot \cos(\gamma) \cdot \sin(\gamma) + L_r^2 - L_f^2] \cdot \cos(p) \cdot \sin(p)$$

$$\tau_4 = (L_f^2 + L_r \cdot L_f) \cdot \cos(\gamma) \cdot \sin(\gamma) - h \cdot (L_f + L_r) \cdot \sin(\gamma)^2$$

$$\tau_5 = [(-2 \cdot L_r \cdot L_f - 2 \cdot L_f^2) \cdot \cos(\gamma) \cdot \sin(\gamma) + 2 \cdot h \cdot (L_f + L_r) \cdot \sin(\gamma)^2] \cdot \cos(p)^2$$

and

$$\lambda(p, \gamma) = (-\sin(p) \cdot \cos(\gamma)^2 + \sin(p)) \cdot m \cdot g \cdot h + (\cos(p) \cdot \cos(\gamma)^2 - \cos(p)) \cdot m \cdot g \cdot L_r$$

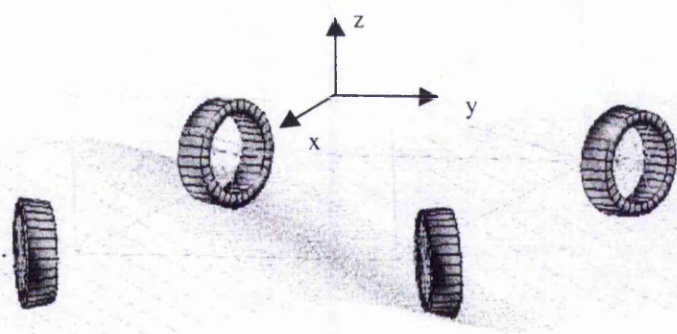


Figure 1. Definition of vehicle coordinate axes

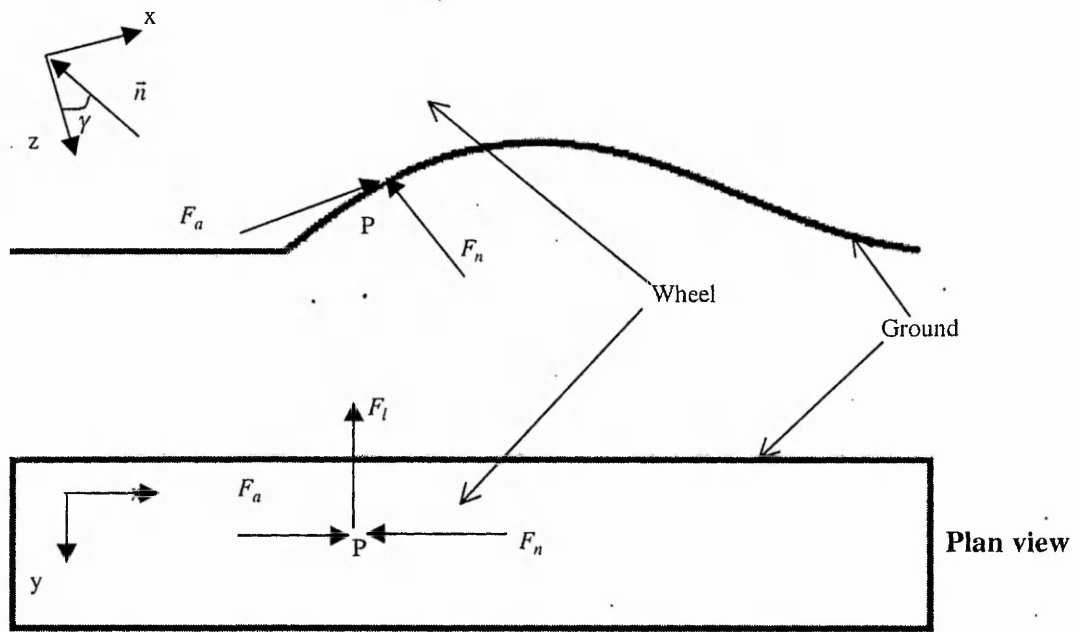


Figure 2. Geometry of wheel-ground contact and definitions of wheel-ground forces.

Table 1. Dimensions of the mobile platform for the case study.

Symbol	Description	Value
L_f	Longitudinal distance of front axle from the vehicle centre of mass	0.6 m
L_r	Longitudinal distance of rear axle from the vehicle centre of mass	0.46 m
h	Height of centre of mass from the wheel centres	0.4 m
R	Radius of wheels	0.1 m
I_y	Pitch moment of inertia of the platform	47 kg-m^2
m	Mass of the platform and payload	270 kg

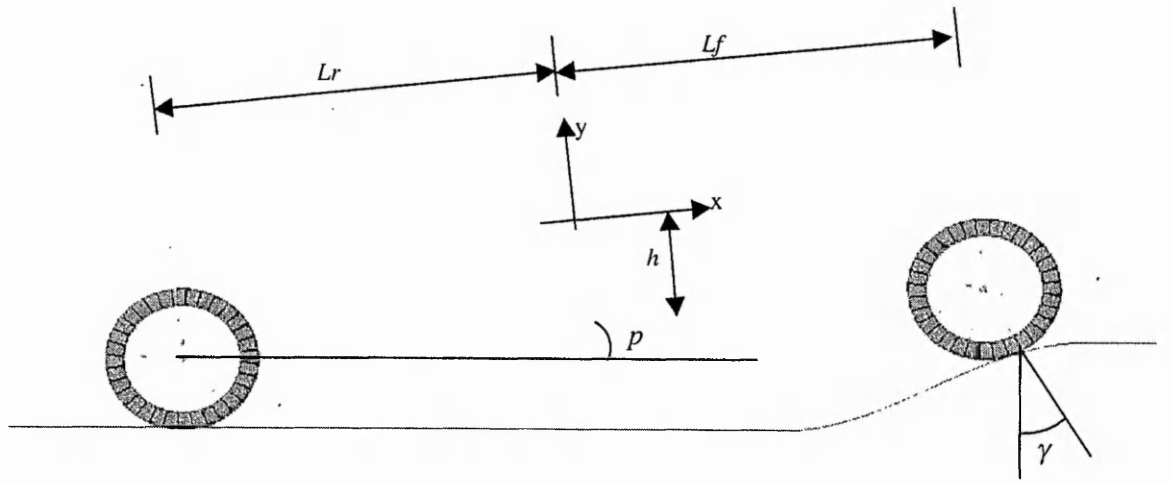
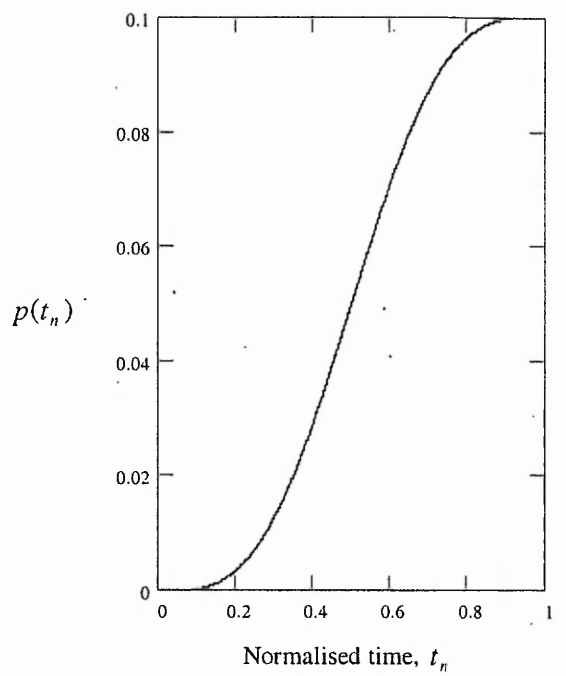
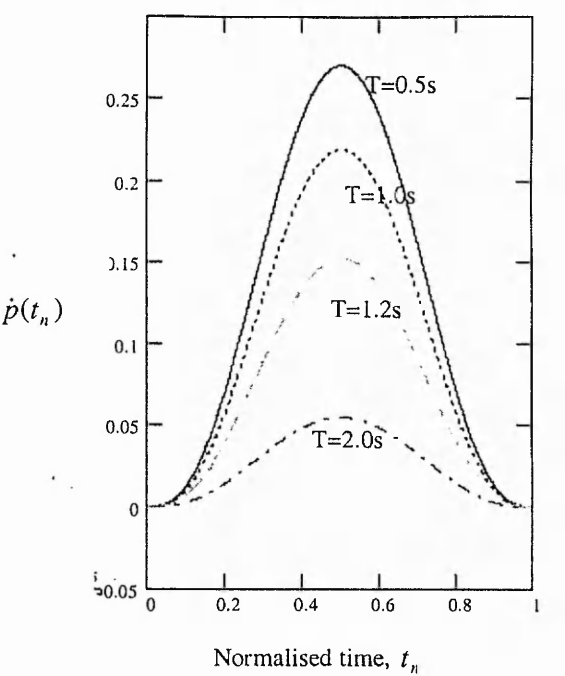


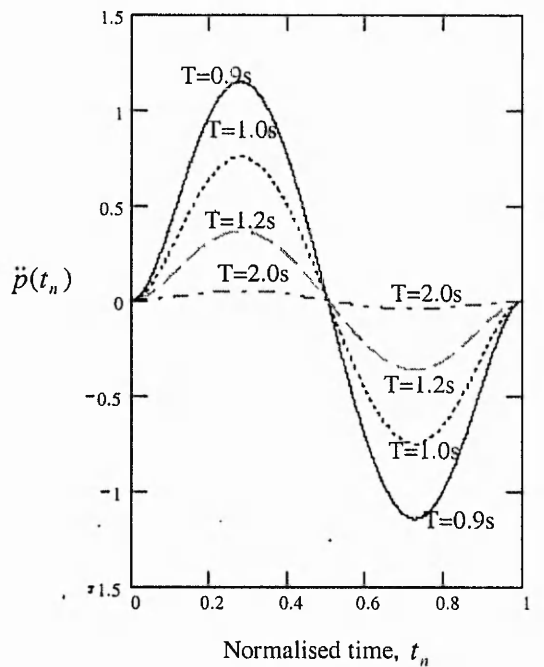
Figure 3. A mobile platform with front obstacle (laterally symmetrical).



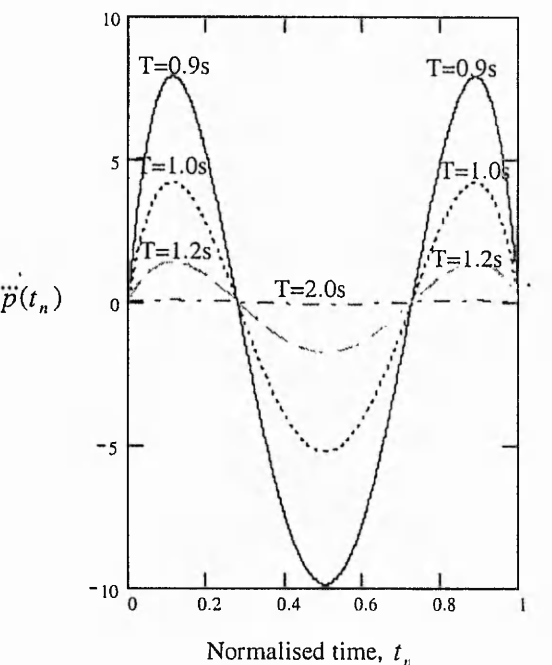
a)



b)



c)



d)

Figure 4. a) Displacement b) velocity c) acceleration d) jerk versus time plots of a polynomial trajectory function.

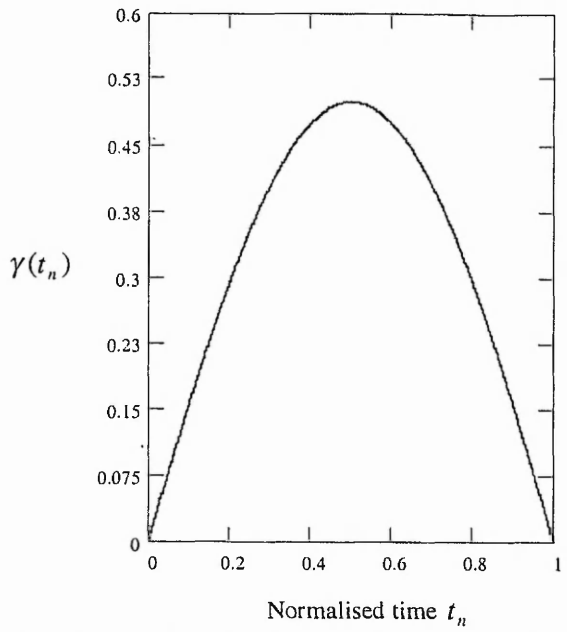


Figure 5. The time parametrised ramp profile angle considered in the simulation.

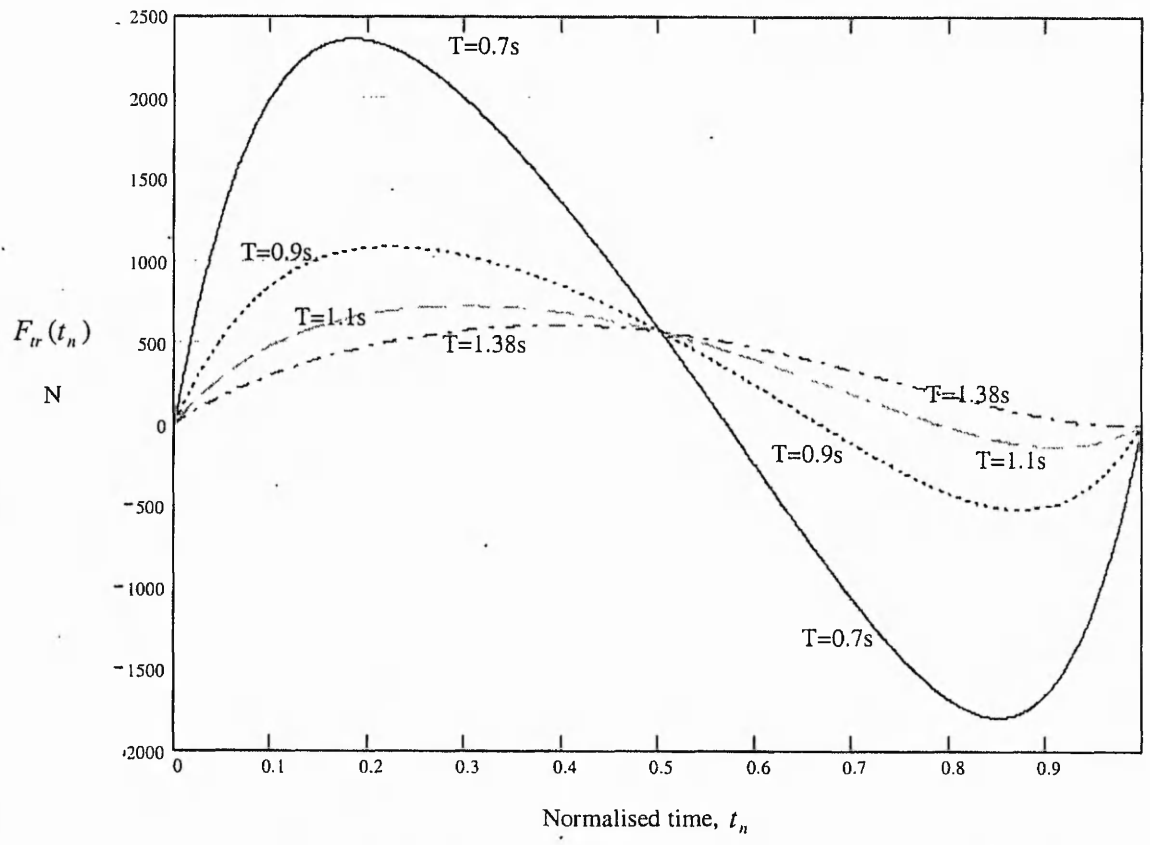


Figure 6 Traction force requirement when manoeuvre in time $T \leq 1.38\text{s}$.

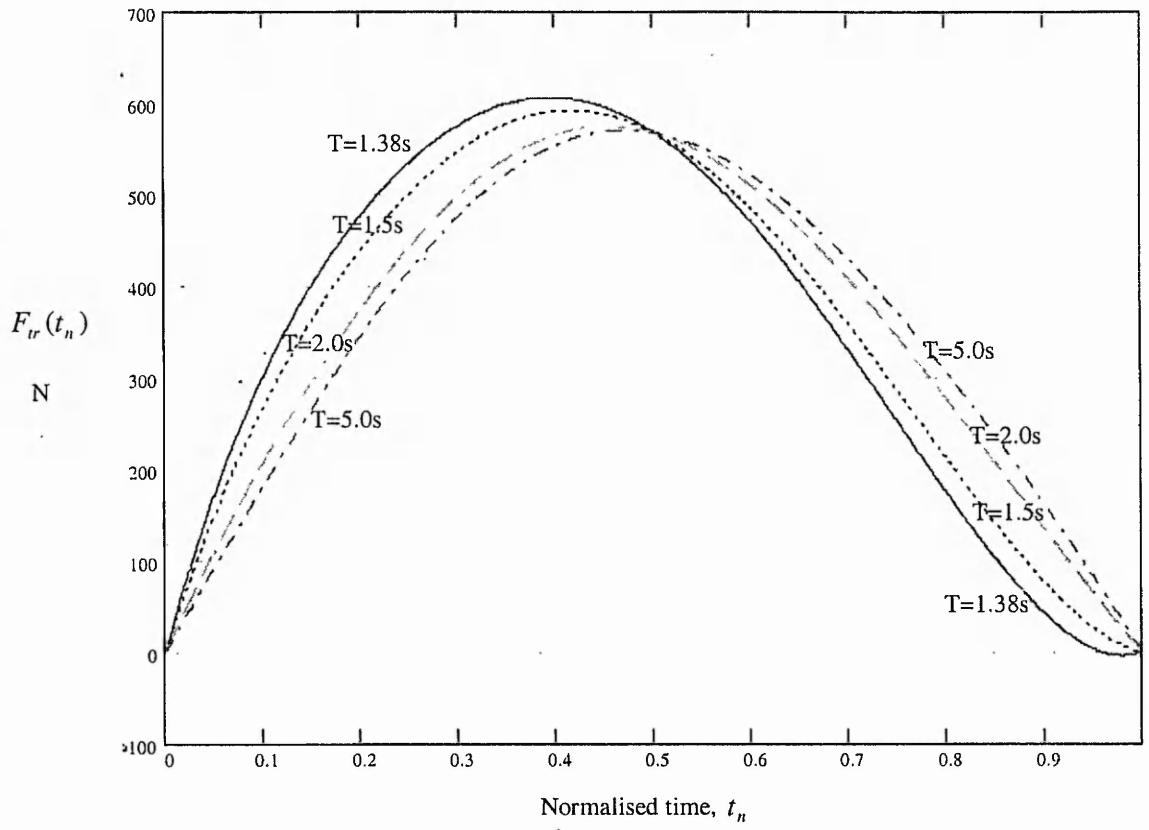


Figure 7 Traction force requirement when manoeuvre in time $T \geq 1.38s$.

Shock Response Analysis of WMRs

A. Ayalew and E. Lai

The Nottingham Trent University, Department of Mechanical Engineering, Nottingham.

S. O. Oyadiji

University of Manchester, School of Engineering, Manchester.

ABSTRACT

An investigation has been carried out to analyse the shock response of a wheeled mobile robot (WMR) when one of its wheels comes into contact with an unexpected surface obstacle. By means of the modal superposition technique, the dynamic loads at different points on the mobile platform are computed using the ANSYS® finite-element package. Three forms of shock pulse loading have been considered: rectangular, triangular and sinusoidal. The amplitude of each harmonic component is determined by means of Fourier expansion and the results for each of the three cases of loading are then compared. The results show that the highest level of dynamic forces occurred in the first harmonic, with the rectangular pulse producing the highest dynamic loading of nearly 7 times the peak magnitude of the shock pulse, the sinusoidal pulse at about 6 times and the triangular pulse at about 5 times. Since shock absorbers are not normally used for WMRs, the work has highlighted the need for developing new wheel materials that can attenuate the impact loading before it propagates to the structure of the platform.

1. INTRODUCTION

Vibration analysis of vehicles fitted with a suspension system has been explored extensively due to the high motivation stimulated by the automotive industry. The advent of passive and active suspension systems has greatly improved ride-comfort, road holding and vehicle stability of passenger cars [1]. However, there is a lack of good understanding of dynamic problems related to vehicles that can not take advantage of such advances in suspension systems.

Wheeled Mobile Robots (WMRs) are commonly designed without a well-defined suspension system. These vehicles are vulnerable to the effects of vibration because they often carry delicate

sensors and computing hardware, in addition to loose payloads on the platform. A limited amount of literature is available in the area of robotics research that gives consideration to WMR interaction with road obstacles. A four-wheeled mobile robot with a variable structure that can pass over step obstacles has been proposed in [2]. The vehicle can switch between two running modes. When the robot is working on a smooth surface it has a car like, four-wheeled structure. When it passes over an obstacle the vehicle changes its structure and becomes a two-wheeled robot running like an inverted pendulum supported by wheels. After the front axle of the WMR has flown over the obstacle it touches the ground in a controlled manner so that soft-landing of the wheels can be achieved with minimum shock loads applied to the vehicle structure. However, the complexity of the vehicle structure and the hardware requirement for the control and instrumentation make the practical application of the technique prohibitive.

Stochastic vibration of manipulators mounted on mobile robots has been discussed in [3], where only the structural dynamics of the manipulator was considered. The displacement of the manipulator tip resulting from stochastic vibration inputs at the wheel of the mobile robot has been analysed. It was suggested that vehicle suspension damping would be needed to minimise error in manipulator control. However, the work did not address the shock response of the mobile platform to suddenly applied excitation loads. Dupont and Yamajako [4] have pointed out that for large displacements the structural dynamics of a body takes place at a much faster rate than its gross motion dynamics. This observation has been taken into account in the present work when analysing the dynamics of the structure by ignoring the effect of the gross motion of the mobile robot.

It is important to have a good understanding of the shock response of the platform when it comes into contact with an obstacle, particularly for safe path planning of wheeled mobile robot navigating on an uneven terrain. Criteria based on acceptable magnitude of dynamic load on the platform can be established to assist the controller of the robot to take appropriate actions.

This paper describes the outcomes of an investigation into the shock response of a WMR excited by three forms of shock pulses: rectangular, sinusoidal and triangular. Attempts have been made to keep the method of analysis simple so that it can be incorporated in motion control systems for mobile robots.

2. MODELLING THE FAST DYNAMICS OF THE ROBOTIC VEHICLE

Assuming the platform is discretised into n points, the fast dynamics system of equations of motion of the structure is given by:

$$M\ddot{U} + C\dot{U} + KU = F \quad (1)$$

where M , C and K are $n \times n$ mass, damping and stiffness matrices, respectively. U is the nodal displacement vector in the generalised coordinates and F is the vector of excitation forces.

If the dimensions of a vehicle are known a finite element (FE) model can be developed for the platform and Equation (1) can be used to determine the response of the vehicle at various points

on the structure due to external forces. Assuming that there is negligible damping in the structure, Equation (1) can be simplified to:

$$M\ddot{U} + KU = F \quad (2)$$

There are two methods available to determine the response of the structure to external excitations based on Equation (2). The first method involves the explicit integration of the equation. This method which is based on time-stepping integration of a system of equations is often slow, making it impractical for real-time motion control schemes.

The second method, known as the 'modal superposition principle', involves the determination of the responses to different modes of vibration of the structure separately and then combining them to obtain a total response. This technique is fast and is well suited for incorporation into a motion control strategy. Advantages can be taken of the fact that natural frequencies and associated modal shapes of the vehicle need be computed only once. Consequently, a reasonably accurate response can be obtained by considering the first few natural frequencies and their corresponding modal shapes [5]. For ease of implementation, the present investigation is carried out by means of the modal superposition technique.

Let Λ and Φ be the matrices of eigenvalues λ_i and eigenvectors ϕ_i respectively,

$$\Lambda = \begin{bmatrix} \lambda_1 & & & \\ & \ddots & & \\ & & \ddots & \\ & & & \lambda_n \end{bmatrix} \text{ and } \Phi = [\phi_1 \quad \bullet \quad \bullet \quad \bullet \quad \phi_n] \quad (3)$$

$\lambda_i = \omega_i^2$, where ω_i is the natural frequency of the i^{th} mode of vibration which has a modal shape specified by the vector ϕ_i . A system of decoupled equations of motion can be obtained by transforming Equation (2) into the normal coordinates using the modal matrix Φ . Thus, in terms of the normal coordinates X , the decoupled equations of motion are given by:

$$\ddot{X}(t) + \Lambda X(t) = \Phi^T F(t) \quad (4)$$

The system of decoupled equations in Equation (4) can be solved by treating individual constituent equations as a system of second order equations with a single degree of freedom. Duhamel's integral can be used to obtain the modal responses in the normal coordinates:

$$x_i(t) = \frac{1}{\omega_i} \int_0^t f_i(\tau) \sin(\omega_i(t-\tau)) d\tau + a_i \sin(\omega_i t) + b_i \cos(\omega_i t) \quad (5)$$

$$\text{where } f_i(t) = \phi_i^T F(t) \quad (6)$$

$f_i(t)$ is the projection of the excitation forces into the i^{th} normal coordinate. Equation (5) provides the general solution of the modal response. The integral term represents the steady-state response of the structure, while the other two terms represents its transient response. The present investigation considers only the steady state response of the structure.

An arbitrary periodic excitation force $f_i(t)$ can be decomposed into simple harmonic components by means of Fourier series expansion. The total response of the structure due to an excitation force is the sum of the responses due to individual harmonic components, assuming that the structure is linear.

Hence the Fourier expansion of the modal force $f_k(t)$ for the k^{th} mode of vibration which is truncated after s terms is given by:

$$f_k(t) = \sum_{i=1}^n \sum_{j=1}^s (a_{ij} \sin(p_{ij}t) + b_{ij} \cos(p_{ij}t)) \quad (8)$$

where a_{ij} and b_{ij} are the Fourier coefficients, p_{ij} is the j^{th} harmonic frequency due to the i^{th} force F_i .

The dynamic factor of the steady state response of the k^{th} mode of vibration due to the j^{th} harmonic component of the exciting force applied at nodal point i , which has a frequency p_{ij} , is given by:

$$(d_{ij})_k = \frac{\sqrt{(a_{ij})^2 + (b_{ij})^2}}{1 - \frac{p_{ij}^2}{\omega_k^2}} \quad (9)$$

Hence the steady state modal response of the k^{th} mode due to all excitation forces F_i (x_k), and the steady state response at point p on the platform in the generalised coordinate system (U_p) are given respectively as:

$$x_k = \phi_k \begin{bmatrix} F_1 \left(\sum_{j=1}^s d(\omega_1, p_{1j}) \sin(p_{1j}t) \right) \\ \vdots \\ F_n \left(\sum_{j=1}^s d(\omega_n, p_{nj}) \sin(p_{nj}t) \right) \end{bmatrix}, \quad U_p = (\phi^T)_p \begin{bmatrix} x_1 \\ \vdots \\ x_n \end{bmatrix} \quad (10)$$

3. CASE STUDIES AND RESULTS

Three case studies of the shock response of a four-wheeled mobile robot (WMR) encountering obstacles of different load forms have been investigated. The finite element model of the WMR is shown in Figure 1 and the analysis was carried out by using the ANSYS® software. The present investigation only considered the vibration of the platform without taking into account the contribution made by other components such as wheels and links. The front-right wheel of the vehicle is assumed to experience a sudden shock load of a known profile. Three forms of shock loading have been considered: rectangular pulse, triangular pulse and sinusoidal pulse (Figure 2).

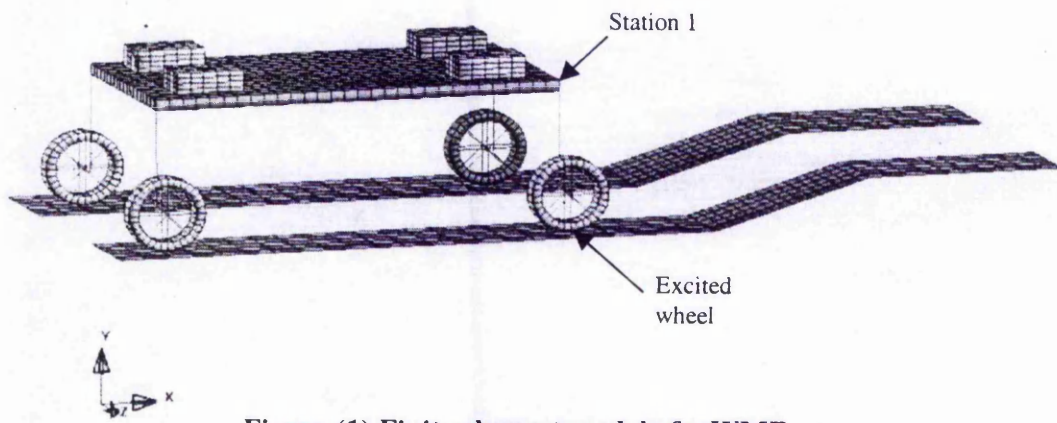


Figure (1) Finite element model of a WMR.

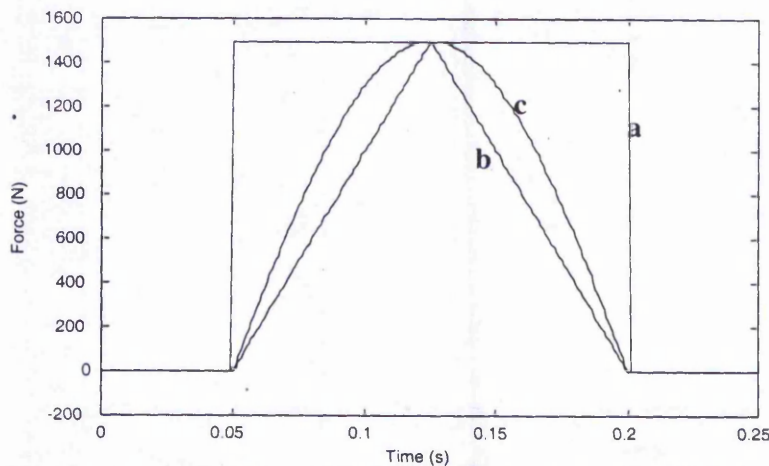


Figure (2). Shock loading curves. a) Rectangular pulse, b) Triangular pulse,
c) Sinusoidal pulse.

Table (1). Summary of natural Frequencies.

Mode No.	Frequency (Hz)	Mode Shape
1	3.82	In phase longitudinal edges bending
2	4.20	Diagonal twisting
3	8.67	Out of phase longitudinal edges bending
4	10.59	In phase lateral edges bending
5	10.94	In phase longitudinal edges bending
6	12.78	Out of phase lateral edges bending
7	15.13	Out of phase longitudinal edges bending
8	17.86	Out of phase longitudinal edges bending
9	22.31	In phase longitudinal edges bending
10	24.30	Out of phase longitudinal edges bending

For ease of comparison, the three shock loading curves are made to have the same peak value of 1500 N and a short duration of 0.15 second. The first ten modal frequencies have been determined by FE analysis and they are summarised in Table 1.

The mobile platform under consideration has a first natural frequency of 3.82 Hz and the fundamental frequency of the excitation force harmonics is 3.98 Hz. All the natural modes of vibrations are excited by all harmonic components of the excitation forces. The amplitude of each harmonic component is determined by means of Fourier expansion and the results for each of the three cases of loading are compared in Figure 3.

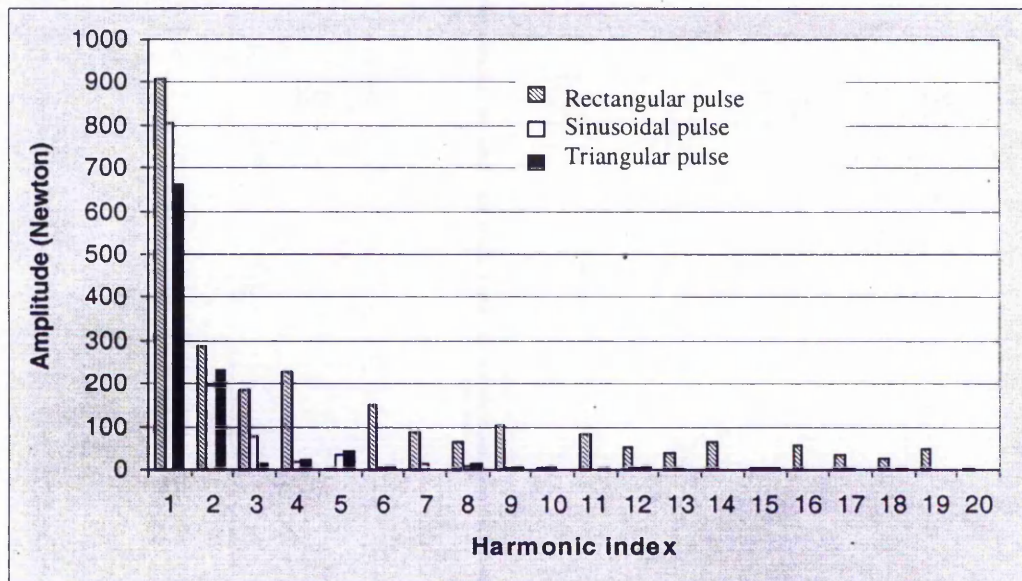


Figure (3). Comparison of amplitudes of excitation forces for the three profiles considered.

The modal dynamic loads can be computed by using Equation (9) for each form of loading. The most critical dynamic loading occurs when any of the harmonic frequencies of the excitation force is close to any of the natural frequencies. Figure 4 shows a detailed analysis of the dynamic forces produced by the first four harmonics of the excitation forces for the three forms of shock loading. It can be seen that the WMR experiences the highest level of dynamic forces in the first harmonic, with the rectangular pulse producing the highest dynamic loading of nearly 7.1 times the peak value of the shock pulse of 1500N (Figure 2). This is followed by the sinusoidal loading at about 6.3 times and the triangular pulse at about 5.2 times.

The general trend of the computed results is in agreement with the expectation that as the amount of work done by the excitation force increases, the level of dynamic loading on the structure also increases. The work done on the system by a particular form of shock loading is proportional to the area under the corresponding loading curve in Figure 2. The time domain analysis as computed by the FE package LSDyna® is provided in Figure 5. The rectangular shock loading is seen to generate the highest acceleration when compared to the sinusoidal and triangular loads.

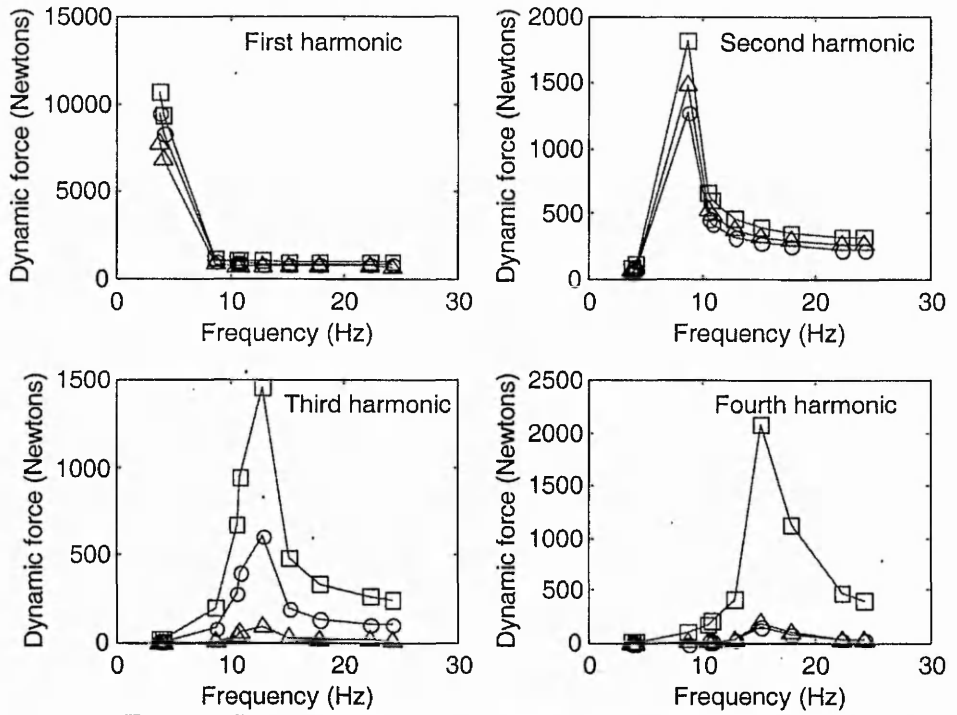


Figure (4). Dynamic loads produced by the first four harmonics.

- Response due to rectangular pulse
- △ Response due to triangular pulse.
- Response due to sinusoidal pulse.

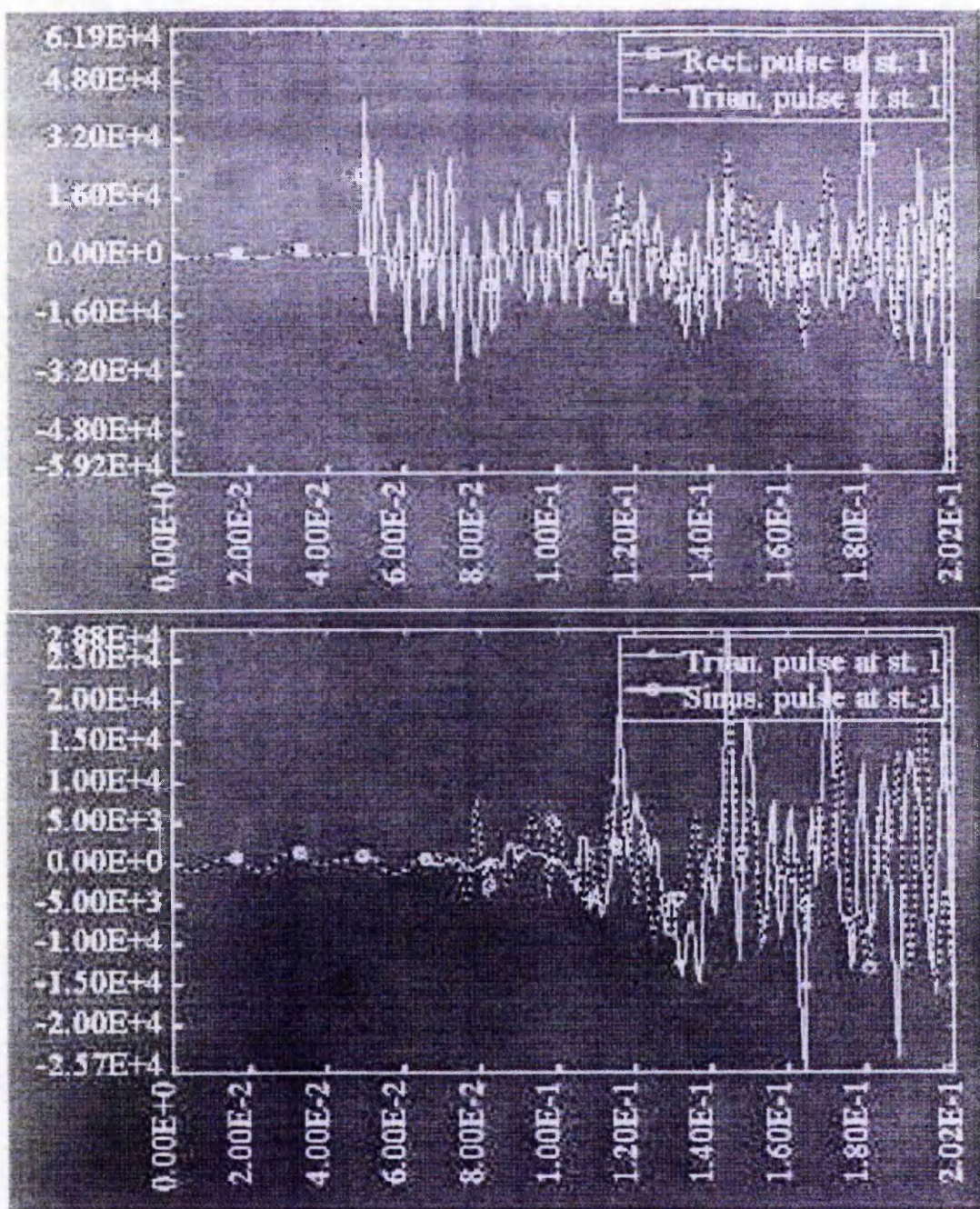


Figure (5) Comparison of acceleration responses at station 1 (Figure 1)

- a) rectangular (solid curve) and triangular (dotted curve) excitations.
- b) triangular(solid curve) and sinusoidal (dotted curve) excitations

CONCLUSIONS

The shock response analysis of a WMR subjected to sudden excitation loads has been carried out. Three different forms of shock loading, namely rectangular, sinusoidal and triangular pulse have been considered and their corresponding modal dynamic forces have been computed. The highest level of dynamic loading has occurred in the rectangular loading followed by the sinusoidal and triangular loading. The results highlight the need for using wheel materials that can attenuate the shock loading before transferring it to the vehicle's structure.

REFERENCES:

- 1 Control of suspensions for vehicles with flexible bodies-Part 1: active suspensions. A Hac, I. Youn and H. H. Chen, Transactions of ASME, Journal of Dynamic Systems, Measurement and Control, Vol. 118, 1996.
- 2 A four-wheeled robot to pass over steps by changing running control modes. O. Matsumoto, S. Kajita, K. Tani, M. Oooto, IEEE International conference on Robotics and automation, 1995.
- 3 Stochastic vibration of a mobile manipulator. U. O. Akpan, M. R. Kujath. Journal of applied mechanics. Vol. 64, No.3, 1997.
- 4 Stability of frictional contact in constrained rigid-body dynamics. P. E. Dupont, S. P. Yamajako. IEEE Transactions on Robotics and Automation, Vol. 13, No. 2, 1997.
- 5 Finite element procedures in engineering analysis. Klaus-Jürgen Bathe. Englewood Cliffs, London, Prentice-Hall, 1982.

Dynamic response of a Wheeled Mobile Robot navigating on an uneven surface

A. Ayalew and E. Lai

The Nottingham Trent University, Department of Mechanical Engineering, Nottingham.

S. O. Oyadji

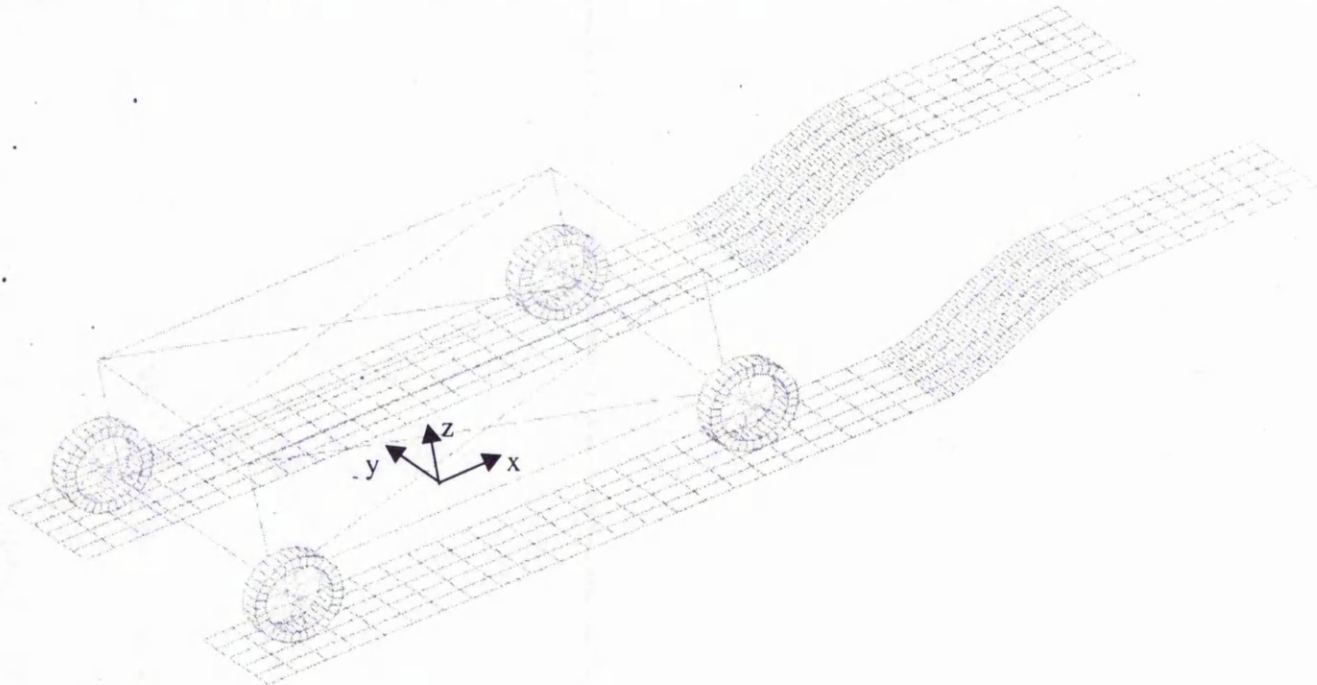
University of Manchester, School of Engineering, Manchester.

ABSTRACT: This paper presents a modeling and simulation technique for analyzing the dynamic behavior of a wheeled mobile robot navigating on an irregular terrain. Particular attention is given to the analysis of the vehicle jerk, as this quantity provides a measure of the payload stability and the smoothness of the vehicle's handling control. The results show that the jerk response of a robotic vehicle may be minimized by regulating the traction forces applied to its wheels. A parametric study has also been carried out to examine the variation of the ideal traction force needed to drive the vehicle over an obstacle with minimum jerk.

1 INTRODUCTION

Many wheeled mobile robot (WMR) control researchers have developed robot control schemes based on kinematic models (Alexander and Madocks, 1989, Muir and Neuman, 1987). However, in the past few years there has been more interest in developing dynamics based control schemes because of their robustness in comparison to kinematic based control techniques. Using a more realistic representation of tyre characteristics, Boyden and

Velinsky (1994) have modelled the dynamics of a three-wheeled mobile robot for high load applications. By observing the lateral drift from the intended trajectory of a kinematically controlled vehicle, this work has demonstrated the importance of vehicle dynamics on the directional accuracy when manoeuvring heavily loaded mobile robots. An experimental investigation of the dynamic behaviour of a WMR moving on a flat terrain was conducted by Mehrabi and Hemami (1993). The work was based on the assumption that the terrain



Figure(1) Coordinate system definition. xyz is the body attached coordinate system.

was smooth so that any surface irregularities could be neglected.

Some consideration has been given to the behaviour of WMRs traversing uneven terrain, but the work is mainly concerned with path planning. Shiller and Gwo (1991) proposed a highly simplified dynamic model in which the vehicle was considered as a point mass with zero moment of inertia. Criteria for stable manoeuvre of a WMR on uneven terrain have been suggested, these include satisfying the following constraints: engine-torque, wheel-ground contact, vehicle sliding and tip-over.

The present study investigates the wheel-ground interaction of a conventionally steered four-wheel WMR navigating on an uneven surface. The generalised equations of motion of the vehicle are derived with respect to the longitudinal, lateral and normal directions. A special case of the wheels of the vehicle encountering a road irregularity while travelling on a straight trajectory is then considered. Particular attention is given to the analysis of the vehicle jerk, as this quantity provides a measure of the stability of the payloads as well as the smoothness of the vehicle's handling control. The jerk response of the vehicle is computed by taking into account the motion of its centre of mass as well as its pitching motion. The results thus obtained permit a suggestion to be made on how the vehicle's jerk response may be minimised through the regulation of the traction forces applied to its wheels. The results may also be used in the development of traction control systems such as those developed in Burg and Blazevic (1997), and Hori et al (1998). Since the vehicle's jerk response is dependent on the geometry of the obstacle, as well as the dimensions and speed of the vehicle, a parametric study is also conducted to examine the variation of the ideal traction force needed to drive the vehicle over an obstacle with minimum jerk.

2 MATHEMATICAL MODELLING.

In general, a wheeled mobile robot taken as a single rigid body, has six degrees of freedom of motion: three translational and three rotational. It is assumed that the inertia and masses of the wheels are very small relative to the inertia and mass of the robotic vehicle. For convenience, a reference coordinate system is attached to the vehicle so that its origin is coincided with the centre of mass of the vehicle (Figure 1). The longitudinal direction of the vehicle is parallel to the x-axis, the lateral direction to the y-axis and the normal direction to the z-axis. Assuming all the wheels are in contact with the ground, the equations of motion of the vehicle are given by:

$$\sum \vec{F}_w + \sum \vec{F}_e = M * \vec{a}_c \quad (1)$$

$$\sum \vec{M}_w + \sum \vec{M}_e = I * \vec{\alpha} \quad (2)$$

where $\sum \vec{F}_w$ and $\sum \vec{F}_e$ are respectively the vector sums of wheel forces and external forces (i.e. gravity etc.). $\sum \vec{M}_w$ and $\sum \vec{M}_e$ are the corresponding moments produced by the wheel and external forces. \vec{a}_c is the acceleration at the centre of mass and $\vec{\alpha}$ is the angular acceleration of the vehicle about the reference coordinate system.

There are three orthogonal forces acting on a wheel: the traction force \vec{F}_a , the lateral force \vec{F}_l and the reaction force \vec{F}_n (Figure 2). The lateral force is a function of the normal force \vec{F}_n , where $\vec{F}_l = \mu_l \vec{F}_n$ (Guntur and Sankar, 1980). The resultant force acting on a wheel, by ignoring the wheel rolling resistance, is given by:

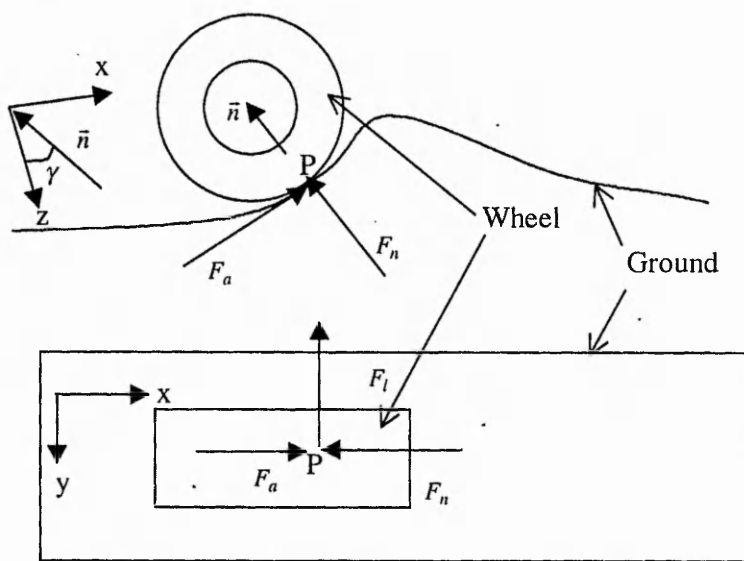


Figure (2) Geometry of wheel-ground contact and definitions of wheel forces.

$$\bar{F}_w = \begin{bmatrix} \cos(\gamma)\cos(\delta) \\ \cos(\gamma)\sin(\delta) \\ \sin(\gamma) \end{bmatrix} F_{tr} + \begin{bmatrix} \mu_l \sin(\delta) - \sin(\gamma)\cos(\delta) \\ -\mu_l \cos(\delta) - \sin(\gamma)\sin(\delta) \\ -\mu_r \sin(\gamma) + \cos(\gamma) \end{bmatrix} F_n \quad (3)$$

where δ is the steering angle of the wheel, μ_l is the coefficient of lateral friction, and γ is the profile angle of the road surface at the point of contact between the wheel and the ground. If the body force is the only external force, then

$$\bar{F}_e = \bar{C}_g W \quad (4)$$

where W is the weight of the vehicle and \bar{C}_g is the vector which projects the gravitational force into the body-attached coordinate system.

Since the reaction force \bar{F}_n is normally unknown quantity, it should be solved along with the translational and rotational accelerations \bar{a}_c and $\bar{\alpha}$. To form a closure model, additional equations are needed. These can be obtained by noting that, at the wheel-ground contact point, the normal component of the acceleration must be zero. Hence,

$$a_{pn} = \bar{a}_p \cdot \bar{n} = 0 \quad (5)$$

$$\text{and } \bar{a}_p = \bar{a}_c + \bar{\omega} \times \bar{\omega} \times \bar{r}_{p/c} + \bar{\alpha} \times \bar{r}_{p/c} \quad (6)$$

The normal vector \bar{n} at the contact point P (Figure 2) is a function of the surface profile and the orientation of the vehicle relative to the terrain. An assumption is made that the geometry of the surface profile can be measured relative to the position of the vehicle.

Now the acceleration \bar{a}_p at the wheel-ground contact point (Equation 6) can be determined by solving Equations 1-4. It can be shown that this acceleration is a function of the traction force \bar{F}_{tr} , the normal force, \bar{F}_n , the angular velocity of the vehicle $\bar{\omega}$ and the profile angle γ . That is,

$$\bar{a}_p = \bar{f}(\bar{F}_{tr}, \bar{F}_n, \bar{\omega}, \gamma)$$

Since $\bar{n} = \bar{n}(\gamma, \bar{\phi})$, Equation 5 can be written as

$$a_{pn} = \bar{a}_p \cdot \bar{n} = g(\bar{F}_{tr}, \bar{F}_n, \bar{\omega}, \gamma, \bar{\phi}) = 0 \quad (7)$$

where $\bar{\phi}$ is a vector of angles (such as Euler's angles), which describes the orientation of the vehicle with respect to the line of action of the gravitational force.

The normal reaction \bar{F}_n at the wheel-ground contact point can be determined from Equation 7, providing the following information is available: the rotational velocity of the vehicle, $\bar{\omega}$; the road profile angles γ ; the orientation of the vehicle relative to the normal

direction and the traction force, \bar{F}_{tr} . Let the solution of Equation 7 be given by:

$$F_n = h(\bar{F}_{tr}, \bar{\omega}, \gamma, \bar{\phi}) \quad (8)$$

Substituting Equation 8 into Equations 1 and 2 allows the accelerations \bar{a}_c and $\bar{\alpha}$ to be determined. Thus,

$$\bar{a}_c = \bar{a}_c(\bar{F}_{tr}, \bar{\omega}, \gamma, \bar{\phi}) \quad (9)$$

$$\bar{\alpha} = \bar{\alpha}(\bar{F}_{tr}, \bar{\omega}, \gamma, \bar{\phi}) \quad (10)$$

The jerk of the centre of mass of the vehicle can be obtained by differentiating Equation 9 with respect to time, that is

$$\begin{aligned} \bar{J}_c = \frac{d}{dt} \bar{a}_c(\bar{F}_{tr}, \bar{\omega}, \gamma, \bar{\phi}) &= \frac{\partial \bar{a}_c}{\partial \bar{F}_{tr}} \frac{d}{dt} \bar{F}_{tr} + \frac{\partial \bar{a}_c}{\partial \bar{\omega}} \frac{d}{dt} \bar{\omega} \\ &+ \frac{\partial \bar{a}_c}{\partial \gamma} \frac{d}{dt} \gamma + \frac{\partial \bar{a}_c}{\partial \bar{\phi}} \frac{d}{dt} \bar{\phi} \end{aligned} \quad (11)$$

Similarly, the jerk due to the pitch angular motion is given by:

$$\begin{aligned} \bar{J}_\alpha = \frac{d}{dt} \bar{\alpha}(\bar{F}_{tr}, \bar{\omega}, \gamma, \bar{\phi}) &= \frac{\partial \bar{\alpha}}{\partial \bar{F}_{tr}} \frac{d}{dt} \bar{F}_{tr} + \frac{\partial \bar{\alpha}}{\partial \bar{\omega}} \frac{d}{dt} \bar{\omega} \\ &+ \frac{\partial \bar{\alpha}}{\partial \gamma} \frac{d}{dt} \gamma + \frac{\partial \bar{\alpha}}{\partial \bar{\phi}} \frac{d}{dt} \bar{\phi} \end{aligned} \quad (12)$$

3 A VEHICLE ON A STRAIGHT TRAJECTORY

3.1 Computation of Traction Force-Profile Angle-Jerk Dependency

The dynamic model described above is applied to the analysis of a wheeled mobile robot traversing a road obstacle while travelling on a straight trajectory (when viewed from the top). The steering angles δ of all the wheels in Equation (3) are equal to zero. As there is no lateral motion the lateral friction coefficient is also equal to zero (Guntur and Sankar, 1980). Thus Equation (3) simplifies to:

$$\bar{F}_w = \begin{bmatrix} F_{wx} \\ F_{wy} \\ F_{wz} \end{bmatrix} = \begin{bmatrix} \cos(\gamma) \\ 0 \\ \sin(\gamma) \end{bmatrix} F_{tr} + \begin{bmatrix} -\sin(\gamma) \\ 0 \\ \cos(\gamma) \end{bmatrix} F_n \quad (13)$$

The accelerations and the jerk response of the vehicle can be determined analytically by solving Equations 9-12. The resulting mathematical expressions are rather lengthy to be produced here. From these expressions the jerk response of the platform, which is of most interest, was computed

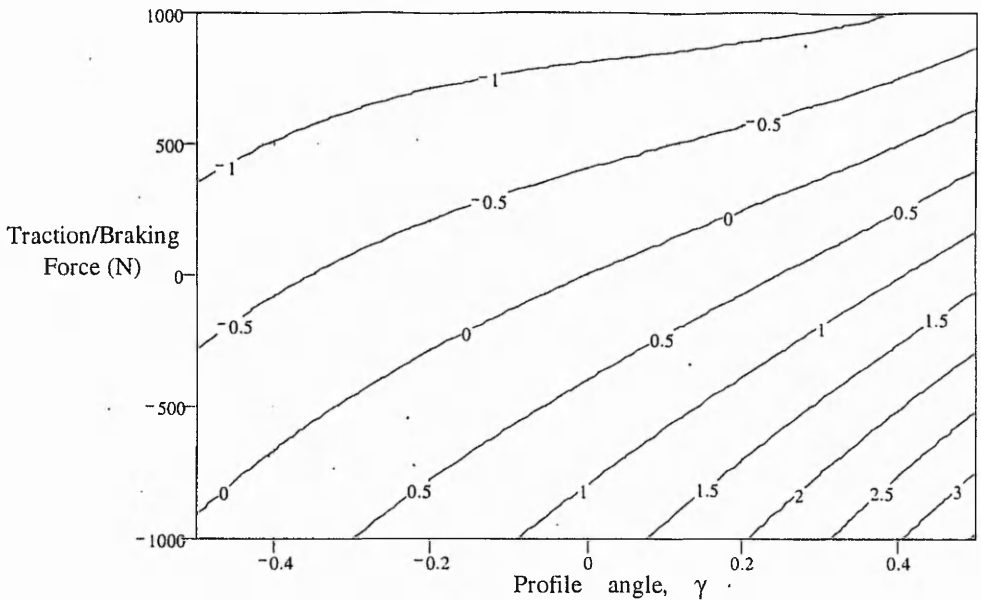


Figure (3) Contour plot of normal jerk of vehicle driven/braked by rear wheels

under the MATHCAD programming environment. The dimensions and properties of the mobile robot used in the computation are as follows.

Vehicle mass	120 kg
Vehicle pitch moment of inertia	40 kg·m ²
Vehicle longitudinal speed	2.0 m/s
Height of centre of mass	0.27 m
Front axle distance from centre of mass	0.8 m
Rear axle distance from centre of mass	1.0 m

The traction forces required to produce normal jerks of the platform within the range -1.0 m/s^3 to 3.0 m/s^3 for profile angles within the range of -0.5 radian to 0.5 radian were computed. The results are displayed as a contour plot in Figure 3. The results also show that the traction force needed to eliminate normal jerk can be either positive or negative. Negative traction forces imply braking forces (for negative profile angles).

3.2 Variation of Traction force with vehicle properties

The idealised traction force required to minimise the jerk depends not only on the surface profile angle but also on the vehicle speed and other geometric parameters of the vehicle including the axle length, height of the centre of mass, mass and pitch moment of inertia. The effects of these parameters on the requirements of the idealised traction force needed to maintain minimum jerk have also been investigated for a profile angle of 17° and the results are shown in Figure 4.

Comparison of Figure 4a and 4b suggests that a better load distribution (one that would require less

traction force to minimise normal jerk) can be achieved by positioning the centre of mass as close as possible to the rear axle. It is worth noting that this observation is applicable only for positive gradient profiles. Furthermore, the lower the height of the centre of mass of a vehicle, the smaller is the requirement of the idealised traction force (Figure 4c). The ideal traction force varies relatively little with the value of pitch moment of inertia (Figure 4e). Figure 4f shows the dependency of the ideal traction force on the velocity of the platform, where it decreases slightly until it reaches a minimum and increases monotonously afterwards.

3.3 Comparison of Jerk Responses

From Figure 3, the traction force required for jerk-free motion for an obstacle profile angle of 17° (0.3 rad.) is approximately 380 N. This traction force was used in LS DYNAm, an independent dynamic simulation package, in order to simulate the jerk response of the vehicle and thereby check that this traction force indeed gives a jerk-free motion. The simulated jerk response over a time period of 0.4 s is shown in Figure 5. It is clearly seen that the ideal traction force of about 380 N does indeed provide an almost jerk-free motion. The figure also shows that when the traction force is greater or less than this ideal value, the jerk response of the vehicle is considerable.

4 CONCLUSION

In this study, a mathematical model has been developed for analysing the dynamic response of a wheeled mobile robot navigating on an uneven terrain. By considering the interaction of the forces at the wheel-ground contact point in conjunction

with a known surface profile, the jerk response of the vehicle has been determined for a range of conditions. Knowledge of the vehicle jerk response allows an assessment to be made of the stability of the payload and the smoothness of the vehicle's handling control. The methodology has been applied to a simple case of a rear-wheel driven vehicle

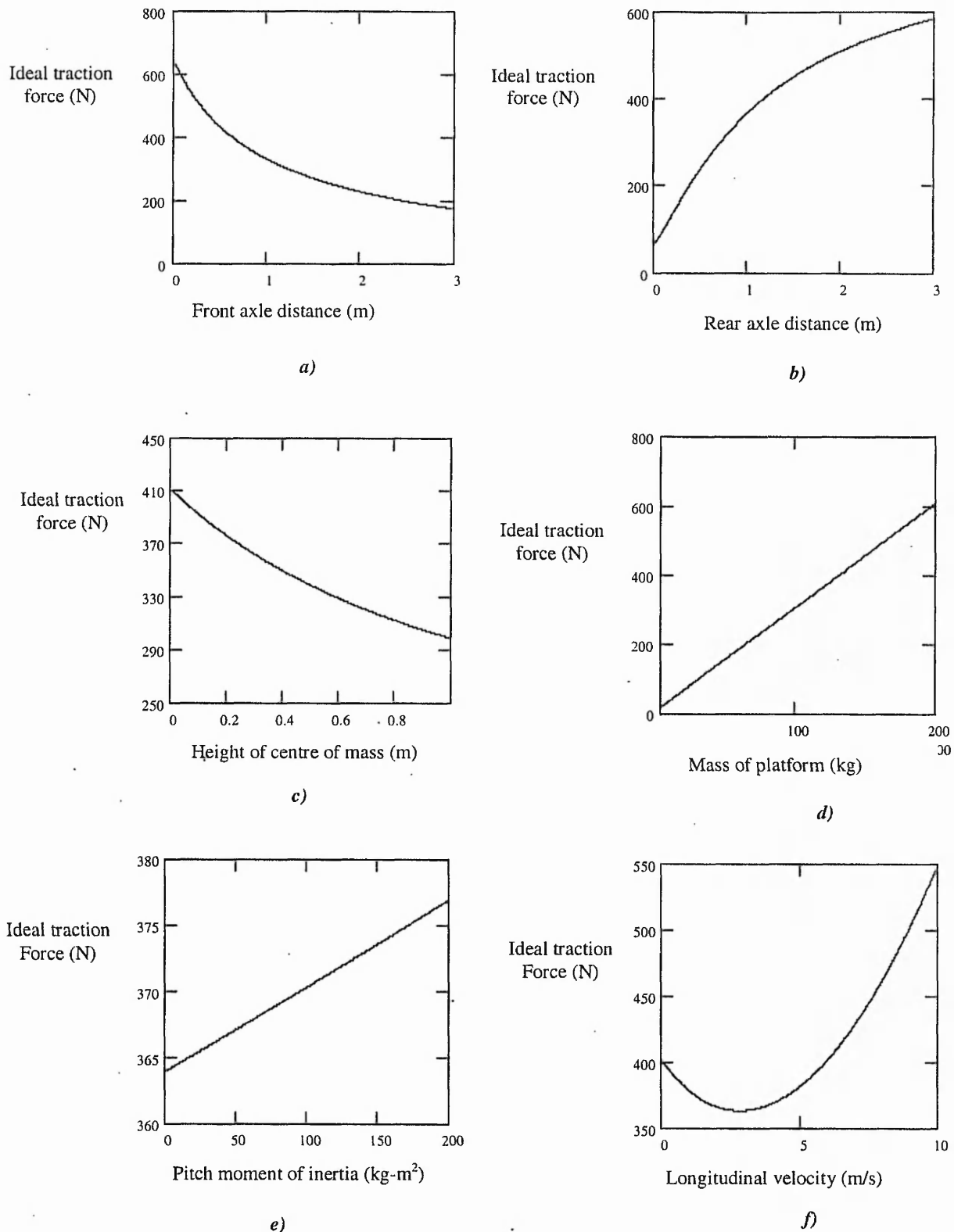


Figure (4) Dependence of the ideal traction force needed for a zero normal jerk motion, with respect to vehicle dimensions and speed.

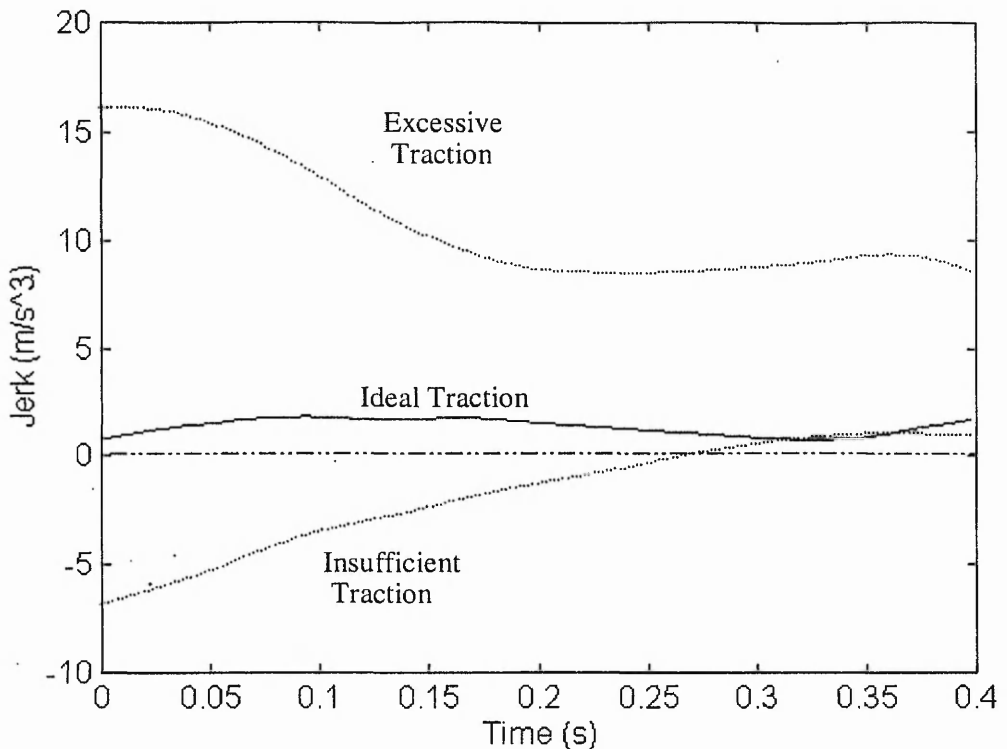


Figure 5 Comparison of jerk responses for three levels of applied traction force: Insufficient, Ideal and Excessive traction Forces

traversing front wheel obstacles. Simulation results show that it may be possible to minimise the vehicle jerk by regulating the traction forces supplied to the wheels. However, the ideal traction force for minimum jerk is also found to be dependent on other parameters including velocity speed and properties of the vehicle. The results presented here may be used in the development of traction control systems for robotic vehicles.

Mehrabi, M. G., Cheng, R.M.H. and Hemami, A., 1993, "Dynamic Modelling of Wheeled Mobile Robots Theory and Experiment," *Second IEEE Conference on Control Applications*, Vancouver, pp. 659-665.

Muir, Patrick F and Neuman, Charles P. Kinematic Modelling of Wheeled Mobile Robots *Journal of Robotic Systems*, 1987, Volume (4), pp. 281-340

Shiller, Z., and Gwo, Y., 1991, "Dynamic Motion Planning of Autonomous Vehicles," *IEEE Transactions on Robotics and Automation*, pp. 241-249.

REFERENCES

- Alexander, J. C., and Maddocks, J. H., 1989, "On The Kinematics of Wheeled Mobile Robots," *The International Journal of Robotics Research*. Vol. 8, No. 5.
- Boyden, F. Demick and Velinsky, A Steven Dynamic Modelling of Wheeled Mobile Robots for High Load Applications, Proceedings - IEEE International Conference on Robotics and Automation, 1994, No.pt 4, pp.3071-3078
- Burg, Jan van der and Blazevic, Pierre, Anti-lock braking and traction control concept for all-terrain robotic vehicle. Proceedings - IEEE International Conference on Robotics and Automation, 1997, Vol.2, pp.1400-1405
- Guntur, R. and Sankar, S; "A friction circle concept for Dugoff's tyre friction model", International Journal of Vehicle Design, vol 1 no 4, 1980.
- Hori, Yoichi , Yasushi, Toyoda and Tsuruoka, Yoshimasa, Traction Control of Electric Vehicle: Basic Experimental Results Using the Test EV "UOT Electric March", *IEEE Transactions on Industry Applications*, Sep-Oct 1998, Vol.34, No.5, pp. 1131-1138

DETC99/VIB-8243

MINIMUM JERK TRACTION CONTROL OF A WHEELED MOBILE ROBOT MOVING OVER A HUMP

A. Ayalew , E. Lai*
Dept. of Mech. & Manuf. Eng.
The Nottingham Trent University
Nottingham, NG1 4BU
England
Fax:+44-115-9486506
E-mail: eugene.lai@ntu.ac.uk

S. O. Oyadji
School of Engineering
The University of Manchester
Manchester, M13 9PL
England
Fax:+44-161-2754346
E-mail: sooyadji@fs1.eng.man.ac.uk

ABSTRACT

A new technique is presented for the minimization of jerk for wheeled mobile robots (WMRs) traveling on uneven terrain. A robot may jerk as it traverses a road obstacle. Consequently, wheel-ground contact loss is one of the undesirable dynamic effects that can cause loss of control and robot instability. By considering the dynamics of the robot with respect to the longitudinal, pitching and vertical motions of the platform, the new technique calculates the dynamic compensation needed to ideally counter the onset of jerk by controlling the magnitude of the input drive torque to the wheels. Simulation results showed that the technique has the potential to substantially reduce the magnitude of jerk of a WMR during longitudinal maneuver over a road obstacle with a positive gradient.

Keywords: Traction control, mobile robots, jerk, dynamics.

1 INTRODUCTION

In the past decade, progress has been made in the development of motion control techniques for wheeled mobile robots (WMRs) maneuvering on smooth terrain. Kinematic- and dynamic-based control methodologies have been proposed and implemented for indoor applications of WMRs (Deng and Brady, 1993, Mehrabi, et. al (1993), Alexander and Maddocks, 1989). Most of the existing models are often based on two key assumptions, namely, (i) the wheels of a robot are in permanent contact with the road surface, and (ii) the terrain is smooth. However, in a real industrial environment, wheeled robots will encounter surface irregularities such as bumps and cracks. Consequently, a wheeled robot may jerk and wheel-ground contact loss is one of the undesirable dynamic effects that can cause loss of control. This arises because a non-contacting wheel

* To whom all correspondences should be sent.

can not generate either steering or traction forces. Furthermore, the stability of the payload on the robot's platform is another concern.

Consideration has been given to the dynamic behavior of a vehicle moving on uneven terrain with respect to path planning. Siméon (1991) studied the geometry of a three-wheel mobile robot and its kinematic constraint in order to plan trajectories on a three-dimensional, terrain represented by polygonal patches. The proposed method is based on the hypothesis that the platform of the robot is deemed to be stable when the line of action of its gravitational force intersects a polygon determined from knowledge of the wheel contact points. Hait and Siméon (1996) considered the motion planning of an articulated vehicle composed of three axles connected to the chassis by joints allowing roll and pitch movements. In an extension of an earlier work Siméon and Dacre-Wright (1993) developed a new method to examine the computed road paths and, where appropriate, to devise a new trajectory in order to avoid wheel-terrain collision that might result in the vehicle's body coming into contact with the rough terrain. Although the approach considered the likelihood of wheel-terrain collision in the path planning criteria, no account was taken of the consequential dynamic effects on the vehicle.

A traction-force prediction scheme for navigating wheeled robots over rough terrain was proposed by Ben Amar, et al. (1993), based on the assumption of non-slip wheels. The scheme considered the interaction between the wheels and the ground, taking into account the vehicle kinematics and terrain geometry. A method for planning the motions of autonomous vehicles moving on general terrain was presented by Shiller and Gwo (1991). The method is based on a highly simplified dynamic model of the vehicle, where it is reduced to a point mass and all moments of inertia are ignored. However, a number of factors were considered in the model including vehicle dynamics, terrain topography, obstacles and surface mobility.

No previous work on wheeled mobile robots, to the best of our knowledge, has addressed the issues pertaining to (i) dynamic stability with respect

to the maintenance of wheel-ground contact and, (ii) payload stability on rigid robot platforms travelling over rough terrain. Whether the wheel and the ground should remain in contact during motion depends on the acceleration at the contact points (Baraff, 1993, Featherstone, 1987). Dynamic constraint requires that for wheel-ground contact to be maintained continuously, not only the normal contact point accelerations should be zero (Fig. 2.), but their rate of change (i.e. jerk) must also be zero. Thus, if the normal acceleration has a value greater than zero at any time t then contact is lost immediately afterwards. It should be noted that this acceleration can never be less than zero for rigid bodies, as this would imply that the wheel has penetrated the road surface or vice versa. For our analysis, an assumption has been made that both the wheel and the road surface are rigid. Furthermore, the normal accelerations are functions of the road surface geometry, the angular and translational velocities and accelerations of the vehicle. Another issue of concern relates to the stability of the payload on the platform of a wheeled robot moving over rough terrain.

Both issues, wheel-ground contact and payload stability, can be addressed simultaneously for road obstacles having a small dimension relative to the size of the vehicle (in terms of its length and height of the centre of mass). For a large vehicle passing over a relatively small obstacle, the problem of jerk minimisation at all points can be conveniently considered as a problem of jerk minimisation at the centre of mass.

NOMENCLATURE

F_a	traction force
F_n	normal reaction force
\tilde{F}_w	resultant wheel force
I	moment of inertia
I_y	pitch moment of inertia
\tilde{J}	jerk
M_y	pitching moment
R_x, R_y	axle forces
\tilde{a}	acceleration

k	index
m	mass
\tilde{r}	position vector
r_w	wheel radius
v_x, v_z	translational velocities
x, y, z	coordinates
$\tilde{\alpha}$	angular acceleration
α_y	pitch angular acceleration
δ	steering angle
μ_l	coefficient of lateral friction
μ_r	coefficient of rolling resistance
γ	road profile gradient angle
$\tilde{\omega}$	angular velocity
ω_y	pitch angular velocity

2 MODELLING

Consider a four-wheeled rigid robotic vehicle initially travelling along a straight path (Fig. 1.). Two coordinate systems can be used for the analysis of the vehicle's motion, namely, a fixed (inertial) coordinate system in space or a moving (non-inertial) system attached to the vehicle. In the present study it is considered more appropriate to analyse the vehicle's motion using a moving, non-inertial, coordinate system. This is because the relative motion rather than the absolute motion of the vehicle is of interest. The aim is to maintain a zero jerk motion of the vehicle so that an observer travelling with the vehicle experiences no jerk. Thus, a set of orthogonal axes is defined at the vehicle's centre-of-mass such that the x -axis is along the direction of travel of the vehicle (i.e. the longitudinal direction). At time t , the wheels (front or rear) of the vehicle traverse a laterally symmetrical road obstacle (hump) with a positive

gradient. As a result, it is subjected to a three-degree-of-freedom motion: pitching motion about the lateral (y) axis; vertical translational motion due to the road obstacle; and longitudinal motion in the direction of travel.

The equations of motion based on the vehicle's coordinate system are given by:

$$\left. \begin{aligned} \sum F_x &= m(\dot{v}_x + v_z \omega_y) \\ \sum F_z &= m(\dot{v}_z - v_x \omega_y) \\ \sum M_y &= I_y \alpha_y \end{aligned} \right\} \quad (1)$$

where m is the mass and I_y is the pitch moment of inertia of the vehicle; v_x and v_z are respectively the longitudinal and the vertical velocities; ω_y is the pitch angular velocity and α_y is the pitch angular acceleration of the platform. It should be noted that the $v^* \omega$ terms arise as a consequence of using a coordinate system attached to the vehicle (D'Souza, and Garg, 1984).

The resultant force \tilde{F}_{wk} acting on the wheel k at the wheel-ground contact point can be written as (Fig. 2.):

$$\tilde{F}_{wk} = \tilde{A}_k F_{ak} + \tilde{N}_k F_{nk} \quad (2)$$

where F_{ak} and F_{nk} are respectively the magnitudes of the traction and normal reaction forces at the wheel. The coefficient vectors \tilde{A}_k and \tilde{N}_k are given by:

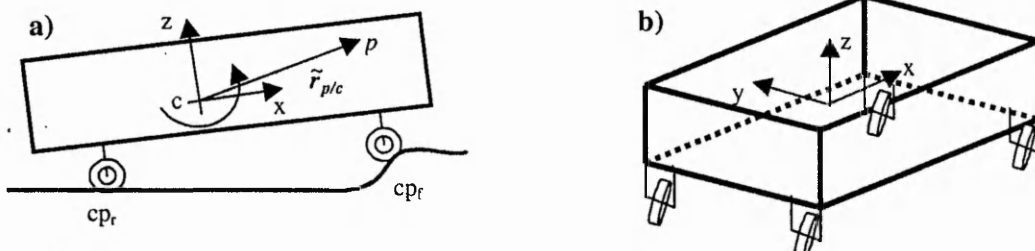


Figure 1. a) The three active degrees of freedom when passing over a hump. **b)** Coordinate system definition.

$$\tilde{\mathbf{A}}_k = \begin{bmatrix} \cos(\gamma_k) \cos(\delta_k) \\ \cos(\gamma_k) \sin(\delta_k) \\ \sin(\gamma_k) \end{bmatrix},$$

$$\tilde{\mathbf{N}}_k = \begin{bmatrix} -\mu_{rk} \cos(\gamma_k) \cos(\delta_k) + \mu_{lk} \sin(\delta_k) - \sin(\gamma_k) \cos(\delta_k) \\ -\mu_{rk} \cos(\gamma_k) \sin(\delta_k) - \mu_{lk} \cos(\delta_k) - \sin(\gamma_k) \sin(\delta_k) \\ -\mu_{rk} \sin(\gamma_k) + \cos(\gamma_k) \end{bmatrix}$$

μ_{lk} is the lateral friction coefficient, δ_k is the steering angle and μ_{rk} is the rolling resistance coefficient. γ_k is the angle that specifies the direction of the normal reaction force and it also defines the gradient of the ground profile at the point of contact. While Eq. (2). describes the contact forces for the general case of a steered wheel attached to a platform travelling along a curved trajectory in a three-dimensional space, simplification can be achieved by limiting the investigation to the case of a laterally symmetric surface and assuming that there is no lateral movement of the vehicle (i.e. $\delta_k = 0$). This assumption reduces the problem to one of a planar motion.

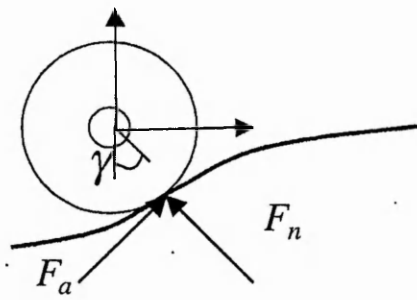


Figure 2. The geometry of wheel forces.

For an arbitrary point p on the vehicle platform (Fig. 1.), its instantaneous acceleration is given by:

$$\tilde{\mathbf{a}}_p = \tilde{\mathbf{a}}_c + \tilde{\boldsymbol{\omega}} \times (\tilde{\boldsymbol{\omega}} \times \tilde{\mathbf{r}}_{p/c}) + \tilde{\boldsymbol{\alpha}} \times \tilde{\mathbf{r}}_{p/c} \quad (3)$$

where $\tilde{\mathbf{r}}_{p/c}$ is the position of the point p relative to the center-of-mass c of the platform.

Two additional constraint equations can be derived by considering the normal components of the

accelerations of the front and rear wheel contact points, cp_f and cp_r (Fig. 1.), which must be zero. Thus,

$$\tilde{\mathbf{a}}_{cp_f} \cdot \tilde{\mathbf{n}}_f = 0 \text{ and } \tilde{\mathbf{a}}_{cp_r} \cdot \tilde{\mathbf{n}}_r = 0 \quad (4)$$

where $\tilde{\mathbf{n}}_f$ and $\tilde{\mathbf{n}}_r$ are the normals to the road profile at the wheel contact points. The normal wheel reaction forces, the acceleration $\tilde{\mathbf{a}}_c$ of the center-of-mass of the platform and the pitch angular acceleration α_y can be obtained by solving Eq. (1). – (4). simultaneously.

It can be seen that the rate of change of acceleration (jerk), $\tilde{\mathbf{J}}_p = \left(\frac{d\tilde{\mathbf{a}}_p}{dt} \right)$, at point p can be determined from the time derivative of Eq. (3). Thus, the jerk is comprised of three constituent parts, namely:

1. The rate of change of the center-of-mass acceleration ($\tilde{\mathbf{J}}_c = \frac{d}{dt} \tilde{\mathbf{a}}_c$),
2. The rate of change of the centrifugal acceleration ($\tilde{\mathbf{J}}_a = \frac{d}{dt} (\tilde{\boldsymbol{\omega}} \times (\tilde{\boldsymbol{\omega}} \times \tilde{\mathbf{r}}_{p/c}))$)
3. The rate of change of the tangential acceleration ($\tilde{\mathbf{J}}_\alpha = \frac{d}{dt} (\tilde{\boldsymbol{\alpha}} \times \tilde{\mathbf{r}}_{p/c})$).

For small surface irregularities, the pitch angular velocity and angular acceleration are usually very small. Consequently the contribution of the centrifugal acceleration term is negligible compared to the other two terms. Hence the problem of minimization of the total jerk can be reduced to one of minimizing the translational jerk at the center of mass and the pitch angular jerk of the platform. Since $\tilde{\mathbf{a}}_c$ and α_y are functions of the gradient of the road profile γ , the longitudinal velocity v_x and the vertical velocity v_z , the translational and pitch angular jerks are given by:

Translational jerk along x

$$J_{cx} = \frac{da_{cx}}{dt} = \frac{\partial a_{cx}}{\partial \gamma} \frac{d\gamma}{dt} + \frac{\partial a_{cx}}{\partial v_x} \frac{dv_x}{dt} + \frac{\partial a_{cx}}{\partial v_z} \frac{dv_z}{dt} \quad (5)$$

translational jerk along z

$$J_{cz} = \frac{da_{cz}}{dt} = \frac{\partial a_{cz}}{\partial \gamma} \frac{d\gamma}{dt} + \frac{\partial a_{cz}}{\partial v_x} \frac{dv_x}{dt} + \frac{\partial a_{cz}}{\partial v_z} \frac{dv_z}{dt} \quad (6)$$

pitch angular jerk

$$J_{ay} = \frac{d\alpha_y}{dt} = \frac{\partial \alpha_y}{\partial \gamma} \frac{d\gamma}{dt} + \frac{\partial \alpha_y}{\partial v_x} \frac{dv_x}{dt} + \frac{\partial \alpha_y}{\partial v_z} \frac{dv_z}{dt} \quad (7)$$

$$\text{and } \frac{d\gamma}{dt} = \frac{dy}{dx} \frac{dx}{dt} = \frac{dy}{dx} v_x \quad (8)$$

Since we are dealing with acceleration with respect to a non-inertial-frame-of reference $x-y-z$, the jerk being considered is one sensed by an observer translating as well as pitching with the vehicle. The term $\frac{dy}{dx}$ is the curvature of the road profile at the point of contact, which can be estimated for a continuous, smooth profile by differentiating the history of γ with respect to the longitudinal displacement x .

3 THEORETICAL ANALYSIS

As mentioned earlier, the jerk brought about by the vehicle traversing a hump with a positive gradient, as experienced by an observer travelling with the vehicle, depends mainly on two factors: the geometry of the road profile and the magnitude of the traction force. The idealised functional relationships between these parameters have been computed for the translational jerk (in the longitudinal and vertical directions) as well as the pitch angular jerk. Since the zero-jerk line in all three cases are found to have identical traces (i.e. coincidental), only the results for the longitudinal jerk are presented in the form of a contour plot in Fig. 3a. Figure 3b. shows the corresponding longitudinal acceleration. The dimensions, and the longitudinal velocity, of the vehicle are given in Section 4. The zero contour line in Fig. 3a. defines the conditions needed for an ideal jerk-free motion.

The usefulness of Fig. 3a. and Fig. 3b. for determining the total traction force needed to avoid the onset of jerk can be demonstrated by means of the following example. For convenience, the zero-jerk line and the zero-acceleration line are re-plotted in Fig. 4a. Consider an instance when the vehicle is required to traverse a surface whose profile gradient γ has a value of 0.2, an ideal total traction force of 160 N is needed to avoid the onset of longitudinal jerk. In this case, the total traction force is made up of two elements: a traction force at zero acceleration (approximately 70 N) and an additional traction force for compensating the jerk ($160N - 70N = 90N$).

As the value of γ can vary continuously, it follows that the total traction force required to maintain permanent wheel-ground contact must also vary accordingly. Furthermore, because of the identical zero-jerk trace for both translational jerk and pitch angular motion jerk, the results suggest that a single traction force applied to the wheels would help to ensure that the jerk in all motions is instantaneously zero.

The question on which pair of wheels (the rear or the front) should be used to generate the necessary traction force has also been investigated. Figure 4b. shows a comparison of the theoretical traction force needed for zero-jerk motions between front-wheel traction and rear-wheel traction, when the front wheels traverse a road obstacle. It can be seen that for moderate surface gradients (i.e. $\gamma < 0.2$), the choice is unimportant. However, for larger values of γ , front-wheel traction would be more preferable as lower traction forces are needed to achieve the same outcome. It is worth noting that similar results were obtained for the case of the rear wheels traversing the same road obstacle.

By considering the equilibrium of the wheels (axle) facing the obstacle, an expression for the angle γ can be derived based on knowledge of the axle forces as follows:

$$\gamma = 2 * \arctan \left[\frac{1}{R_x + F_a} \left(R_y \pm \sqrt{R_y^2 + R_x^2 - F_a^2} \right) \right] \quad (8)$$

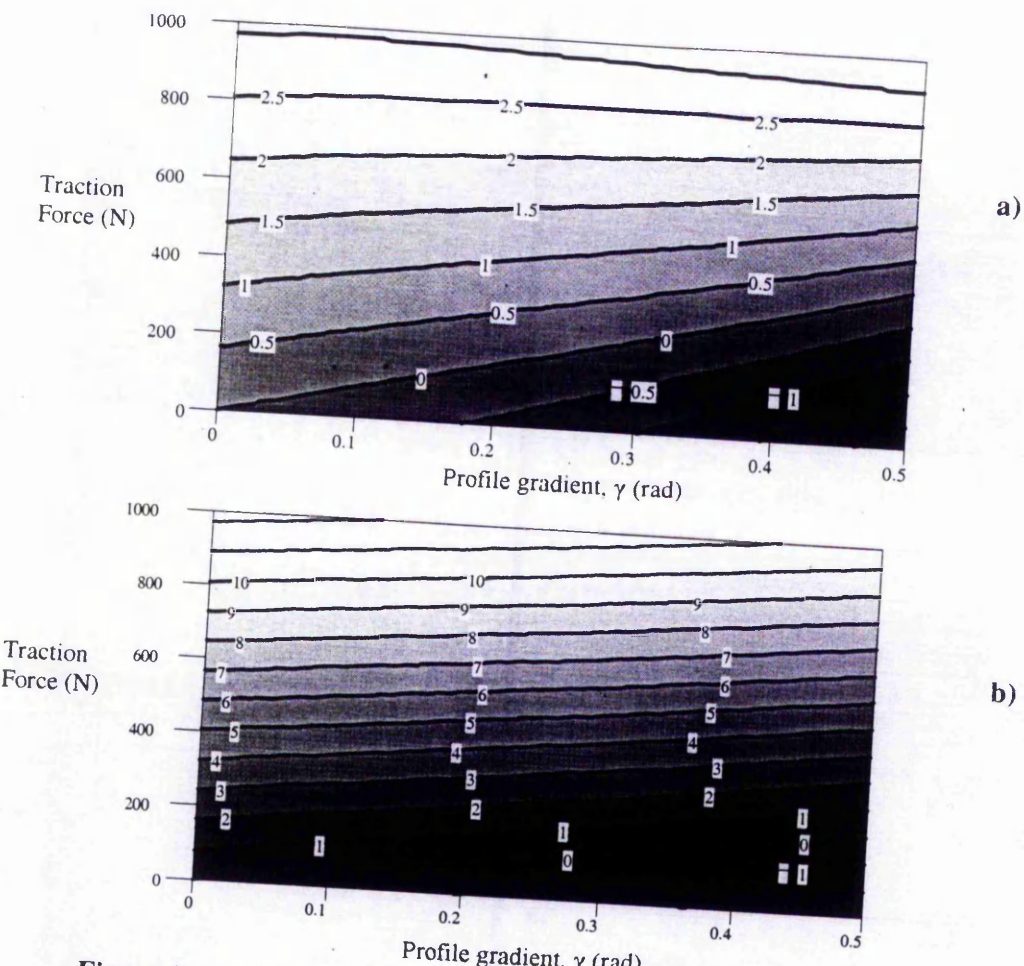


Figure 3. a) Contour plot of the longitudinal acceleration jerk. b) Contour plot of longitudinal acceleration.

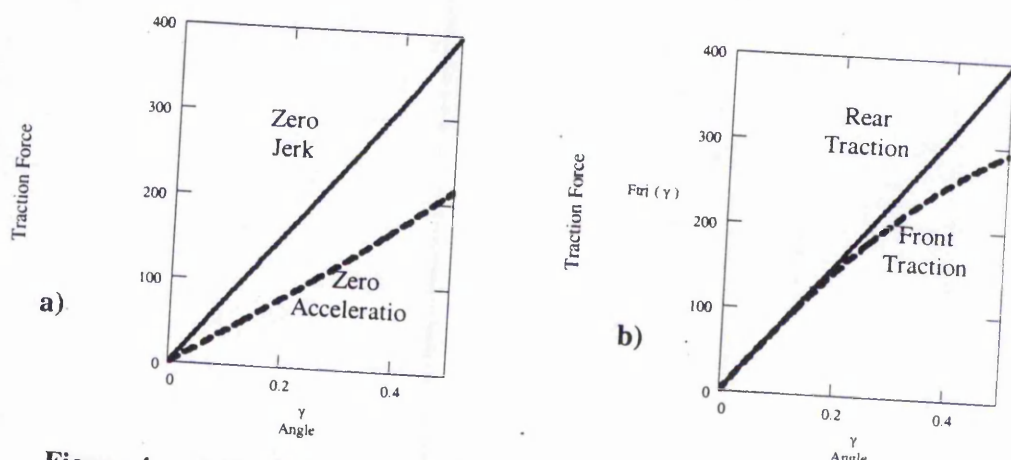


Figure 4. a) Conditions for zero jerk motion and zero longitudinal acceleration
b) Front and rear wheel traction for a zero jerk motion.

where R_x and R_y are respectively the longitudinal and vertical axle forces, which may be measured by suitable load cells; F_a is the corresponding traction force. The latter is the ratio of the driving torque to the radius of the wheels (assuming non-slip condition).

One way of utilizing the results of this work is to devise a scheme (Fig.5) for regulating the motor torque applied at the wheels in order to minimize the vehicle jerk. In this scheme, an ideal torque is calculated from Eqs. (5-7) using input values of vehicle mass, inertia, dimensions and velocity. Also needed is knowledge of the surface profile angle, which can be determined from Eq. (8) based on measurements of axle load and a feedback measure of the driving torque. The ideal torque is used as an input to the torque controller which in turn regulates the power supply to the motor and hence the driving torque.

4 A CASE STUDY

The effectiveness of the proposed technique for jerk minimization was assessed by means of a dynamical model of a four-wheeled mobile platform.

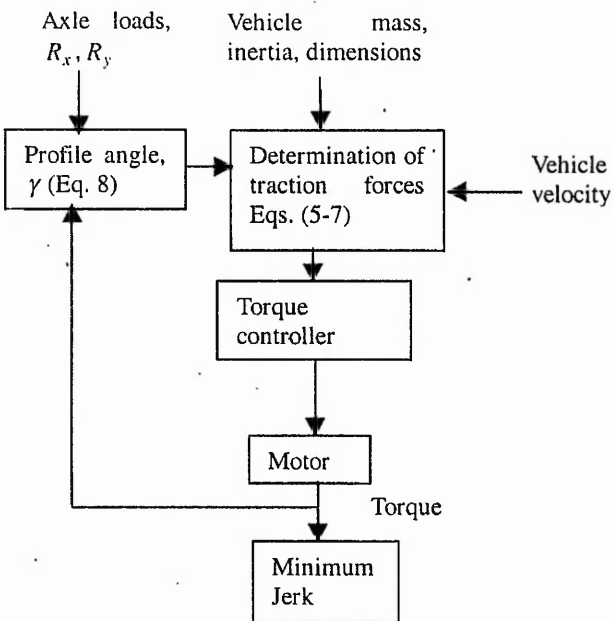


Figure 5 Implementation of the control scheme.

The model enables the dynamic response of the platform to be simulated for a specified surface profile condition. In particular, analysis of the interaction between a wheel and the road surface requires integration of the equations of motion. For this reason, simulation study was carried out using the program LS-DYNA (Livermore, 1997) as its computational environment can handle numerical integration relatively well. As a case study, the front wheels of the model vehicle were required to traverse a laterally symmetrical road obstacle in the form of a ramp having an elevation of 25 degrees from the horizontal. Rear-wheel traction was assumed. For illustrative purposes, only the longitudinal results are considered in the case study. The overall dimensions of the model and other parameters used in the numerical analysis are listed below.

Distance between front and rear axles, $L=2.4$ m;
Distance between front axle and center of mass, $L_r=1.2$ m;
Height of center of mass, $H=0.4$ m;
Wheel radius, $R=0.1$ m;
Total mass of vehicle, $m=80$ kg;
Pitch moment of inertia, $I_y=116$ kg-m²;
Longitudinal velocity of vehicle, $v_x=1$ m/s.

From the results of the theoretical analysis, an ideal traction force of 350 N was needed to avoid the onset of jerk when the mobile platform moved over the ramp. The time history of the nodal acceleration at the center-of-mass of the dynamical model was computed by using LS-DYNA for each of the following three traction forces applied at the wheels. The accelerations were then differentiated to determine the jerks.

1. A traction force of 200 N (i.e. insufficient traction force).
2. An ideal traction force of 350 N.
3. A traction force of 500 N (i.e. excessive traction force).

Figure 6. shows the longitudinal jerk response for the three levels of applied traction forces when $\gamma = 25^\circ$. Although the ideal traction condition should give a

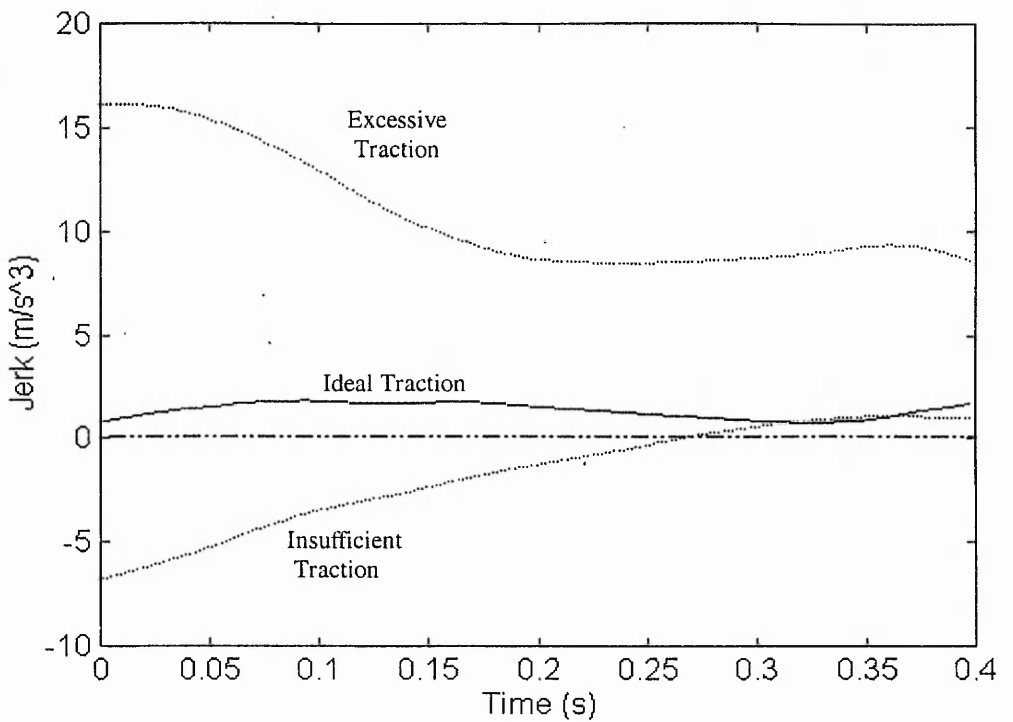


Figure 6 Comparison of jerk responses for three levels of applied traction force: Insufficient, Ideal and Excessive traction Forces

jerk response close to zero, numerical and modeling approximations in the dynamical model have resulted in deviations shown in the figure. However, the importance of jerk minimization by controlling the traction force applied at the wheels is clear. For excessive applied traction force, the vehicle exhibits a longitudinal jerk response while accelerating up the ramp. The opposite is also true for insufficient traction force.

5 CONCLUSIONS

A new technique has been presented for the minimisation of jerk for wheeled mobile robots travelling on uneven terrain. Central to this technique is a new dynamic model that allows the conditions for a theoretical zero-jerk motion to be identified. Simulation results showed that the jerk motions of the wheeled mobile robot could be minimised by controlling the traction forces applied at the wheels. Selection of an appropriate traction force requires only knowledge of the geometry of the road profile,

which can be determined from measurements of the axle forces on the wheels while traversing the road obstacle.

REFERENCES

- Alexander, J. C., and Maddocks, J. H., 1989, "On The Kinematics of Wheeled Mobile Robots," *The International Journal of Robotics Research*. Vol. 8, No. 5.
- Baraff, D., 1993, "Issues in Computing Contact Forces for Non-penetrating Rigid Bodies," *Algorithmica*, pp. 292-352.
- Ben Amar, F., Bidaud, P., and Ben Ouezdou, F., 1993, "On Modeling and Motion planning of Planetary Vehicles," *Proceeding of the 1993 IEEE/RSJ International Conference on Intelligent Robots and Systems*, pp. 1381-1386.
- D'Souza, A. F. and Garg V. K., 1984, *Advanced Dynamics, Modeling and Analysis*. Prentice-Hall, Inc., pp. 95-97.

Deng, Z., and Brady, M., 1993, "Dynamics and Control of a Wheeled Robot," *Proceedings, The American Control Conference*, San Francisco, pp. 1830-1834.

Featherstone, R., 1987, *Robot Dynamics Algorithms*. Kluwer Academic Publishers, pp.153-195.

Hait, A., and Siméon, T., 1996, " Motion Planning on Rough Terrain for an Articulated Vehicle in Presence of Uncertainties," *IEEE International Conference on Intelligent Robots and Systems*, Vol.3, pp. 1126-1133.

Livermore Software Technology Corporation, 1997, "LSDYNA Users Manual."

Mehrabi, M. G., Cheng, R.M.H. and Hemami, A., 1993, "Dynamic Modelling of Wheeled Mobile Robots Theory and Experiment," *Second IEEE Conference on Control Applications*, Vancouver, pp. 659-665.

Shiller, Z., and Gwo, Y., 1991, "Dynamic Motion Planning of Autonomous Vehicles," *IEEE Transactions on Robotics and Automation*, pp. 241-249.

Siméon, T., 1991, "Motion Planning for a Non-holonomic Mobile Robot on 3-dimensional Terrain," *IEEE/RSJ International Workshop on Intelligent Robots and Systems, IROS'91*, Osaka, Japan, pp. 1455-1460.

Siméon, T. and Dacre-Wright, B, 1993, "A Practical Motion Planner for All-Terrain Mobile Robots," *IEEE International Conference On Intelligent Robots and Systems*, Yokohama, Japan, pp. 1357-1363.

Minimum jerk traction of a wheeled mobile robot passing over a hump

A. Ayalew, E. Lai

Dept. of Mech. & Manuf. Eng.
The Nottingham Trent University
Nottingham NG1 4BU
assefa.ayalew@ntu.ac.uk, e.lai@ntu.ac.uk

S. O. Oyadji

School of Engineering
The University of Manchester
Manchester M13 9PL
sooyadji@fs1.eng.man.ac.uk

Abstract

In this work a new technique for minimising jerk during longitudinal manoeuvre of a wheeled mobile robot traversing fixed road obstacles, which have positive gradient geometry, is presented. The dynamics of the robot with respect to the longitudinal, pitching and vertical motions of the platform are considered. The work has demonstrated that by controlling the drive torque input to the wheels, the platform can move over a positive-gradient hump with minimal jerk. This helps to minimise the possibility of wheel-ground contact loss, thus ensuring the stability of payload on wheeled mobile robots which are often used for transporting materials over uneven factory shop floors.

1. Introduction

There has been progress in the control of wheeled mobile robots, which are manoeuvred, on smooth terrain. Both kinematic- and dynamic-based control methodologies have been implemented for ideal indoor applications with no road obstacles [1][2][3]. But in a real industrial workspace these robots will encounter various obstacles like humps and cracks, which can bring about unwanted dynamic effects. Loss of control forces due to wheel-ground contact loss is one of such unwanted effects. This is because a wheel that has lost its contact with the ground can not generate either steering or traction forces. Consequently, it will be difficult to control the vehicle smoothly with a possible adverse impact on the stability of the payload on the platform.

Some consideration has been given to vehicle behaviour while moving on uneven terrain with respect to path planning. Siméon [4] considered the stability of a mobile platform as deemed to be satisfactory, when the line of action of the force of gravity on the vehicle intersected the polygon prescribed by the wheel contact points. In the path planning criteria used by Hait et al. [5], road paths that were likely to lead to wheel-terrain collision were included in the analysis but without considering the consequences. Ben Amar et al. [6] proposed a traction-force prediction scheme for vehicles travelling on uneven terrain based on the criteria that the wheels do not slip.

A highly simplified dynamics model has been presented by Shiller et al. [7] for vehicles travelling on uneven terrain. In this model a vehicle is reduced to a point mass so that the inertia effects can be ignored. No previous work, to the best of our knowledge, has addressed the issue of dynamic stability, in relation to the maintenance of wheel-ground contact and payload stability, for rigid mobile platforms travelling over road humps.

The validity of the constraint governing the wheel-ground contact is dependent on the acceleration at a contact point [8][9]. For a wheel to remain in contact with the road surface the normal component acceleration at the point of contact must be zero. If this component of acceleration is greater than zero at some time t , then contact is lost immediately after that instant. The acceleration can never be less than zero for rigid bodies, as this would imply that the wheel has penetrated the road surface. It is assumed that both the wheel and the road surface are rigid.

For contact to be maintained continuously, not only that the normal contact point accelerations must be zero but also their rate of change (jerk) must also be zero.

The normal accelerations are functions of the geometry of the road surface, and the angular and translational velocities and accelerations of the platform. By considering the case of a three-degree-of-freedom motion of a platform traversing a laterally symmetrical road obstacle (Figure 1), the present study attempts to address the issue pertaining to the maintenance of wheel-ground contact. The analysis assumes that the road obstacles have relatively small dimensions compared to the size of the vehicle (length of the vehicle and height of its centre of mass).

2. Modelling

Consider a rigid four-wheeled platform moving over a positive gradient hump. The wheels (front or rear) are subjected to a three degrees of freedom motion, namely, pitching motion about the lateral axis, longitudinal and vertical translational motion (Figure 1).

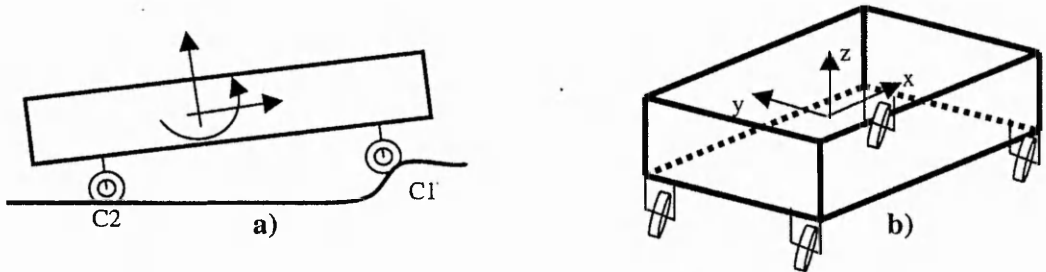


Figure 1. a) The three active degrees of freedom when passing over a hump.
b) Co-ordinate system definition.

The Newton's equations of motion, based on a co-ordinate system ($x-y-z$) attached to the vehicle's centre-of-mass can be written as:

$$\sum F_x = m(\ddot{v}_x + v_z \omega_y), \quad \sum F_z = m(\ddot{v}_z - v_x \omega_y), \quad \sum M_y = I_y \alpha_y \quad (1)$$

where m is the mass and I_y is the pitch moment of inertia, v_x and v_z are the longitudinal and the vertical velocities, respectively, ω_y is the pitch angular velocity, and α_y is the pitch angular acceleration of the platform.

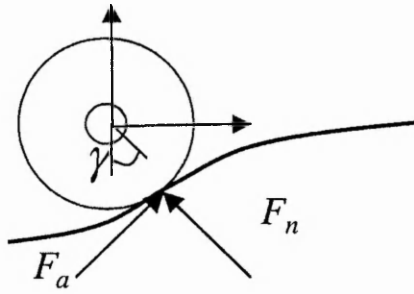


Figure 2. The geometry of wheel forces.

The wheel forces at the wheel k can be written as (Figure 2):

$$F_{wk} = A_k F_{ak} + N_k F_{nk} \quad (2)$$

F_a and F_n are the traction and normal reaction forces. A_k and N_k are given by:

$$A_k = \begin{bmatrix} \cos(\gamma_k) \cos(\delta_k) \\ \cos(\gamma_k) \sin(\delta_k) \\ \sin(\gamma_k) \end{bmatrix}, \quad N_k = \begin{bmatrix} -\mu_{rk} \cos(\gamma_k) \cos(\delta_k) + \mu_{lk} \sin(\delta_k) - \sin(\gamma_k) \cos(\delta_k) \\ -\mu_{rk} \cos(\gamma_k) \sin(\delta_k) - \mu_{lk} \cos(\delta_k) - \sin(\gamma_k) \sin(\delta_k) \\ -\mu_{rk} \sin(\gamma_k) + \cos(\gamma_k) \end{bmatrix}$$

μ_l is the lateral friction coefficient and μ_r is the rolling resistance coefficient, δ is the steering angle of the wheel, and γ is the angle which specifies the direction of the normal reaction force, it is also the gradient of the profile of the road surface at the point of contact. Although the contact forces (Equation 2) have been written for the most general case of a steered wheel, the present study concentrates on the special case of the longitudinal motion of a four-wheel vehicle. Hence the lateral friction forces are neglected with $\delta_k = 0$.

The acceleration at an arbitrary point p on the platform is written as:

$$\mathbf{a}_p = \mathbf{a}_c + \boldsymbol{\omega} \times \boldsymbol{\omega} \times \mathbf{r}_{p/c} + \boldsymbol{\alpha} \times \mathbf{r}_{p/c} \quad (3)$$

where $\mathbf{r}_{p/c}$ is the position of the point p with respect to the platform's centre of mass c .

Two other equations are needed for solving the equations of motions for the unknown accelerations and wheel reactions forces. These can be derived from the normal

acceleration components of the rear and front wheel contact points, C1 and C2 (Figure 1). Let \mathbf{n}_1 and \mathbf{n}_2 be the normal vectors to the road surface at the front and rear wheel contact points, respectively, and let \mathbf{a}_1 and \mathbf{a}_2 be the corresponding accelerations.

Thus,

$$\mathbf{a}_1 \cdot \mathbf{n}_1 = 0 \text{ and } \mathbf{a}_2 \cdot \mathbf{n}_2 = 0 \quad (4)$$

The equations of motion (Equation 1) can be solved to find the normal wheel reaction forces, the platform's centre of mass acceleration \mathbf{a}_c and its pitch angular acceleration α_y , after substituting for the wheel forces given in Equations 2 and using the Equations 3 and 4.

The rate of change of acceleration, that is jerk, at the point p on the platform, $\mathbf{J}\mathbf{e}_p$, is given by the differential of the right hand side of Equation 3 with respect to time. It is evident that this quantity is the sum of the jerk of the centre of mass ($\mathbf{J}\mathbf{e}_c = \frac{d}{dt} \mathbf{a}_c$), the rate of change of the centrifugal acceleration term, $\frac{d}{dt}(\omega \times \omega \times \mathbf{r}_{pc})$, and the rate of change of the tangential acceleration term, $\frac{d}{dt}(\alpha \times \mathbf{r}_{pc})$.

The centrifugal acceleration term contributes a jerk, which is proportional to the third power of the pitch angular velocity and another term, which is proportional to the product of the pitch angular velocity and the pitch angular acceleration. Since the angular velocity and angular acceleration are very small in so far as small size road obstacles are concerned, the contribution of the centrifugal acceleration term can be neglected. Hence the total jerk can be minimised by minimising the translational jerk at the centre of mass and the pitch angular jerk of the platform. Since we are dealing with acceleration with respect to a non-inertial-frame-of reference x - y - z , the jerk we are dealing with is one sensed by an observer moving with the vehicle.

The components of \mathbf{a}_c are functions of the gradient of the road profile γ , the longitudinal velocity v_x , and the vertical velocity v_z hence the differentiation of acceleration \mathbf{a}_c with respect to time is carried out in the following manner.

$$\mathbf{J}\mathbf{e}_c = \frac{d\mathbf{a}_c}{dt} = \frac{\partial \mathbf{a}_c}{\partial \gamma} \frac{d\gamma}{dt} + \frac{\partial \mathbf{a}_c}{\partial v_x} \frac{dv_x}{dt} + \frac{\partial \mathbf{a}_c}{\partial v_z} \frac{dv_z}{dt} \quad (5)$$

Similarly, for the pitching motion, the jerk is calculated as:

$$\mathbf{J}\mathbf{e}_{\alpha_y} = \frac{d\alpha_y}{dt} = \frac{\partial \alpha_y}{\partial \gamma} \frac{d\gamma}{dt} + \frac{\partial \alpha_y}{\partial v_x} \frac{dv_x}{dt} + \frac{\partial \alpha_y}{\partial v_z} \frac{dv_z}{dt} \quad (6)$$

$$\frac{d\gamma}{dt} = \frac{d\gamma}{dx} \frac{dx}{dt} = \frac{d\gamma}{dx} v_x \quad (7)$$

The term $\frac{d\gamma}{dx}$ is the curvature of the road profile at the point of contact and can be estimated for a continuous, smooth profile by differentiating the record of γ with respect to longitudinal displacement x .

3. Theoretical Results

The jerks of the translational motions of the centre of mass and the pitch angular motion of the platform, as felt by an observer travelling with the vehicle, are mainly functions of the geometry of the profile and the magnitude of the actuating forces. By solving the relevant governing equations, the relationship between the traction force requirement and the road surface profile (in terms of γ) can be established. For example, consider a mobile robot of the following geometric dimensions, and inertia and kinematic parameters:

Distance between front and rear axle, $L=2.2$ m;

Distance between front axle and centre of mass, $L_r=1.0$ m;

Height of centre of mass, $H=0.42$ m;

Total mass of vehicle, $m=50$ kg;

Pitch moment of inertia, $I_y=80$ kg-m²;

Longitudinal velocity of vehicle, $v_x=2.5$ m/s.

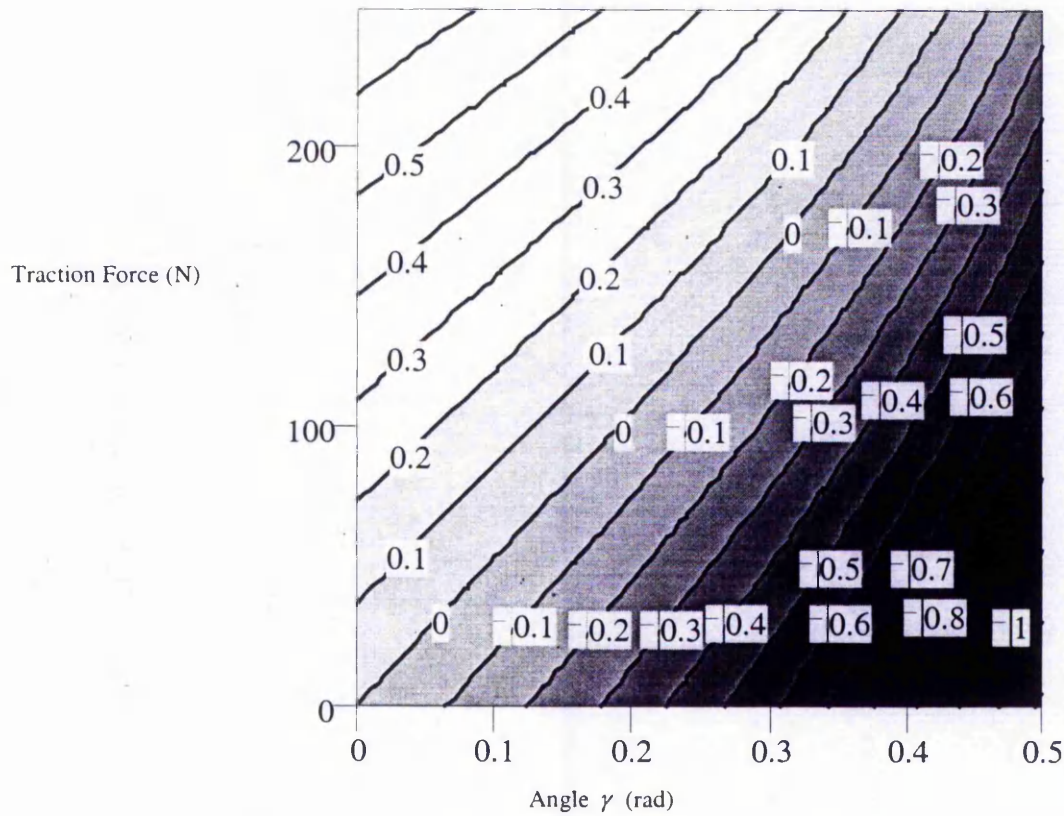


Figure 3-a) Contour plot of the longitudinal jerk.

Using the above information, the jerks (Equation 5-6) and accelerations (Equation 1) become functions of two variables, namely the wheel traction force (F_t) and the profile gradient (γ). The functional relationship between jerk/acceleration, traction force (F_t) and profile gradient (γ) can be represented graphically in the form of contour plots. In this example we have used a traction force ranging from zero to 250 N and profile gradient ranging from zero (corresponding to flat surface) to 0.5 radians ($\approx 30^\circ$ inclination from the horizontal).

For each pair of values of traction force and profile gradient, that is (F_t, γ) , the corresponding values of jerk and acceleration were computed using Equations (1), (5) and (6). The results are depicted as contour plots of longitudinal jerk and longitudinal acceleration in Figures 3-a and 3-b respectively. In Figure 3-a, the family of curves denote lines of constant jerk while the numerical values associated with each curve indicate the numeric values of the jerk. Similarly, in Figure 3-b, the family of curves denote lines of constant acceleration while the numerical values associated with each curve indicate the numeric values of the acceleration.

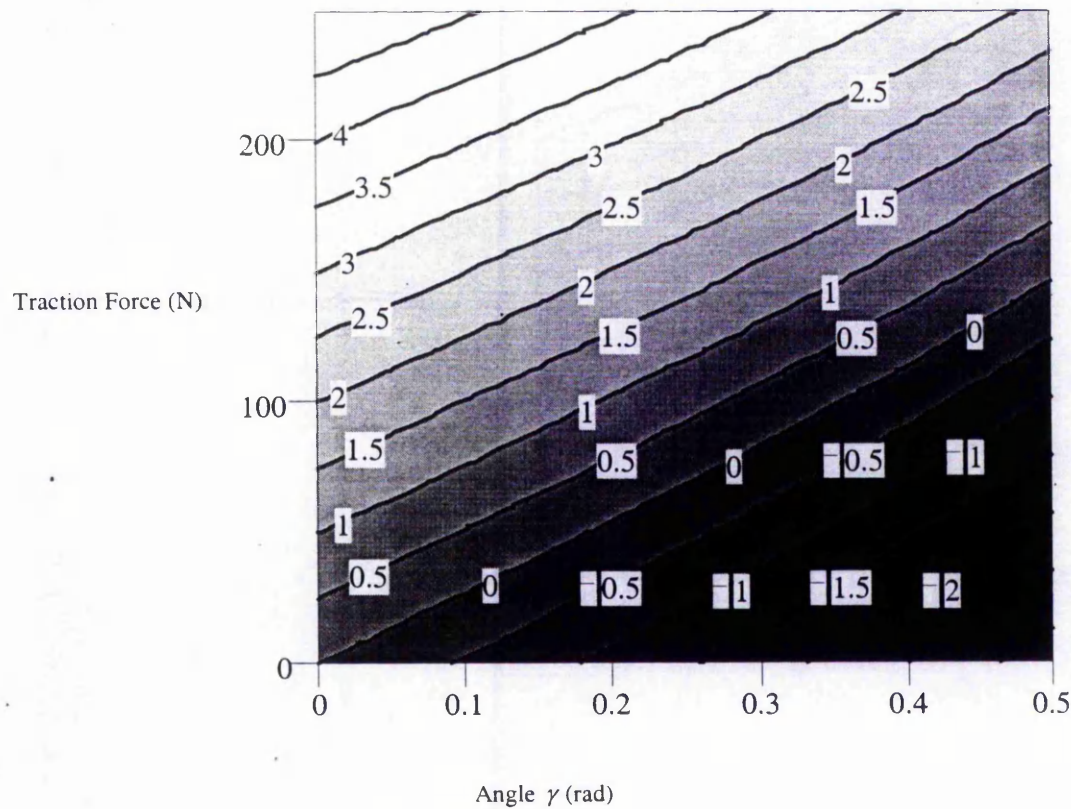


Figure 3-b) Contour plot of longitudinal acceleration

The zero contour line in Figure 3-a represents the conditions required for a theoretical jerk-free motion, if a proper actuating force is selected as a function of the geometry

of the profile. It has also been that an identical zero-jerk contour line is present in both components of the translational motions (vertical and longitudinal), as well as the pitch angular rotation. Hence, it can be concluded that for a given profile gradient, an appropriate traction force can be determined and applied to the wheels in order to ensure that the jerk in all motions is instantaneously zero. It should be noted that the longitudinal jerk and the longitudinal acceleration can not be simultaneously zero. The desired state is for the jerk to remain at zero throughout the duration of the motion of the mobile robot. This requires that the robot's longitudinal acceleration be positive.

4. Conclusions

A technique has been presented for the minimisation of jerk during longitudinal manoeuvre of a wheeled mobile robot traversing fixed road obstacles, which have positive gradient geometry. This can be accomplished by controlling the traction forces applied at the wheels. The traction force requirement for a given application can be determined from knowledge of the geometry of the road profile and vehicle dimensions.

5. References

1. Z. Deng and M. Brady, "Dynamics and Control of a Wheeled Robot," *Proceedings of the American Control Conference*.
2. M. G. Mehrabi and A. Hemami, "Dynamic Modelling of Wheeled Mobile Robots. Theory and Experiment," *Second IEEE Conference on Control Applications*. September 1993.
3. J.C. Alexander and J.H. Maddocks, "On The Kinematics of Wheeled Mobile Robots," *The International Journal of Robotics Research*. Vol. 8, No. 5. Oct 1989.
4. T. Simeon, "Motion Planning for a Non-holonomic Mobile Robot on 3-dimensional Terrain," *IEEE/RSJ International Workshop on Intelligent Robots and Systems, IROS'91*.
5. A. Hait and T. Simeon, "Motion Planning on Rough Terrain for an Articulated Vehicle in Presence of Uncertainties," *IEEE International Conference on Intelligent Robots and Systems, 1996*.
6. F. Ben Amar, Ph. Bidaud and F. Ben Ouezdou, "On Modelling and Motion planning of Planetary Vehicles," *Proceedings of the 1993 IEEE/RSJ International Conference on Intelligent Robots and Systems*.
7. R. Featherstone. Robot Dynamics Algorithms, *Kluwer Academic Publishers*. 1987.
8. D. Baraff, "Issues in Computing Contact Forces for Non-penetrating Rigid Bodies," *Algorithmica*, 1993.
9. Z. Shiller and Y. Gwo, "Dynamic Motion Planning of Autonomous Vehicles," *IEEE Transactions on Robotics and Automation*. 1991